

**Evolution equation models for
the advective transport during spring
and
the fasting physiology during winter
of age-0 Pacific herring in Prince William Sound, Alaska**

**Results from projects J, U, T and I
of the Sound Ecosystem Assessment Program[†]**

Vincent Patrick*

J. SEA Information Systems and Model Development (Proj. 320J)

Jennifer R. Allen	Alaska Digital Graphics, PO Box 212806, Anchorage AK 99521
C. A. Berenstein	Math and Inst. for Systems Res., U. Maryland, College Park MD 20742
Stephen Bodnar	Juneau, Alaska
Charles S. Falkenberg	ECologic Corp., 19 Eye St. NW, Washington, D.C. 20001
Tasuki Hirata	Tysons Corner, VA
Eddy Jin	U. of Toronto, Toronto, Ontario, Canada
Meibing Jin	Inst. for Marine Science, U. Alaska, Fairbanks AK 99775
Ravi Kulkarni	Grafikon Ltd and Adv. Vis. Lab., U. Maryland, College Park MD 20742
Doran M. Mason	Great Lakes Envir. Res. Lab., NOAA, Ann Arbor MI 48105
C. N. K. Mooers	Rosenstiel Sch. Marine & Atmos. Sci., U. Miami, Miami FL 33149
Roy Murray	Juniper Systems & Campbell Scientific
Ricardo H. Nochetto	Mathematics, U. Maryland, College Park MD 20742
Vincent Patrick (PI)	Inst. Sys. Res. & Adv. Vis. Lab., U. Maryland, College Park MD 20742
Sridhar Rao	Amazon.com, Seattle, WA
Jia Wang	Intl. Arctic Res. Cntr. & Inst. Mar. Sci., U. Alaska, Fairbanks AK 99775

U. SEA Fish Energetics (Proj. 320U)

A. J. Paul (PI)	Seward Lab., Inst. Mar. Sci., U. Alaska-Fairbanks, Seward AK 99664
-----------------	--

T. SEA Juvenile Herring Habitat and Growth (Proj. 320T)

Evelyn D. Brown	Inst. of Marine Sci., U. Alaska, Fairbanks AK 99775
Robert J. Foy	Inst. of Marine Sci., U. Alaska-Fairbanks, Kodiak AK
Michele Frandsen	Inst. of Marine Sci., U. Alaska, Fairbanks AK 99775
Brenda L. Norcross (PI)	Inst. of Marine Sci., U. Alaska, Fairbanks AK 99775
Jody Seitz	Anchorage AK
Kevin D. E. Stokesbury	Cntr. Mar. Sci. & Tech., U. Mass. Dartmouth, New Bedford MA 02744

I. SEA Stable Isotopes in Food Webs (Proj. 320I)

Thomas Kline (PI)	Pr. William Sound Sci. Cntr., PO Box 705, Cordova AK 99574
John Williams	Cordova, AK 99574

[†] Projects in the Sound Ecosystem Assessment (SEA) Program, Restoration Project 320 of the *Exxon Valdez* Oil Spill Trustee Council; partial project list identifying projects directly contributing to this documentation.

* email vince@isr.umd.edu, ph 301-405-7937, FAX 301-405-0720

Abstract

Two models are presented which together address the objective of the Sound Ecosystem Assessment Program to quantitatively represent the time evolution of age-0 (first year of life) subpopulations of Pacific herring (*Clupea pallasii*). For these models the first year of life is represented as hatching followed by three disjoint time intervals, with each interval characterized by a single dominant process: spring through mid-summer, advective transport of larvae; mid-summer through fall, feeding and growth; and winter through early spring, fasting. Models were developed for the first and third time intervals; these two are the subject of this report.

The model for advective transport and fate of larvae is the result of three separate model developments: the implementation of the Mellor-Blumberg 3D primitive equation circulation model for PWS (Wang, Mooers and others, J. SEA); the representation of larval advection as composite Lagrangian particles (Wang, M. Jin and others, J. SEA); and the representation of larval initial conditions, behavior, and mortality (Norcross and others, T. SEA). A primary application is the losses for an age-0 subpopulation in PWS due to advection of larvae out of PWS. It is shown that the assumption of a constant, spatially uniform predation loss rate greatly simplifies the comparison of the time evolution of loss due to advection relative to that due to predation. This comparison is applied to a full simulation for 1996 with the result that the advective loss is negligible.

After the period of advective drift the age-0 subpopulation ceases to make significant spatial movements and is represented as a discrete collection of stationary subpopulations indexed by site. For the fasting period and for each site-indexed subpopulation the following is assumed: *i.*) observable initial physiological conditions at an observable initial time for fasting; *ii.*) observable environmental forcing during fasting; *iii.*) total fasting until an observable end-of-fast time in spring. During the fasting period the four non-negligible tissue types—lipid, protein, ash, and water—are represented as an initial value problem for a system of ordinary differential equations, and fasting survival is represented as a region of viability in a four-dimensional physiology space (Patrick, Mason and others, J. SEA). The model is calibrated using laboratory studies of fasting (Paul, U SEA), and validated using the two observables physiology and survival for a set of study sites (U. SEA and T. SEA).

Both models are required for the determination of the time evolution of the age-0 subpopulation. The site-specific fasting survival is useful only in the context of the global distribution of the subpopulation among the possible sites. This distribution at the start of fasting is approximately given by the distribution at the end of the period of larval drift.

Keywords: marine ecosystem, evolution equations, numerical simulation, Prince William Sound, larval advection, physiology, bioenergetics, winter fasting, Pacific herring

Citation: Patrick, V. (2000). Evolution equation models for the advective transport during spring and the fasting physiology during winter of age-0 Pacific herring in Prince William Sound, Alaska. Results from projects J, U, T and I of the Sound Ecosystem Assessment Program. ISR Technical Report 2000-XX, Institute for Systems Research, University of Maryland, College Park MD 20742.

Preface for the ISR Technical Report

In March 1989 the Prince William Sound (PWS) ecosystem was abruptly perturbed by the *Exxon Valdez* oil spill (EVOS). However, the consequences of that perturbation were poorly understood due to the lack of models for the perturbed system and the lack of sufficient data to fully represent the state of the system at times preceding or following the perturbation. During 1993 Prof. Carlos Berenstein of ISR, along with R. Kulkarni and C. C. Goodrich of the Advanced Visualization Lab (AVL), provided support for V. Patrick to plan and to begin a new model development effort in collaboration with the Prince William Sound Science Center in Cordova Alaska. In September of 1993 the progress of that initial planning effort was incorporated into a larger science planning project established by the leadership of the PWS commercial fishing industry and sponsored by the *Exxon Valdez* Oil Spill Trustee Council (EVOSTC). In April 1994 the Science Plan [PWS93] was approved and the Sound Ecosystem Assessment (SEA) Program was begun. The objective was the quantitative representation of the subsystems of Prince William Sound presently generating the juvenile subpopulations of pink salmon and Pacific herring. These two species had been identified as damaged by the oil spill. Since their combined commercial harvest was the primary economic resource for Cordova, the outcome of the development effort would have significance beyond its technical objectives. A public overview of the SEA program and of the performance of the models was presented at the 10th anniversary symposium in Anchorage in March 1999.

The ISR and AVL planning initiative of 1993 became the Information Systems and Model Development (ISMD) project of the SEA Program. The ISMD project was one of 13 projects; it was responsible for the evolution equation models and for establishing the required computing and communications infrastructure at the Cordova site.

This Technical Report is adapted from one of the final reports for the ISMD project, the final report for the models for Pacific herring. It consists of four parts: a section describing the application context and project background, a “User’s Guide,” a “Validation Reference,” and a “Calibration Reference.” The format of this report is itself the result of a development effort. The format and the specific sections were created to serve as a candidate for a way to meet the needs of each of the groups to be served by the SEA Program: the technical development community, the scientific review committee, the program initiators from commercial fishing, marine resource managers, and those involved in the planning and oversight of oil spill protection and response for PWS.

Contributors

Each objective of the Sound Ecosystem Assessment (SEA) program required the use of multiple disciplines, and, conversely, each discipline was required by multiple program objectives. This scenario is routine for engineering projects and a typical approach is the use of the “matrix-management” organizational structure. Specifically, the scientific and technical disciplines—the “functional lines” of the organization—are shared across an orthogonal set of “project lines.” A structure based solely upon either the disciplines or the objectives either is impossible or requires extensive and inefficient duplication.

The “functional” structure of the SEA Program “matrix” consisted of thirteen discipline-specific projects. Each of these SEA projects was then to provide all of the Program requirements associated with that discipline. The objectives, the schedule, and the resources allocated to each project were established by the requirements of the shared SEA Program objectives.

This approach has consequences which are well known in project management but are much less familiar in the marine sciences. For example, the approach requires that no one project has exclusive “ownership” of any of the program objectives. There are contributing sub-objectives which in many cases are “within discipline” and can therefore be meaningfully attributed to a single project. However, any of the serious Program objectives requires the combined contributions from at least three projects and in many cases a majority of the projects.

This is well illustrated by the SEA models for juvenile Pacific herring. The results described in this technical report depend upon the direct contributions from the four SEA projects identified on the title page [PAB⁺00, PAB⁺98, Pau99, NBF⁺99, Kli99]. In addition to these four there are two further projects whose contributions are essential to the results provided by these four. The Juvenile Herring Habitat and Growth Project was integrally dependent upon contributions from the acoustics project (project 320N) [TK99]; the development and the applications of the circulation model are dependent upon information provided by the observational physical oceanography project (project 320M) [VIT99].

The following table contains additional information about the investigators and the four projects which contributed directly to the information contained in this document.

Contributors

contributor	in-project address	present address	email
J. SEA			
Information Systems and Model Development, Restoration Project 320J			
Jennifer R. Allen	PWSSC	Alaska Digital Graphics	jralen@alaska.net
C. A. Berenstein	UMD-ISR & Math	UMD-ISR & Math	carlos@isr.umd.edu
Stephen Bodnar	PWSSC	Juneau, Alaska	sbodnar@alaska.net
Charles S. Falkenberg	AVL	EcoLogic Ltd	csfalk@ecologic.net
Tasuki Hirata	UMD-ISR	Tysons Corner, VA	suki@eng.umd.edu
Eddy Jin	U. Toronto	U. Toronto	ejin@utoronto.ca
Meibing Jin	IARC & UAF-IMS	IARC & UAF-IMS	mbj@ims.uaf.edu
Ravi Kulkarni	AVL & Grafikon	AVL & Grafikon	ravi@avl.umd.edu
Doran M. Mason	Purdue	NOAA GLERL	mason@glerl.noaa.gov
C. N. K. Mooers	RSMAS U. Miami	RSMAS U. Miami	cmooers@rsmas.miami.edu
Roy Murray	Utah State	Juniper Systems	
Ricardo H. Nochetto	UMD Math	UMD Math	rhn@math.umd.edu
Vincent Patrick (PI)	PWSSC	UMD, ISR & AVL	vince@isr.umd.edu
Sridhar Rao	PWSSC & UMD	Amazon.com	cfynx@eng.umd.edu
Jia Wang	RSMAS & IARC	IARC & UAF-IMS	jwang@iarc.uaf.edu

U. SEA**Fish Energetics, Restoration Project 320U**

A. J. Paul (PI)	UAF-IMS Seward	UAF-IMS Seward	ffajp@uaf.edu
-----------------	----------------	----------------	---------------

T. SEA**Juvenile Herring Habitat and Growth, Restoration Project 320T**

Evelyn D. Brown	UAF-IMS	UAF-IMS	ebrown@uaf.ims.edu
Robert J. Foy	UAF-IMS	UAF-IMS	foy@ims.alaska.edu
Michele Frandsen	UAF-IMS	UAF-IMS	frandsen@ims.alaska.edu
Brenda L. Norcross (PI)	UAF-IMS	UAF-IMS	norcross@ims.uaf.edu
Jody Seitz	UAF-IMS	UAF-IMS	jody@pwssc.gen.ak.us
Kevin D. E. Stokesbury	UAF-IMS	U. Mass.	kstokesbury@umassd.edu

I. SEA**Stable Isotopes in Food Webs, Restoration Project 320I**

Thomas Kline (PI)	PWSSC	PWSSC	tkline@pwssc.gen.ak.us
John Williams	PWSSC	Cordova, AK	williams@pwssc.gen.ak.us

acronyms for contributor home institutions

acronym	organization	address
AVL	Advanced Visualization Lab, Office of Info. Technol.	UMD College Park MD
IARC	International Arctic Research Center	Fairbanks AK
IMS	Institute of Marine Science	UAF Fairbanks AK
ISR	Institute for Systems Research	UMD College Park MD
PWSSC	Prince William Sound Science Center	Cordova AK
RSMAS	Rosenstiel School of Marine & Atmospheric Science	Miami FL
UAF	University of Alaska - Fairbanks	Fairbanks AK
UMD	University of Maryland	College Park MD

Bibliography

- [Kli99] Thomas C. Kline. Stable isotopes as food-web tracers. In R. T. Cooney, editor, *Sound Ecosystem Assessment (SEA) - An Integrated Science Plan for the Restoration of Injured Species in Prince William Sound*, Final Report Ch 6. Exxon Valdez Oil Spill Trustee Council, Anchorage, AK, June 1999.
- [NBF⁺99] Brenda L. Norcross, Evelyn D. Brown, Robert J. Foy, Michele Frandsen, Jody Seitz, and Kevin D. E. Stokesbury. Juvenile herring growth and habitats. In R. T. Cooney, editor, *Sound Ecosystem Assessment (SEA) - An Integrated Science Plan for the Restoration of Injured Species in Prince William Sound*, Final Report Ch 10. Exxon Valdez Oil Spill Trustee Council, Anchorage, AK, June 1999.
- [PAB⁺98] Vincent Patrick, Jennifer R. Allen, C. A. Berenstein, Stephen Bodnar, Charles S. Falkenberg, Tasuki Hirata, Eddy Jin, Meibing Jin, Ravi Kulkarn, Doran M. Mason, C. N. K. Mooers, Roy Murray, Ricardo H. Nochetto, Sridhar Rao, and Jia Wang. Information Systems and Model Development. In R. T. Cooney, editor, *Sound Ecosystem Assessment (SEA) - An Integrated Science Plan for the Restoration of Injured Species in Prince William Sound*, 1994, 95, 96, 97 Annual Reports, Ch 7. Exxon Valdez Oil Spill Trustee Council, April 1995–1998.
- [PAB⁺00] Vincent Patrick, Jennifer R. Allen, C. A. Berenstein, Stephen Bodnar, Charles S. Falkenberg, Tasuki Hirata, Eddy Jin, Meibing Jin, Ravi Kulkarn, Doran M. Mason, C. N. K. Mooers, Roy Murray, Ricardo H. Nochetto, Sridhar Rao, and Jia Wang. Information systems and model development. In R. T. Cooney, editor, *Sound Ecosystem Assessment (SEA) - An Integrated Science Plan for the Restoration of Injured Species in Prince William Sound*, Final Report Ch 7. Exxon Valdez Oil Spill Trustee Council, Anchorage, AK, 2000. in preparation.
- [Pau99] A. J. Paul. Fish energetics. In R. T. Cooney, editor, *Sound Ecosystem Assessment (SEA) - An Integrated Science Plan for the Restoration of Injured Species in Prince William Sound*, Final Report Ch 11. Exxon Valdez Oil Spill Trustee Council, Anchorage, AK, June 1999.
- [PWS93] PWSFERPG. Sound Ecosystem Assessment Initial science plan and monitoring program. Technical report, PWSFERPG, Cordova, AK, 1993.
- [TK99] G. L. Thomas and J. Kirsch. Nekton-plankton acoustics. In R. T. Cooney, editor, *Sound Ecosystem Assessment (SEA) - An Integrated Science Plan for the Restoration of Injured Species in Prince William Sound*, Final Report Ch 9. Exxon Valdez Oil Spill Trustee Council, Anchorage, AK, June 1999.
- [VIT99] Shari L. Vaughan, Shelton M. Gay III, and Loren B. Tuttle. Observational physical oceanography. In R. T. Cooney, editor, *Sound Ecosystem Assessment (SEA) - An Integrated Science Plan for the Restoration of Injured Species in Prince William Sound*, Final Report Ch 8. Exxon Valdez Oil Spill Trustee Council, Anchorage, AK, June 1999.

Chapter 7 Document 1

Application information for the models for larval advective drift and age-0 winter fasting for Pacific herring

J. SEA
and
U. SEA, T. SEA, I. SEA

1. Introduction

This section presents selections from items developed initially to serve as an on-line component of a final reporting to the sponsor[†] and to the industry group which had initiated the effort. For this ISR Technical Report the selections are drawn from the background information rather than from those items developed for use as on-line end-user tutorials. The tutorials were simplifications of some of the technical results and were prepared prior to this report. The presentation in this Technical Report replaces the earlier tutorials.

On the other hand, the background information is still useful. It is noted at several places in this report that the presentation assumes an “informed reader” with respect to the application issues and the motivation for the R&D effort. The background selections here provide some basic information regarding the Prince William Sound marine ecosystem, the economics and social issues of commercial fishing in southcentral Alaska, and the significance of the juvenile subpopulations of exploited marine species to the management and the tracking of marine subsystem dynamics.

[†] Primary support during 1994–1999 provided by the Exxon *Valdez* Oil Spill Trustee Council, Restoration Project 320J.

Sustaining support during 1998–1999 for the circulation model development and for the PWSSC computing infrastructure provided by the Oil Spill Recovery Institute, Cordova Alaska.

Version 3 of the fasting model and all of the final documentation for the ISMD projects are due to private financing from V. Patrick for ISMD IR&D and to continued long term sustaining support from Grafikon Ltd and from the Advanced Visualization Lab of the University of Maryland.

2. A brief history of ISMD prior to 1994

The “virtual” group that later formed the Information Systems and Model Development project became interested in the mathematical and information technology issues posed by the Prince William Sound (PWS) marine systems in November 1992. The interest was the result of an invitation by the director of the Prince William Sound Science Center (www.pwssc.gen.ak.us) to visit Cordova Alaska and to review a newly established program for a community GIS information center and to discuss the contemporary issues for the PWS marine system following the Exxon Valdez oil spill of March 1989. As a result of that visit and ensuing events, AVL and Carlos Berenstein of ISR (www.isr.umd.edu) provided support during 1993 for an application initiative with two objectives: *i*) mathematical models and numerical methods for remote subarctic marine systems and *ii*) the facilitation of model development projects at remote sites through the use of contemporary network and information technologies, especially those for collaborative and distributed R&D.

The first objective for 1993 was a technical and financial plan to connect the remote Cordova site to the Internet. The purpose here was to establish connectivity at a bandwidth sufficient for the remote community to utilize effectively and to real advantage the technical and computational assets available at major national centers. An optimally cost efficient technical design was developed, but the best design was fully an order of magnitude more expensive than the equivalent service in any major population center of the United States. No financial plan could be found whereby so large a cost factor could be accommodated given the existing national and regional investment schedules for telecommunications and community Internet access.

In July 1993 there was a second invited visit to Cordova. During that week the course was set for the second of the two objectives: in collaboration with David Eslinger (then at UA Fairbanks, now at the NOAA Coastal Services Center) a first draft was sketched which specified, albeit only coarsely, the targeted marine subsystems but specified quite specifically the approach for their mathematical representation. In early August, however, the initiative appeared to lack key required elements with no evident means for correcting the situation. Equal in importance to the lack of a viable financial plan was the lack of an adequately well-posed problem statement, the lack of a specific application with measurable technical significance or societal relevance, and the apparent lack of sufficient system-specific and issue-specific knowledge to correct either deficiency. This assessment, however, was premature, for activities in other parts of the same community soon resolved these apparent gaps.

The devastating economic consequences of back-to-back exceedingly low and unanticipated returns for PWS pink salmon for 1992 and 1993 were compounded by the collapse of the Pacific herring fishery in 1993. These two fish species are respectively the first and second largest economic resources for the PWS fishing fleet. The economic consequences were worst for seine vessel permit holders, for this vessel type is used exclusively for the harvest of these two species in Prince William Sound. Seine vessel permit holders reside in communities throughout southcentral Alaska, but a major fraction reside and harbor their vessels in Cordova. More important than the residency is the fact that fleet support and the processing of the fleet harvest is by far the primary industry for Cordova. Whereas Valdez, Homer, Seward, and Whittier each are home ports for the seine fleet, each of these has a more diverse economy in which commercial fishing is a significantly smaller component than is the case for Cordova. The unfortunate events of 1992 and 1993 provided, especially in Cordova, the focus and performance measures that were heretofore missing.

In addition to eventually establishing a problem statement and performance measures, the events of 1992 and 1993 also established an unprecedented industry-directed R&D initiative for the PWS marine system. The proximity in time to the Exxon Valdez Oil Spill could not be overlooked despite the on-going litigation over fate and effects of the spill for the marine bio-production system. The seine fleet approached the Exxon Valdez Oil Spill Trustee Council (EVOSTC) with the appropriateness of an industry-directed R&D effort at this juncture. Such an effort would be a part of the then commencing "Restoration" program, the second phase of the EVOSTC administration of the spill settlement funds. By virtue of a unique presentation technique, the seine fleet representatives on August 12, 1993, secured an industry-directed R&D investment of \$5million for each of five years. (This was later reduced to a \$20million investment over five years at a declining investment schedule, and hereafter only the actual lower investment schedule will be referenced.) Given the gravity of the purpose, the cost for network access that heretofore had been prohibitive was now a reasonable and justifiable expense. Access to the necessary resources and capabilities could now be assumed, and after September, 1993, the focus could turn to the issues of the problems to be solved and the implementation plan for obtaining the solutions.

In a remarkable history that has not been adequately documented, the ad hoc group of seine fleet representatives responsible for establishing the program then passed the task of the problem statements and the implementation plan to a second ad hoc committee, the Prince William Sound Fisheries Ecosystem Research Planning Group (PWSFERPG). This committee was significantly smaller than the first but had an expanded representation. It was, in effect, an industry and resource management consortium comprised of individuals from the commercial fleet, from Prince William Sound Aquaculture Corporation (pink salmon hatcheries), and from the Cordova office of the Alaska Department of Fish and Game. There was official inclusion and consultation with additional representation, however, it was the individuals from these three groups who carried out the work of the consortium.

A planning process was begun in September 1993 that would last for more than three months. The planning was the primary work for the initiating participants of PWSFERPG and for many of the technical persons who were selected as part of the planning process. The scientific and technical persons had equal responsibilities for establishing the plan and at the conclusion were to then carry out that plan.

We conclude the history here, and jump ahead to December 1993 at which time the the planning was concluded with the release of the Sound Ecosystem Assessment (SEA) Science Plan. That plan contained in effect two industry-directed problem statements which hereafter are referred to as the PWSFERPG-directed problem statements.

Although the problem statements were the joint product of all contributors, these statements were not based upon scientific curiosity or a search for yet another "most significant" variable in ecosystem"health." Rather, the statement is the result of over 40 man-months of concentrated effort to select wisely from the open issues in PWS marine bio-production. The problems selected were those whose solution could be realized with the knowledge of the day. More importantly, the solutions would contribute measurably to never again being unable either to anticipate events such as those which occurred in 1992 and 1993 or, once such events had occurred, to resolve their origins in the preceding time evolution of the bio-production system. The SEA Science Plan contained an outline of an implementation plan which was further developed during the spring of 1994. In April

1994 the EVOSTC provided financial support for the first year of the Sound Ecosystem Assessment (SEA) Program. SEADATA was one of a dozen projects in the SEA program, each project organized by technical discipline. The issues that were to be addressed and the problems that were to be solved by SEADATA are the focus of this document. However, the interdependencies of the projects make the various efforts largely inseparable. Therefore, these other efforts will of necessity be referenced throughout. The reports and results from these companion efforts were in some cases made available for on-line publication at the SEA Program web site www.pwssc.gen.ak.us/sea The SEA web site is no longer actively maintained. Consequently, reports not available on-line will not be appearing at some future date. In such cases one must contact the Trustee Council office for distribution of the documentation.

3. The SEA investment: economic context

The investment made in industry-directed R&D over the period of April 1994 through March 1999 was approximately \$20million. If the investment schedule had been flat the rate would have been \$4million for each of the five years. In fact, the schedule was declining, but for the comparisons here we use the average annual rate.

3.1 Equivalent to fleet IR&D at 20% of total revenue

The annual adult hatchery pink salmon returns for release years since the beginning of coded-wire tagging in 1987 through 1996 (release year) shows a maximum sound-wide return of 31million. (This upper bound was exceeded by release year 1998 that has just returned during the past summer, but we use the historical maximum for this comparison.) Recent prices for pink salmon have been approximately \$0.15 per pound and returning adults are approximately 3 pounds. That is, each adult is worth \$0.50 to the fleet, and the total annual revenue for the entire hatchery pink salmon harvest is about \$15million for harvests at the historical maximum. Wild stock pink salmon returns have recently averaged 6million adults, so at best there is an additional \$3million per year, but we shall not include wild stock value in this discussion. Pacific herring harvest annual values have been suppressed since the sharp decline in 1993. An approximation is that the value to the fleet adds another \$5million to the \$15million from pink salmon. The total ex-vessel annual revenue for the two species addressed in the SEA R&D is approximately \$20million. That is, the SEA five year R&D effort was equivalent to a full year annual harvest revenue. In other terms, the annual expenditure on average for SEA was equivalent to a 20% re-investment rate for IR&D, the usual acronym for "Internal R&D." This, of course, has not included value added by processors. The comparison is made here without consideration of this additional value to the region from the harvest.

3.2 Twice the annual PWS RCAC operating budget

Until 1999 PWS Regional Citizens's Advisory Council conducted all of its advisory functions, monitoring, oversight, and some R&D with a \$2million annual budget. On average the industry directed R&D conducted by SEA was carried out at a schedule twice that for PWS RCAC.

3.3 Not quite four times the annual operating budget for OSRI

The Oil Spill Recovery Institute has taken over some of the SEA R&D efforts with the intent of moving these to full implementation. It is worth keeping in mind that for the five years of SEA the annual budget was nearly four times the \$1.2million annual operating budget for OSRI. Given the scope of the OSRI mission and the extent of the community served by that mission, one might expect that no more than one-third of the annual budget would be allocated to topic areas that were part of the SEA R&D effort. In this case the annual SEA investment rate is about 12 times that which OSRI will invest annually. Given that there were typically ten or so projects in SEA, the OSRI investment schedule is sufficient to support about 75% of a single one of larger SEA projects which averaged from \$500K to \$800K annually; it alternatively can support fully a single one of the smaller SEA projects which averaged \$150K to \$300K annually plus 50% again. Since none of the

SEA projects individually had industry relevance such an investment rate will never be capable of sustaining any of the SEA objectives in their original formulation. For any fleet relevance a total redesign effort is required comparable to that which was done in the fall of 1993.

3.4 Two-thirds of the EVOS planned Restoration Reserve investment schedule

The investment schedule mentioned by EVOS for the GEM effort is \$6million annually. The SEA investment rate will then have been on average 66% of the total planned investment rate for all future monitoring to be conducted by the EVOSTC Restoration Reserve Fund.

3.5 Technology transfer and utilization at practical IR&D schedules

The United States places great importance on its technical edge in the new global economy. The federal government makes major expenditures for industry-applicable R&D. One example from a closely related area is the extensive collection of USDA programs in support of aquaculture. There are similar expenditures for R&D efforts in areas of interest to commercial fishing industry; the bulk of these efforts are carried out by NOAA on behalf of the industry.

Unlike telecommunications and satellite industries who have NASA created university Centers for the Commercialization of Space, commercial fishing has the benefit of the NOAA laboratories and centers for industry-applicable R&D support. This means that the past five year investment in non-federal commercial fishing directed R&D is a rare anomaly. The challenge for for the PWS fleet is to use this investment effectively given that the project and the results are outside the conventional industry support system.

The first task is for the fleet to promptly and thoroughly carry out its review and evaluation of the effort and determine a means to secure a proper return for the amount invested. The PWS fleet must look to the investigators to complete as full a technology transfer as possible while that technology is still accessible and the corporate knowledge still intact. This is precisely what these pages seek to deliver to the fleet from the investigators who carried out the SEADATA project.

We have in mind as the minimum acceptable outcome that the SEA investment in the very near future begin to deliver a return comparable to that which would come from having placed the entire \$20million in any income producing investment—such as treasury bonds. A modest 5% return would be \$1million annually, which is roughly a 5% improvement in the profitability of commercial fishing. Just as it would have taken five years to accumulate the full \$20million in T-bonds, it took five years to accumulate the SEA results. Our goal in these pages is work with the fleet to find the 5% return to the industry in the SEA solutions to the PWSFERPG problems.

4. The PWSFERPG problem statements

Over three months of concentrated effort by more than fifteen individuals from diverse fields gave the SEA effort its most valuable asset: two well-posed problem statements. If the problem statements had been ineptly constructed no amount of effort, no number of dollars, and no greater aggregation of data would have led to a positive outcome. Everything hinges on the quality of what went into the formulation of the problem.

The figure below states in overly condensed form the two problem statements. It then also shows those sections of the implementation concept presented in the SEA Plan that fell to the SEADATA project.

The boxes with dotted boundaries indicate the large portion of SEA that was NOT among the SEADATA tasks. The boxes are not to scale with respect to either level of effort or scope of responsibility.

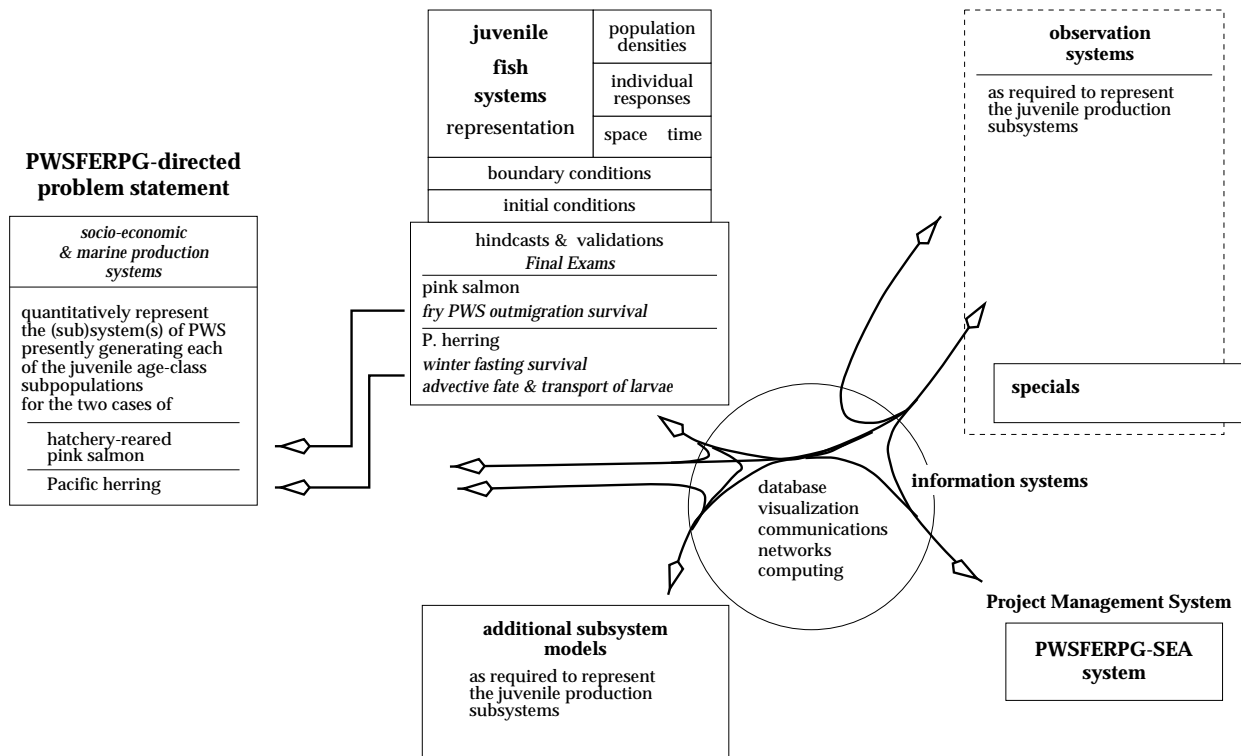


Figure 1.

The box marked Specials refers to first and second year tasks in which certain new sensor technologies were brought on-line and the fourth of the major model efforts begun. These are described in the "initiatives & spinoffs" section.

5. The Pacific herring models: Why Bother?

The purpose of SEA in general – and of the various models in particular – was to realize an major incremental improvement on the ability to track the production processes of PWS for the two fisheries that provide the economic basis for the region, and for Cordova in particular. The processes that sustain adult populations are different from those involved in the formation of new juvenile populations. Neither sets of processes were quantitatively understood. As a result there has been no means to address the tasks of optimization and efficiency that are fundamental to any production-based industry.

The issue of little or no quantitative theory or model sufficient for any meaningful tracking of the time evolution of these production systems was highlighted by the perturbation to the system due to the Exxon Valdez oil spill. With no means to track the system without perturbation, there was of course no means to track any consequences or determine differences in the system functions with a major perturbation. In this situation, there is no means to effectively protect the production system from events associated with the multiple uses of the marine system.

These two related purposes – economics and protection – are the two fundamental objectives of the model development effort. In the SEA program the focus was on the production processes for the juvenile populations. The overwinter survival of age-0 is but one of the processes. But it occurs at the transition between a period of very high mortality and the age-1 period in which mortality is much lower. Consequently, the successful realization of models that adequately represent the fasting processes and the consequent mortality will enable tracking of the population and the approximation of the future exploitable stocks by the upper bound associated with survival of the age-0 winter.

The following graphical depiction (ignore any numbers) of the ADFG ASA analysis shows the manner in which the overwinter model serves as one part of the extension of this analysis to age-0.

Estimated Naturally Spawning Population (millions) ASA

YEAR	AGE							mt	tons
	3	4	5	6	7	8	9		
1999	66.0	195.0	52.2	30.8	30.9	61.5	5.9	47927	52831
2000	19.4	154.8	177.5	33.7	20.3	21.0	45.3	60253	66417
2001	21.8	42.3	131.7	112.6	20.6	12.6	37.0	50760	55953



YEAR	AGE										mt	t
	0	1	2	3	4	5	6	7	8	9		
1999				66.0	195.0	52.2	30.8	30.9	61.5	5.9	47927	52831
2000				19.4	154.8	177.5	33.7	20.3	21.0	45.3	60253	66417
2001				21.8	42.3	131.7	112.6	20.6	12.6	37.0	50760	55953

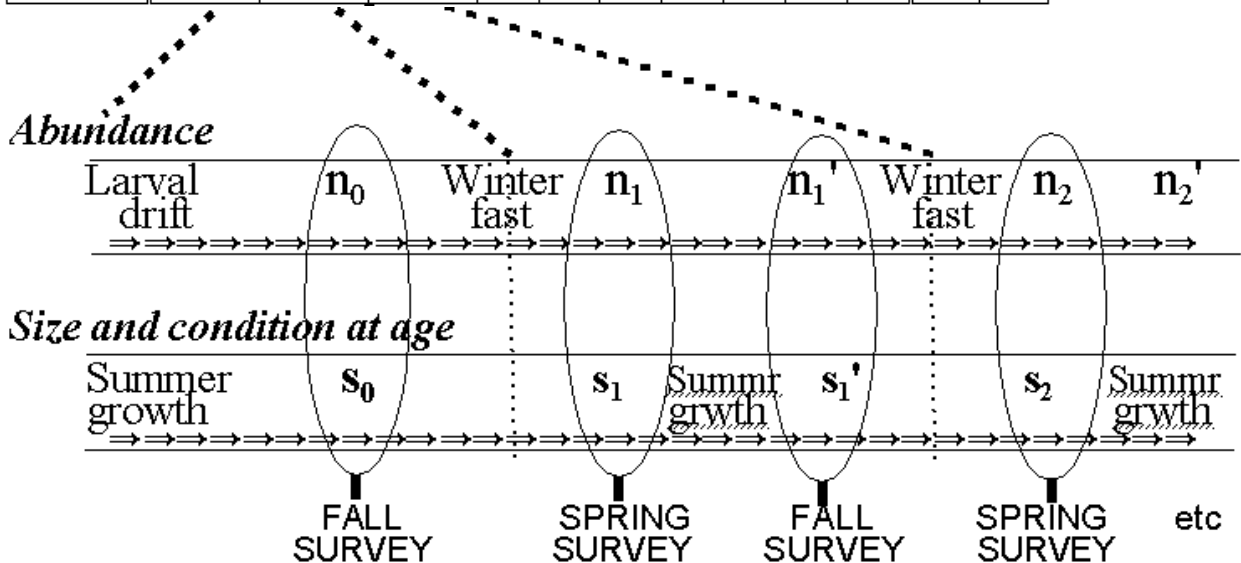


Figure 2. A graphical illustration of the role of the outputs of the SEA models for Pacific herring used in the context of one of the standard tools for resource management, the “Age Structure Analysis” of a population. **Note:** all numbers shown are purely fictional—there is no correspondence with any actual population sizes.

6. The geographic domain

For obvious reasons remote sensing and mapping projections have become closely linked. The projection for the SEA bathymetry dataset was chosen during the first year at the same time that decisions were made regarding a projection for the SEA AVHRR datasets. There was no compelling reason to use anything other than the same projection for the SST data and for the PWS gridding itself, and there are obvious advantages for using the same projection for both.

The "equal area" projections have advantages for imaging sensors with arrays of equal-sized pixels. Gary Drew (USGS) urged use of the Albers conic equal-area projection with parameters

* parallels 55 and 65 degrees N * origin at -154 longitude, 50 latitude

Drew noted that both the state and the federal agencies used Albers for remote sensing data but that the two differed on the specific parameters. (My recollection is that the above is the federal "standard.")

Gary Drew and Dave Eslinger settled on this choice for their AVHRR data. This same choice was used for the bathymetry gridded data set. During the following spring Jia Wang used the bathymetry grid to define the grid for the circulation model. This projection is now a factor in the development of forcing data for the circulation model and in the development of applications of the model. Since the choice of projection is about to be a factor throughout the project, it looks prudent to sort out any issues and problems with its use.

Figure 3 shows the domain used for the SEA R&D program in the context of the larger map of southcentral Alaska. Note in particular that one consequence of the choice of projection is that the "y-coordinate" of the projection is nowhere tangent to lines of longitude anywhere in the study domain.

Figure 4 shows an expanded view of the study domain. In this view the outlined rectangular domain identifies the region that was regularly gridded and used for the implementation of the circulation model. The model domain was constrained as shown in Figure 4 due to the limited extent of the available bathymetry data in 1994. (In recent years the EEZ bathymetry data was declassified and is now available. This new resource will enable the extension of model domain to the full region of interest.) The domain shown in Figure 4 is the domain used for the larval advection simulation described in Document 2 of this report.

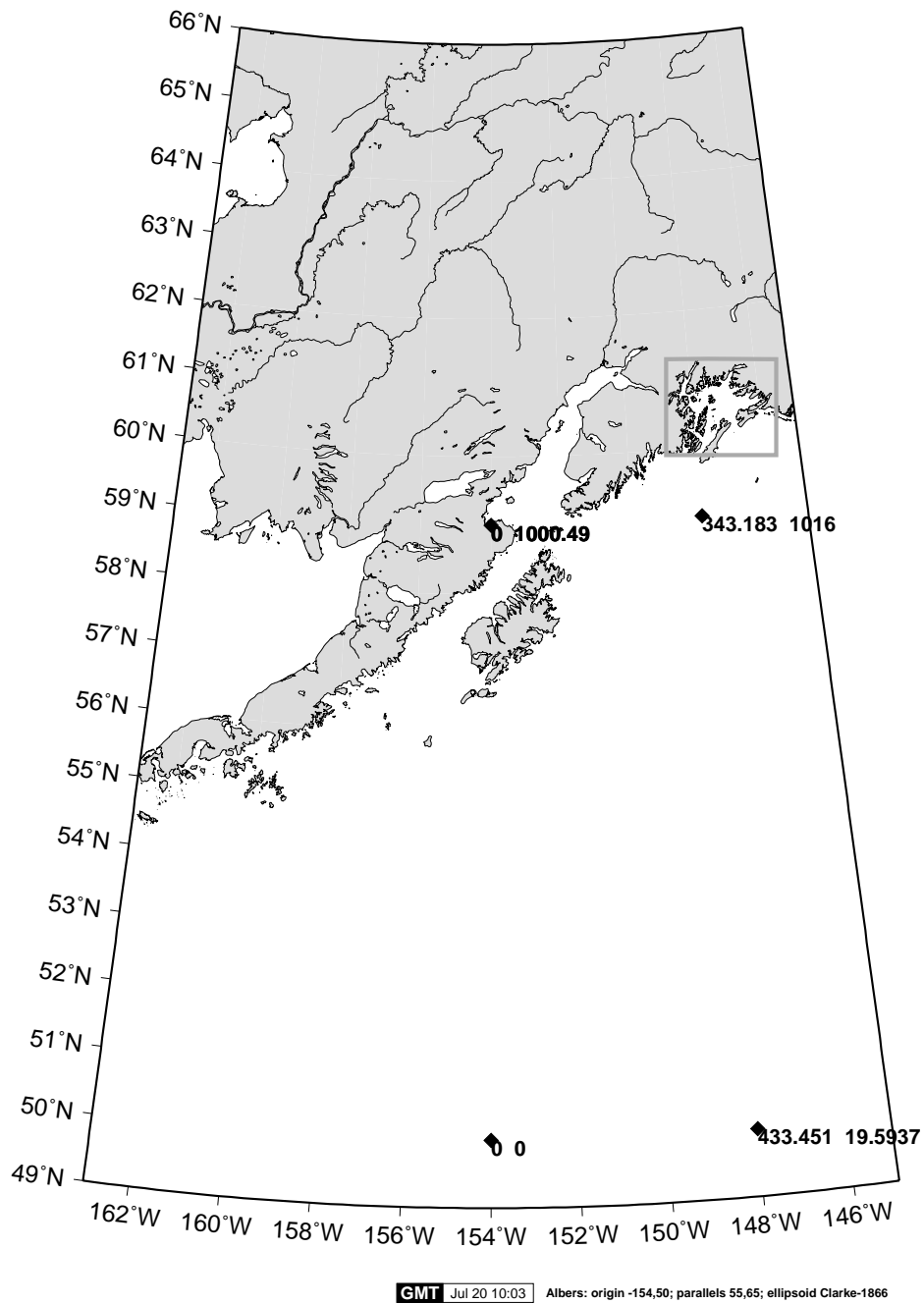
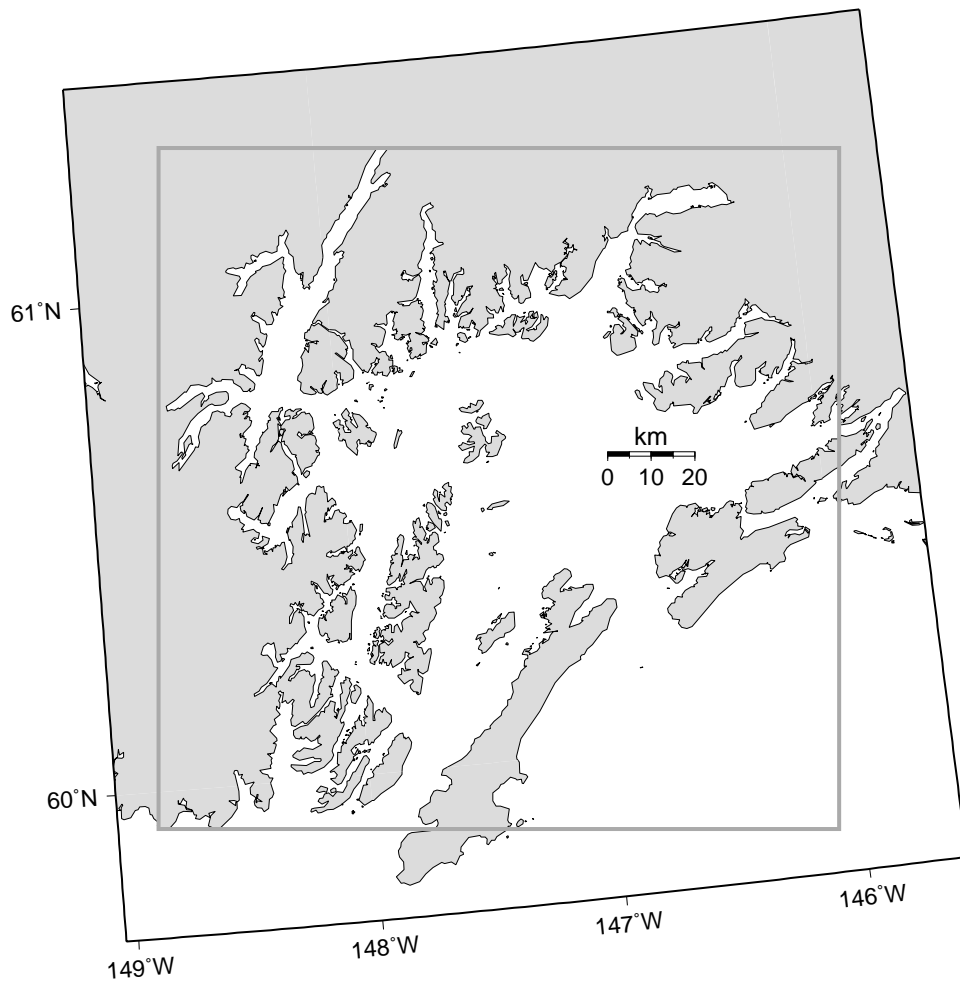


Figure 3. Albers “154 50” projection of southcentral Alaska with the study domain indicated. The origin of the projection and the coordinates for a few points are shown.



GMT Jul 20 05:01 Albers: origin -154,50; parallels 55,65; ellipsoid Clarke-1866

Figure 4. The Albers “154 50” projection of the study region. The outlined regions is that which is represented in the SEA circulation model and hence the region represented in the larval advection simulation of this report.

Chapter 7 Document 2

A Concise User's Reference for the models for larval advective drift and age-0 winter fasting for Pacific herring

J. SEA
and
U. SEA, T. SEA, I. SEA

1. Introduction

This section is in the form of a “User’s Reference,” but one that is restricted to the information required to begin using the current version of the models. It is intended to serve as a single source document for the equations and for the applicability for each of the models for juvenile Pacific herring developed by the Information Systems and Model Development (ISMD)[†] project of the Sound Ecosystem Assessment (*SEA*) Program. The goal is to provide an informed end-user with the information needed to construct an implementation plan incorporating the overwinter fasting model and the circulation model and to then conduct a breadboard analysis to determine the efficacy and cost-to-benefit ratio of that implementation plan.

The format and organization of the section parallels the order in which a user would apply each of the various models during the course of a one year cycle. Since there are extensive interdependencies between the ISMD models and the developments and deliverables of other *SEA* projects, this format requires that these interdependencies be made explicit and included in the presentation. In particular, this section presents all of the major components, or modules, of the juvenile herring models with guidance regarding the resource documentation for those components developed by other projects. In the case of components developed by other projects, this section provides a brief summary from the point of view of a user seeking to apply the models for larval advective transport and fate and for age-0 overwinter fasting.

This section is intended as a “quick reference pull-out” for an informed end-user. It is designed to be a part of a more complete User’s Reference Manual. In addition, the User’s Reference Manual is but one part of the documentation for the ISMD model development and the reader is directed to other sections for information regarding the motivation, development, calibration, validation, and

[†] Primary support during 1994–1999 provided by the Exxon *Valdez* Oil Spill Trustee Council, Restoration Project 320J.

Sustaining support during 1998–1999 for the circulation model development and for the PWSSC computing infrastructure provided by the Oil Spill Recovery Institute, Cordova Alaska.

Version 3 of the fasting model and all of the final documentation for the ISMD projects are due to private financing from V. Patrick for ISMD IR&D and to continued long term sustaining support from Grafikon Ltd and from the Advanced Visualization Lab of the University of Maryland.

**Structure of the documentation for the solutions to the PWSFERPG problems
contained in the Final Report of the
Information Systems and Model Development Project**

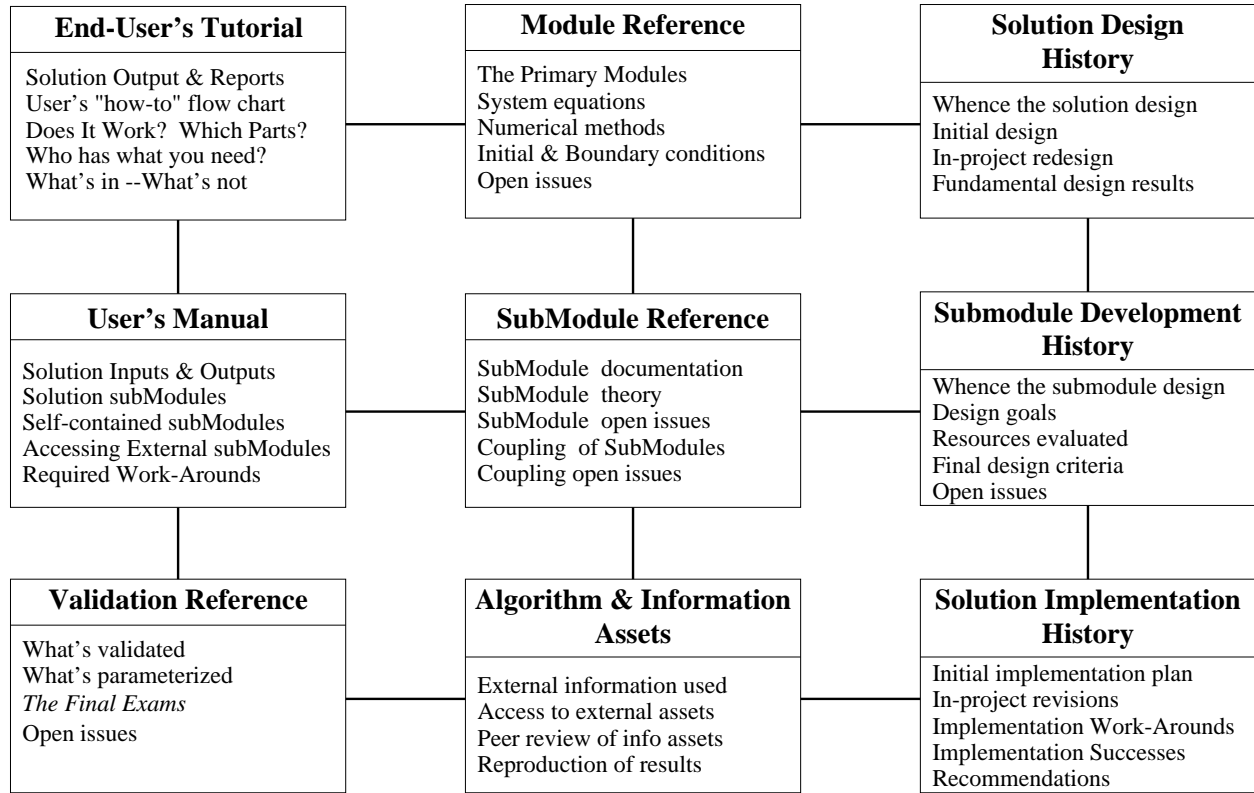


Figure 1. Structure of the document and the relationships between sections. (All sections in the figure do not appear in this first draft of the Final Report.)

history of the ISMD models. These other sections of this documentation and their relationship to this Concise Reference can be seen in the diagram of the document structure shown in Figure 1.

1.1 The annual cycle and sequence of the juvenile herring models

There is a natural ordering for the components of the juvenile herring models that arises from a fundamental design feature: the objective of the *SEA* modelling effort was to quantitatively represent only very short time intervals and to select those intervals whose end-points were naturally associated with the capability of measurements providing data for model validation or data assimilation. As a consequence of this fundamental design objective, the individual components of the juvenile herring models consist of a model for each of an ordered sequence of time intervals, with each interval bounded by monitoring conducted at the interval end-points. This is immediately clear from the graphical representation of the model and monitoring components shown in Figure 2. The order of presentation of this section follows the annual cycle shown in Figure 2. In Figure 2 the direction of increasing time during the year is from bottom to top—the March at the

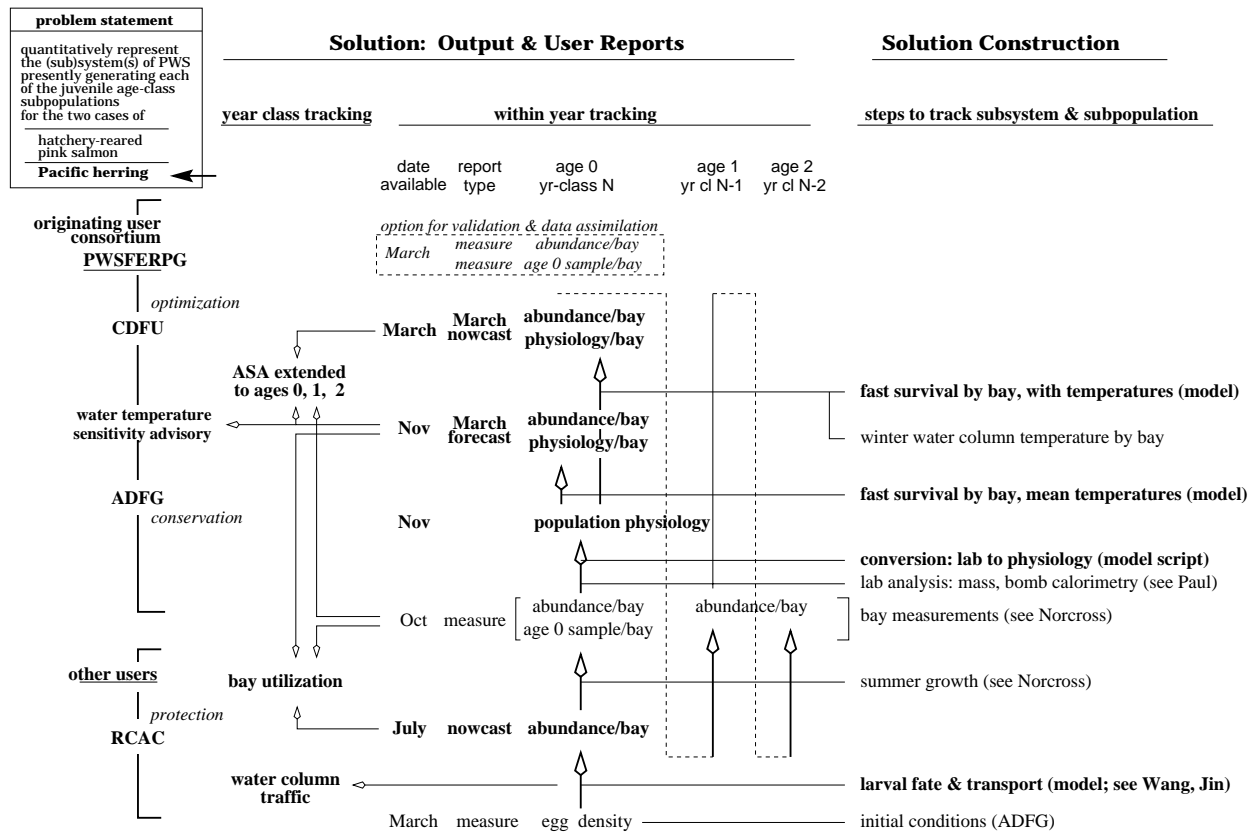


Figure 2. The annual cycle for the models and the monitoring for tracking the development of the juvenile subpopulations of Pacific herring.

top of the figure is one year later than the March at the bottom.

Figure 2 is extracted from the “User’s Tutorial” section of this document. It is assumed that the contents of the figure are familiar to the reader—for example, the organizations identified as the primary end-users and the topics identified as the primary areas of application shown in the left-most columns of the figure.

The right-most column, from bottom to top, is the order followed in this concise reference. The “steps” listed in the right-most column are the “major modules” of the juvenile herring models. Each of these is a subsection of this concise reference. There are nine such steps or modules shown in Figure 2. The four steps shown in bold in Figure 2 were the development responsibility of the ISMD project. The column in Figure 2 labeled “date available” identifies the specific month during the “application year” in which the output of the module becomes available to the end-users and to the next module in the annual sequence.

2. Concise descriptions of model components

2.1 Spawn deposition survey

The first module is the field estimation during April of the shoreline density of herring eggs in Prince William Sound. The *spawn deposition survey* was developed by the Alaska Department of Fish and Game (ADF&G) to exploit a directly measurable variable having a fundamental link to the number of sexually mature adults in the population. Central to the development of the survey was the determination of the quantitative properties of the relationship between the observed variable and the population numbers. The spawn deposition survey is used here not for its original purpose but rather to provide initial boundary conditions for the next component in the sequence of juvenile herring models, the model for the advective transport and fate of the herring larvae. In the event that ADF&G makes no in-season observation of the April egg density, then a “most probable” set of initial conditions for the larval drift model must be constructed from historical data and from any available contemporary information.¹

We turn next to establishing some basic notation. The following notation brings together in the form of end-user application equations results presented in the Juvenile Herring Growth and Habitats report (Ch. 10 of the *SEA* Final Report)[NBF⁺99], results from the “Circulation Model” section of this document, and the original plans and objectives of the 1993 *SEA* Science Plan [PWS93].

Let $\varphi_Y(x, t)$ denote a line-source flux of larvae entering the water column at shoreline position x and time t for spawning year Y . That is, $\varphi_Y(x, t)$ is the number of larvae per unit length of coastline per unit time emerging from the spawning site x at time t during spring of year Y . Let \mathcal{C} denote the one-dimensional coastline of PWS. Because of the modelling objective we restrict \mathcal{C} to the subset that is within the boundaries of the present version of the PWS circulation model domain. (See the “Algorithms and Information” section.) For any given year Y spawning occurs only over a subset \mathcal{C}_Y of the full coastline \mathcal{C} . Similarly, larvae emerge only during a short time interval I_Y . The subset \mathcal{C}_Y is that part of the entire shoreline \mathcal{C} which has spawn, and the measure of the subset, denoted $|\mathcal{C}_Y|$, is the widely used egg distribution variable “kilometers of spawn.”

The line-source flux of larvae φ_Y from shore to water column is the initial boundary condition for the representation of larvae within the PWS circulation model. This boundary condition is non-zero only over the subset \mathcal{C}_Y of the shoreline and only during the time interval I_Y . This is commonly described using the notion of “support”: the flux has support in $\mathcal{C}_Y \times I_Y$. The information sought in this first model component is the magnitude of the flux and the nature and extent of its support.

The basic zero-order estimate for the flux φ_Y is obtained by making a one-step survival factor reduction of the flux that would occur if the total accumulation of eggs observed during the spawn deposition survey were to survive and successfully hatch into larvae. The use of a survival fraction is equivalent to assuming that the incubation period loss rate is linearly dependent upon egg density. The egg losses are accumulated until hatching begins but ignored during the short hatching period I_Y . (This is the approach used by Norcross; see page 14 of Ch. 10 in which the survival factor 0.067

¹ At the end of November 1999 ADF&G advises that only a sharply reduced spawn deposition survey is being considered for April 2000, one consisting of only the aerial component of the survey protocol.

is used for constructing the initial larval flux for the 1996 simulation.) The mortality losses for the pelagic larvae are dealt with in the circulation model simulation. Let $\varphi_{\text{sp},Y}$ denote the flux estimated directly from egg density reports from the ADF&G spawn deposition survey. This estimate is based upon the maximum observed accumulated egg density at a site. The actual flux of larvae from shore to water column occurring during hatching is then estimated to be $\varphi_Y = \varphi_{\text{sp},Y} s_{e,Y}$, where $s_{e,Y}$ is a constant survival fraction. In particular, the total number of larvae entering the water column $N_{\ell,Y}$ is simply the cumulative total obtained by integrating the flux over all time and over all coastline

$$N_{\ell,Y} = \int_{\mathcal{C}_Y \times I_Y} \varphi_{\text{sp},Y} s_{e,Y} dx dt \quad (1.1)$$

Two of the required items, $\varphi_{\text{sp},Y}(x, t)$ and \mathcal{C}_Y , come directly from the spawn deposition survey. The shoreline survival $s_{e,Y}$ must be obtained separately. However, because it is represented as a constant and because there are no nonlinear density dependencies throughout the remaining collection of models, the survival factor can be applied at any time later in the model sequence, including at the end. The time interval I_Y can be either estimated from historical data (see Ch. 10), estimated from supplementary observations following the spawn deposition survey, or dealt with later through sensitivity tests of the advection outcomes using a range of time durations and a range of time translations for the period of hatching.

The foregoing boundary conditions have thus far been described assuming complete spatial and temporal knowledge of the egg density and the rates of hatching. The notation is likely to be more useful and more transparent if it is restated in the form of discrete approximations. Indeed, in this form the notation will conform better to the format of the data provided by the spawn deposition survey.

There are good reasons to use discrete approximations. First, there is little reason to use other than a uniform rate of hatching during the time period I_Y . Norcross, Wang, and Jin used the period May 1 through May 15 as the time interval for hatching and computed the larval flux by assuming constant and uniform flux within a discrete finite set of spawning sites. Although at best there may be some in-season information regarding expansion, contraction, or translation of I_Y from a historical mean, there is likely little information for other than a uniform rate approximation for hatching. Second, there is limited basis and no real motivation to use other than a finite set of spawning sites with at most a few discrete values for egg density within each site.

Let $\mathcal{C}_{Y,i}$, $i = 1, \dots, n$ be a partitioning of the domain \mathcal{C}_Y into a discrete set of n non-overlapping shoreline subdomains; within each such subdomain the flux of larvae $\varphi_{\text{sp},Y}(x, t)$ is approximated by a constant $\varphi_{\text{sp},Y,i}$. Let $N_{\ell,Y,i}$ denote the cumulative flux of larvae into the water column from site i . Specifically,

$$\mathcal{C}_Y = \bigcup_{i=1}^n \mathcal{C}_{Y,i} \quad (1.2)$$

$$\varphi_{\text{sp},Y}(x, t) = \begin{cases} \varphi_{\text{sp},Y,i} & \text{for } x \text{ in } \mathcal{C}_{Y,i} \text{ and } t \text{ in } I_Y \\ 0 & \text{otherwise} \end{cases} \quad (1.3)$$

$$N_{\ell,Y,i} = \varphi_{\text{sp},Y,i} s_{e,Y} |\mathcal{C}_{Y,i}| |I_Y| \quad (1.4)$$

$$N_{\ell,Y} = \sum_{i=1}^n N_{\ell,Y,i} \quad (1.5)$$

where $|I_Y|$ is the duration of the hatching interval I_Y and $|\mathcal{C}_{Y,i}|$ is the length of the shoreline subset $\mathcal{C}_{Y,i}$.

The spawn deposition variable “accumulated number of eggs per site” $N_{\text{egg},Y,i}$ is, with the foregoing assumptions regarding $s_{e,Y}$, related to $N_{\ell,Y,i}$ by $N_{\text{egg},Y,i} = N_{\ell,Y,i}/s_{e,Y}$. With spawn deposition survey reports for $N_{\text{egg},Y,i}$ and $\mathcal{C}_{Y,i}$, $i = 1, \dots, n$, and with estimates for $s_{e,Y}$ and for I_Y , the desired initial boundary conditions for larval advection are

$$\mathcal{C}_Y = \bigcup_{i=1}^n \mathcal{C}_{Y,i} \tag{1.6}$$

$$\varphi_{\text{sp},Y,i} = N_{\text{egg},Y,i}/(|\mathcal{C}_{Y,i}| |I_Y|) \tag{1.7}$$

$$\varphi_Y(x, t) = \begin{cases} \varphi_{\text{sp},Y,i} s_{e,Y} & \text{for } x \text{ in } \mathcal{C}_{Y,i} \text{ and } t \text{ in } I_Y \\ 0 & \text{otherwise} \end{cases} \tag{1.8}$$

Eqs 1.6, 1.7 and 1.8 are the equations for the outputs from this first module in the sequence.

In the following tables we express the simulation input used by Norcross, Wang and Jin for 1996 (Ch. 10, *SEA Final Report*) in terms of the objects defined in this section.

hatching time period and egg survival

hatching time period	hatching duration	shoreline egg survival
I_Y	$ I_Y $ (da)	$s_{e,Y}$
May 01 – May 15	15	0.067

spawning site specifications

index	site domain	site measure	max egg count	flux (uncorrected)	larvae hatched
i	$\mathcal{C}_{Y,i}$	$ \mathcal{C}_{Y,i} $ (km)	$N_{\text{egg},Y,i}$ (10^9)	$\varphi_{\text{sp},Y,i}$ ($10^9/\text{km}/\text{da}$)	$N_{\ell,Y,i}$ (10^9)
1	Montague	24.0	1460	4.06	97.9
2	Northeast	15.6	950	4.06	63.7
3	East	3.6	219	4.06	14.7
4	North Shore	1.2	73	4.06	4.9

For their simulation for 1996 Norcross, Wang and Jin used the ADF&G total egg count of 2677×10^9 allocated to each site in proportion to the site length. Hence, with a common value $|I_Y| = 15$ for all sites the line flux $\varphi_{\text{sp},Y,i}$ is the same for each site. The heading “uncorrected” notes that the shoreline egg survival factor of 0.067 has not yet been applied.

2.2 Advective transport and fate of herring larvae

The *larval drift* model uses the PWS circulation model, if available, to track the advective transport of herring larvae from the time of hatching in May, with conditions as specified in §2.1, through a time in late July at which one of three fates is registered to have occurred: mortality, exit, or retention in a bay or fjord. For a notation, each of these three fates is associated with a value for the index $k = -1, 0, 1, \dots, m$. Let $N_{M,Y,k}$ denote the number of age-0 juveniles in year Y with fate k and let the index value k be assigned as follows:

$k = -1$	mortality during advection;
$k = 0$	exit from PWS;
$k = 1, \dots, m$	arrival and retention at one of m bays or fjords within PWS.

We next combine this fate index k with the notation from §2.1 to have a notation sufficient for presenting the end-user equations associated with the larval drift component of the juvenile herring models. First, using what we have so far, we can state the basic conservation relationship that must hold between the input obtained from the spawn deposition module and the output fates from the larval drift model,

$$N_{\ell,Y} = \sum_{k=-1}^m N_{M,Y,k} \quad (2.1)$$

Since the submodel for larval drift within the circulation model provides for the tagging of each larva (more precisely, each advective group) with its hatch site, each fate-class subpopulation has associated with it information regarding the contribution of each of the spawning sites $\mathcal{C}_{Y,i}$ to that subpopulation. Specifically, a basic data format for the output of the drift model is

$$N_{M,Y,k}^i \quad \text{for } i = 1, \dots, n \text{ and } k = -1, 0, 1, \dots, m$$

where $N_{M,Y,k}^i$ denotes the number of age-0 with fate k and hatched at spawn site $\mathcal{C}_{Y,i}$.

There are the two obvious conservation relationships,

$$N_{M,Y,k} = \sum_{i=1}^n N_{M,Y,k}^i \quad (2.2)$$

$$N_{\ell,Y,i} = \sum_{k=-1}^m N_{M,Y,k}^i \quad (2.3)$$

It is helpful to view the model output $N_{M,Y,k}^i$ as a $(m+2) \times n$ matrix M . Specifically, let the matrix M be defined by

$$M_{ki} = N_{M,Y,k}^i \quad k = -1, 0, 1, \dots, m, \quad i = 1, \dots, n$$

That is, the i^{th} column of M is the decomposition of the subpopulation from spawning site $\mathcal{C}_{Y,i}$ into the $m+2$ sub-subpopulations for each of the possible fates, and the k^{th} row is the decomposition

of the age-0 subpopulation with fate k into its spawning site source sub-subpopulations. Explicitly, the drift model output in the format of the post-metamorphosis population structure matrix M is

$$M = \begin{pmatrix} N_{M,Y,-1}^1 & N_{M,Y,-1}^2 & \cdots & N_{M,Y,-1}^n \\ N_{M,Y,0}^1 & N_{M,Y,0}^2 & \cdots & N_{M,Y,0}^n \\ N_{M,Y,1}^1 & N_{M,Y,1}^2 & \cdots & N_{M,Y,1}^n \\ \vdots & \vdots & \ddots & \vdots \\ N_{M,Y,m}^1 & N_{M,Y,m}^2 & \cdots & N_{M,Y,m}^n \end{pmatrix} \quad (2.4)$$

The array in Eq 2.4 provides a complete view of the information provided by the output of the larval drift model. All of the information will not be of equal accuracy because of differences in the extent, development status, and verification of the various submodules, but the parts that were developed to address the questions posed in the 1993 *SEA Plan* are mature. We shall return to this topic shortly, but first we will complete the presentation of the notation, the properties and the equations needed to apply the output from the model.

The following are some of the basic properties of the population structure used in the larval drift model and displayed in the matrix array of Eq 2.4.

- (i) *The top row lists the mortalities for each spawn site $C_{Y,i}$, $i = 1, \dots, n$. These values are cumulative for mortalities occurring to larvae within PWS; larvae exiting PWS enter permanently the disjoint "exited" subpopulation and thereafter never contribute to this cumulative mortality subpopulation.*
- (ii) *The second row lists the number from each spawn site $C_{Y,i}$, $i = 1, \dots, n$ having exited PWS. Larvae exiting are drawn from the surviving, within-PWS subpopulation; once exited there is no return.*
- (iii) *Row $j + 2$ is a list for bay j , $j = 1, \dots, m$, of the number originating from spawn site $C_{Y,i}$, $i = 1, \dots, n$ and both surviving and achieving terminal fate within PWS at bay j .*
- (iv) *Taking the sum across all columns yields, in row order,*
 - the total number of mortalities (while in PWS), $N_{M,Y,-1}$*
 - the total number having exited PWS, $N_{M,Y,0}$*
 - the total number surviving and reaching bay j , $N_{M,Y,j}$, $j = 1, \dots, m$*
- (v) *Taking the sum across rows for column i yields the total number of larvae $N_{\ell,Y,i}$ hatched from spawning site $C_{Y,i}$, $i = 1, \dots, n$*

Dividing the entries in a given column by the column sum separates the role of advective drift from that of the initial egg density. Define an advective fate transition matrix A by

$$A_k^i = N_{M,Y,k}^i / N_{\ell,Y,i} \quad (2.5)$$

Let the n subpopulations representing the hatched larvae for each spawning site be the components of the column vector $\mathbf{N}_{\ell,Y}$ and let the $m + 2$ fate-class subpopulations be the components of a second column vector $\mathbf{N}_{M,Y}$,

$$\begin{aligned} \mathbf{N}_{\ell,Y} &= (N_{\ell,Y,1}, \dots, N_{\ell,Y,n})^t \\ \mathbf{N}_{M,Y} &= (N_{M,Y,-1}, N_{M,Y,0}, N_{M,Y,1}, \dots, N_{M,Y,m})^t \end{aligned}$$

Then the “fate-class” vector is related to the “hatch-site” by matrix multiplication by A ,

$$\begin{aligned} \mathbf{N}_{M,Y} &= \mathbf{A} \mathbf{N}_{\ell,Y} \\ \text{or, equivalently,} & \\ N_{M,Y,k} &= \sum_{i=1}^n A_k^i N_{\ell,Y,i} \end{aligned} \tag{2.6}$$

The matrix A is similar to a transition matrix from Markov processes in that all entries are less than one and each column sums to unity. It is useful to see explicitly the column vectors and the fate transition matrix,

$$\begin{pmatrix} N_{M,Y,-1} \\ N_{M,Y,0} \\ N_{M,Y,1} \\ \vdots \\ N_{M,Y,m} \end{pmatrix} = \begin{pmatrix} A_{-1}^1 & A_{-1}^2 & \dots & A_{-1}^n \\ A_0^1 & A_0^2 & \dots & A_0^n \\ A_1^1 & A_1^2 & \dots & A_1^n \\ \vdots & \vdots & \ddots & \vdots \\ A_m^1 & A_m^2 & \dots & A_m^n \end{pmatrix} \begin{pmatrix} N_{\ell,Y,1} \\ N_{\ell,Y,2} \\ \vdots \\ N_{\ell,Y,n} \end{pmatrix} \tag{2.7}$$

The focus in the 1993 *SEA* Plan was on first the possibility and second the frequency of PWS circulation scenarios wherein differences between numbers of larvae exiting PWS and numbers retained were sufficient to make a noticeable difference in the consequent age-0 population. The Plan acknowledged that the period of larval drift was one of rapid population dynamics with major changes in mortality rates due to predation and to the sensitivity of survival to the timing of suitable phytoplankton forage in relation to yolk sac exhaustion. The *SEA* Plan looked to the larval drift model as the means to establish tracking and testing of the impacts of the relationship between flushing versus retention on juvenile population formation. It did not propose any attempt to account for absolute population sizes during the first summer of life.

By the close of the *SEA* program in March 1999 the circulation model development had progressed to the point that the the model output specified in either Eq 2.4 or Eq 2.7 could be generated for calendar year 1996. The results of the advective drift simulation for 1996 conducted by Norcross, Wang, and Jin are described in Ch. 10 and the status of the model development is presented in the “Circulation Model” section of this document. However, the circulation model development had not progressed to this point early enough in the program so that questions regarding flushing versus retention could be evaluated through the simulation of various circulation scenarios. In this presentation we will use the results from the 1996 simulation to show the maturity of the advective transport model.

The presentation is in two parts. The first part covers the use of the circulation model and the larval drift module to assess the original *SEA* Plan question regarding retained versus exited larvae. The second part describes the use for problems that were not fully anticipated in 1993.

2.2.1 The significance of retained versus exited larvae for the age-0 population.

The original *SEA* Plan question of retained versus exited larvae was not concerned with the specific fate of the advective transport only whether the advective path remained within PWS or exited.

Therefore, the arrays in Eqs 2.4 and 2.7 have more detail than is needed and in fact that detail will confuse rather than clarify the significance of the model output. The post-metamorphosis matrix in Eq 2.4 is condensed by replacing all bays with their sum but expanded by adding the column totals and row totals to the top and left of the array, respectively.

$$\begin{array}{l}
 N_{M,Y,-1} \\
 N_{M,Y,0} \\
 \sum_{k=1}^m N_{M,Y,k}
 \end{array}
 \begin{pmatrix}
 N_{\ell,Y,1} & N_{\ell,Y,2} & \dots & N_{\ell,Y,n} \\
 N_{M,Y,-1}^1 & N_{M,Y,-1}^2 & \dots & N_{M,Y,-1}^n \\
 N_{M,Y,0}^1 & N_{M,Y,0}^2 & \dots & N_{M,Y,0}^n \\
 \sum_{k=1}^m N_{M,Y,k}^1 & \sum_{k=1}^m N_{M,Y,k}^2 & \dots & \sum_{k=1}^m N_{M,Y,k}^n
 \end{pmatrix}
 \quad (2.8)$$

Next we proceed to fill in the array in Eq 2.8 with values from the 1996 larval drift simulation. The totals at the top are the “larvae hatched” shown in the table in §2.1. The first row of the matrix is the cumulative mortalities for larvae in PWS by spawn site. The second row in the matrix is taken from Figure 10 of Ch. 10 of the *SEA* Final Report. The third row of the matrix is taken from the text with corrections described later. The mortalities are computed using the conservation identity Eq 2.3.

larval drift simulation model output at Aug 01 1996

from initial conditions in §2.1 and mortality rate 0.050/da

displayed in post-metamorphosis population structure matrix format

$$\begin{array}{r}
 181. \quad 97.9 \quad 63.7 \quad 14.5 \quad 4.85 \\
 177. \left(\begin{array}{cccc} 95.0 & 62.8 & 14.3 & 4.71 \end{array} \right) \\
 1.78 \left(\begin{array}{cccc} 1.6 & 0.10 & 0.0002 & 0.08 \end{array} \right) \\
 2.41 \left(\begin{array}{cccc} 1.3 & 0.90 & 0.21 & 0.06 \end{array} \right)
 \end{array}
 \quad (2.9)$$

displayed as a spawn-site to fate transition matrix multiplication

$$\begin{pmatrix} 177. \\ 1.78 \\ 2.41 \end{pmatrix} = \begin{pmatrix} 0.971 & 0.986 & 0.986 & 0.971 \\ 0.0163 & 0.00157 & 0.000014 & 0.0165 \\ 0.0133 & 0.0141 & 0.0142 & 0.0133 \end{pmatrix} \begin{pmatrix} 97.9 \\ 63.7 \\ 14.5 \\ 4.85 \end{pmatrix}
 \quad (2.10)$$

We next present the application equations required to use the model output shown in Eqs 2.9 and 2.10. In particular, the significance of the values for the the cumulative mortalities, the cumulative losses due to exits, and the cumulative retained subpopulation is not self-evident. As is often the case with numerical simulation models, qualitative analysis is required to make use of the simulation capability. For example, the fact that the exited subpopulation and the retained subpopulation is similar in size is misleading and in fact is irrelevant to the *SEA* Plan question regarding significance of retention and exit for age-0 population formation. In fact, the correct interpretation for the 1996 simulation is the following.

Larval drift 1996 simulation, Result 1. *For the case of constant pelagic mortality rate μ_Y , with $\mu_Y = 0.050 \text{ da}^{-1}$, the result of the larval drift numerical simulation for calendar year 1996 is that the effect of larvae exiting PWS by advective transport is inconsequential to the formation of the age-0 population in 1996.*

The qualitative analysis whereby Result 1 is established follows, with examples using the output of the 1996 simulation.

First, we observe that the size of the “retained” sub-population is rapidly changing and the value at any one time alone is not indicative of the contribution of advective exits of larvae to the formation of the subsequent age-0 population. This simply reflects the magnitude of the mortality rate during larval drift. For the 1996 simulation it was assumed that the mortality for pelagic larvae was linear with density of larvae, that the rate was constant throughout the simulation, and that the value was $\mu_Y = 0.050 \text{ da}^{-1}$. Since $\ln(2)/0.05 = 14$, or

$$e^{-\mu_Y \cdot 14} = 0.5 \quad (2.11)$$

the surviving and retained subpopulation is decreasing by half every fourteen days. As will be seen, the rate of exit, or flushing, of larvae in the 1996 simulation was very small relative to the mortality rate. Hence, the 14 da halving of the retained population should be a dominant feature of the simulation output, with the time t dependence $\exp(-0.05 \cdot t)$ only slightly underestimating the change in the population size. This is indeed the case as can be seen from the tabulation of the model simulation results noted in the text of Ch. 10, pg 15, of the *SEA* Final Report.

date	retained and surviving in PWS
16 Jun	0.15
01 Jul	0.07
01 Aug	0.013

We need a definition for that which we seek. Let $N_{M,Y,\text{ret}}^i$ denote the subpopulation from spawn site i that is still retained within PWS,

$$N_{M,Y,\text{ret}}^i = \sum_{k=1}^m N_{M,Y,k}^i \quad (2.12)$$

Let $\widehat{N}_{M,Y,\text{ret}}^i$ be similarly defined for a special scenario with the same initial conditions and the same mortality rate but with no advective exits from PWS. We refer to “the retained subpopulation” in this special case even though retention is total and the surviving population is the result of the action of the mortality process alone. For spawn site i we seek the ratio Θ_i of the size of the retained subpopulation established with advective exits to the size of the retained subpopulation established with no advective exits, both at time t ,

$$\Theta_i = N_{M,Y,\text{ret}}^i / \widehat{N}_{M,Y,\text{ret}}^i \quad (2.13)$$

With the present minimal mortality model it is not necessary to try to construct a circulation model simulation in which there are no advective exits. The solution for the retained and surviving subpopulation can be expressed in closed form; it is the solution to the following elementary differential equation.

$$\frac{d\widehat{N}_{M,Y,\text{ret}}^i}{dt} = \varphi_{Y,i} |\mathcal{C}_{Y,i}| x_{I_Y}(t) - \mu_Y \widehat{N}_{M,Y,\text{ret}}^i, \quad \widehat{N}_{M,Y,\text{ret}}^i(0) = 0, \quad i = 1, \dots, n$$

$$x_{I_Y}(t) = \begin{cases} 1 & \text{for } t \text{ in } I_Y \\ 0 & \text{otherwise} \end{cases} \tag{2.14}$$

where $\varphi_{Y,i}$ and μ_Y and $|\mathcal{C}_{Y,i}|$ are constants.

The solution is

$$\widehat{N}_{M,Y,\text{ret}}^i(t) = \varphi_{Y,i} |\mathcal{C}_{Y,i}| |I_Y| \frac{1 - e^{-\mu_Y |I_Y|}}{\mu_Y |I_Y|} e^{-\mu_Y(t-|I_Y|)} \quad \text{for } t > |I_Y| \tag{2.15}$$

where $t = 0$ corresponds to the time at which hatching begins and $|I_Y|$ is the duration of the period of hatching. From §2.1 $N_{\ell,Y,i} = \varphi_{Y,i} |\mathcal{C}_{Y,i}| |I_Y|$, hence the solution can be expressed in more familiar terms and we save this as Property 1 of the analysis.

Larval drift model, Property 1. *For the case of constant pelagic mortality rate μ_Y and for the special circulation scenario of no advective exit of larve, the surviving (and retained) subpopulation from spawn site i at time t is*

$$\widehat{N}_{M,Y,\text{ret}}^i(t) = N_{\ell,Y,i} \frac{1 - e^{-\mu_Y |I_Y|}}{\mu_Y |I_Y|} e^{-\mu_Y(t-|I_Y|)} \quad \text{for } t > |I_Y| \tag{2.16}$$

where $|I_Y|$ is the duration of hatching, $N_{\ell,Y,i}$ is the total number of larvae hatched at site i , and $t = 0$ corresponds to the start of hatching. The solution is linear with respect to initial number of larvae but is otherwise independent of the spawn site.

Property 1 is the core utility for using the larval drift model to evaluate advective exits versus advective retention in population formation. The following table computes the ratio Θ_i using the simulation output results shown in the population structure matrix Eq 2.9 or the transition matrix Eq 2.10. Since $t = 93$ for Aug 01 1996

$$\widehat{N}_{M,Y,\text{ret}}^i(t) = N_{\ell,Y,i} \cdot 0.704 \cdot 0.0202 = N_{\ell,Y,i} \cdot 0.0142$$

1996 larval drift simulation: evaluation of advective exit of larvae on age-0

$\mu_Y = 0.050$ for simulation date Aug 01 1996

index	site domain	retain, w/ exits	retain, no exits	reduction from exits
i	$\mathcal{C}_{Y,i}$	$\frac{N_{M,Y,\text{ret}}^i}{N_{\ell,Y,i}}$	$\frac{\widehat{N}_{M,Y,\text{ret}}^i}{N_{\ell,Y,i}}$	Θ_i
1	Montague	0.0133	0.0142	0.94
2	Northeast	0.0141	0.0142	0.99
3	East	0.0142	0.0142	1.00
4	North Shore	0.0133	0.0142	0.94

There is clearly inconsequential loss incurred due to advective exits.

There are some open issues that can be considered in any new application implementation plan.

Larval drift model, Open Issue 1. *The conclusions in Result 1 and the reduction ratio Θ_i in the table above have an incompletely evaluated dependence upon the value assumed for the mortality rate μ_Y .*

This open issue is due to the manner in which the two processes—advective exit from PWS and individual mortality in PWS—each function to the exclusion of the other. An individual who is a mortality is no longer a candidate for advective exit and visa versa. This means that the process with the higher rate will accumulate a larger fraction of the individuals. As time progresses, the magnitude of the impact of the slower process becomes negligible for there are no longer individuals in sufficient number for the consequences to be apparent in the population. The open issues arise from consideration of the fact that there is a time delay associated with advective exit that is not the case for the mortality process. Similarly, late season advective transport out of PWS will not have the same consequences for the population as early season advective transport.

The application designer may wish to test a conclusion for a given year using a smaller mortality rate. From numerical considerations alone and not from any consideration of realism, a factor of five reduction of mortality rate would suffice to show whether the mortality rate is selectively filtering some of the consequences of advective transport. On the other hand, for scenarios with strong advective consequences, the application plan should consider a test using a larger mortality rate.

In the analysis we computed Θ_i for a single time. Since the variable Θ_i is the primary measure of the impact of advective exit upon population formation, it is advisable to track this quantity for all time during the simulation. It is likely that advective exit has rather strong peaks during the 90 da period of larval drift. These peaks will be apparent in the time series output for Θ_i . The time record for Θ_i is the quantity that measures the impact of advective exit on the age-0 population; if that impact is a priority for the application plan then tracking of Θ_i is an essential model output.

2.2.2 New applications for the larval drift model

During the six years since the construction of the *SEA* Plan the applicability of the larval drift model has expanded beyond the basic comparison of the retention versus exit of larvae. There are two major new applications and both are shown in Figure 2.

First, whereas the distribution of surviving larvae throughout the course of the advective transport was once viewed as a means to obtain the terminal distribution, it is now itself an equally important model output. This new value for the time evolution of the larval population during the May through July journey through PWS is due to the increased interest in the use of oil dispersants in PWS as an option for oil-spill response. The function of a dispersant is to remove the spill from the surface of the water and distribute it throughout the water column. The merit of this response technology for PWS has been under review for the past several years. The time evolution of the larval herring population as it travels through PWS is a key piece of information for designing an optimal application strategy with respect to dispersants.

The second application area that was unanticipated in the original *SEA* Plan is the use of the post-metamorphosis matrix to characterize the relative distribution of metamorphosed juveniles among the m bays and fjords of PWS. The original focus was solely on the collective “retained”

versus “exited” subpopulations without regard to the manner in which the “retained” individuals were distributed. The new interest in the terminal distribution arises from the basic question of whether in any given year the transport has led to equal distribution of juveniles among available terminal sites or whether it has led to high densities in a few sites with the remainder underutilized. This information is clearly contained in the post-metamorphosis matrix in Eq 2.4. However, the application design whereby “retention” at a bay or fjord is registered is not fully developed. At present we have the population shoreline distributions as shown in Figure 8 of Ch. 10. These provide a first means to assess the relative difference in the densities at the terminal sites. These already have the potential to contribute to a more well informed sampling plan for the fall pre-fasting juvenile survey.

2.3 Summer growth

In this summary we skip over the period from July through October for the juvenile populations, in particular for the age-0 population. The study of growth and habitats during this period was the focus of the Juvenile Herring Growth and Habitat project [NBFSS] and the interested reader is referred to Chapter 10 of the *SEA* Final Report. The summer months are a time of rapid changes in both the size and the physiology of the juvenile subpopulations due to both growth and predation. Because the quantitative representation of these processes presented major technical challenges and because these processes acted upon age-0 at a time period further removed than the subsequent winter survival from the first available corroborating, fishery-dependent information for the age-3 year class, the summer months were not a topic of study in the original 1993 *SEA* Plan. This topic was added in 1995 after the project was underway. It was understood at that time that the effort would provide information needed for a future quantitative representation but that such a representation was well beyond the scope of the *SEA* Program. The information resources established regarding summer growth processes are documented in Ch. 10.

It was understood in 1993 that there would not be a tight connection between the model output for larval advective transport and the findings from a fall measurement of the juvenile population density and structure. In the original *SEA* Plan the fall sampling and survey is for all practical purposes viewed as the source of the "initial conditions" for the overwinter fasting model. This remains the case. However, the original *SEA* Plan did not anticipate the magnitude of the differences in population structure between bays for a given fall. The original concept was one of greater uniformity and a sound-wide impact of winter fasting across the juvenile population as a whole. It is the present need to revise this first conceptualization that has increased the attention given to the role of advective transport of larvae in establishing the juvenile population. The model for larval advective transport has a new relevance as a source of information for use in the design of minimum cost fall sampling plans. The summer growth and habitat study has confirmed the conjecture of the original *SEA* Plan regarding the rapid time dynamics of the age-0 population structure during summer. The interested reader will see from the reports that the summer processes narrow but do not close the gap between those bays with very large age-0 populations in early summer and those with very small populations. Consequently, the larval advection nowcasts in July should indeed provide projections that are useful in the prioritization of bays for fall monitoring. With this we pass over the summer and enter the fall. The task for the fall is the resetting of the information regarding the age-0 population, information that ideally was last updated in July or August through nowcasts from the advective transport model and from any consequent observations for validation or data assimilation.

2.4 Fall monitoring of juvenile herring

This is an in-situ monitoring module wherein the juvenile subpopulations resident in the bays are surveyed and sampled. All aspects of the design, implementation, and execution of the monitoring program for juvenile herring was conducted by other projects. This section will cover issues and findings regarding fall monitoring that are tightly linked to any application of the ISMD models.

From the perspective of model applications the central objectives for monitoring are to obtain sufficiently accurate approximations for two basic objects—population density² and population physiology—for the age-0, -1, and -2 subpopulations occurring in each bay or fjord³ (i.e., site) in the monitoring plan.

2.4.1 The links between larval drift and winter fasting: Open Issues

The fall monitoring for population density is only recently being considered as an observational link between the larval drift model and the model for overwinter fasting. The larval drift model output regarding the population distribution of post-metamorphosis juveniles is now being examined for the guidance it can provide regarding the site selection for monitoring. Conversely, the results of the fall monitoring can serve either as validation tests for the larval drift model (albeit with considerable noise in the coupling) or as the source of data for assimilation in which the drift forecasts and the fall observations are combined. The degree to which the population distribution forecasts from the larval drift model will persist through late summer and into fall remains an Open Issue. The progress of the development of the circulation model only now is sufficient for simulation trials in which this question can be addressed. The 1993 *SEA* Plan was based on the assumption that the fall monitoring for population density would establish independently the initial conditions for the winter fasting model. The 1993 Plan did not formulate either the possibility or the utility of linking the distribution information from the larval drift model for July and August with the population density monitoring conducted in the ensuing fall.

In a similar way the monitoring for population physiology is only recently being considered in the context of the output of the larval drift model. It was typically viewed solely as the source of initial conditions for winter fasting or the source of final conditions for summer growth processes with little relation to the output of the drift model. There is observational evidence for the occurrence of large differences in the size of bay-specific post-metamorphosis subpopulations and large differences in the fall physiology of these subpopulations. The feasibility of such differences has led to revisions

² The term density is used herein to mean “Something that can be integrated over any subset of the domain in question (e.g., over a depth interval of a bay) to obtain the accumulated amount of the quantity of the density (e.g., individual age-0 herring) occurring in the subset; the something can vary with time.” Thus, the so-called “population abundance” is the integral of the population density over the entire domain. Confusion arises if it is unclear whether the density is considered to be known *globally* (i.e., everywhere in the domain) or only *locally* (i.e., for some relatively small subset of the domain). Herein we use density in the global sense and explicitly indicate if there is only local information. Consequently, a determination of population density implies the ability to compute “abundance.”

³ Since we will not need to identify the site topography, we will use only the term bay or site to indicate location.

of prior thinking regarding the acceptability of using a canonical representation for age-0 (or age-1) juveniles across all rearing sites.

Among the revisions is a re-examination of the information resources available for tracking bay-specific population density. In particular, the output of the larval drift model is seen to be an immediately available source of this information for age-0 population distribution for the period from May through August.

However, the progress to date is consistent with only the more limited goals of the 1993 *SEA* Plan. As a consequence, with this section the focus turns away from the larval drift model to the winter fasting model and the needs of that model for initial conditions. Although the presentation will have that focus, any new implementation plan should *not* restrict itself to the discussion that follows but rather should incorporate the extended utility of the larval drift model as a companion to this monitoring module and to the subsequent modules for the winter fasting model.

2.4.2 Post-monitoring analyses

The state of the technology for monitoring in the marine sciences still requires large scale transport of people and equipment to temporary and mobile remote facilities for extended periods of time. Little of the effort is automated and all information, even sensor derived data, requires significant post-monitoring direct manipulation. None of the techniques can be said to be “remote” and near realtime means within a few weeks.⁴ In particular, there are extensive post-monitoring protocols associated with both the population density and the population physiology. In the sequence for this Concise Reference we omit the so called “post-processing” tasks for the population density. These procedures are well known and well established and are described in Ch. 9 [TK99] and Ch. 10 [NBF⁺99] of the *SEA* Final Report. However, this effort resulted in new developments in the post-monitoring analyses for the population physiology. Consequently, in this sequence we have two modules—§2.5 Laboratory Analysis and §2.6 Fall juvenile physiology by bay—that are in fact two post-monitoring analyses required to establish the population physiology objectives of the fall monitoring.

For the remainder of this section we shall address in turn the various issues associated with fall monitoring, especially those that were programmatic parts of the original 1993 *SEA* Plan. We shall report how each issue was addressed during the *SEA* Program and which of these remains Open Issues to be resolved in a forthcoming implementation plan.

2.4.3 Site selection and Times: Issues related to fasting models

Some aspects of site selection for overwinter fasting have been indicated in prior sections, such as the new interest in the outcome of larval drift with respect to the uniformity of utilization of rearing sites. From the perspective of the fasting model this is the most important site and time issue. Two lesser issues are the following.

Preferred time is after fall feeding From the point of view of the overwinter fasting model, the time of fall sampling should be *after* fall feeding has concluded or, at the least, after it has decreased to a

⁴ This is a very optimistic schedule. The interested reader may wish to compare NWS information practices and the NASA programs for peer-review and publication of datasets.

level that is “representative” of the remainder of the winter. This assumes that either of these two specifications can be made precise. Assuming that is the case, then sampling can occur any time following the cessation of significant feeding. Specifically, the model is constructed to represent a winter period during which there is complete fasting. The fall monitoring results will (unless modified) be interpreted as representing a population that henceforth does not feed until March.

Consider using sites that are extremes and “worst cases” In its basic form the winter fasting model is useful to the extent two underlying assumptions hold.

- A1 the observed changes in the population structure during winter reflect mortality losses from fasting; conditions sufficient for this assumption to hold are the more restrictive and specific assumptions of
 - (a) site fidelity, and
 - (b) the structural changes during winter due to predation mortality are similar to those due to fasting mortality or, alternatively, are negligible in comparison to fasting mortality;
- A2 the fasting during winter can be assumed to be total, that is, any intake alters the physiology only negligibly.

Sites having previously shown evidence of poor conformance with either of these assumptions are useful for establishing worst case bounds for model performance.

2.4.4 Site selection and Times: Solutions and fixes

For this past effort the specification of the sites and times for the fall monitoring was the responsibility of the observational projects, especially the Juvenile Herring Growth and Habitat (JHGH) project and the Fish Energetics (FE) project. Investigations regarding the times and nature of fall feeding and winter fasting were conducted by the JHGH project, in particular by R. J. Foy. Consult the Juvenile Herring Growth and Habitat Final Report [NBF⁺99] for the design of the monitoring plan and its schedule and for the findings regarding fall and winter feeding and fasting.

The model development of this project was guided by the recommendations from A. J. Paul (FE project) and R. Foy (JHGH project) regarding the time period for fasting. The recommendation (personal communication) was to use a single fixed time period for age-0 winter fasting for all years and all bays: November 01 through mid-March.

It remains an open issue whether the fall monitoring used for initial conditions in this effort occurred before or after the onset of fasting. Moreover, a quantitative definition of winter feeding with which to adequately ask the question is not yet in place. Any new implementation plan will have the benefit of the work of Foy regarding fall and winter diets [NBF⁺99]. If we go by the above fixed date recommendation then nearly all fall sampling occurred before the end of fall feeding—as early as Oct 03. (See §2.3 of the “Validation Reference” document.)

There is a simple resolution, and it is due to the properties of the fasting model and of the model-determined survival forecasts. §2.7 of this document and §2.2 of the “Validation Reference” show the extent to which the fasting survival estimates are quite tolerant of considerable error in the specification of fasting interval translations, water temperature, and even fast interval duration. The tolerance decreases only in cases of very low survival, and these occur as a result of unfavorable initial physiological conditions. This property of the model, and presumably of the age-0 physiology,

allows any number of a posteriori adjustments to be made for early fall monitoring. The adjustment used here was selected for numerical simplicity.

The foregoing resolution is in part due to the modelling approach. One seeks to characterize accurately an *extreme* among all outcomes rather than the most likely outcome. This is a general design approach that is used throughout all of the *SEA* model development. In the case of a scalar such as survival it means modelling to represent either the upper or the lower bound. This has several advantages:

- by definition extremes have no (or sharply reduced) "variability";*
- testing and validation objectives are unambiguous;*
- solutions are available for coping with uncertain forcing and initial conditions.*

In the present situation the winter fasting model was developed to represent total fasting during a presumed fasting interval. The goal then is for the physiology in the model simulation to be more depleted than the observed physiology. With this approach uncertainty regarding initial conditions is handled by choosing accommodations that are either neutral or underestimate the benefit to the individual during the unknown course of events. For example, if fasting is assumed to begin on Oct 22 and the fall monitoring occurred on Oct 03, we assume that during the period from Oct 03 to Oct 22 the individual feeds in a manner that exactly sustains his physiological state of Oct 03 with no gain or loss. That is, the individual is advanced to Oct 22 with conditions unchanged from the date of the monitoring. A side benefit is that any translation of the fasting interval incurs no change in the initial conditions. This allows testing such translations without imposing a requirement to construct a scheme for revised initial conditions more complex than the most simple one of keeping them constant.

2.4.5 Monitoring age classes: Issues

The conjectures regarding the vulnerability of juveniles to winter fasting presented in the 1993 *SEA* Plan [PWS93] included both the age-0 and the age-1 juveniles. A determination was made during the course of the *SEA* effort that the age-1 subpopulation was not significantly vulnerable to winter fasting. This determination was made prior to the development of the first version of the fasting model and was not further considered during the period of model development. This leaves the following issues open relative to the objectives of the 1993 *SEA* Plan.

- (i) We are not able in this Concise Reference to contribute to the determination of vulnerability for age-1 juveniles. It is indeed feasible and even probable that winter fasting mortality during the second winter does not significantly contribute to the formation of the adult population. However, we cannot offer any quantitative evidence for or against based upon the present winter fasting model and simulations with age-1 initial fall conditions.
- (ii) We are unable to report on bay-specific physiological differences in fall for age-1 juveniles. It is unknown whether the between-bay fall physiological status for age-0 is similarly reflected in the status for age-1 or whether there is evidence for coupling between age-0 and age-1 with respect to fall physiological state.
- (iii) The present version of the winter fasting model is calibrated and validated for *only* age-0 juvenile herring. There is no basis whatsoever for the use of the model for age-1 and age-2 juveniles. The extension of the current model to these age classes can be done by applying

the methods described in the “Validation Reference” section of the model documentation.

Any implementation plan should incorporate resolution of these open issues. These issues should be addressed in the reverse order of the above listing:

- (i) Calibrate and validate the fasting model for age-1 and age-2.
- (ii) Extend bay-specific physiology monitoring and model output to age-1 and age-2.
- (iii) Confirm the preliminary assessment regarding vulnerability for age-1 and age-2 juveniles.

2.4.6 Monitoring population density: Issues

The determination of the total number of juveniles herring in the fall for each monitored site was left ambiguous in the original *SEA* Plan. This was because the Plan placed a high priority on avoiding intractably long time intervals and intractably large spatial domains. In the case at hand, the overwinter fasting process met these objectives—if certain assumptions regarding the ability to represent sound-wide effects for juvenile herring from site-specific information could be confirmed.

The first working assumption for the winter survival modelling is that for a given year fasting survival was a sound-wide feature. That is, the winter survival for the bulk of the juvenile population could be extrapolated from a knowledge of fasting survival for a subset of all bays in Prince William Sound. It was fully expected that population density was not a sound-wide feature. The working assumption was that the fall physiology would be sufficiently uniform to allow one to assess the impact to the juvenile population from a determination of winter survival using a subsample of all sites. The assumption of relatively uniform survival eliminated the need for a sound-wide (global) determination of population density.

The second working assumption was that there was a degree of permanence to the population structure within each of the various bays. This permanence assumption is required to be able to validate a winter survival model using fall and spring monitoring of the same bay. A sufficient condition for this permanence is the stronger assumption of negligible immigration and emigration between sites. That is, each site was in effect a closed juvenile rearing domain.

A third assumption was that the impact of predation upon the population structure from fall to spring would not alter the physiological structure in a manner that would make validation of the fasting model impossible.

In §2.6 we shall see examples wherein the first assumption does not hold. It is premature to totally discard the first working assumption for the significance of the exception has not been fully assessed. However, this assessment is now an Open Issue, one that must be incorporated in any forthcoming implementation plan.

The second and third assumptions, however, have held up rather well during the testing and validation of the winter fasting model. It was never the intent to prove or disprove these assumptions. Such a task requires an undertaking on the scale of that which the *SEA* Plan was seeking to avoid. Rather, the tests are used to determine whether the simulation results are consistent with the assumptions. The complete collection of all validation tests based on field datasets is presented in the “Validation Reference” in §2.1 and §2.2. Direct observations of physiological changes from fall to spring are consistent with the so-called “site fidelity” assumption. In only one case is there reason to look to first winter predation mortality at a level near to or greater than fasting mortality for consistency between simulated winter fasting survival and alternately determined winter survival.

The working assumptions had consequences for the design of the monitoring plan for population density. If indeed the survival for a subset of bays can be extended to the larger domain as a uniform feature, then there is no need to know the actual population density of a bay. What is needed is a measure for the population density of a bay that is consistent for that bay. Since the measure would be used at most to compare fall and winter population size for use with simulations of survival, the measure did not need to be absolute. There was no need to make population density comparisons between bays, only within a bay over single season time intervals.

To this end Stokesbury, Norcross Peters, Kirsch, and Thomas developed a “relative density” measure for monitored bays. The design of the monitoring approach and the post-monitoring procedures are described in Ch. 9 [TK99] and Ch. 10 [NBF⁺99] of the *SEA* Final Report. The “relative density” is a consistent measure for a bay but cannot be used to compare different bays. This measure has been used as one of the validation tests for the the winter fasting model.

The “relative density” has undergone a first extension. Norcross has sought to extend the Stokesbury estimate to an absolute “abundance” estimate. This is a first effort to move the present protocol to one suitable for system-wide calculations.

2.4.7 Monitoring population density: Open Issues

What was not known in 1993 was the extent to which initial physiology conditions for a given year would differ between bays. If the indications are confirmed regarding significant differences for survival between bays in a given year, then a population density measure which is applicable for all bays is needed to infer the impact of winter survival upon the development of the age-0 subpopulation.

It is still possible to realize the goal of the *SEA* Plan to eschew a sound-wide population density measurement for age-0. The larval drift model has the potential of providing the information whereby a small and cost-effective fall monitoring plan will still suffice for the determination of impact of fasting on population formation. The larval drift model output is looked to for the relative size of the populations of post-metamorphosis juveniles in all bays of PWS. This output will provide the means to stratify the fall monitoring. To confirm the basis of the stratification and to obtain the correct weighting to use in extending the survival values to the PWS population, the present version of the “relative density” measure for population density monitoring must be enhanced to a sound-wide measure or to an absolute measure of either bay population abundance or population density.

The incorporation of a plan for the resolution of these open issues is a priority for any new implementation plan, for the goal of the extension of the ADF&G ASA model to juvenile populations depends upon this resolution.

Hereafter, this Concise Reference focuses on the modelling of the fall to winter fasting. The extension of these results to the ASA format will require revised population density estimates.

2.5 Laboratory Analysis

The essential input for the winter fasting model is the fall initial physiological condition of an individual at the start of a presumed winter fast. The output of the model consists in part of the physiological condition of that individual at each time during the fast until its conclusion. That is, the model represents the time evolution of an individual during the course of total fasting, with the physiology of the individual at the start of the fast specified, the temperature during the fast specified, and with the activity level assumed to be sufficiently low to be neglected. The model is a non-autonomous (time is explicit due to the time varying temperature) system of ordinary differential equations of initial value type, with one equation for each constituent variable of the physiology. In this section we review the post-monitoring laboratory analyses whereby the values for each constituent variable of the physiology are determined for an individual.

In practice, the laboratory analysis is organized around a sample set of individual juvenile herring—a sample set that had been constructed to provide a good representation of the distribution of physiological states in a given subpopulation at the time the sample was collected. In the *SEA* Program the Juvenile Herring Growth and Habitat (JHGH) project [NBF⁺99] was responsible for the selection of the times, sites, and delivery of field samples for laboratory analysis. The Fish Energetics (FE) project [Pau99] was responsible for the laboratory analysis of juvenile herring for the purpose of determining their physiological state.⁵ But the sample set is a facet of the monitoring plan and not an aspect of the laboratory analyses. In this section the focus is on only the laboratory procedures, with each procedure presented in terms of the analysis of a single sample element, i.e., of a single individual juvenile herring.

2.5.1 The physiological space \mathcal{P}

As is well know, there is negligible carbohydrate in the tissue of fish [SN90]. Consequently, the basic physiological state—the so-called “proximate analysis” [VPPLR97]—of an individual is specified by the values for four variables: mass of protein m_P , mass of lipid m_L , mass of ash m_A , and mass of water m_W . These values are the so-called “whole body mass” for each of the four non-negligible categories of body matter. (When reference is made to an actual number for one of these masses, the unit for that number is gram.)

This familiar “proximate analysis” for an individual specifies a point (m_P, m_L, m_A, m_W) in a 4-dimensional space, the space of four positive real numbers, commonly denoted by \mathbb{R}_+^4 . It will be helpful to select a specific name and a symbol for this space. We refer to \mathbb{R}_+^4 with coordinate variables (m_P, m_L, m_A, m_W) as *the physiological space* and denote this space by \mathcal{P} .

Let us denote an individual juvenile herring by the symbol ω . We can now think of the proximate analysis as a mapping of the individual herring to a point in \mathcal{P} and denote that mapping by $h_{\mathcal{P}}$. With this we can write

$$(m_P, m_L, m_A, m_W) = h_{\mathcal{P}}(\omega) \tag{5.1}$$

⁵ All observation information for the juvenile herring program is managed and maintained by each of the participating observation projects in its own separate, internal data system. The interested reader can contact the project investigator for information on the full scope of the sampling and analyses conducted by that project during the *SEA* Program. For a point of contact see the project Final Report.

The purpose of this module in the sequence is the execution of the laboratory procedures whereby one does this mapping. In particular, the designer of an implementation plan must select from among several possible laboratory analysis procedures and then specify what is required from the laboratory analysis. Each of the various procedures can, if properly specified, provide the data needed to realize the mapping $h_{\mathcal{P}}$. We begin with guidelines that apply regardless of the choice of analysis method.

Guideline 1. *We want to be able to compute using the results from the lab analysis all four coordinate variables of \mathcal{P} .*

Explanation. Although we noted that the physiological state is a point in the 4-dimensional space \mathbb{R}_+^4 , there are circumstances when one can get by with fewer than all four coordinate variables. The point here is that in the case of fasting we need to know the full specification of the physiology to determine the consequent fate of the individual.

The purpose of the guideline is to emphasize the distinction between fasting and the simpler scenario of near-normal growth in near-normal environments. In the latter case the well known “Wisconsin” bioenergetics model for growth of fish requires that one know only one variable, the wet mass $m_{\text{WWT}} = m_{\text{P}} + m_{\text{L}} + m_{\text{A}} + m_{\text{W}}$. This one variable is the model input and the model output. In this case the laboratory analysis is quite simple—requires only one measurement for it so happens that the one variable in the model is also a variable that is an output of a single laboratory measurement. This approach suffices for near-normal circumstances for two reasons: (i) during normal growth each of the four coordinates of \mathcal{P} are adequately well approximated by a constant multiple of m_{WWT} —that is, we *can* approximately recover \mathcal{P} from the one variable; and (ii) the extent to which the actual values for the coordinates deviate from this approximation is of no consequence.

This does not work at all with fasting. One coordinate is constant, two decrease but at different rates that likely depend on the present physiological state, while the fourth (according to one conjecture) goes up to compensate for the decrease in the others. Clearly, no fixed constant ratio relative to wet mass will suffice. Even more important is that the degree that one or another of the coordinates differs from the “norm” is of major consequence: it determines whether the individual lives or dies.

Although we well may discover as a result of a successful and mature model that the time evolution of the fasting physiology occurs in a hyperspace of \mathcal{P} , now is not the time to be guessing what that hyperspace may be and begin looking for quick fixes intended to reduce the dimensionality of the question.

There is a practical aspect to Guideline 1: it imposes no cost whatsoever. It is free. This is the bottom-line message of Guideline 2—we need only do what is done conventionally already in conjunction with a few basics.

Guideline 2. *To determine experimentally the four variables m_{P} , m_{L} , m_{A} , m_{W} the laboratory analysis must determine the values for four functionally independent variables (each of which is a function of m_{P} , m_{L} , m_{A} , m_{W}).*

Explanation. This guideline is a restatement of lessons from high school algebra: If one has four unknowns then one needs four equations to be able to find a solution. In this context, the four quantities being measured represent the values for four equations in which the four vari-

ables m_P , m_L , m_A , m_W are the unknowns. Guideline 1 explained that we do wish to determine m_P , m_L , m_A , m_W empirically; this Guideline states the consequence for the laboratory analysis.⁶

There are three measurements that are common to any laboratory analysis, dry mass m_{DWT} , wet mass m_{WWT} , and the mass of ash m_A . This specifies three of the four equations,

$$m_{DWT} = m_P + m_L + m_A \quad (5.2)$$

$$m_{WWT} = m_P + m_L + m_A + m_W \quad (5.3)$$

$$m_A = m_A \quad (5.4)$$

The fourth measurement distinguishes between the various laboratory analysis options.

Bomb calorimetry: whole body energy E in kiloJoules

$$E = \hat{E}_L m_L + \hat{E}_P m_P, \quad \hat{E}_P \text{ and } \hat{E}_L \text{ constants;} \quad (5.5)$$

Nitrogen analysis: whole body mass of nitrogen m_N in grams

$$m_N = m_P k_N, \quad k_N \text{ constant;} \quad (5.6)$$

Solvent analysis: whole body protein plus ash

$$m_{\text{solv}} = m_P + m_A \quad (5.7)$$

The reader has likely recognized that for each of the three options all of the equations are linear in m_P , m_L , m_A , m_W . Recall that if the four equations are linearly independent then there is a unique solution for m_P , m_L , m_A , m_W that is itself linear in terms of the four measured variables.⁷ The solutions for each of the three analyses are for reference presented in §2.6. Here we add some brief comments on each of the three methods.

2.5.2 The options for the laboratory analysis

Bomb calorimetry measures the whole body energy content in the sense of the energy produced by the heat of combustion of the body tissues. In this effort we use the approximation that the energy bearing constituents of the physiology are lipid and protein. In the case of protein, this heat of combustion energy differs from that available to organisms as a consequence of metabolism of the consumed tissue. According to Schmidt-Nielsen [SN90] the energy available from consumed protein is 4.3 kcal/g whereas bomb calorimetry produces 5.3 kcal/g. This difference is due to the difference

⁶ This guideline is often overlooked. The consequences are that analyses can be "ill-posed" or under-determined and the results found to vary in an apparently random manner. Such results can be incorrectly attributed to system "variability."

⁷ To date we have found no evidence that this basic relationship between the physiological variables m_P , m_L , m_A , m_W and either of the three sets of four empirically measured variables has been noted, although it obviously is routinely used. The use of ratios rather than the variables used here changes these linear relationships into nonlinear ones. The routine preference for ratios may tend to make these simple linear systems less apparent.

in the end product: urea for metabolism and nitrogen for bomb calorimetry. For the purpose here only the heat of combustion need be considered.

A linear relation between whole body energy and the masses of lipid and protein is the result of the conventional linear assumption regarding the relationship between the species-specific mix of proteins and lipids and the total energy content of that mix. The energy content of all protein in an individual is assumed adequately approximated by a constant multiple \widehat{E}_P of the mass of all protein. Similarly, the energy content from all lipid in an individual is represented as a constant multiple \widehat{E}_L of the total lipid mass. It is well known that each type of lipid and each type of protein differs in energy content. It is an empirical approximation that the mix of the various types within the two categories lipid and protein is, for each species, such that the total energy from all protein or all lipid is related to the total mass of each by the two constant factors \widehat{E}_P and \widehat{E}_L . These constants are applicable to the energy determined by a bomb calorimetry analysis of a “whole body” tissue subsample. Specifically, the “whole body energy” of an individual as determined by bomb calorimetry is the sum of the energies from the two energy bearing constituents. In terms of the coordinates (m_P, m_L, m_A, m_W) the whole body energy E is determined by

$$E = \widehat{E}_L m_L + \widehat{E}_P m_P \quad (\text{bcal})$$

Heats of combustion for protein \widehat{E}_P and for lipid \widehat{E}_L are reported by Schmidt-Nielsen [SN90] to be

$$\widehat{E}_P = 5.3 \text{ kcal g}^{-1} = 22.2 \text{ kJ g}^{-1} \quad (1a)$$

$$\widehat{E}_L = 9.4 \text{ kcal g}^{-1} = 39.3 \text{ kJ g}^{-1} \quad (1b)$$

and by Morowitz (pg 202) [Mor78] to be

$$\widehat{E}_P = 23.64 \text{ kJ g}^{-1}$$

$$\widehat{E}_L = 39.75 \text{ kJ g}^{-1}$$

The latter pair is from a table in which Morowitz presents the values as being representative for “Meat, fish.” It is useful to keep in mind that this pair is among the largest in the table in general, and in particular the values are higher than the means across all trophic levels—means taken across levels from plants through beef and birds. The values from Schmidt-Nielsen have been used in this effort as the starting point.

The document on model set-up and calibration describes the basis for using a lower energy density for protein. In particular, the most recent trials with the Phow model are based on

$$\widehat{E}_P = 18.8 \text{ kJ g}^{-1}$$

$$\widehat{E}_L = 39.3 \text{ kJ g}^{-1}$$

In nitrogen analysis the whole body mass of nitrogen m_N is measured. This mass is then related to protein mass by assuming a constant value k_N for the ratio m_N/m_P . It is customary to assume the value of 0.16 for this ratio. This special value for k_N is denoted here by \tilde{k}_N . However, the ratio is not well represented as a constant, for its value ranges from less than 0.12 to greater than 0.20., that is, k_N is typically in the interval $k_N \pm 0.25 \cdot \tilde{k}_N$.

Once a choice (or calibration) of k_N has been fixed, then the observation variable m_N is related to the (m_P, m_L, m_A, m_W) coordinates by

$$m_N = m_P k_N \quad (\text{N2})$$

The solvent analysis method uses the solubility of lipid and the low solubility of protein and ash to extract lipid and leave in place the protein and ash. The ash is then measured in the same manner as is used if lipid were present. We assume here that the ash determinations here are equivalent to the two preceding methods. The linear equation associated with the solvent method is simply the mass remaining after the solvent treatment m_{solV} in terms of the coordinates (m_P, m_L, m_A, m_W) :

$$m_{\text{solV}} = m_P + m_A \quad (\text{solV})$$

2.6 Inverse transformations: lab measurements to physiology

The forward and inverse transformations for the analyses of §2.5 follow with current parameters.

bomb calorimetry: $(m_P, m_L, m_A, m_W) \longrightarrow (E, m_{\text{DWT}}, m_{\text{WWT}}, m_A)$ $\hat{E}_P = 18.8$, $\hat{E}_L = 39.3$

$$E = \hat{E}_L m_L + \hat{E}_P m_P \quad (\text{e})$$

$$m_{\text{DWT}} = m_L + m_P + m_A \quad (\text{d})$$

$$m_{\text{WWT}} = m_L + m_P + m_A + m_W \quad (\text{w})$$

$$m_A = m_A \quad (\text{a})$$

b.c. inverse: $(E, m_{\text{DWT}}, m_{\text{WWT}}, m_A) \longrightarrow (m_P, m_L, m_A, m_W)$

$$m_P = \frac{-E + \hat{E}_L(m_{\text{DWT}} - m_A)}{\hat{E}_L - \hat{E}_P} \quad (6.1)$$

$$m_L = \frac{E - \hat{E}_P(m_{\text{DWT}} - m_A)}{\hat{E}_L - \hat{E}_P} \quad (6.2)$$

$$m_A = m_A \quad (6.3)$$

$$m_W = m_{\text{WWT}} - m_{\text{DWT}} \quad (6.4)$$

nitrogen analysis: $(m_P, m_L, m_A, m_W) \longrightarrow (m_N, m_{\text{DWT}}, m_{\text{WWT}}, m_A)$ $k_N = 0.18$

$$m_N = k_N m_P \quad (\text{n})$$

$$m_{\text{DWT}} = m_L + m_P + m_A \quad (\text{d})$$

$$m_{\text{WWT}} = m_L + m_P + m_A + m_W \quad (\text{w})$$

$$m_A = m_A \quad (\text{a})$$

n.a. inverse: $(m_N, m_{\text{DWT}}, m_{\text{WWT}}, m_A) \longrightarrow (m_P, m_L, m_A, m_W)$

$$m_P = \frac{m_N}{k_N} \quad (6.5)$$

$$m_L = m_{\text{DWT}} - m_A - m_N/k_N \quad (6.6)$$

$$m_A = m_A \quad (6.7)$$

$$m_W = m_{\text{WWT}} - m_{\text{DWT}} \quad (6.8)$$

solvent analysis: $(m_P, m_L, m_A, m_W) \longrightarrow (m_{\text{solv}}, m_{\text{DWT}}, m_{\text{WWT}}, m_A)$

$$m_{\text{solv}} = m_P + m_A \quad (\text{solv})$$

$$m_{\text{DWT}} = m_L + m_P + m_A \quad (\text{d})$$

$$m_{\text{WWT}} = m_L + m_P + m_A + m_W \quad (\text{w})$$

$$m_A = m_A \quad (\text{a})$$

s.a. inverse: $(m_{\text{solv}}, m_{\text{DWT}}, m_{\text{WWT}}, m_A) \longrightarrow (m_P, m_L, m_A, m_W)$

$$m_P = m_{\text{solv}} - m_A \quad (6.9)$$

$$m_L = m_{\text{DWT}} - m_{\text{solv}} \quad (6.10)$$

$$m_A = m_A \quad (6.11)$$

$$m_W = m_{\text{WWT}} - m_{\text{DWT}} \quad (6.12)$$

2.7 November forecast of winter fasting survival by bay

This section presents everything required to construct a bay-specific November forecast of age-0 spring survival due to winter fasting. There are a number of submodules required to implement the November forecast. Before turning to the specifics of the submodules and the role of each in the construction of the forecast, it is best to have a concise statement of what it is we are to construct. The next section attempts to provide such a statement. The sections thereafter provide the detailed descriptions.

2.7.1 Summaries of the 9 steps for a November forecast of spring survival

Let k , $k = 1, \dots, m$, be the index for a set of m bays. A November forecast of spring survival is to be prepared for each of the m bays. Let Ω_k^\bullet denote the fall field sample set of age-0 herring extracted from bay k , and let t_k^\bullet denote the time at which field sample set was taken. As before, $\omega \in \Omega_k^\bullet$ denotes an individual age-0 herring ω in sample set Ω_k^\bullet . The notation $|\Omega_k^\bullet|$ is used to denote the number of elements in the finite set Ω_k^\bullet , which in this case is the number of individual juvenile herring in the field sample set Ω_k^\bullet .

By November each of the fall field sample sets Ω_k^\bullet , $k = 1, \dots, m$, has been taken (§2.4), each sample set Ω_k^\bullet has undergone laboratory analysis (§2.5), and each analysis has been converted to physiological variables (§2.6). That is, for each bay k we have the representation of the fall initial conditions for the physiology of the age-0 subpopulation of bay k

$$\{(m_P, m_L, m_A, m_W) = h_P(\omega) : \omega \in \Omega_k^\bullet\}, \quad \text{at } t = t_k^\bullet \quad (7.1)$$

To construct in November a forecast of fasting survival at the start of spring feeding one first must construct two “climatological” approximations. These two are the first of the new submodels introduced in this section and a statement of their function follows.

1. *Expected fasting interval.* Three “climatological mean” times (dates) are required.

- (1) the expected time $\tilde{t}_{0,k}$ of the onset of fasting in fall in bay k ;
- (2) the expected time $\tilde{t}_{1,k}$ of the cessation of fasting in spring in bay k ;
- (3) an upper bound $\tilde{t}_{\max,k}$ for the time in spring at which fasting ends in bay k —that is, fasting does not continue beyond time $\tilde{t}_{\max,k}$;
- (4) the time interval for fasting extended to the foregoing upper bound $\tilde{I}_k = [\tilde{t}_{0,k}, \tilde{t}_{\max,k}]$.

2. *Expected water temperature time-series.* The model for the physiological response to fasting is temperature dependent. The forecast requires the construction of a “climatological mean” water temperature time-series $\tilde{T}_k(t)$, for $t \in \tilde{I}_k$, representative of the water temperature at the expected location and depth in bay k for age-0 herring at time t .

3. *A patch for differences between t_k^\bullet and $\tilde{t}_{0,k}$.* The physiological response model requires as an input the initial physiology for an individual ω at the start of fasting $\tilde{t}_{0,k}$,

$$\{(m_P, m_L, m_A, m_W) = h_P(\omega) : \omega \in \Omega_k^\bullet\}, \quad \text{at } t = \tilde{t}_{0,k} \quad (7.2)$$

Since the field sample set (Eq 7.1) describes the condition of individuals at time t_k^\bullet , a procedural “patch” is needed. One option is a procedure whereby the conditions in Eq 7.1 are “advanced” or

“retarded” from t_k^\bullet to the time $\tilde{t}_{0,k}$ at which fasting is presumed to begin. A second option is to change $\tilde{t}_{0,k}$ from the “climatological” start time to the field sample time t_k^\bullet .

4. *The physiological response model.* The core model for the time evolution of the physiological response of each individual ω to fasting can be described as the map Φ from (i) the initial physiological conditions $h_{\mathcal{P}}(\omega)$, (ii) the initial time $\tilde{t}_{0,k}$, (iii) the climatological mean temperature time-series \tilde{T}_k , and (iv) time t to \mathcal{P} , that is, to the values for $m_{\mathcal{P}}$, $m_{\mathcal{L}}$, $m_{\mathcal{A}}$, $m_{\mathcal{W}}$,

$$(m_{\mathcal{P}}(t), m_{\mathcal{L}}(t), m_{\mathcal{A}}(t), m_{\mathcal{W}}(t)) = \Phi(t; h_{\mathcal{P}}(\omega), \tilde{t}_{0,k}, \tilde{T}_k) \quad (7.3)$$

5. *The partition of \mathcal{P} into alive vs dead.* A second model describes the partitioning of the physiology space \mathcal{P} into two disjoint subsets, the subset \mathcal{P}^\square which is compatible with life and the subset \mathcal{P}^* which is not compatible with life. In particular, if the response model Φ takes an individual's initial condition $h_{\mathcal{P}}(\omega)$ into the \mathcal{P}^* subset of \mathcal{P} , then that individual ω is modelled as having died. The time t' at which $(m_{\mathcal{P}}(t'), m_{\mathcal{L}}(t'), m_{\mathcal{A}}(t'), m_{\mathcal{W}}(t'))$ first passes from \mathcal{P}^\square to \mathcal{P}^* is the survival time for ω and is denoted by t^* . This defines a map from the initial condition $h_{\mathcal{P}}(\omega)$ to the variable time,

$$t^*(h_{\mathcal{P}}(\omega)) = \sup\{t' \in \tilde{I}_k : \Phi(t'; h_{\mathcal{P}}(\omega), \tilde{t}_{0,k}, \tilde{T}_k) \in \mathcal{P}^\square \text{ for all } t \in [\tilde{t}_{0,k}, t']\} \quad (7.4)$$

In Eq 7.4 the action of the sup (“supremum”) operator is to find the largest time t' such that throughout the entire prior time interval $[\tilde{t}_{0,k}, t']$ the physiological response model Φ remained in \mathcal{P}^\square .

6. *The forecast of survival progression $\tilde{S}_k(t)$.* We now can state that which we seek, the forecast for the progression of the survival of the age-0 population in bay k in spring. In Eq 7.4 we have associated with each ω in Ω_k^\bullet a survival time $t^*(h_{\mathcal{P}}(\omega))$. The subset of individuals in Ω_k^\bullet remaining alive at time t is therefore the subset of Ω_k^\bullet for which the survival time t^* is greater than t . That is, the set of survivors in the simulation at time t is

$$\{\omega : \omega \in \Omega_k^\bullet \text{ and } t^*(h_{\mathcal{P}}(\omega)) > t\} \quad (7.5)$$

The forecast for the progression of the population survival fraction $\tilde{S}_k(t)$ at time t is constructed by computing the fraction of the fall field sample set Ω_k^\bullet in the set of survivors (Eq 7.5) at time t ,

$$\tilde{S}_k(t) = \frac{|\{\omega : \omega \in \Omega_k^\bullet \text{ and } t^*(h_{\mathcal{P}}(\omega)) > t\}|}{|\Omega_k^\bullet|} \quad (7.6)$$

7. *The forecast of spring survival.* The forecast of spring survival due to fasting losses alone is the survival progression time-series evaluated at the “climatological mean” time for cessation of fasting

$$\tilde{S}_k^\circ = \tilde{S}_k(\tilde{t}_{1,k}) \quad (7.7)$$

8. *Advisory information by bay.* In §2.9 the procedure is described for constructing a refined version of the foregoing forecast by replacing the “climatological” approximations with information

that becomes available during the November to March fasting period. The acquisition of that information, however, involves allocation and prioritization of monitoring effort. The November forecast provides the advisory information whereby the significance of any winter and spring bay-specific monitoring can be quantified. Here considerations are restricted to information about a specific bay separate from its role as a part of a larger system. Sound-wide issues make up a separate submodel that follows.

A moments reflection makes clear that the time evolution of the survival fraction $\tilde{S}_k(t)$ is not the result of some process wherein the rate of decrease is linearly related to $\tilde{S}_k(t)$. That is, $\tilde{S}_k(t)$ does not decrease exponentially nor is it asymptotic to zero for large t . Rather, if fasting were to continue indefinitely $\tilde{S}_k(t)$ goes to zero in some finite time $t_{S=0}$. From this simple thought experiment we can expect to find that $\tilde{S}_k(t)$ has the following behavior

$$\lim_{t \rightarrow \tilde{t}_{0,k}} \tilde{S}_k(t) = 1 \quad (7.8)$$

$$\lim_{t \rightarrow \tilde{t}_{0,k}} \frac{d \log \tilde{S}_k(t)}{dt} = 0 \quad (7.9)$$

$$\lim_{t \rightarrow t_{S=0}} \tilde{S}_k(t) = 0 \quad (7.10)$$

$$\lim_{t \rightarrow t_{S=0}} \frac{d \log \tilde{S}_k(t)}{dt} = -\infty \quad (7.11)$$

One way to represent this behavior using the survival forecast is to list the “population halving times”

$$t_{2^{-1}}, \quad t_{2^{-2}}, \quad t_{2^{-3}}, \quad t_{2^{-4}}, \quad t_{2^{-5}}, \quad \dots \quad (7.12)$$

where

$$\tilde{S}_k(t_{2^{-1}}) = 1/2, \quad \tilde{S}_k(t_{2^{-2}}) = 1/4, \quad \dots, \quad \tilde{S}_k(t_{2^{-4}}) = 1/16, \quad \tilde{S}_k(t_{2^{-5}}) = 1/32, \quad \dots \quad (7.13)$$

If the November forecast indicates that at the end of fasting a twenty day extension of fasting would half the population, then one would have an interest in increasing the accuracy of the forecast, especially if the population to be effected were significant. Conversely, if at the end of fasting it takes 40 days to half the population, then sources of error will not effect the survival outcome significantly.

9. System-wide advisory information. Of course, any forecast for survival is of little interest if it applies to a site with a negligible part of the population. There are two sources of system-wide population information potentially acquired through these juvenile herring models: the outcome of the larval drift model §2.2 and the results from the fall population density determinations §2.4.

If neither of the two sources of system-wide population information is available at the time of the November survival forecast, then the advisories above may serve to confirm that none is needed or they may provide a prioritized list of sites for late fall monitoring of age-0 population density.

2.7.2 The “climatological” time approximations (1.) and the time “patch” (3.)

The current version of the winter fasting model uses the following climatological approximations

for fasting time specifications for all bays k

Table 7.1 expected begin and end times and “patched” initial time

event	notation	date	Julian day	Julian day+	duration
expected start of fast	$\tilde{t}_{0,k}$	Oct 22	295	295	
expected end of fast	$\tilde{t}_{1,k}$	Mar 05	64	429	
max “end of fast”	$\tilde{t}_{\max,k}$	Apr 01	91	456	
expected fast interval		Oct 22 – Mar 05			134
max “fast interval”	\tilde{I}_k	Oct 22 – Apr 01			161
simultn. init. time	$\tilde{t}_{0,k}^\bullet$	$\max\{\tilde{t}_{0,k}, t_k^\bullet\}$			
simultn. fast interval		$[\tilde{t}_{0,k}^\bullet, \tilde{t}_{\max,k}]$			

In the foregoing table the column “Julian day+” is the Julian day increased by 365 for all events occurring in the spring, that is, for events occurring in the second of the two calendar years involved in the winter fasting period. The offset for leap years is ignored: the change of any of the entries by a single day has negligible effect on the outcome. The “expected” dates are a current best guess. That is, with the current calibration and the values in the table simulation results are consistent with observations. That consistency would be essentially unaltered if the start and end dates were both shifted by equal amounts. (As will seen, such a translation changes only the temperature time-series during fasting and that change is relatively small—fall days replace spring days or visa versa.) The implementer of an application is safe in making such shifts without materially effecting the calibration presented here.

It is, rather, the duration of the fast that much more strongly impacts the outcome. Thus, changes to either the start or the end date separately can be expected to yield different outcomes. Consequently, the time “patch” is shown explicitly in the table. The notation $\tilde{t}_{0,k}^\bullet$ is introduced to denote the time that is used as the initial time for the simulation that generates the forecast. In the current version of the “patch” $\tilde{t}_{0,k}^\bullet$ is either the expected start time $\tilde{t}_{0,k}$ or the field sample time t_k^\bullet . Specifically, it is whichever of the two times that is later. The specification $\tilde{t}_{0,k}^\bullet = \max\{\tilde{t}_{0,k}, t_k^\bullet\}$ implements the following “patch” procedure:

If $t_k^\bullet < \tilde{t}_{0,k}$ then it is expected that at the time of the fall sample fall feeding was still underway and fasting had not begun. However, we lack both a model and sufficient foraging information to make a quantitative estimate of the impact of this expected feeding. Consequently, we adopt the simplest assumption computationally: the feeding is sufficient for the physiology to remain constant. Thus, the physiology condition from the field sample set is simply advanced in time from t_k^\bullet to $\tilde{t}_{0,k}$ and the simulation initial time $\tilde{t}_{0,k}^\bullet$ is set equal to $\tilde{t}_{0,k}$.

If $\tilde{t}_{0,k} < t_k^\bullet$ then the fall sample set is expected to have occurred during fasting. In this case the physiology is expected to reflect losses incurred by fasting. If one were to “back-up” the simulation initial time to $\tilde{t}_{0,k}$ then the losses would be incurred twice. In this case the “patch” involves no approximation but rather simply setting the simulation initial time $\tilde{t}_{0,k}^\bullet$ to the fall field sample time t_k^\bullet .

The choice of April 01 as the upper bound for the end of fasting is almost certainly not a least upper bound. This date arises from laboratory calibration tests and is retained to cover the period used in those tests.

2.7.3 The “climatological” temperature time-series approximation (2.)

Early in the development of the fasting model it was recognized that a mean temperature change of fully 1C was required to produce a change equivalent to just over 5% expansion or contraction of the fasting period. From Table 7.1 the expected fasting interval is 134 da hence the approximate equivalence that 1 week longer fasting is offset by 1C colder water temperature, and conversely. In the early development period prior to simulations with actual observations a 1 week expansion or contraction appeared quite small but a 2C change in the mean was expected to be of some consequence.

It is worth emphasizing that the nature of the temperature effect is approximately linear so time intervals of temperature above and below the climatological mean are offsetting. The foregoing effect from a 2C change in the mean requires that there be the equivalent of a shift of the temperature by 2C throughout the entire fasting period. A shift by this amount for half of the period is equivalent to a sustained shift of only 1C.

In the later stages of the model development the testing of the model with existing physiological data sets was constrained by the lack of *in situ* temperature information and in some cases by unresolved quality control questions. This motivated the search for an alternative to direct observations. That search resulted in the development of the 2-node linear element model for the annual water temperature time-series. Specifically, it was found that all available temperature observations (all sites, all years) for the upper 50m of the water column were within upper and lower bounds set by $\pm 2\text{C}$ translations of the “climatological mean” temperature time-series defined by the temperature at two unique, fixed dates in the year and linear interpolation for all other time.

The effectiveness of this approximation is shown in Figure 7.1. The two-node linear element approximation along with its translations by $\pm 2\text{C}$ is shown along with the overlay of temperature data provided by the Juvenile Herring Growth and Habitats project [NBF⁺99]. The dates and temperature values for the two nodes of the approximation are listed in Table 7.2.

**Table 7.2: 2-node linear element approximation
time and temperature at nodes**

node	date	Julian day	temperature (C)
1	Mar 16	\hat{t}_0 75	\hat{T}_0 4
2	Nov 01	\hat{t}_1 305	\hat{T}_1 10

The equations for the temperature time-series approximation \tilde{T}_k follows. The notation for the node time (\hat{t}_0 and \hat{t}_1) and for the node temperature (\hat{T}_0 and \hat{T}_1) is shown in Table 7.2 adjacent to the values used in the approximation. In the following equations we make no correction for leap years since the error is not significant. The equations as written apply to t in the range -60 to 440 Julian

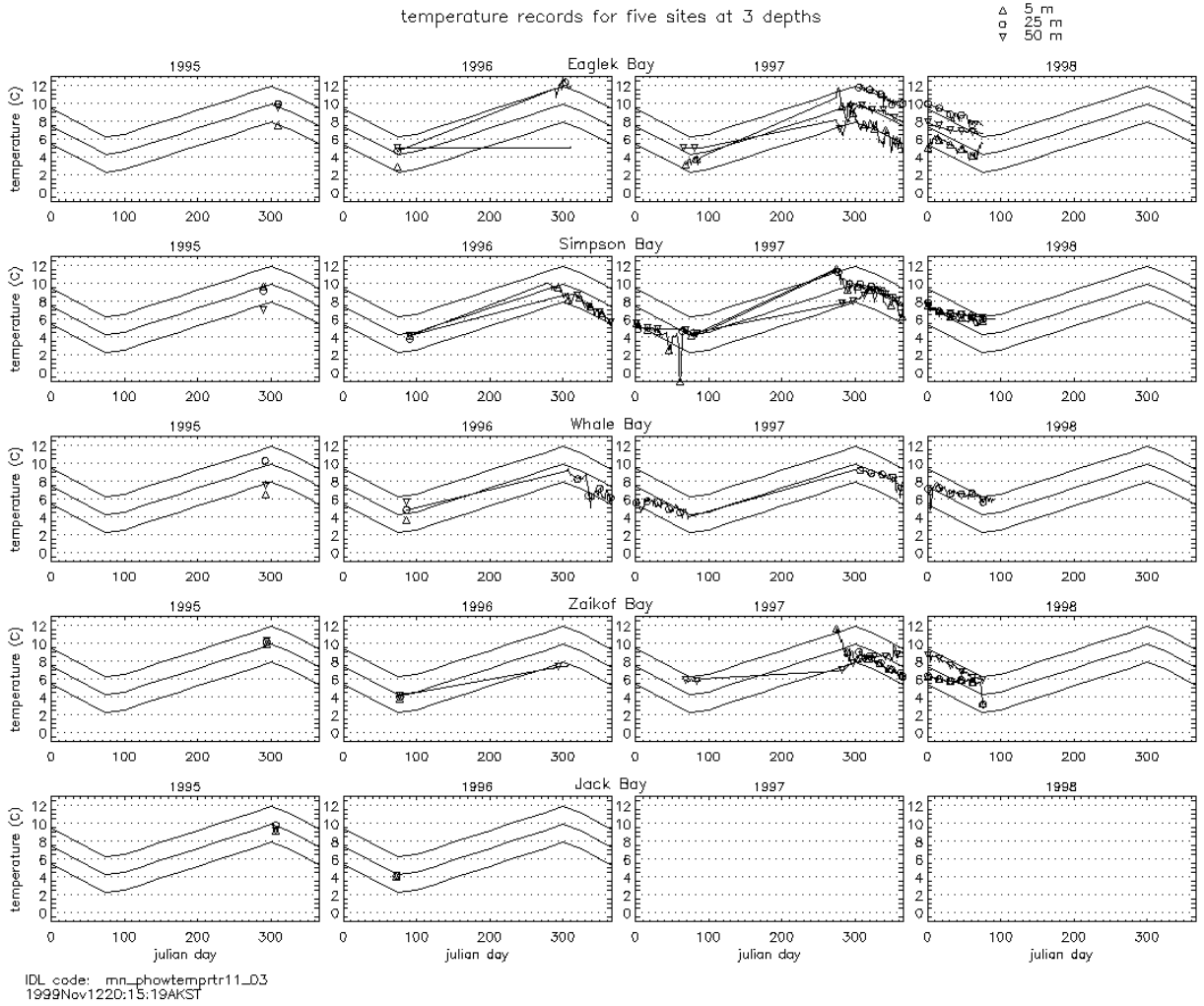


Figure 7.1 Temperature time-series data from winter monitoring of selected bays conducted by the Juvenile Herring Growth and Habitat project [NBF+99]. Data are from continuously logged thermistor arrays or from CTD casts. Records for 5m, 25m, and 50m were provided for use in this model development and are shown in this figure. Also shown is the 2-node linear element approximation and the upper and lower bound approximations obtained from $\pm 2C$ offsets.

day. In practice the code is written so that t is between 0 and 366.

$$\tilde{T}_k(t) = \begin{cases} \frac{\hat{T}_1(\hat{t}_0 - t) + \hat{T}_0(t - (\hat{t}_1 - 365))}{\hat{t}_0 - (\hat{t}_1 - 365)} & \text{for } t \leq \hat{t}_0 \\ \frac{\hat{T}_1(t - \hat{t}_0) + \hat{T}_0(\hat{t}_1 - t)}{\hat{t}_1 - \hat{t}_0} & \text{for } \hat{t}_0 < t \leq \hat{t}_1 \\ \frac{\hat{T}_1(\hat{t}_0 + 365 - t) + \hat{T}_0(t - \hat{t}_1)}{\hat{t}_0 + 365 - \hat{t}_1} & \text{for } \hat{t}_1 < t \end{cases} \quad (7.14)$$

The model development during 1999 has increasingly relied upon the approximation in Eq 7.14. It has been a priority to keep the model solution readily implemented with office automation software, yet the model does involve an integration of the temperature time-series. If one relies solely on empirical data then one must implement a numerical integration routine that is compatible with undocumented and varying data formats from a variety of sources. Although this is not impossible, it is cumbersome and costly for occasional use. The 2-node linear element approximation is readily integrated analytically and the result is an expression similar to Eq 7.14. One then can use the approximation in two ways:

- (i) The forecast can be constructed for the expected approximation of the temperature time-series and for both the upper and the lower bounding time-series; the two extreme forecasts provide an immediate test of the sensitivity of the forecast to temperature differences as well as upper and lower bounds for the forecast.
- (ii) In the event there is temperature data for the fasting period one can use the mean from the observations and the mean from the approximation to compute an offset for the approximation. The actual data need not be directly ingested into the model code.

These are the methods that have evolved during the past year and are the basis for this November forecast component of the models. Prior to the routine use of the approximation the focus had been on the use of near realtime data and nowcasting during the progression of the fast.

2.7.4 The model for the physiological response to fasting (4.)

The fasting model is the result of adapting the compensatory growth modelling work of Kooijman [Koo86] and of Nisbet, Ross, Brooks, Gurney, McCauley, Murdoch, Broekhuizen, Jones, and Bryant [RN90, NRBar, GMNM90, MMNC90, BGJB94] to an early set of process conjectures due primarily to Paul [Pau99] and to the data on juvenile Baltic herring contained in the dissertation of Arrhenius [Arr95a].

The physiological response we seek is the path through \mathcal{P} that starts at $(m_P, m_L, m_A, m_W) = h_{\mathcal{P}}(\omega)$ at time $t = \tilde{t}_{0,k}^{\bullet}$ under the conditions that the temperature T is \tilde{T}_k . The path is defined by specifying the instantaneous rates of change for each of the coordinate variables m_P , m_L , m_A , m_W for the time interval relevant to site-year k

$$\begin{aligned} \frac{dm_P}{dt} &= F_P \\ \frac{dm_L}{dt} &= F_L \quad \text{for } \tilde{t}_{0,k}^{\bullet} \leq t < \tilde{t}_{\max,k} \\ \frac{dm_A}{dt} &= F_A \quad \text{and } (m_P, m_L, m_A, m_W)(\tilde{t}_{0,k}^{\bullet}) = h_{\mathcal{P}}(\omega) \\ \frac{dm_W}{dt} &= F_W \end{aligned} \tag{7.15}$$

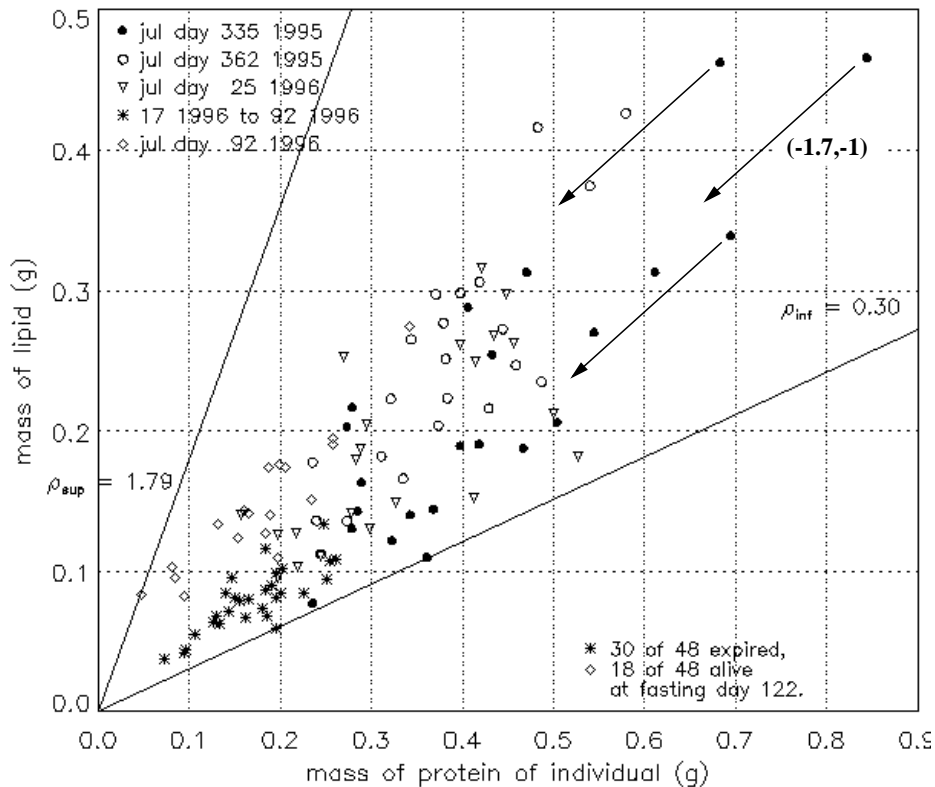
This says, for example, that if we were to watch ω at time $\tilde{t}_{0,k}^{\bullet}$ as it moved through \mathcal{P} by looking at its path projected to the $m_P \times m_L$ plane, as in Figure 7.2, we would see it moving at that instant in the direction of (F_P, F_L) . In Figure 7.2 we have illustrated this by drawing the vector $(-1.7, -1)$ at the position in $m_P \times m_L$ of three such ω 's. We are showing the direction of (F_P, F_L)

mass of lipid vs mass of protein
for fasting age-0 Pacific herring
SEA juvenile herring fasting model
calibrated to Seward Lab study 95-96

$$\hat{E}_L = 39.3, \hat{E}_P = 18.8$$

ash from std length

$$m_A = 1.89e-07 * s^{3.108}$$



run ID = 1999Nov1719:34:27AKST
IDL code = mn_phowSLfastng37.pro

obsrvd tank temp + 0.0C; obsrvd m_{DWT} , m_{WWT} , E
estimated m_{ash} ; modelled $m_{lip}(t)$, $m_{prot}(t)$

Figure 7.2 Direction of response to fasting in $m_P \times m_L$ illustrated using the results from the 1995-1996 Seward Laboratory fasting study conducted by A. J. Paul [Pau99].

by normalizing by $-F_L$ and then assuming that $F_P/F_L = 1.7$. (For this display the length of the vector is immaterial, we are concerned only with direction in $m_P \times m_L$.) The points displayed in Figure 7.2 are actual physiological conditions in $m_P \times m_L$ from the 1995-1996 Seward Laboratory fasting experiment conducted by A. J. Paul [NBF+99]. We have positioned the three vectors at the physiological conditions of three individuals whose state was measured at the first sample time Dec 01. All individuals measured on Dec 01 are shown with the graphical symbol \bullet . The individuals measured at the second sample time Dec 27 are shown with the graphical symbol \circ . One can compare the assumed direction of change $(-1.7, -1)$ with the actual measurements in the Seward Lab study at the first and second sample times as well as at subsequent sample times. These issues are the substance of the ‘‘Calibration Reference’’ and are dealt with quantitatively in that document.

Recall Guideline 2 from §2.4—we have four unknowns F_P, F_L, F_A, F_W so we need four equations to have a model. Let R denote the metabolic requirements during winter fasting. Let \hat{E}_P and \hat{E}_L

denote the energy in kiloJoules (by bomb calorimetry) in one gram of protein and lipid respectively, and let δ_P , δ_L , δ_A , δ_W denote the density (gram per cc) of protein, lipid, ash, and water respectively. Let A_{L2P} be a constant. The collection of models implemented and considered in this effort for the physiological response to fasting is specified by the following four equations,

$$\text{energy conservation} \quad \widehat{E}_P F_P + \widehat{E}_L F_L - R = 0 \quad (7.16)$$

$$\text{protein:lipid withdrawal} \quad F_P - A_{L2P} F_L = 0 \quad (7.17)$$

$$\text{constant ash} \quad F_A = 0 \quad (7.18)$$

$$\text{water rebalance} \quad \begin{cases} F_W = 0 & \text{constant } m_W \\ F_P + F_L + F_A + F_W = 0 & \text{constant wet mass} \\ \frac{F_P}{\delta_P} + \frac{F_L}{\delta_L} + \frac{F_A}{\delta_A} + \frac{F_W}{\delta_W} = 0 & \text{constant volume} \end{cases} \quad (7.19)$$

The basis for the formulation is considered fully in the ‘‘Calibration Reference’’ and other documents, but the essentials are straightforward. Equation (7.16) is the constraint due to zero intake: the metabolic requirements must be fully recovered by the rates of withdrawal of the two energy bearing tissue types.⁸ Equation (7.17) is an assumption regarding the relative rates for withdrawal of protein versus lipid during fasting. The ‘‘Calibration Reference’’ expands upon what is evident in Figure 7.2: protein is consumed during fasting and $F_P = 0$ is not a good approximation; the full scope of available empirical evidence is too sparse to refine (7.17) beyond the present linear approximation; and the linear approximation is sufficient to realize the goal of a lower bound for the physiology at the late stages of total winter fasting. Equation (7.18) follows from the assumption of zero intake and the further assumption that in such cases there is no change in the skeletal structure and negligible change in any other mineral constituents of the body that contribute to the ash category.

The relations for mass of water m_W reflect the diversity of conjectures that guided the initial model development. The first conjecture is the simplest and is in fact is a conjecture from the numerical rather than the biological contributors. However, one can conjecture that if ash is constant then it is not an unreasonable approximation to assume water is also constant. The second assumption, that wet mass (or ‘‘wet weight’’) is constant, is the conjecture encountered most frequently. The third is a variant of the second; it was first heard as the proposed mechanism underlying the second conjecture. Therefore, during the model development we formulated both the conjectured mechanism and the consequent empirical approximation.

It is straightforward that either of the three will produce quite similar outcomes. The mass of water is 80% of the wet mass. During fasting at most 50% of the remaining mass may be lost, so one expects to see the mass of water change by at best 10% under either the constant wet mass or constant volume assumptions. This change has insignificant impact on any of the metabolic

⁸ The careful reader will have seen in (7.16) that we used the value \widehat{E}_P identified earlier as the full heat of combustion energy for protein in an equation accounting for energy recovered from protein by metabolism. One could decrement \widehat{E}_P in (7.16) to address that difference. We have omitted any adjustment of \widehat{E}_P in this version of the model and present the basis for this omission in the ‘‘Calibration Reference.’’

processes that may have m_w as a variable for any of the formulations know or considered. To the extent quantitative information is available we find mass of water increases slightly in the early stage of fasting but thereafter decreases, with a significant net loss, during the later stages of fasting. (See the "Calibration Reference" document in this report.) The second and third assumptions in (7.17) imply that m_w is monotonically increasing throughout fasting. As a consequence, the current version of the model is fully developed and calibrated using the first assumption in (7.17) for the rate of change of m_w .

With (7.16-7.19) the model in (7.15) will be defined once R is specified. Contemporary bioenergetics models are empirical models wherein the dependence upon physiological, environmental, and a behavioral variables is specified using a product of functions of single variables. For example, the instantaneous energy flux R at time t required to sustain all metabolic processes (alternatively referred to as "respiration") is represented by

$$R(m, T(t), \alpha) = C_0 f_m(m) f_T(T(t)) f_\alpha(\alpha) \tag{7.20}$$

where m is some mass, T is temperature, and α the so-called "activity factor." For our needs we assume a fixed contribution from "activity" and incorporate $f_\alpha(\alpha)$ into the constant C_0 . We adopt the existing approximations for temperature (for example, see Arrhenius [Arr95a, Arr95b])

$$f_T(T) = e^{\gamma T}, \quad \text{where } \gamma \text{ is a constant} \tag{7.21}$$

We generalize three methods X for accounting for the roles of the various tissue types in setting the metabolic rate

$$f_{m,X}(m_P, m_L, m_A, m_W) = \left(C_{0,X} \sum_{i=P,L,A,W} C_{i,X} m_i \right)^k, \quad \text{for } X = \text{LP, CE, WWT} \tag{7.22}$$

The coefficients $C_{0,X}$ and $C_{i,X}$ are given in Table 7.1.

Table 7.1 Coefficients for three formulations of metabolic cost as a function of tissue type

X	$C_{0,X}$	$C_{P,X}$	$C_{L,X}$	$C_{A,X}$	$C_{W,X}$
LP	$C_{0,LP}$	1	1	0	0
CE	$C_{0,CE}$	\hat{E}_P	\hat{E}_L	0	0
WWT	1	1	1	1	1

The coefficient $C_{0,X}$ is used solely to allow the use of an overall constant C_0 that is close to or identical to that which is routinely in use based on parameterization with the WWT coefficients. For example, assuming dry mass of 20% of wet mass and ash that is 10% of dry mass, then $C_{0,LP} = 5.56$.

The reason to examine the three formulations for $f_{m,X}$ is that both the WWT and the CE formulation are widely used but differ markedly in the representation of what is setting the metabolic rates. In the WWT formulation the mass of water dominates: during fasting $f_{m,WWT}(m_P, m_L, m_A, m_W)$ is

for all practical purposes a constant whose value is established by m_w . Any change in the mass of any other constituent can be neglected and, as noted above, m_w changes but not more than $\pm 20\%$.

In contrast, the CE formulation discards water and ash and scales protein and lipid to their “carbon equivalent” mass. This increases the role of lipid by over a factor of 2 relative to protein. Since the relative change for lipid is greater than that for any other constituent, the CE formulation is the one in which R will change the most due to physiological change.

The current version of the model uses the LP coefficients. The LP formulation does not have changes in the metabolic rate dominated by the large and stable water mass and it does not increase the effect of lipid mass change relative to that of protein. The LP coefficients are an intermediate formulation. In addition we find it more reasonable for metabolic cost of lipid to be comparable to that of protein rather than a factor of two larger. The LP coefficients have the added benefit of removing water as a variable in R . The LP and CE coefficients agree on this; this aspect of the two has thus far seemed worth retaining.

For reference (7.15) is rewritten with the foregoing applied. Let $(m_{P,0}, m_{L,0}, m_{A,0}, m_{W,0})$ denote any initial point in \mathcal{P} at initial time t_0 . The path in \mathcal{P} is then

$$\begin{aligned}\frac{dm_P}{dt} &= A_{L2P} \frac{dm_L}{dt} \\ \frac{dm_L}{dt} &= \frac{C_0 C_{0,LP}^k (m_P + m_L)^k e^{\gamma T(t)}}{\widehat{E}_L + A_{L2P} \widehat{E}_P} \\ \frac{dm_A}{dt} &= 0 \\ \frac{dm_W}{dt} &= 0\end{aligned}\tag{7.23}$$

for $t_0 \leq t < \tilde{t}_{\max,k}$

$$\text{and } (m_P, m_L, m_A, m_W)(t_0) = (m_{P,0}, m_{L,0}, m_{A,0}, m_{W,0})$$

This system is quite simple and has the analytic solution

$$\begin{aligned}m_P(t) &= A_{L2P} (m_L(t) - m_{L,0}) + m_{P,0} \\ m_L(t) &= m_{L,0} + \frac{m_{L,0} + m_{P,0}}{1 + A_{L2P}} \left[-1 + \left[1 - \frac{C_0 C_{0,LP}^k (1-k)(1 + A_{L2P}) \int_0^t e^{\gamma T} dt}{(\widehat{E}_L + A_{L2P} \widehat{E}_P)(m_{L,0} + m_{P,0})^{1-k}} \right]^{1/(1-k)} \right] \\ m_A(t) &= m_{A,0} \\ m_W(t) &= m_{W,0}\end{aligned}\tag{7.24}$$

The values for constants appearing in 7.24 are

$C_{0,LP} = 5.56 \text{ gm}^{-1}$		fixed; to adjust LP to WWT
$\gamma = 0.548 \text{ C}^{-1}$	$k = 0.773$	prior bio-energetics [Arr95a]
$\widehat{E}_L = 39.3 \text{ kJ g}^{-1}$		animal physiology [SN90, Mor78]
$\widehat{E}_P = 18.8 \text{ kJ g}^{-1}$	$A_{L2P} = 1.7$	this work & Seward Lab [Pau99]
	$C_0 = 0.0285 \text{ kJ da}^{-1}$	

The integral $\int_{t_0}^t e^{\gamma T(s)} ds$ appearing in (7.24) can be computed by a variety of methods depending on what one is starting with. To present a complete closed form solution for the physiology we provide the integral for the case T is the climatological mean time series \tilde{T}_k described in (7.14). The integral in this case is readily evaluated and more involved to express than compute. In the following the notation is the same as that for (7.14). Recall that the 2-node approximation uses two fixed times $\hat{t}_0 = 75$ and $\hat{t}_1 = 305$, in Julian day. We neglect the extra day for leap years and use 365 for year length. For a “mean” year the temperature at \hat{t}_0 is $\hat{T}_0 = 4\text{C}$ and at \hat{t}_1 it is $\hat{T}_1 = 10\text{C}$. One can adjust either \hat{T}_0 or \hat{T}_1 either up or down if there is monitoring information. Figure 7.1 show the linear approximation for \hat{T}_0 and \hat{T}_1 set to the two “mean” values and also both shifted by +2C and by -2C. For the task at hand, estimating forthcoming winter survival in November, one can use the “mean” and then examine the significance of, say, either a +2C or -2C change in water temperature.

Let b_w and b_s denote the slopes of the winter and summer approximations

$$b_w = -\frac{\hat{T}_1 - \hat{T}_0}{\hat{t}_0 + 365 - \hat{t}_1} \quad \text{and} \quad b_s = \frac{\hat{T}_1 - \hat{T}_0}{\hat{t}_1 - \hat{t}_0}$$

Then the integral $\int_{t_0}^t e^{\gamma T(s)} ds$ is given in terms of b_w and b_s and the value of the approximation (7.14) at the endpoints t_0 and t , that is, $\tilde{T}_k(t_0)$ and $\tilde{T}_k(t)$

$$\int_{t_0}^t e^{\gamma T(s)} ds = \left\{ \begin{array}{ll} \text{if } t_0 < \hat{t}_1 \text{ then} & \\ \frac{e^{\gamma \tilde{T}_k(t)} - e^{\gamma \tilde{T}_k(t_0)}}{b_s} & \text{if } t < \hat{t}_1 \text{ and } t \text{ in same year} \\ \frac{e^{\gamma \hat{T}_1} - e^{\gamma \tilde{T}_k(t_0)}}{b_s} + \frac{e^{\gamma \tilde{T}_k(t)} - e^{\gamma \hat{T}_1}}{b_w} & \text{if } t \geq \hat{t}_1 \text{ and } t \text{ in same year} \\ \frac{e^{\gamma \hat{T}_1} - e^{\gamma \tilde{T}_k(t_0)}}{b_s} + \frac{e^{\gamma \tilde{T}_k(t)} - e^{\gamma \hat{T}_1}}{b_w} & \text{if } t < \hat{t}_0 \text{ and } t \text{ in next year} \\ \frac{e^{\gamma \hat{T}_1} - e^{\gamma \tilde{T}_k(t_0)}}{b_s} + \frac{e^{\gamma \hat{T}_0} - e^{\gamma \hat{T}_1}}{b_w} + \frac{e^{\gamma \tilde{T}_k(t)} - e^{\gamma \hat{T}_0}}{b_s} & \text{if } t \geq \hat{t}_0 \text{ and } t \text{ in next year} \\ \text{if } t_0 \geq \hat{t}_1 \text{ then} & \\ \frac{e^{\gamma \tilde{T}_k(t)} - e^{\gamma \tilde{T}_k(t_0)}}{b_w} & \text{if } t \geq \hat{t}_1 \text{ and } t \text{ in same year} \\ \frac{e^{\gamma \tilde{T}_k(t)} - e^{\gamma \tilde{T}_k(t_0)}}{b_w} & \text{if } t < \hat{t}_0 \text{ and } t \text{ in next year} \\ \frac{e^{\gamma \hat{T}_0} - e^{\gamma \tilde{T}_k(t_0)}}{b_w} + \frac{e^{\gamma \tilde{T}_k(t)} - e^{\gamma \hat{T}_0}}{b_s} & \text{if } t \geq \hat{t}_0 \text{ and } t \text{ in next year} \end{array} \right. \quad (7.25)$$

2.7.5 The partition of \mathcal{P} into *alive* vs *expired* (5.)

This step is the simplest. The “Calibration Reference” shows the basis for the partition of \mathcal{P} into

the two disjoint subsets

$$\begin{aligned} \text{alive : } \quad \mathcal{P}^\square &= \{ (m_P, m_L, m_A, m_W) : m_L > L_* m_A \} \\ \text{expired : } \quad \mathcal{P}^* &= \{ (m_P, m_L, m_A, m_W) : m_L \leq L_* m_A \} \end{aligned} \quad (7.26)$$

where $L_* = 0.70$

2.7.6 Forecasting the progression of survival by bay (6.,7., and 8.)

By means of the three steps specified above in (7.14), (7.24), and (7.25) we can now compute for any time t the physiological status (m_P, m_L, m_A, m_W) of an individual ω in Ω_k^\bullet who had commenced fasting at time $\tilde{t}_{0,k}^\bullet$ with initial conditions $(m_{P,0}, m_{L,0}, m_{A,0}, m_{W,0}) = hP(\omega)$ and who is expected to experience temperatures given by \tilde{T}_k . The three steps are condensed into the map Φ

$$(m_P(t), m_L(t), m_A(t), m_W(t)) = \Phi(t; (m_{P,0}, m_{L,0}, m_{A,0}, m_{W,0}), \tilde{t}_{0,k}^\bullet, \tilde{T}_k) \quad (7.27)$$

$$= \Phi(t; hP(\omega), \tilde{t}_{0,k}^\bullet, \tilde{T}_k) \quad \text{for } \omega \text{ in } \Omega_k^\bullet \quad (7.28)$$

$$\begin{aligned} &= \left(\Phi_P(t; hP(\omega), \tilde{t}_{0,k}^\bullet, \tilde{T}_k), \Phi_L(t; hP(\omega), \tilde{t}_{0,k}^\bullet, \tilde{T}_k), \right. \\ &\quad \left. \Phi_A(t; hP(\omega), \tilde{t}_{0,k}^\bullet, \tilde{T}_k), \Phi_W(t; hP(\omega), \tilde{t}_{0,k}^\bullet, \tilde{T}_k) \right) \\ &\quad \text{for } \omega \text{ in } \Omega_k^\bullet \end{aligned} \quad (7.29)$$

where the coordinate variables are written as functions of time. The same information has been written three different ways because at this juncture we must make the transition from the focus on a single individual of (7.27) to a focus on a sample set such as Ω_k^\bullet . The use of (7.28) and (7.29) is the means to expand the focus from one initial condition $(m_{P,0}, m_{L,0}, m_{A,0}, m_{W,0})$ to an entire sample set of initial conditions $\{ (m_P, m_L, m_A, m_W) = hP(\omega) : \omega \text{ in } \Omega_k^\bullet \}$. In (7.28) we have a notation for the four coordinates as a point in \mathcal{P} ; in (7.29) we add a subscript to Φ so that we can refer to each coordinate variable as it appears in the sample set Ω_k^\bullet . Since we can compute (7.29) for each ω in Ω_k^\bullet and for any time t during winter, we can now make the November forecast of survival for members of Ω_k^\bullet at any time during winter. Recall that $|\text{set}|$ means count the members in the set.

$$\begin{aligned} \tilde{S}_k(t) &= \frac{|\{ \omega \text{ in } \Omega_k^\bullet : \Phi_L(t; hP(\omega), \tilde{t}_{0,k}^\bullet, \tilde{T}_k) > L_* \Phi_A(t; hP(\omega), \tilde{t}_{0,k}^\bullet, \tilde{T}_k) \}|}{|\Omega_k^\bullet|} \\ &= \frac{|\{ \omega \text{ in } \Omega_k^\bullet : \Phi(t; hP(\omega), \tilde{t}_{0,k}^\bullet, \tilde{T}_k) \text{ in } \mathcal{P}^\square \}|}{|\Omega_k^\bullet|} \end{aligned} \quad (7.30)$$

Both forms say the same thing. The first, however, is more explicitly expressed in terms of things we know how to compute. The second says the same thing once we recall what is required to be in the *alive* subset \mathcal{P}^\square of \mathcal{P} . (We have, in effect, “pulled-back” the set \mathcal{P}^\square from \mathcal{P} into the sample set Ω_k^\bullet ; in (7.30) we are computing the relative number in the “pull-back.”)

Figure 7.3 illustrates the steps in (7.29) and (7.30) through a graphical display of an actual November forecast of spring survival. The figure shows the fall and the forecast distributions of sample

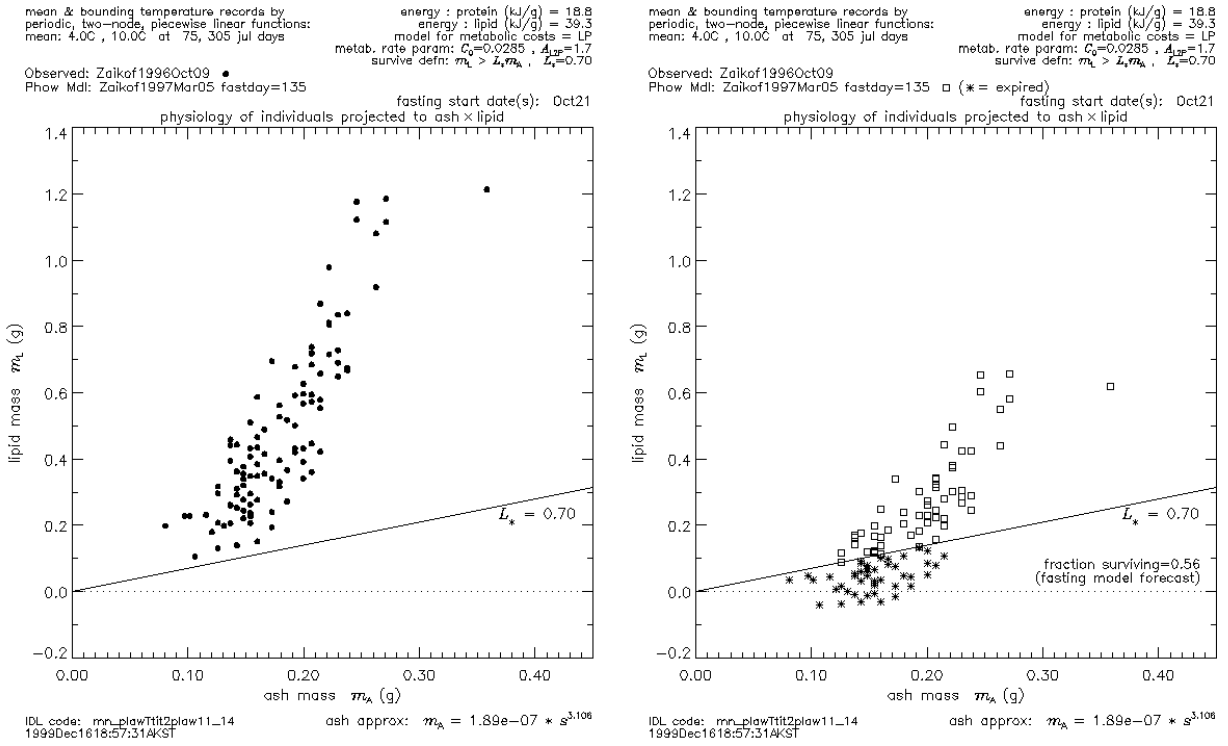


Figure 7.3 November forecast of March fasting survival based on fall physiology monitoring for Zaikof Bay 1996

set Ω_k^\bullet in \mathcal{P} , where k is Zaikof Bay, Oct 09 1996. The time of the fall monitoring t_k^\bullet is Oct 09. Since this is prior to the presumed start of fasting, the monitoring results are assumed to remain fixed until the start of fasting on Julian day 295 or Oct 21 and hence initial time $\tilde{t}_{0,k}^\bullet$ is set to Oct 21.

The left panel is a scatterplot of these initial conditions projected to the $m_A \times m_L$ plane showing

$$\bullet \left\{ (m_A, m_L) = \left(\Phi_A(\tilde{t}_{0,k}^\bullet; h_{\mathcal{P}}(\omega), \tilde{t}_{0,k}^\bullet, \tilde{T}_k), \Phi_L(\tilde{t}_{0,k}^\bullet; h_{\mathcal{P}}(\omega), \tilde{t}_{0,k}^\bullet, \tilde{T}_k) \right) : \text{for } \omega \text{ in } \Omega_k^\bullet \right\}$$

The right panel shows the results of using (7.14), (7.24), and (7.25) to compute the March forecast. It shows the physiology of each ω in Ω_k^\bullet at the expected fasting end-time $\tilde{t}_{1,k}$ under the assumed temperature scenario \tilde{T}_k .⁹ The right panel scatterplot shows

$$\square \left\{ (m_A, m_L) = \left(\Phi_A(\tilde{t}_{1,k}; h_{\mathcal{P}}(\omega), \tilde{t}_{0,k}^\bullet, \tilde{T}_k), \Phi_L(\tilde{t}_{1,k}; h_{\mathcal{P}}(\omega), \tilde{t}_{0,k}^\bullet, \tilde{T}_k) \right) : \text{for } \omega \text{ in } \Omega_k^\bullet \right. \\ \left. \text{and } m_L > L_* m_A, \right\}$$

$$* \left\{ (m_A, m_L) = \left(\Phi_A(\tilde{t}_{1,k}; h_{\mathcal{P}}(\omega), \tilde{t}_{0,k}^\bullet, \tilde{T}_k), \Phi_L(\tilde{t}_{1,k}; h_{\mathcal{P}}(\omega), \tilde{t}_{0,k}^\bullet, \tilde{T}_k) \right) : \text{for } \omega \text{ in } \Omega_k^\bullet \right. \\ \left. \text{and } m_L \leq L_* m_A, \right\}$$

⁹ All such information, including all calibration settings, run date, and code file, can be found in the header and the footer of each graphical display appearing in these documents.

Given the results from this model development, the $m_A \times m_L$ plane is the convenient one to use to see the partition between alive and expired in \mathcal{P} in general and, more to the point, to see the movement during winter of members of Ω_k^* through the *alive* subset toward the *expired* subset. Figure 7.3 shows only one snapshot of that winter long movement—one taken at or near the end of fasting. It is the snapshot that serves as the estimator of overall winter survival due to fasting effects. The fraction of Ω_k^* alive at the time of the snapshot is shown in the lower right of the right panel, 0.56. This is the survival estimate $\tilde{S}_k(\tilde{t}_{1,k})$ of (7.30). It is simply the ratio of the number of \square 's to the number of \bullet 's in Figure 7.3.

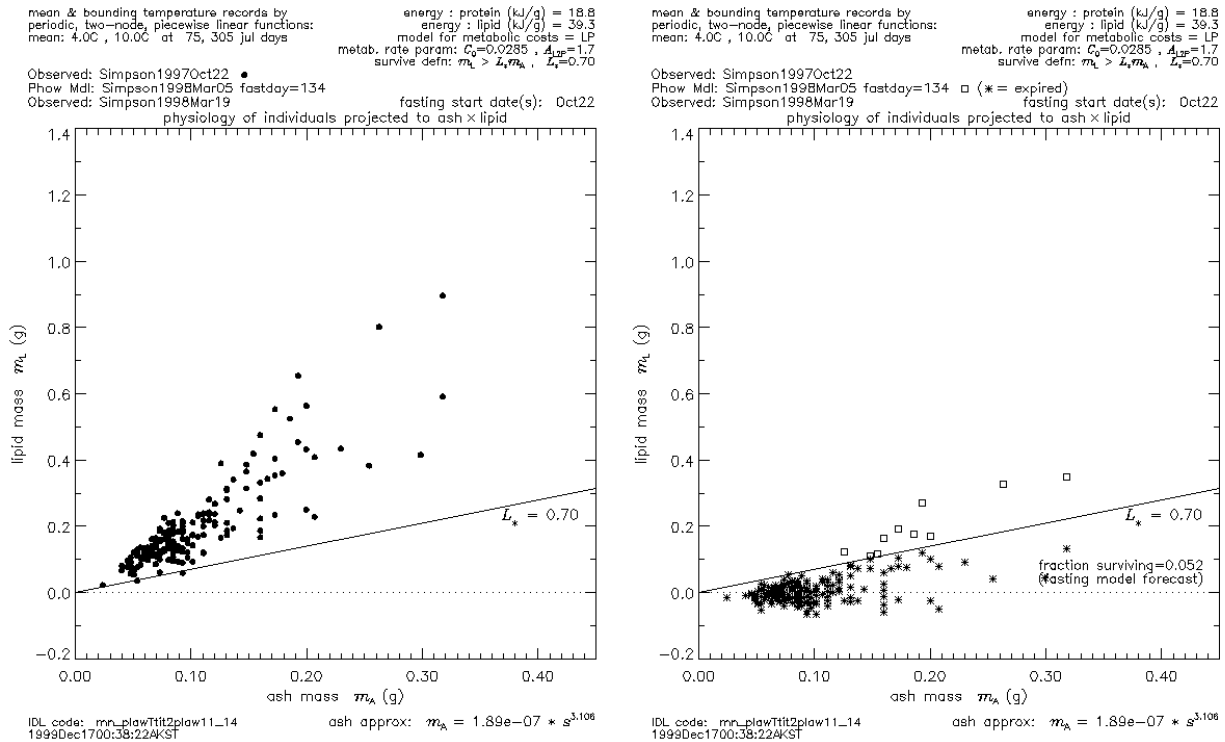


Figure 7.4 November forecast of March fasting survival based on fall physiology monitoring for Simpson Bay 1997

There are reasons to want to see more information about the movement of a given Ω_k^* through \mathcal{P} . Figure 7.4 illustrates one of the primary reasons.

In the case of Simpson Bay, winter 1997-1998, the forecast is that there is a lot of movement from *alive* to *expired* that took place well before the end of fasting. If we had seen this in November 1997 we could well have wished to see if this scenario was really going to happen and, if so, would it make any difference to the overall PWS age-0 population. Figure 7.4 provides some motivation for computing \tilde{S}_k for time t in between the expected start and end of fasting. We know how to do that from (7.14), (7.24), and (7.25) and the results are shown in Figure 7.5.

For Zaikof during winter 1996-1997 the age-0 population halved in about 130 days. The half times for Simpson during winter 1997-1998 are approximately 70, 100, 110, 135, Of course, at fast day

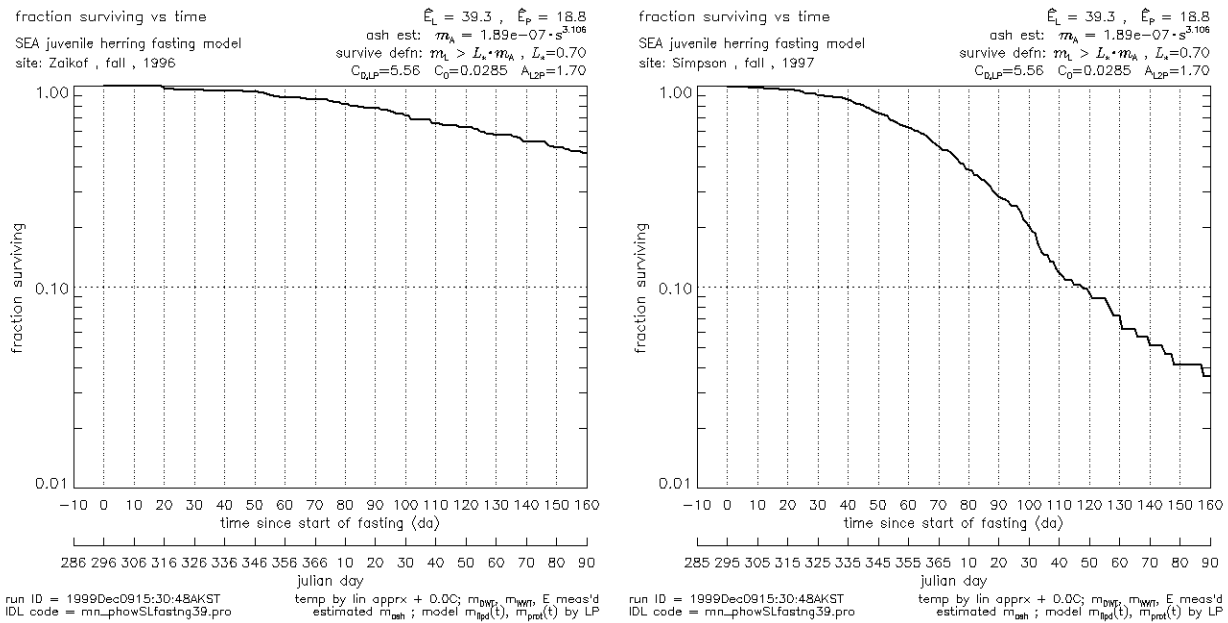


Figure 7.5 Progression of winter survival for Zaikof 1996 and Simpson 1997 based on fall physiology monitoring and model forecast.

110 the size of the sample set Ω_k^\bullet is reduced to one-eighth of its original size and the realism of the progression of survival is diminished. But we do see that around day 100 of fasting this population was halving in under 2 weeks. At that rate of decline the assumptions used to construct the overall survival estimate have greater relative impact on the survival estimate than will be the case for Zaikof 1996. For Zaikof 1996 the assumptions used to construct Figure 7.5 are quite adequate. Whether they are adequate for Simpson depends upon what fraction of the PWS population is being halved during the two weeks around fastday 110.

Figures 7.3 and 7.4 and Figure 7.5 show the first two of three methods for using the (7.14), (7.24), and (7.25) with fall monitoring information in November. The third way is a technique whereby one can visualize what is in the three figures just reviewed without doing *any* of the calculations. Or rather, the calculations are done only once. The method uses special structure of this specific formulation of the model. As the model is refined a similar simplification may not be available. To the extent this version of the model has sufficient realism then the technique is available for a quick first assessment of the situation contained in fall monitoring information.

In (7.4) we defined the “survival time” function t^* . For a given temperature time series \tilde{T}_k the “survival time” function t^* takes an initial condition $(m_{P,0}, m_{L,0}, m_{A,0}, m_{W,0})$ and tells us how long that condition can survive during winter fasting. It tells the time of transition from \mathcal{P}^\square to \mathcal{P}^* . In general t^* depends on the four variables m_P, m_L, m_A, m_W . Since m_W does not appear anywhere, t^* really depends only on m_P, m_L, m_A . It turns out that t^* depends only on the 2-dimensional subspace $\{(m_P + L * m_A, m_L - L * m_A) : (m_P, m_L, m_A, m_W) \text{ in } \mathcal{P}\}$. One can think of $m_L - L * m_A$ as the “lipid reserves” (since the amount $L * m_A$ is not available for metabolism). For lack of a better notation we use “reserves” for both and define $m_{P,res} = m_P + L * m_A$ and $m_{L,res} = m_L - L * m_A$. The

significance is that we can use the plane $m_{P,res} \times m_{L,res}$ for visualizing the level sets or the “contour lines” for constant survival time t^* . In particular, we need no fall data; we need only the mean time series \tilde{T}_k and the model calibration to generate Figure 7.6.

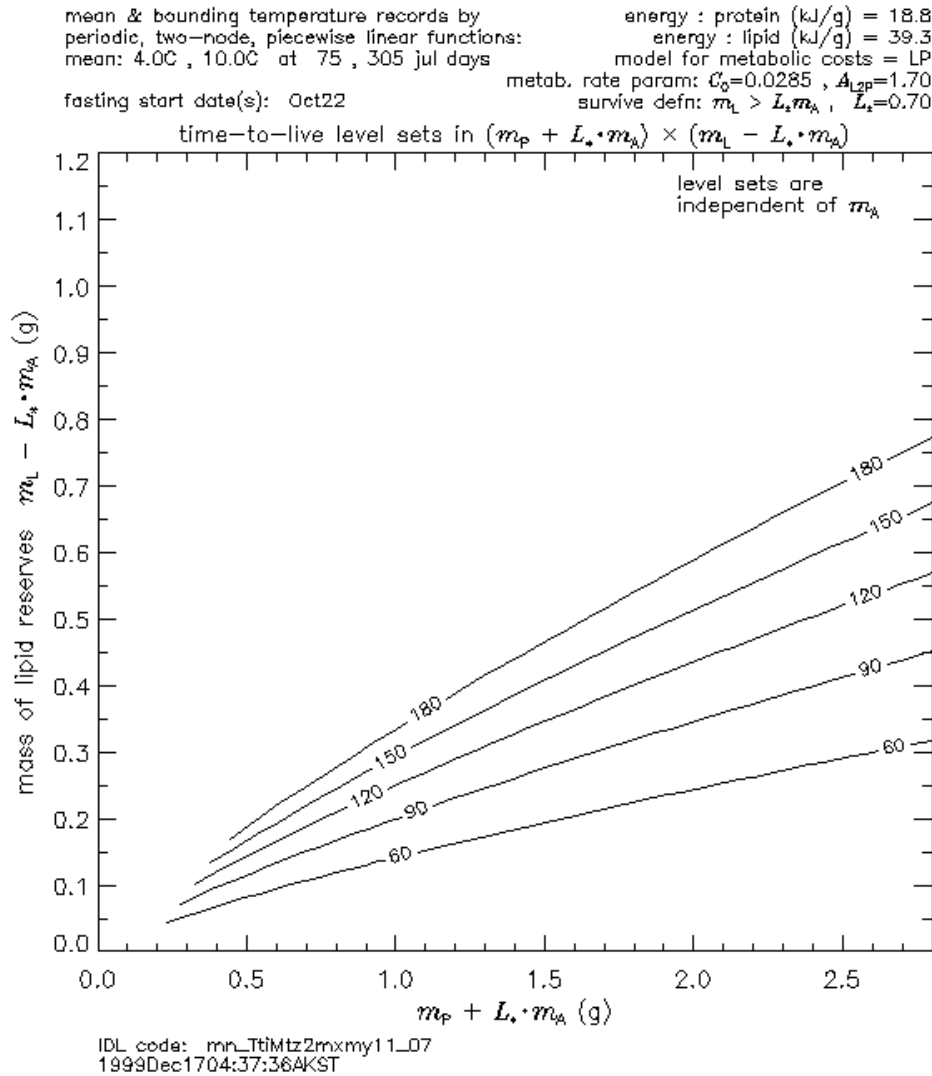


Figure 7.6 Level sets for constant survival times in the $m_{P,res} \times m_{L,res}$ plane. The level sets are at 30da intervals.

With Figure 7.6 one can, by whatever means, including by hand, take the November monitoring report, transform it to the physiological variables m_P , m_L , m_A , m_W , project it to the $m_{P,res}$, $m_{L,res}$ variables, and plot the results on Figure 7.6. This is in effect what is done to generate Figure 7.7. Although one does not have a value for survival without considerable further effort, one does however have with nearly no effort at all most of the bottom line regarding Zaikof 1996 and Simpson 1997.

The display in Figure 7.7 has a few features not shown in the “template” version in Figure 7.6. In

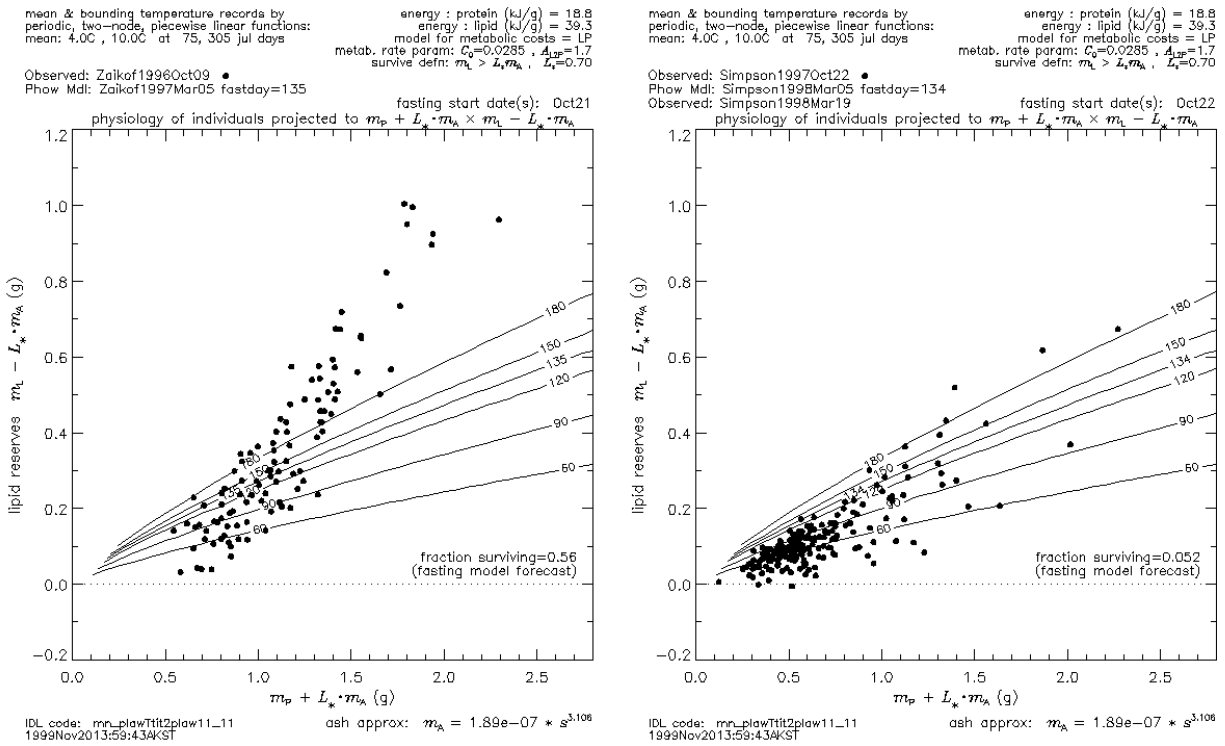


Figure 7.7 The “template” in Figure 7.6 used with Zaikof 1996 and Simpson 1997.

Figure 7.7 the estimated end-of-fast time is added to the list of displayed level sets (i.e., “contour lines”). Second, the lipid reserve axis is translated in order to show negative values. The region $m_{L,res} \leq 0$ is \mathcal{P}^* and this region is used when model output for a spring forecast is displayed in $m_{P,res}$, $m_{L,res}$ coordinates.

There is yet another use for Figure 7.6. This format is by far the simplest means to gauge the sensitivity of the forecast to assumptions regarding start time and water temperature. Figure 7.8. shows the degree to which the level sets are shifted by altering the start time ± 15 days, that is to start dates of Oct 07 or Nov 06. As expected, trading time in cold spring water for warmer Oct water raises each level set. The second panel shows the consequences of a shift of the mean temperature by $\pm 2C$. The dashed level sets are the unshifted sets, the ones shown in Figure 7.6. The level set for higher and lower water temperature appear above and below the dashed, unshifted level sets. As expected, a 2C temperature shift moves a level set about half the distance to the neighboring level set. Since level sets are shown for 30 days intervals, the 2C change therefore produces the same change as a 15 day change in fast duration. (Said another way, a level set for $t^* = 90$ with a -2C shift falls close to the level set for $t^* = 120$ with a +2C shift: an overall 4C shift spans the 30 day separation. This use of Figure 7.6 equates start time and temperature errors to changes in fast duration. However, the significance of the equivalent fast duration change for survival at site k requires one to use Figure 7.6 with actual monitoring data as was done in Figure 7.7.

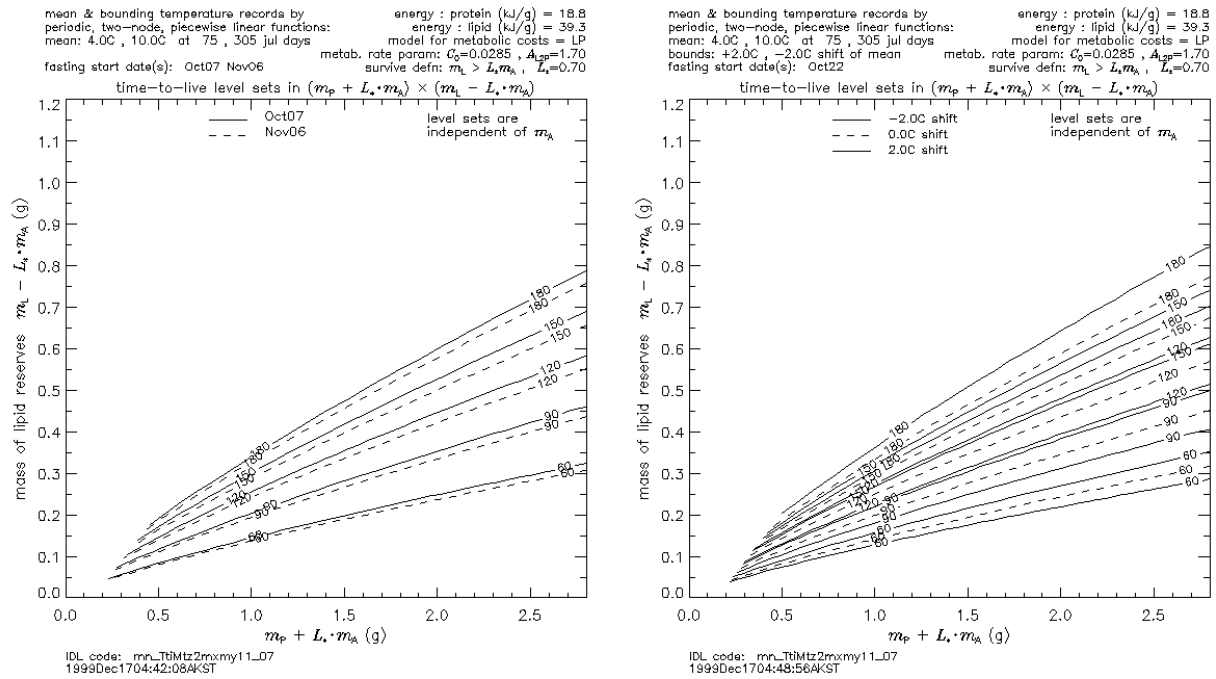


Figure 7.8 The “template” Figure 7.6 used to display the sensitivity of the forecast to assumptions regarding start time for fasting and winter water temperature.

2.7.7 The significance for the system (9.)

This last of the nine steps listed at the outset of §2.7 must remain incomplete. We have shown how to make the November forecasts of winter survival for any bay with fall monitoring data. We have seen how to assess whether the forecast can likely be in error by 10% or 50% or 100%. The likelihood of increased error increases as survival decreases. Both the increased error and the increased mortality are indicators for an “alert” or an “advisory” regarding the forecast. The item needed to weigh the significance of such an alert or advisory is an estimate for the fraction of the PWS population having been advected to that specific site. The potential utility of the foregoing in the development of the extended ADF&G ASA model will emerge as the advective fate of larvae is added to the information presented above.

2.8 Winter environmental monitoring by bay

Any model implementation plan should include a contingency plan for site-specific measurements. The primary role of this document is to enable the end-user to have all of the application-specific information needed to prepare the plan. The precise nature of the resulting monitoring plan will depend upon the fall survival forecast as well as the specific goals for the application plan. The range of options is beyond the scope of this "Concise User's Reference."

2.9 March nowcast of winter fasting survival by bay

This section serves as a placeholder for the end-user. In those cases where an actual realization of a model implementation plan has found winter monitoring justified, the end-user will then use the results of that monitoring to revise and update the forecasts constructed in the preceding November. It is possible there is no winter monitoring and hence no updates.

Bibliography

- [Arr95a] Fredrik Arrhenius. *Feeding Ecology of Baltic Sea Herring (*Clupea harengus* L.)—field and model studies of a dominant zooplanktivor*. PhD dissertation, Stockholm University, Department of Systems Ecology, 1995.
- [Arr95b] Fredrik Arrhenius. *Feeding Ecology of Baltic Sea Herring (*Clupea harengus* L.)—field and model studies of a dominant zooplanktivor*. PhD dissertation, Stockholm University, Department of Systems Ecology, 1995.
- Chapter VI: Bioenergetics of young-of-the-year herring (*Clupea harengus* L.) and a revision of a bioenergetics model
- [BGJB94] N. Broekhuizen, W. S. Gurney, A. Jones, and A. D. Bryant. Modelling compensatory growth. *Functional Ecology*, 8:770–782, 1994.
- [GMNM90] W. S. C. Gurney, E. McCauley, R. M. Nisbet, and W. W. Murdoch. The physiological ecology of *Daphnia*: a dynamic model of growth and reproduction. *Ecology*, 71:716–732, 1990.
- [Koo86] S. A. L. M. Kooijman. Population dynamics on the basis of budgets. In J. A. J. Metz and O. Diekman, editors, *The dynamics of physiologically structured populations*, pages 266–297. Springer-Verlag, Berlin, 1986.
- [MMNC90] E. McCauley, W. M. Murdoch, R. M. Nisbet, and W. S. C. Gurney. The physiological ecology of *Daphnia*: Development of a model of growth and reproduction. *Ecology*, 71, 1990.
- [Mor78] H. J. Morowitz. *Foundations of Bioenergetics*, chapter 14, pages 197–212. Academic Press, New York, 1978.
- [NBF⁺99] Brenda L. Norcross, Evelyn D. Brown, Robert J. Foy, Michele Frandsen, Jody Seitz, and Keven Stokesbury. Juvenile Herring Growth and Habitats. In R. T. Cooney, editor, *Sound Ecosystem Assessment (SEA) - An Integrated Science Plan for the Restoration of Injured Species in Prince William Sound*, Final Report, Ch 10. Exxon Valdez Oil Spill Trustee Council, June 1999.
- [NRBar] R. M. Nisbet, A. H. Ross, and A. J. Brooks. Empirically-based dynamic energy budget models: theory and an application to ecotoxicology. preprint, to appear.
- [Pau99] A. J. Paul. Fish Energetics. In R. T. Cooney, editor, *Sound Ecosystem Assessment (SEA) - An Integrated Science Plan for the Restoration of Injured Species in Prince William Sound*, Final Report, Ch 11. Exxon Valdez Oil Spill Trustee Council, June 1999.
- [PWS93] PWSFERPG. Sound Ecosystem Assessment Initial science plan and monitoring program. Technical report, PWSFERPG, Cordova, AK, 1993.
- [RN90] A. H. Ross and R. M. Nisbet. Dynamic models of growth and reproduction for the mussel *Mytilus edulis* (L.). *Functional Ecology*, 4:777–787, 1990.

- [SN90] Knut Schmidt-Nielsen. *Animal Physiology: Adaptation and Environment*. Cambridge University Press, Cambridge, 4 edition, 1990.
- [TK99] G. L. Thomas and J. Kirsch. Nekton-Plankton Acoustics. In R. T. Cooney, editor, *Sound Ecosystem Assessment (SEA) - An Integrated Science Plan for the Restoration of Injured Species in Prince William Sound*, Final Report, Ch 9. Exxon Valdez Oil Spill Trustee Council, June 1999.
- [VPPLR97] T. I. Van Pelt, J. F. Piatt, B. K. Lance, and D. D. Roby. Proximate composition and energy density of some north Pacific forage fish. *Comp. Biochem Physiol.*, 118A(4):1393–1398, 1997.

Chapter 7 Document 3

Validation Reference for the models for physiological response and survival of age-0 Pacific herring during winter fasting

J. SEA
and
U. SEA, T. SEA, I. SEA

1. Introduction

This document presents the results from validation testing of the most recent version¹ of the model for the physiology and survival of age-0 Pacific herring during winter fasting. The winter fasting model tested herein is the product of the Information Systems and Model Development (ISMD) project² of the Sound Ecosystem Assessment (*SEA*) Program, with essential contributions from the Juvenile Herring Growth and Habitats project [NBF⁺99], the Fish Energetics (FE) project [Pau99], and the Stable Isotopes project [Kli99].

This “Validation Reference” is designed for use with with the full documentation of the model for winter fasting. (Figure 1 shows the full documentation set in a two-dimensional array.) The presentation of the validation tests assumes a working familiarity with the purposes and the essential features of the model (see “Concise User’s Reference” and “User’s Tutorial”) and an understanding of the model calibration (see “Calibration Reference”). A central purpose of the documentation is to provide the end-user the means to reproduce all of the results presented in these reports. This goal is especially important in the case of these validation tests for it is these tests that will be a key factor in any implementation plan and consequent cost-benefit analysis. The test results presented here can be reproduced using the model formulas presented in the “Concise User’s Reference” in conjunction with the data resources described in the document “Algorithms and Information Assets.”

¹ Version 3, Jul 1999, implemented the model processes associated with parameters L_* , P_* , and A_{L2P} . Version 3.1, Nov 1999, is a full recalibration of the model based on a more complete assessment of the physiological structure of the two Seward Laboratory test populations.

² Primary support during 1994–1999 provided by the Exxon *Valdez* Oil Spill Trustee Council, Restoration Project 320J.

Sustaining support during 1998–1999 for implementation of the circulation model and for the PWSSC computing infrastructure provided by the Oil Spill Recovery Institute, Cordova Alaska.

Version 3 of the model and this final documentation of the ISMD project were made possible by private financing from V. Patrick for ISMD IR&D and by the continued long term sustaining support from Grafikon Ltd and from the Advanced Visualization Lab of the University of Maryland.

**Structure of the documentation for the solutions to the PWSFERPG problems
contained in the Final Report of the
Information Systems and Model Development Project**

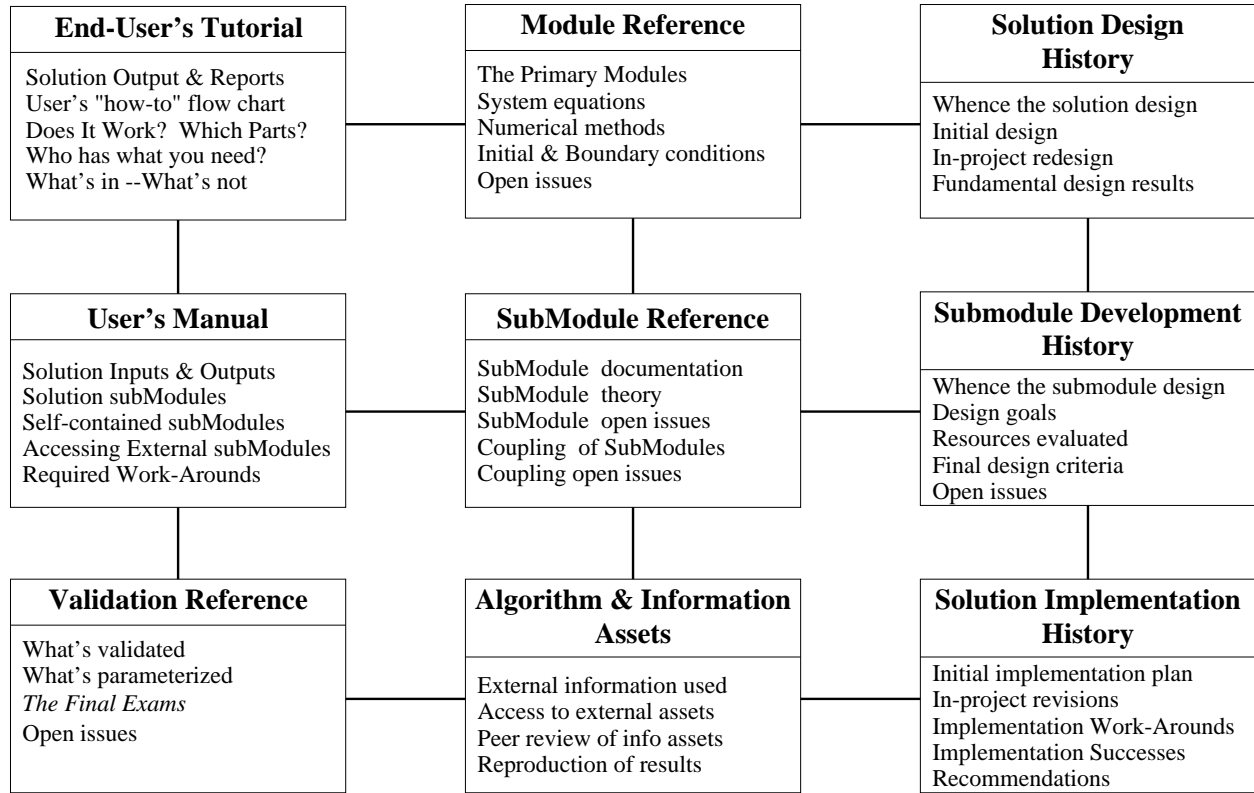


Figure 1. Structure of the document and the relationships between sections. (All sections in the figure do not appear in this first draft of the Final Report.)

The boundary between the tests presented here and those presented in the companion document “Calibration Reference” is to some degree arbitrary. The boundary has been set by restricting this document to those tests that *are not* utilized in any manner to set any of the model parameters. The model tested herein has been set by a parameterization procedure that uses separate datasets and analyses uniquely adapted to those datasets. A review of the “Calibration Reference” shows that the calibration procedures in fact overdetermine the parameters and that this overdetermination is a source of further validation of the model. One consequence of this choice for the boundary is that all tests presented here utilize information obtained from the field monitoring program whereas all tests in “Calibration Reference” utilize information from the Seward Laboratory controlled environment fasting experiment.

Because the tests described herein are based upon field monitoring data, this document will be directly applicable to the design of any future model implementation plan. These validation tests offer the application designer a preview of possible findings from future monitoring and a listing of the validation issues to be asked in the context of those findings. For example, the tests provide

one means to evaluate the so-called “site fidelity” assumption. They also provide insight into the suitability of the assumption that predation makes only a second order change in physiological population structure that is set primarily by fasting survival. But their primary purpose is the assessment of the accuracy of the November forecasts and the March nowcasts for survival. To complete that assessment we will show how to use the results presented to estimate the upper and lower bounds for changes due to errors in field-determined parameters and time-series. This estimate in conjunction with the methods in the “Concise User’s Reference” enables the application developer to optimally allocate his monitoring resources.

The context for these validation tests is the one-year model application cycle shown in Figure 2. In Figure 2 the direction of increasing time is from bottom to top and the span of time from bottom to top is one year—the March at the top of the figure is one year later than the March at the bottom.

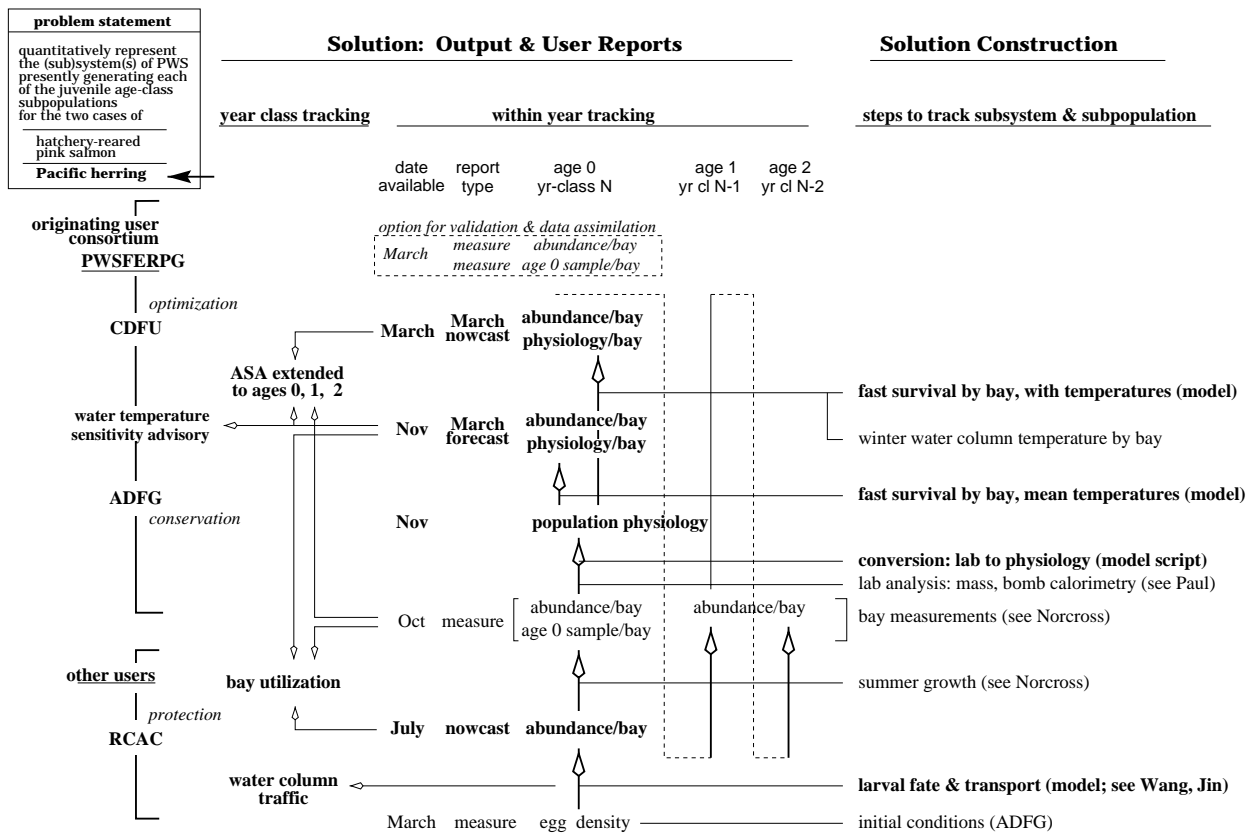


Figure 2. The annual cycle for the models and the monitoring for tracking the development of the juvenile subpopulations of Pacific herring.

2. Validation tests

The validation tests are presented in three sections. The first two sections correspond to two distinct monitoring datasets: (i) the laboratory analyses of sample sets from the age-0 subpopulation in fall and in the following spring for the same bay, and (ii) the relative density assessments of Stokesbury for age-0 and age-1 subpopulations in fall and in the following spring or fall for the same bay. These are two distinct and independently determined assessments of the age-0 population development and therefore offer two independent validation tests of the winter fasting model. The fasting model itself has two submodels: the submodel for the time evolution of the physiological state of an individual, and the submodel representing the partitioning of the physiological state space into the two subsets *alive* and *dead*. We will see in this section how each submodel is validated, jointly and separately, through testing with the two datatypes.

The model for the time evolution of the physiology is tested by comparing the bay-specific forecasts of spring physiology—forecasts based on the initial conditions established by fall monitoring—with the observed spring physiology established by direct monitoring of the same bay. If available, information on the time series of water temperature is incorporated into the forecast. The field monitoring samples and temperature time-series are due to the Juvenile Herring Growth and Habitats project (JHGH) [NBF⁺99]. The subsequent laboratory analyses whereby the physiology is established is due to the Fish Energetics project (FE) [Pau99]. The JHGH and FE projects made available a collection of datasets for age-0 herring for fall and spring and a separate collection of datasets for water temperature time series. From that collection there were five “site-year” datasets with the requisite fall-spring pairing. Only a subset of the five had companion datasets for winter water temperature. In order to make full use of the available monitoring information assest, a temperature time-series approximation was developed and an error analysis carried out to demonstrate that the climatological temperature approximation is quite adequate for the purposes of the winter fasting model.

The submodel for fast-induced mortality is field validated by an assessment of how well the observed physiology in spring (and to a limited degree in fall) conforms to the model specified partitioning of the physiological space. The forecast for fast-induced mortality is a forecast of that subset of physiological states that cannot appear in the spring monitoring sample. Similarly, the survival forecast indicates the subset of all physiological states that can and should appear. In particular, the forecast is explicit about the boundary between surviving and expired. The degree to which the spring monitoring results are consistent with these three features are a field-derived validation test for for the model representation of viable versus unviable physiological states.

The second dataset type, the bay-specific relative density assessment, provides a validation test for the model forecast of spring survival. Since this forecast is obtained by combining the viable-unviable partition and the state of the physiology for each individual in the subpopulation sample at the assumed end of fasting, this is a validation test of the two submodels functioning in concert. Stokesbury has reported on his relative density findings, and from those reports there are two cases which can be used directly for model testing and two additional cases which can be used if we accept some reduced accuracy for the validation test. In this later case we compare the model forecast for winter fasting survival with the Stokesbury report for survival of age-0 from the first fall to the fall one year hence. The so-called “site-fidelity” assumption implies that the age-1 relative density in fall is bounded above by the age-0 relative density of the same bay in the preceding

spring. Hence, the survival of age-0 from first fall to the following fall for a given bay is a lower bound for age-0 winter survival. For example, if there is no spring relative density assessment for a specific bay but there is an assessment in the following fall for age-1 from which fall-to-fall survival is 0.90, then the survival for the first winter was necessarily no less than 0.90. Conversely, if the fall-to-fall survival is very low then there is little that can be inferred regarding fall-to-spring (winter) survival. However, we can look at the fall-to-spring and the fall-to-fall survival assessments as part of a consistency or quality control procedure. We do this for one of the relative density reports wherein the winter survival computed from relative density exceeds unity by more than can be expected from measurement noise. In this case we consider the consequences of viewing the fall-to-fall survival as the more reliable of the two estimates. In this particular case we clearly do not have a validation test in even a loose sense, but we have nevertheless included this case in the presentation.

A short third section presents in one place all of the survival forecasts constructed using the winter fasting model. Here one can see each of the available datasets for fall condition used to generate a site-specific survival estimate. This section is provided in anticipation of future information in the Alaska Department of Fish & Game Age-Structure Analysis which can be meaningfully related to these site-year survival estimates. This section, then, is provided in the spirit of an “in-progress validation.”

2.1 Validation tests using fall & spring observed physiology

Five tests are presented in which model forecasts of spring physiology are compared with the spring physiology determined by field survey.

2.1.1 Data resources

The information resources available for the sites monitored by the JHGH project differs greatly. This project, with the assistance of the JHGH and FE projects, inquired regarding the existence of applicable information resource types and then inquired regarding the availability of those resource types for common sites for any sequential fall and spring. From the findings of these inquiries applicable data subsets were then made available to this project for the tests described in this section. The results of that process of inquiry and submission are summarized in Table 1.1.

Table 1.1: fall–spring data resources available for model testing

site	1995		1996			1997		1998	
	fal t_k^\bullet	wnt T_k	spr t_k°	fal t_k^\bullet	wnt T_k	spr t_k°	fal t_k^\bullet	wnt T_k	spr t_k°
Jack Bay	Nov 03 307	ctd	Mar 12 72						
Simpson Bay	Oct 16 289	ctd	Mar 07 67	Oct 03 277	log	Mar 05 64	Oct 22 295	log	Mar 19 78
Whale Bay	Oct 19 292	ctd	Mar 24 84		log			log	

Table 1.1 identifies the three distinct sites used in the physiology validation tests. All three sites

had fall–spring monitoring datasets for one winter, the 1995–1996 winter. One site, Simpson Bay, has fall–spring monitoring datasets for all three winters, 1995–1996, 1996–1997 and 1997–1998.

The third row of the table header recalls the notation developed in the “Concise User’s Reference.” The times of the fall and spring field samples for bay k are denoted by t_k^\bullet and t_k° respectively. The temperature time-series for winter for bay k is denoted T_k . This notation differs only in that the index k is used to identify site-year rather than only the bay or site. This extended meaning for the index k eliminates the need for any added notation to identify different winters at a common site. To keep this meaning clear we shall refer to site-year k rather than bay k in this document. The use of symbolic superscripts to distinguish fall and spring events is to directly link the notation to the information presented graphically. If one looks ahead to any of the figures for the validation tests one sees that the symbols \bullet and \circ appearing here as superscripts for fall and spring observations are the same symbols used to display graphically data from fall and spring observations.

The entry “log” in the winter (“wnt”) column indicates that a temperature time-series record was measured by the JGHG project for that bay. These measurements were by a fixed thermistor array with sensors at a fixed set of depths. The entry “log” in Table 1.1 indicates that a temperature time-series dataset from that effort has been made available. For most time periods temperatures for the 5m, 25m and 50m depths are available. The 25m depth is recommended by Stokesbury of JGHG as the dominant depth of winter residency for age-0 herring. The entry “ctd” indicates that no time-series monitoring data are available; instead temperature data for the depths corresponding to the data logging effort were extracted from isolated “CTD” casts and provided for use in these tests. The full record of the temperature time-series is shown graphically in Figure 1.1. See also the document “Algorithms and Information Assessts.”

The dates in the fall and spring columns of Table 1.1 are the times at which the collection of age-0 samples occurred. These dates are shown for in two formats: “Mon Da” and Julian day.

2.1.2 Simulation scenarios

To carry out the simulations of the time evolution of the age-0 physiology, the information in Table 1.1 is recast to that shown in Table 1.2.

**Table 1.2: fasting start & stop times
and temperature shifts for the approximating time-series**

site	1995		1996			1997		1998	
	fal $\tilde{t}_{0,k}^\bullet$	wnt \tilde{T}_k	spr $\tilde{t}_{1,k}^\circ$	fal $\tilde{t}_{0,k}^\bullet$	wnt \tilde{T}_k	spr $\tilde{t}_{1,k}^\circ$	fal $\tilde{t}_{0,k}^\bullet$	wnt \tilde{T}_k	spr $\tilde{t}_{1,k}^\circ$
Jack Bay	Nov 03 307	+0	Mar 05 64						
Simpson Bay	Oct 22 295	+0	Mar 04 64	Oct 21 295	-2	Mar 05 64	Oct 22 295	+0	Mar 05 64
Whale Bay	Oct 22 295	+0	Mar 05 64						

The fall and spring observation dates are recast to reflect the initial and final times for the simulation of fasting. Only the fall monitoring of Jack Bay occurred after the presumed start of fasting on

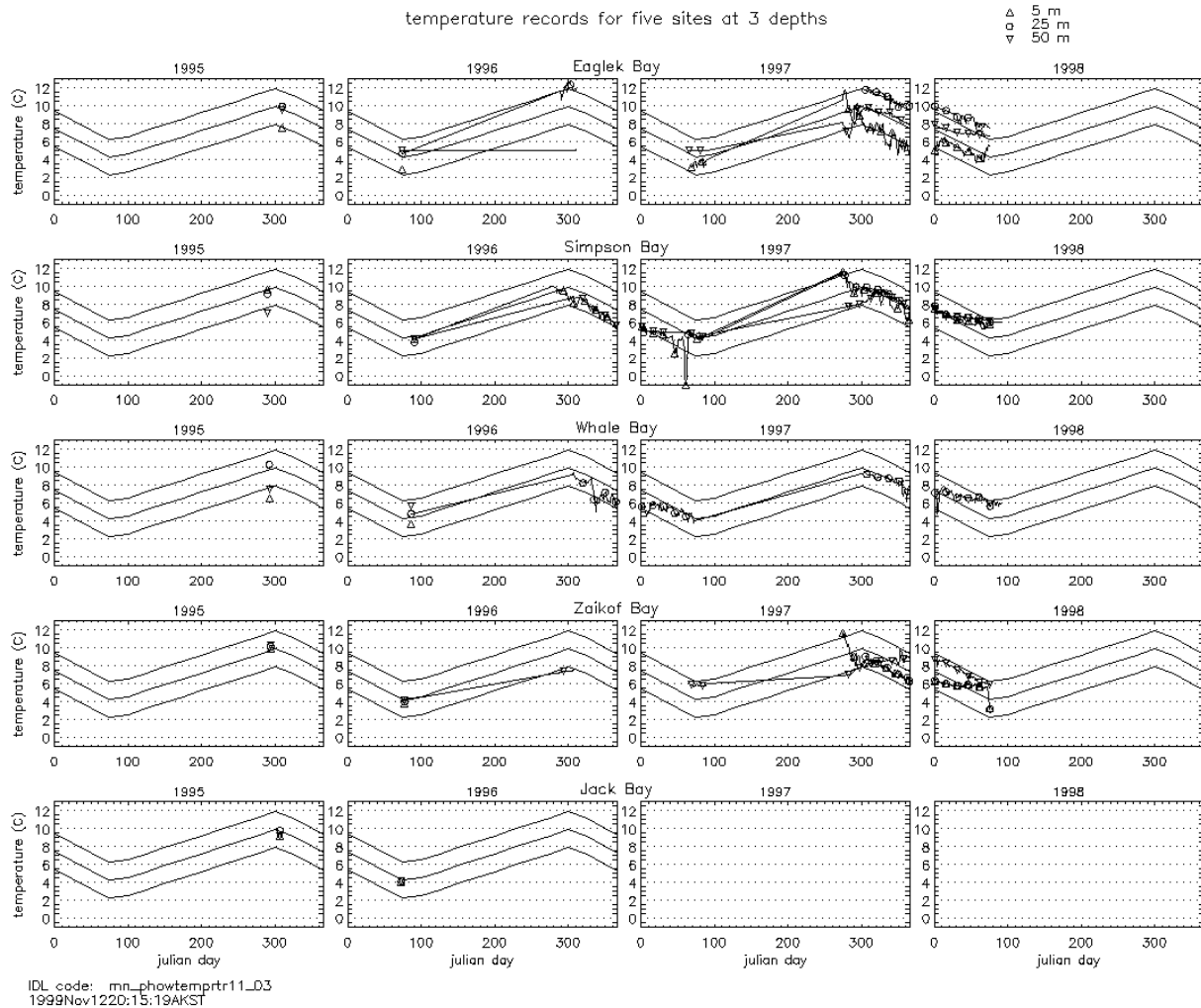


Figure 1.1 Graphical overview of all data resources for water column temperature time-series used in model validation testing. All temperature datasets provided by R. Foy of JHGH.

Julian day 295; for all other cases the date in Table 1.1 was advanced to Julian day 295 to obtain the initial time for the simulation. All spring observation dates occur after the presumed end of fasting on Julian day 64. In the validation tests we will make the same assumption as was made for the fall: if observations in spring occur after the end of presumed fast it is assumed that the period of feeding is sufficient to exactly offset metabolic costs, hence the physiological state is constant during the time from end of fast to observation date. As a consequence, validation testing is done with the physiology obtained on Julian day 64 for all five test cases. Table 1.2 recalls the notation for these simulation start and end times that result from the foregoing fusion of the observation times with the expected times for beginning and ending of fasting. The start and end times for the physiology simulations for these validation tests are denoted $\tilde{t}_{0,k}^{\bullet}$ and $\tilde{t}_{1,k}^{\circ}$ respectively. The addition of the accent symbol \sim indicates that the value is result of an analysis that precedes the actual simulation.

The temperature time-series or CTD cast information is recast into a temperature shift by an integer number of degrees Celsius of the 2-node linear element approximation of the climatological temperature time-series. The unshifted approximation and the $+2^\circ\text{C}$ and the -2°C shifts are shown in Figure 1.1. The use of the 2-node linear element approximation and the small set of possible shifts simplifies greatly the task of dealing with many issues evident in Figure 1.1: different data types; options regarding methods for integration; options for and extent of smoothing; and the primary habitat of juvenile herring at the various periods of the winter fast. The ‘‘Concise User’s Reference’’ describes explicitly the steps whereby Table 1.2 is obtained from Table 1.1. The notation for the approximating temperature time-series for site-year k is denoted \tilde{T}_k .

The information in both Table 1.1 and Table 1.2 is restated in the legends at the top of each of the figures used to present the validation results. Thus, the information regarding the rectification of observation dates to fasting dates and the method of assimilation of temperature data is self-contained in each of the validation figures.

The foregoing describes the manner in which the data resources from field monitoring are used in the following tests. In addition, the legend for each figure shows the model calibration parameters used in the test. All of the parameterization is fixed throughout all of the validation tests and reflects the values used in Version 3.1 of the winter fasting model.

2.1.3 Validation testing in \mathcal{P}

The validation testing of the physiology model requires the comparison of two finite sample populations each of which is distributed in the 4-dimensional space \mathcal{P} . The space \mathcal{P} is defined in the ‘‘Concise User’s Reference’’ to be the 4-dimensional space of positive real numbers with the coordinate variables (m_P, m_L, m_A, m_W) . The methods in the ‘‘Concise Users’s Reference’’ specify all of the procedures that define the mapping $h_{\mathcal{P}}$ from an individual age-0 herring ω to its physiological state $(m_P, m_L, m_A, m_W) = h_{\mathcal{P}}(\omega)$.

The two finite sample populations are the fall and the spring sample sets for a given site-year k , denoted Ω_k^\bullet and Ω_k° respectively. The fall initial conditions for site-year k consist of the collection of points in \mathcal{P}

$$\{ (m_P, m_L, m_A, m_W) = h_{\mathcal{P}}(\omega) : \omega \in \Omega_k^\bullet \} \quad \text{for} \quad \min\{t_k^\bullet, \tilde{t}_{0,k}^\bullet\} \leq t \leq \tilde{t}_{1,k}^\circ \quad (1.1)$$

and the spring observations for site-year k consist of the collection of points in \mathcal{P}

$$\{ (m_P, m_L, m_A, m_W) = h_{\mathcal{P}}(\omega) : \omega \in \Omega_k^\circ \} \quad \text{for} \quad \tilde{t}_{1,k}^\circ \leq t \leq \max\{t_k^\circ, \tilde{t}_{1,k}^\circ\} \quad (1.2)$$

The model for the time evolution of the physiology in site-year k is the map for each time t from an initial point $(m_P, m_L, m_A, m_W) = h_{\mathcal{P}}(\omega)$ in \mathcal{P} at initial time $\tilde{t}_{0,k}^\bullet$, with forcing temperature time-series \tilde{T}_k , to a new point $(m_P(t), m_L(t), m_A(t), m_W(t))$ in \mathcal{P} representing the new state of individual ω at time t ,

$$(m_P(t), m_L(t), m_A(t), m_W(t)) = \Phi(t; h_{\mathcal{P}}(\omega), \tilde{t}_{0,k}, \tilde{T}_k) \quad (1.3)$$

In this notation the spring forecast for the physiological state of individual ω from the fall sample Ω_k^\bullet is

$$(m_P(\tilde{t}_{1,k}^\circ), m_L(\tilde{t}_{1,k}^\circ), m_A(\tilde{t}_{1,k}^\circ), m_W(\tilde{t}_{1,k}^\circ)) = \Phi(\tilde{t}_{1,k}^\circ; h_{\mathcal{P}}(\omega), \tilde{t}_{0,k}, \tilde{T}_k) \quad (1.4)$$

For the validation tests we must compare two samples and not the time evolution of an individual ω .³ The set points in \mathcal{P} obtained by applying the model in (1.4) to the fall collection of points in \mathcal{P} described in (1.1) is

$$\{ (m_P, m_L, m_A, m_W) = \Phi(\tilde{t}_{1,k}^\circ; \omega, \tilde{t}_{0,k}^\bullet, \tilde{T}_k) : \omega \in \Omega_k^\bullet \} \quad (1.5)$$

Before the set of forecast points in \mathcal{P} (1.5) can be compared to the observed points in \mathcal{P} (1.2) we must sort those in (1.5) according to whether they should occur in a field observation. The “Concise User’s Reference” describes the model whereby a point (m_P, m_L, m_A, m_W) in \mathcal{P} is classified as *alive* or *expired* as a consequence of fasting. That is, \mathcal{P} is partitioned into two disjoint subsets \mathcal{P}^\square and \mathcal{P}^* for *alive* and *expired* respectively. The “union” set operator \cup and the “intersection” set operator \cap are useful in this context. The space \mathcal{P} is the union of the two partitions,

$$\mathcal{P} = \mathcal{P}^\square \cup \mathcal{P}^*$$

and those individuals in the forecast are assigned to *alive* or *expired* status according to whether their final state is in \mathcal{P}^\square or in \mathcal{P}^* ,

$$\text{alive: } \mathcal{P}^\square \cap \{ (m_P, m_L, m_A, m_W) = \Phi(\tilde{t}_{1,k}^\circ; \omega, \tilde{t}_{0,k}^\bullet, \tilde{T}_k) : \omega \in \Omega_k^\bullet \} \quad (1.6)$$

$$\text{expired: } \mathcal{P}^* \cap \{ (m_P, m_L, m_A, m_W) = \Phi(\tilde{t}_{1,k}^\circ; \omega, \tilde{t}_{0,k}^\bullet, \tilde{T}_k) : \omega \in \Omega_k^\bullet \} \quad (1.7)$$

As was noted for the superscripts \bullet and \circ , the symbols \square and $*$ are used in graphical displays to distinguish individuals forecast to be in the subset *alive* and *expired* respectively.

The validation task, then, is to compare the four collection of points in \mathcal{P} described by (1.1), (1.2), (1.6) and (1.7) for $k = 1, \dots, 5$.

A fundamental issue is the definition of the procedure whereby the results from (1.1), (1.2), (1.6), and (1.7) are to be compared. A full definition requires the specification of a measure V that yields a positive scalar value for the extent to which, say, the two populations in (1.2) and (1.6) differ. At this time such a measure is not fully defined. Instead, we show the steps that are now planned for constructing that measure. As will be seen, given the open issues, it is somewhat premature to fix the specific measure. However, from the presentation it will be clear what to include in the measure. It will also be clear that one measure alone is insufficient for there are several issues addressed jointly in these validations tests.

In addition, at this juncture we are as much interested in how the observed and simulated sets differ as in the degree of difference. Because the sets are in the 4-dimensional space \mathcal{P} it is non-trivial to describe “how” they differ. Simple scalar features do not suffice for there are geometric aspects to be considered. The present methods for addressing these two issues—the preliminaries of a measure for differences and the means to see the origins of differences—are presented next.

³ In all of the tests described herein the individual ω is destroyed in the testing.

2.1.4 Comparisons between simulations and observations in \mathcal{P}

The differences between the simulation results and the observations are made apparent by the projections of the space \mathcal{P} to three two dimensional spaces.

$$\begin{array}{ccc}
 & (m_P, m_L, m_A, m_W) & \\
 & \swarrow \quad \downarrow \quad \searrow & \\
 (m_A, m_L) & & (m_P, m_L)
 \end{array} \tag{1.8}$$

The basis for these three projections is found in §2.7 of the “Concise User’s Reference” but the manner in which each of the three is used will be apparent from the description of the results below.

For each of the three projections the four sets of points in \mathcal{P} for fall initial conditions (1.1), spring observations (1.2), simulations of *alive* in spring (1.6), and simulations of *expired* in spring (1.7) are combined into the following 2-by-2 four panel display

	overlay of fall initial conditions (1.1), spring observations (1.2), and spring simulation for <i>alive</i> (1.6) and <i>expired</i> (1.7)
fall initial conditions (1.1)	
spring observations (1.2)	spring simulation for <i>alive</i> (1.6) and <i>expired</i> (1.7)

This display format is used throughout this section. The presentation of the the validation comparisons, therefore, consists of five site-year test cases, three projections per site-year, with four views of the sample sets for each projection. This is the content of Figure 1.2 through 1.17.

The description of the preliminary components for a suitable measure V is contained within the presentation of the validation test results for the first site-year Jack Bay 1995.

2.1.5 Test results for Jack Bay 1995

The three projections of (1.8) for Jack Bay 1995 are shown in Figures 1.2, 1.3, and 1.4. For this first site-year the results are presented with each projection considered separately. Thereafter the results are described in a much more condensed manner with all three projections considered jointly.

Jack Bay 1995 $m_A \times m_L$ The projection (m_A, m_L) (Figure 1.2) is the most immediately informative of the three from the perspective of the end-user interested in population development. The (m_A, m_L) projection provides the explicit display of the partition of the spring forecast into *alive* versus *expired* because the model for the partition is a function of only m_A and m_L

$$\mathcal{P}^\square = \{ (m_P, m_L, m_A, m_W) : m_L > L_* m_A, L_* = 0.70 \} \tag{1.9}$$

Following the practice used in the pink salmon fry survival model tests we identify each component of the preliminary measure V as a numbered “Final Exam Question” (FEQ). The first FEQ is obvious from a brief inspection of the results shown in Figure 1.2.

FEQ 1. *Is the spring observation set consistent with the partition $\mathcal{P} = \mathcal{P}^\square \cup \mathcal{P}^*$ defined in (1.9)?*

Grade. One member of the spring observation sample set, presumably alive when taken in the field, falls in the *expired* partition. All other members of the spring observed set are in the *alive* partition.

From the “Concise User’s Reference” we have the definition of the support of the sample population distributions in the plane defined by the two coordinates m_A and m_L . The support is that subset of the $m_A \times m_L$ plane in which the probability density function for, say, the spring observations or the *alive* subset of the spring simulation is non-zero. From a numerical perspective the support can be defined by constructing a DeLaunay triangulation of the points in the sample set and taking the union over all triangles. Because the support for fall, spring observed and spring simulated has concave-up upper and lower boundaries, one would not use the convex hull of the set. In this document we do not construct an approximation of the support and use temporarily the visualization of that support apparent in Figure 1.2. The comparison of the support for the spring observed versus the spring simulated *alive* is made more precise in the next several FEQs.

The goal of the model is to reflect the extreme scenario of complete fasting for the entire winter. The corresponding FEQ is

FEQ 2. *Does the forecast for the alive subset (or its support) reflect an underestimation of the physiology relative to that found in the spring observations?*

Grade. Pass.

In making this assessment we have made implicit use of the assumption that during winter there is no change in m_A for surviving individuals. That is, m_A is constant. Thus, the overlay in the upper right enables one to visually assess this FEQ.

This is a good point to recall that these validation tests must assess two questions simultaneously: (i) the performance of the model with allowances for the degree to which the underlying assumptions hold, and (ii) the degree to which the findings are consistent with the underlying assumptions. The “Concise User’s Reference” clarifies that the scope of the effort here is not to prove or disprove the underlying assumptions. However, the validation tests must be evaluated for consistency or inconsistency with the assumptions. Two assumptions to be examined are restated here.

- A1 the observed changes in the population structure during winter reflect mortality losses from fasting; conditions sufficient for this assumption to hold are the more restrictive and specific assumptions of
 - (a) site fidelity, and
 - (b) the structural changes during winter due to predation mortality are similar to those due to fasting mortality or, alternatively, are negligible in comparison to fasting mortality;
- A2 the fasting during winter can be assumed to be total, that is, any intake alters the physiology only negligibly.

Assumption A2 is the basis for the property of the model wherein m_A is constant. This is apparent in Figure 1.2: the change from fall to spring in simulation is a movement vertically downward in the $m_A \times m_L$ plane. Assumption A1 and A2 together imply that the spring observed distribution should exhibit specific structural relationships to the fall initial conditions.

FEQ 3. *Is the upper bound for m_A in the spring sample set no greater than that for the fall initial conditions?*

Grade. Pass. One is hard pressed to find any evidence for discarding the site fidelity assumption. We shall see that throughout this evaluation for Jack Bay there is evidence of some feeding and growth either during the winter or during the time period following the cessation of fasting. No attempt was made to apply a statistical test of significance for a difference in the upper bounds. Indeed, prior to such a test there is a need to make more precise the definition of the upper bound in the context of a finite sample from a population. Moreover, there is then the need to define the difference in the upper bounds for the case of two samples from populations which are different. One difference is identified in the next FEQ.

FEQ 4. *Does the support of the spring observed distribution reflect the change in support forecast by fasting losses, in particular, does the lower bound for m_A change between fall and spring in a manner consistent with the simulation?*

Grade. Pass. Although this site-year case has low fasting mortality, nevertheless it does make clear that the mortality impact is such that the lower bound for m_A should increase. The fall to spring observations exhibit an increase, albeit one larger than that forecast. The difference does not seem sufficient to warrant discarding either assumption A1 or A2 or in particular part b of assumption A1.

There are further tests which involve the full support of the sample sets and not their boundaries.

FEQ 5. *Is the support for the spring observation sample set essentially the same as the support of the alive set from the simulation except for a translation in the direction of the m_L coordinate?*

Grade. Pass. This test allows for some feeding either during winter or between the end of fasting and the time of the spring sample. It measures the combined effect of the model acting upon the fall initial conditions together with assumption A1—that the action of the model is the only significant source of change in the population structure.

Testing both assumptions A1 and A2 together with the model requires getting not only the “shape” of the support correct but also its position.

FEQ 6. *Is the support of the spring observation sample set the same as the support of the alive set from the simulation?*

Grade. Not quite. There is evidence in Figure 1.2 that at some point during winter the “low end” of the support was “clipped” in a manner not unlike that exhibited by the simulation (lower right panel), but that prior to the spring sample there was noticeable recovery of lipid. Although it is possible that there was never any approach to the boundary of \mathcal{P}^\square , the “compression” of the extent of the support in the m_L direction suggests otherwise. The result is not inconsistent with the model, for the spring observation on Mar 12 is 8 days later than the presumed end of fasting on Mar 04.

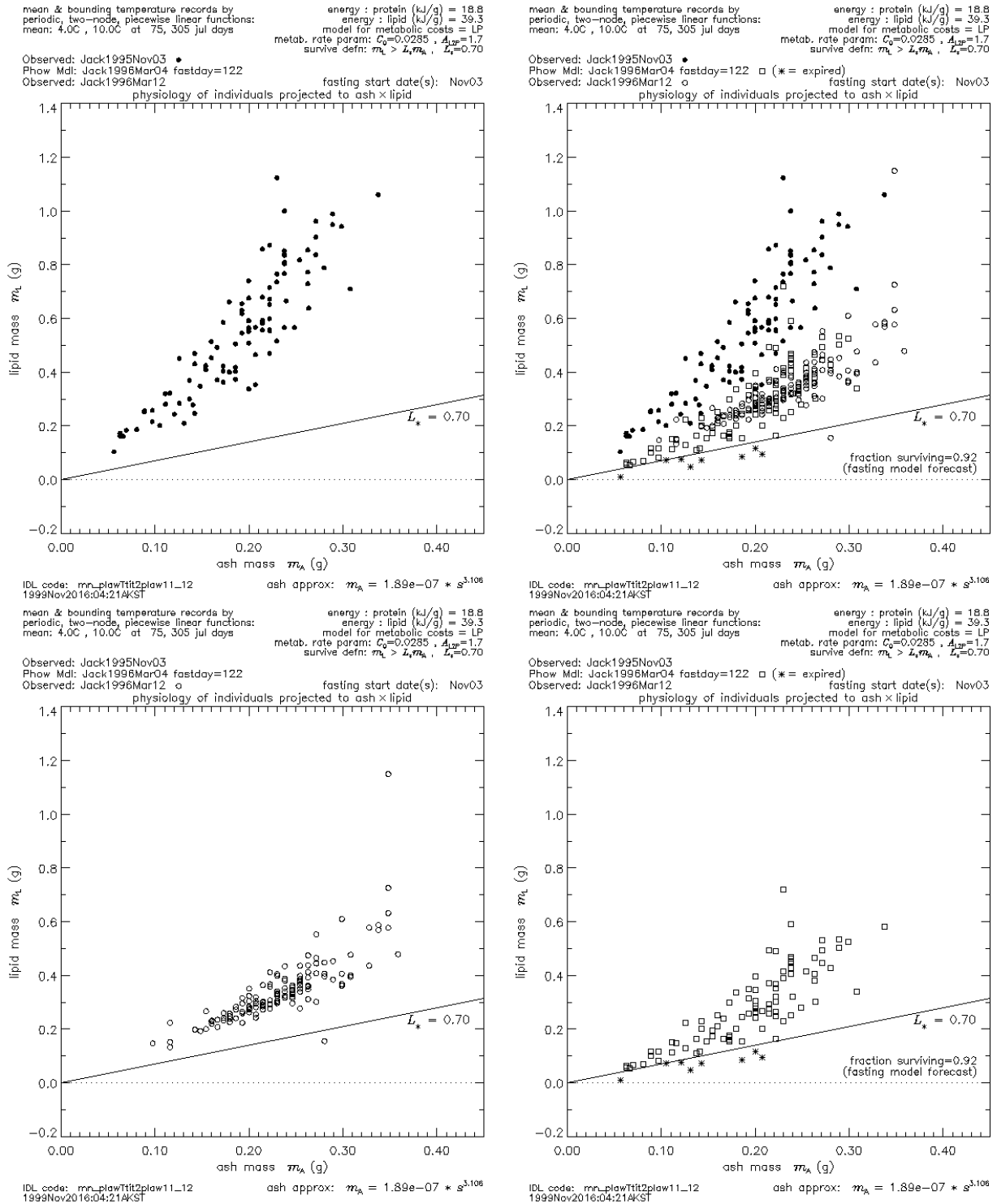


Figure 1.2 Jack Bay 1995 projected to $m_A \times m_L$.

Jack Bay 1995 $m_A \times m_P$ The same FEQs used for the projection to the $m_A \times m_L$ plane apply with only minor change to the projection to the $m_A \times m_P$ plane. However, from the “Concise User’s Reference” we know that the two projections to $m_A \times m_P$ and to $m_P \times m_L$ are relevant only for the assessment of the physiological response model and are not relevant for the survival outcome under the model assumptions for protein use relative to lipid. This is due to the result regarding the partitioning of \mathcal{P} into \mathcal{P}^\square and \mathcal{P}^* described in the “Calibration Reference”; no evidence has been found for any dependence of the partitioning on m_P . Consequently, any revision in the utilization of protein in the manner specified in the model will simply be compensated for by the necessary change in the constant coefficient for metabolic energy requirement when the model is calibrated against experimentally determined changes in lipid and in the occurrence of mortality. Although there is the separate interest in the realism of the physiology model, the realism for protein utilization is not necessary if the assumption is retained that

$$\frac{dm_P}{dt} = A_{L2P} \frac{dm_L}{dt} \quad \text{where } A_{L2P} \text{ is a constant} \quad (1.10)$$

The utilization of m_P *would* be a factor for survival if the assumption in (1.10) were changed to something other than linear.

There is, however, a use for the following assessment beyond the realism of the physiology model. The difference between the spring observations and the spring simulations for protein are conjectured to be more sensitive to the occurrence of winter or spring feeding than the lipid utilization. We shall see in the tests that high survival occurs with larger errors in the estimates for protein usage. The conjecture is then that feeding will offset preferentially the use of protein, leaving any intake shortfall to be covered by lipid reserves. With these qualifiers and conjectures we can return to the Final Exam Questions for the projection to $m_A \times m_P$.

FEQ 1. *Is the spring observation set consistent with the partition $\mathcal{P} = \mathcal{P}^\square \cup \mathcal{P}^*$ defined in (1.9)?*

Grade. Pass. The line $m_P = P_* m_A$ shown in Figure 1.3 is the lower bound for all observed individuals and occurs as the lower bound of those who are in fact alive. All observed individuals having expired are not close to this lower bound. This test is passed as long as there are *no* points below this lower bound regardless of their state.

FEQ 2. *Does the forecast for the alive subset (or its support) reflect an underestimation of the physiology relative to that found in the spring observations?*

Grade. Pass. The forecast for m_P for a given m_A is noticeably lower than what is observed.

FEQ 3. *Is the upper bound for m_A in the spring sample set no greater than that for the fall initial conditions?*

FEQ 4. *Does the support of the spring observed distribution reflect the change in support forecast by fasting losses, in particular, does the lower bound for m_A change between fall and spring in a manner consistent with the simulation?*

Grade for 3 and 4. This is the same question as in the $m_A \times m_L$ projection for the issue is solely the change in the domain for m_A .

FEQ 5. *Is the support for the spring observation sample set essentially the same as the support of the alive set from the simulation except for a translation in the direction of the m_L coordinate?*

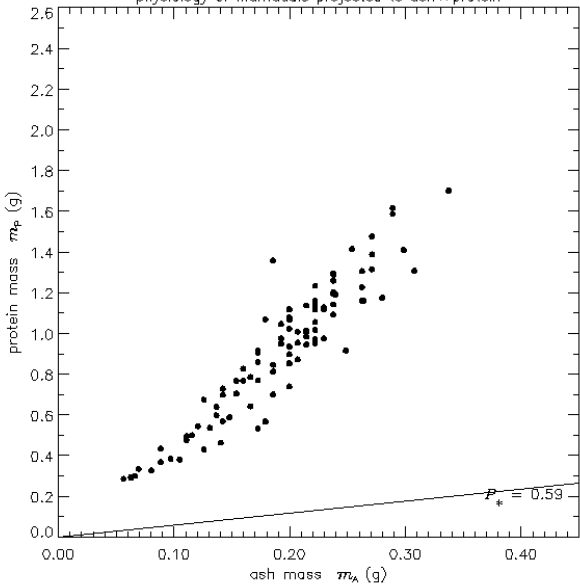
Grade. No. The difference is beyond a translational offset, i.e., a zeroth order error. It is better characterized as a linear scaling. This difference suggests either feeding or the inadequacy of the linear assumption for relative use of lipid versus protein.

FEQ 6. *Is the support of the spring observation sample set the same as the support of the alive set from the simulation?*

Grade. No, fail for $m_A \times m_P$.

mean & bounding temperature records by periodic, two-node, piecewise linear functions: mean: 4.0C , 10.0C at 75, 305 jul days
 energy : protein (kJ/g) = 18.8
 energy : lipid (kJ/g) = 39.3
 model for metabolic costs = LP
 metab. rate param: $C_p=0.0285$, $A_{sp}=1.7$
 survive defn: $m_L > L, m_A$, $L_p=0.70$

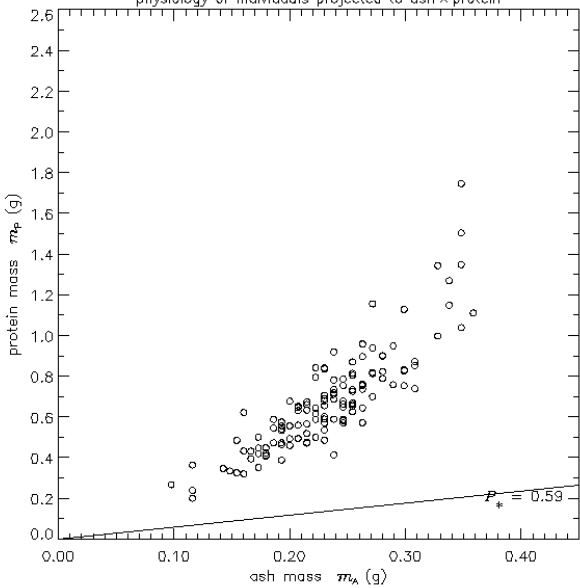
Observed: Jack1995Nov03 •
 Phow Mdl: Jack1996Mar04 fastday=122
 Observed: Jack1996Mar12 ○
 physiology of individuals projected to ash × protein
 fasting start date(s): Nov03



IDL code: mn_plawTtit2plaw11_12
 1999Nov2016:04:21AKST
 ash approx: $m_A = 1.89e-07 * s^{3.106}$

mean & bounding temperature records by periodic, two-node, piecewise linear functions: mean: 4.0C , 10.0C at 75, 305 jul days
 energy : protein (kJ/g) = 18.8
 energy : lipid (kJ/g) = 39.3
 model for metabolic costs = LP
 metab. rate param: $C_p=0.0285$, $A_{sp}=1.7$
 survive defn: $m_L > L, m_A$, $L_p=0.70$

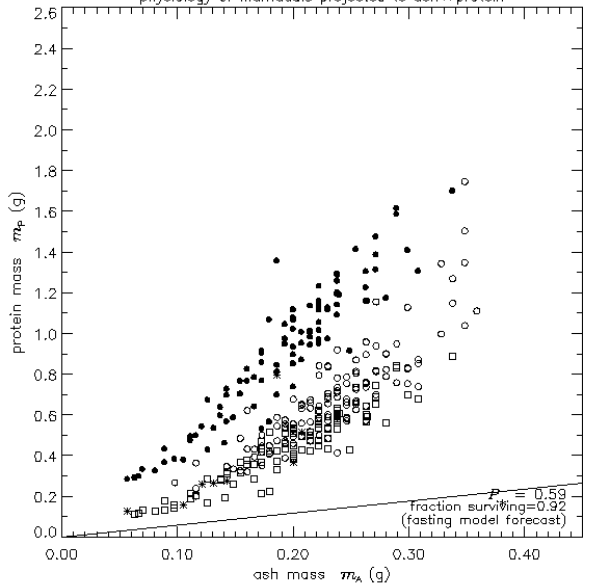
Observed: Jack1995Nov03 •
 Phow Mdl: Jack1996Mar04 fastday=122
 Observed: Jack1996Mar12 ○
 physiology of individuals projected to ash × protein
 fasting start date(s): Nov03



IDL code: mn_plawTtit2plaw11_12
 1999Nov2016:04:21AKST
 ash approx: $m_A = 1.89e-07 * s^{3.106}$

mean & bounding temperature records by periodic, two-node, piecewise linear functions: mean: 4.0C , 10.0C at 75, 305 jul days
 energy : protein (kJ/g) = 18.8
 energy : lipid (kJ/g) = 39.3
 model for metabolic costs = LP
 metab. rate param: $C_p=0.0285$, $A_{sp}=1.7$
 survive defn: $m_L > L, m_A$, $L_p=0.70$

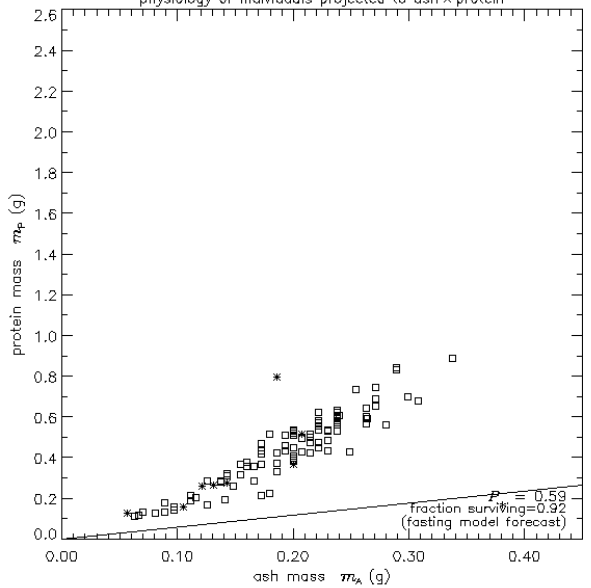
Observed: Jack1995Nov03 •
 Phow Mdl: Jack1996Mar04 fastday=122 □ (* = expired)
 Observed: Jack1996Mar12 ○
 physiology of individuals projected to ash × protein
 fasting start date(s): Nov03



IDL code: mn_plawTtit2plaw11_12
 1999Nov2016:04:21AKST
 ash approx: $m_A = 1.89e-07 * s^{3.106}$

mean & bounding temperature records by periodic, two-node, piecewise linear functions: mean: 4.0C , 10.0C at 75, 305 jul days
 energy : protein (kJ/g) = 18.8
 energy : lipid (kJ/g) = 39.3
 model for metabolic costs = LP
 metab. rate param: $C_p=0.0285$, $A_{sp}=1.7$
 survive defn: $m_L > L, m_A$, $L_p=0.70$

Observed: Jack1995Nov03 •
 Phow Mdl: Jack1996Mar04 fastday=122 □ (* = expired)
 Observed: Jack1996Mar12 ○
 physiology of individuals projected to ash × protein
 fasting start date(s): Nov03



IDL code: mn_plawTtit2plaw11_12
 1999Nov2016:04:21AKST
 ash approx: $m_A = 1.89e-07 * s^{3.106}$

Figure 1.3 Jack Bay 1995 projected to $m_A \times m_P$.

Jack Bay 1995 $m_P \times m_L$ There is only a single FEQ for the projection to $m_P \times m_L$.

FEQ 7. In $m_P \times m_L$ does the spring observed set reflect the assumed linear relationship between the rates of consumption of protein and lipid, $\frac{dm_P}{dt} = A_{L2P} \frac{dm_L}{dt}$, where $A_{L2P} = 1.7$?

Grade. Fair. The simulation and the observation for spring differ since the simulated loss for m_L conforms better to observations whereas the simulation for protein conforms less well.

With the foregoing having established a “grading template,” we can address all three projections at one time for the remaining four site-year test cases.

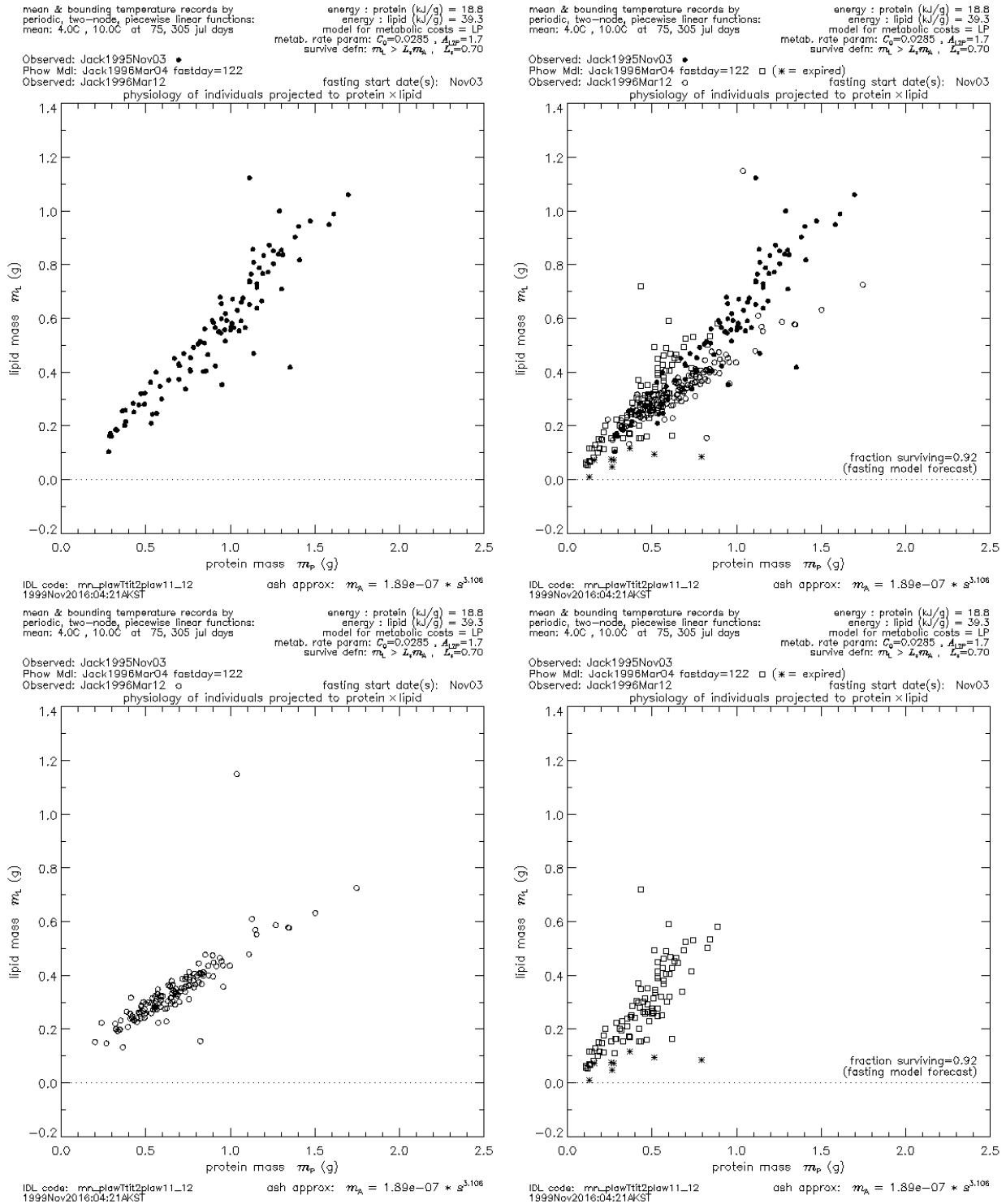


Figure 1.4 Jack Bay 1995 projected to $m_P \times m_L$.

2.1.6 Test results for Simpson Bay 1995

The FEQs are considered for all three projections as a group.

FEQ 1. *Is the spring observation set consistent with the partition $\mathcal{P} = \mathcal{P}^\square \cup \mathcal{P}^*$ defined by $\mathcal{P}^\square = \{ (m_P, m_L, m_A, m_W) : m_L > L_* m_A, L_* = 0.70 \}$*

Grade. Pass.

FEQ 2. *Does the forecast for the alive subset (or its support) reflect an underestimation of the physiology relative to that found in the spring observations?*

Grade. Pass, for both m_L and m_P , with m_P significantly underestimated by the simulation.

FEQ 3. *Is the upper bound for m_A in the spring sample set no greater than that for the fall initial conditions?*

Grade. Pass. The simulation forecasts survival to be 0.64. The lower right panel shows that the third of the fall initial population lost to starvation is from the lower third of the interval of support for the m_A coordinate. It is reasonable to expect the sample distribution to shift as shown in the spring observations. The change in the upper bound for m_A of less than 10% seems not sufficient to challenge assumption A1.

FEQ 4. *Does the support of the spring observed distribution reflect the change in support forecast by fasting losses, in particular, does the lower bound for m_A change between fall and spring in a manner consistent with the simulation?*

Grade. Pass. The loss of one-third of the population from the lower third of the interval of support for m_A is consistent with the spring observations.

FEQ 5. *Is the support for the spring observation sample set essentially the same as the support of the alive set from the simulation except for a translation in the direction of the m_L coordinate?*

Grade. Modest for m_L , poor for m_P . The difference is greater than a simple translation of the simulation. For m_P the difference is beyond a linear scaling of the m_P coordinate. There is, in addition, a spreading of the support in the directions of the m_L and m_P coordinates. There is nothing in the fasting process that can widen the support in this manner, hence one is forced to look to feeding that is non-uniform within the site. Nevertheless, the similarity between the supports for observed and simulated *alive* in the $m_A \times m_L$ plane is reasonable whereas it is less so for the $m_A \times m_P$ plane. The difference between supports projected to $m_A \times m_P$ is significantly more than was the case for Jack Bay. Recall that the difference in $m_A \times m_P$ does not effect the survival estimates.

FEQ 6. *Is the support of the spring observation sample set the same as the support of the alive set from the simulation?*

Grade. Fair for $m_A \times m_L$, No for $m_A \times m_P$.

FEQ 7. In $m_P \times m_L$ does the spring observed set reflect the assumed linear relationship between the rates of consumption of protein and lipid, $\frac{dm_P}{dt} = A_{L2P} \frac{dm_L}{dt}$, where $A_{L2P} = 1.7$?

Grade. The simulation overestimates the use of protein relative to lipid.

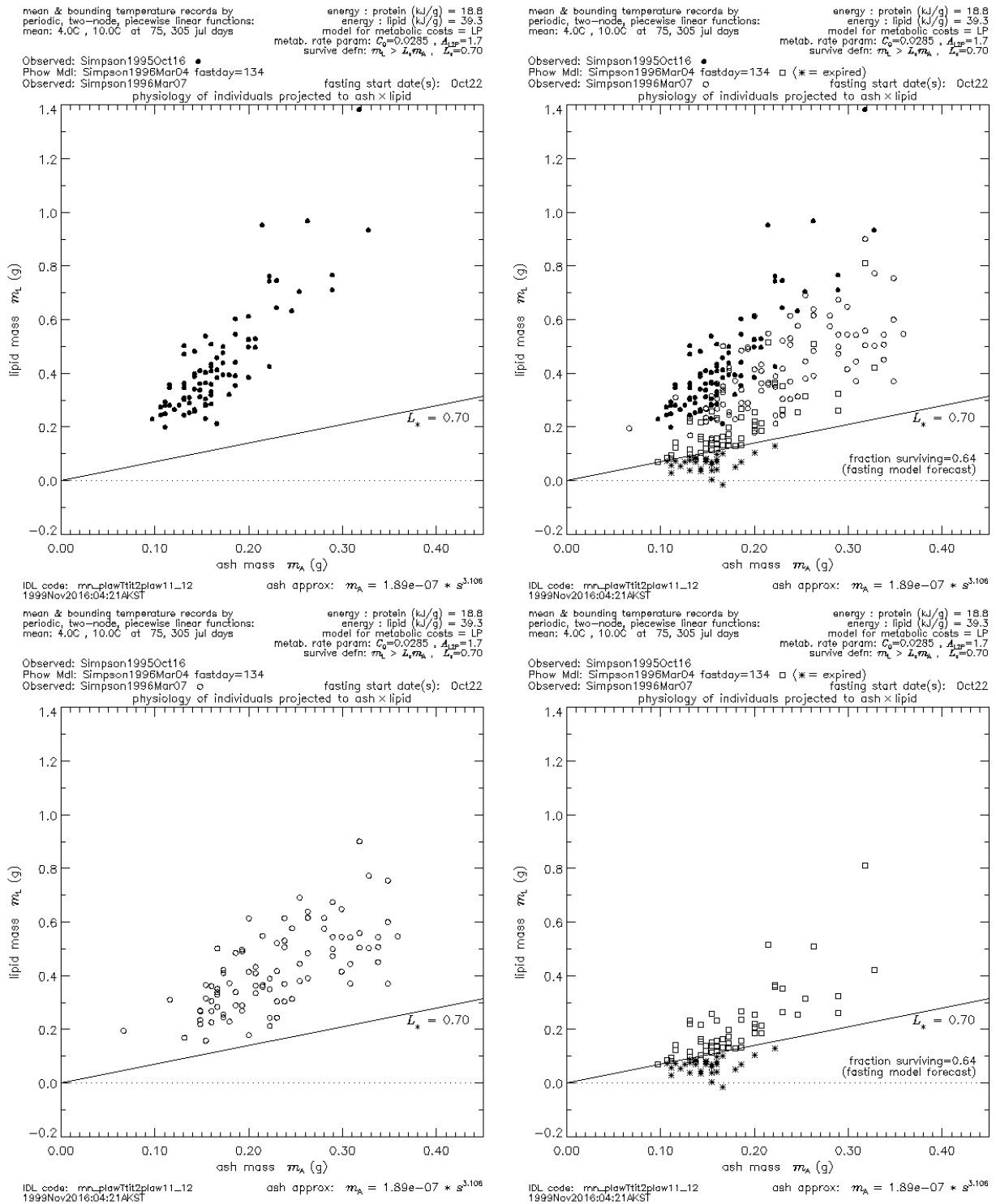


Figure 1.5 Simpson Bay 1995 projected to $m_A \times m_L$.

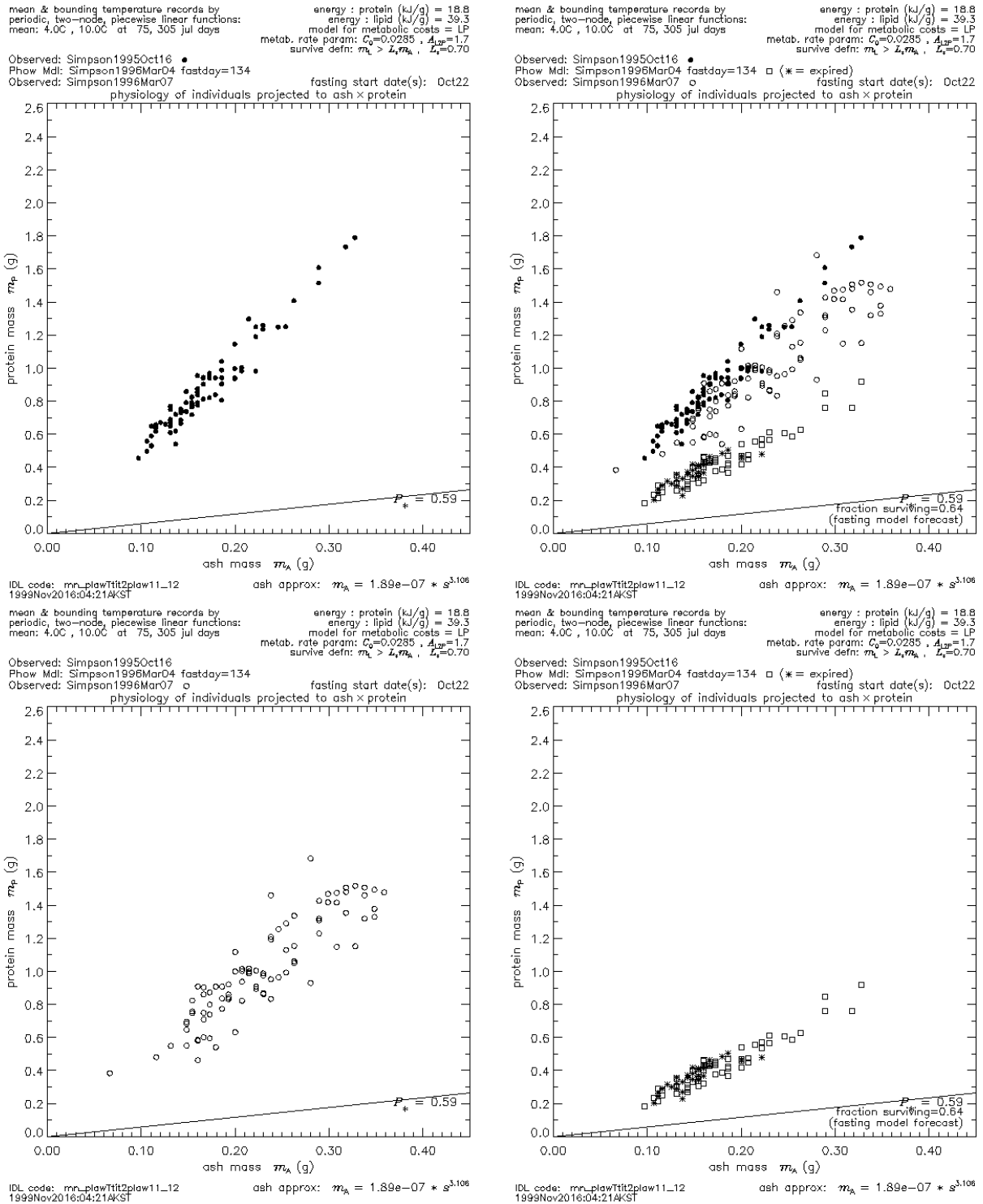


Figure 1.6 Simpson Bay 1995 projected to $m_A \times m_P$.

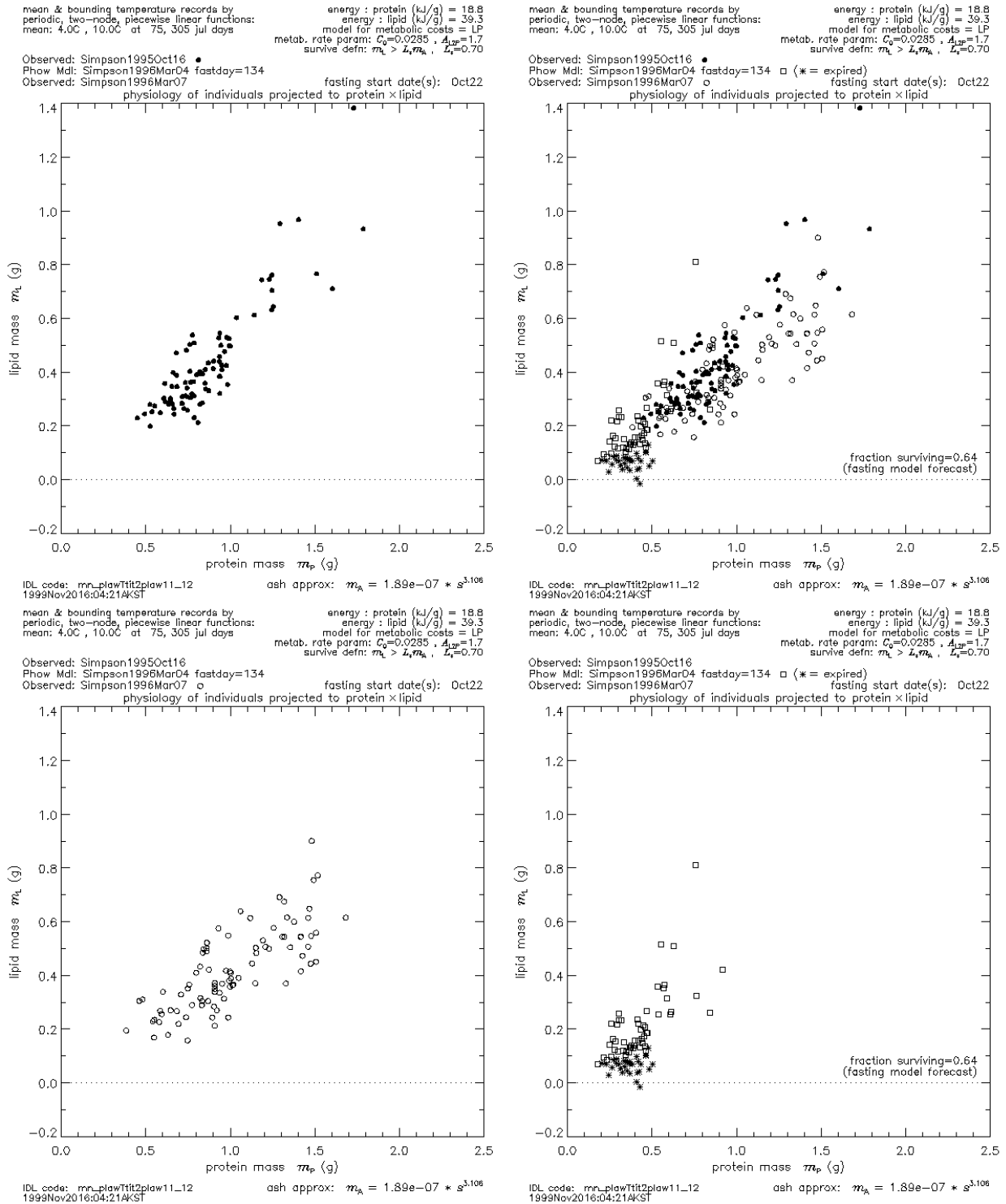


Figure 1.7 Simpson Bay 1995 projected to $m_P \times m_L$.

2.1.7 Test results for Simpson Bay 1996

For Simpson Bay 1996 and 1997 the survival from the simulations are low relative to the other three site-years, 0.18 and 0.052 respectively. We find that in these two cases—cases wherein the outcome is in correspondence with the model assumptions for extreme conditions—the correspondence between spring observations and simulations for m_P is now much better. The correspondence is essentially equal to that for m_L . In the fifth site-year the situation returns to a high survival and the correspondence for m_P similarly returns to the poorer correspondence shown by Simpson Bay 1995 and by Jack Bay 1995.

FEQ 1. *Is the spring observation set consistent with the partition $\mathcal{P} = \mathcal{P}^\square \cup \mathcal{P}^*$ defined by $\mathcal{P}^\square = \{ (m_P, m_L, m_A, m_W) : m_L > L_* m_A, L_* = 0.70 \}$*

Grade. Pass.

FEQ 2. *Does the simulation forecast for the alive subset (or its support) underestimate the physiology relative to that found in the spring observations?*

Grade. Pass. For both m_L and m_P there is noteworthy correspondence between spring observations and the *alive* set from the simulation.

FEQ 3. *Is the upper bound for m_A in spring observations no greater than that for fall?*

Grade. Pass, with allowances for the fact that 82% of the population establishing the fall initial conditions is lost by spring. This loss makes the comparison between simulation survivors and those few in the spring observation set—only 12 in the observation sample set—difficult. The upper bound for spring observations is increased by approximately 20% over that for fall. The simulation survivors at the upper bound lie in the middle of the interval of support for the m_A coordinate for the majority of the spring observation set.

FEQ 4. *Does the support of the spring observed distribution reflect the change in support forecast by fasting mortality losses?*

Grade. Pass. The losses are forecast over an interval of m_A which in the spring observation is essentially lacking members. However, the forecast is not for total loss. The small size of the spring sample cannot be neglected. There is, remarkably one member of the spring observed set with m_A value at the lower end of the simulation range with negligible fasting mortality.

FEQ 5. *Is the support for the spring observation sample set in $m_A \times m_L$ and in $m_A \times m_P$ essentially the same as the support of the *alive* set from the simulation except for a translation in the direction of the m_L or m_P coordinates?*

FEQ 6. *Is the support of the spring observation sample set the same as the support of the *alive* set from the simulation?*

Grade. Pass for both 5 and 6, with allowances as above and with no offset required. This is most readily seen in the upper right overlay panel for both $m_A \times m_P$ and $m_A \times m_L$.

FEQ 7. In $m_P \times m_L$ does the spring observed set reflect the assumed linear relationship between the rates of consumption of protein and lipid, $\frac{dm_P}{dt} = A_{L2P} \frac{dm_L}{dt}$, where $A_{L2P} = 1.7$?

Grade. Pass, with the allowances above. The scenario of low survival in this case has indications of total protein use relative to lipid use consistent with the value $A_{L2P} = 1.7$.

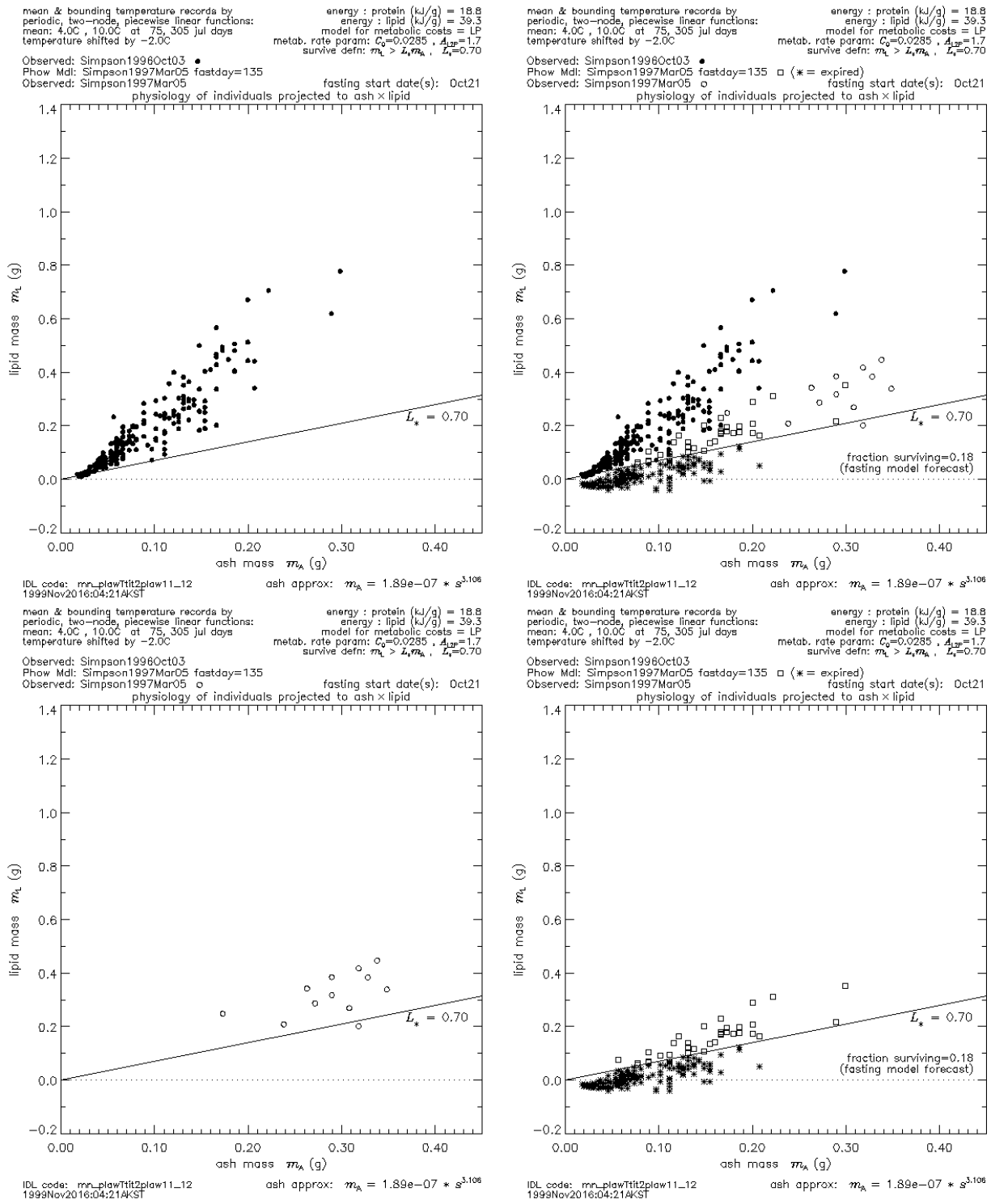


Figure 1.8 Simpson Bay 1996 projected to $m_A \times m_L$.

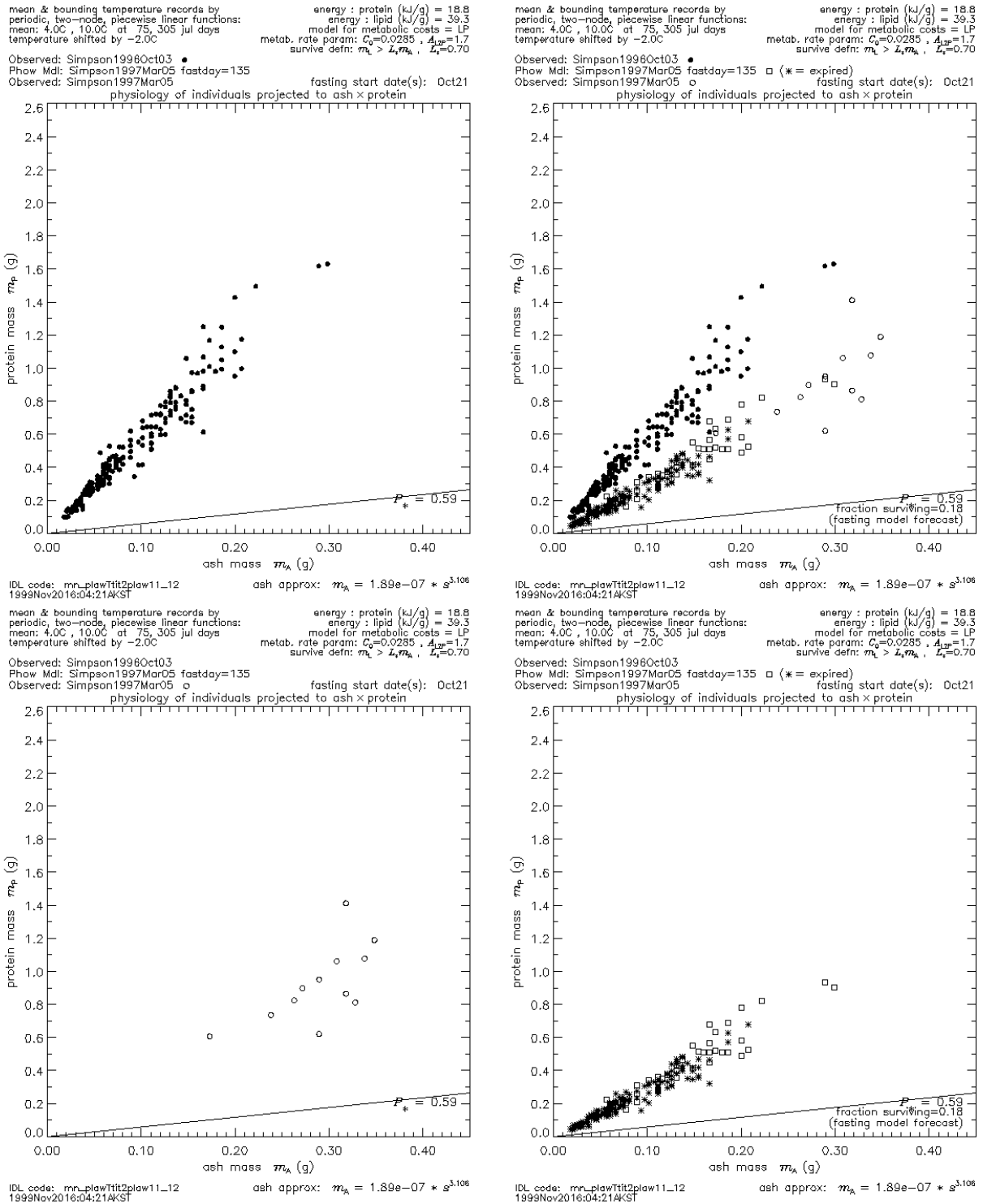


Figure 1.9 Simpson Bay 1996 projected to $m_A \times m_P$.

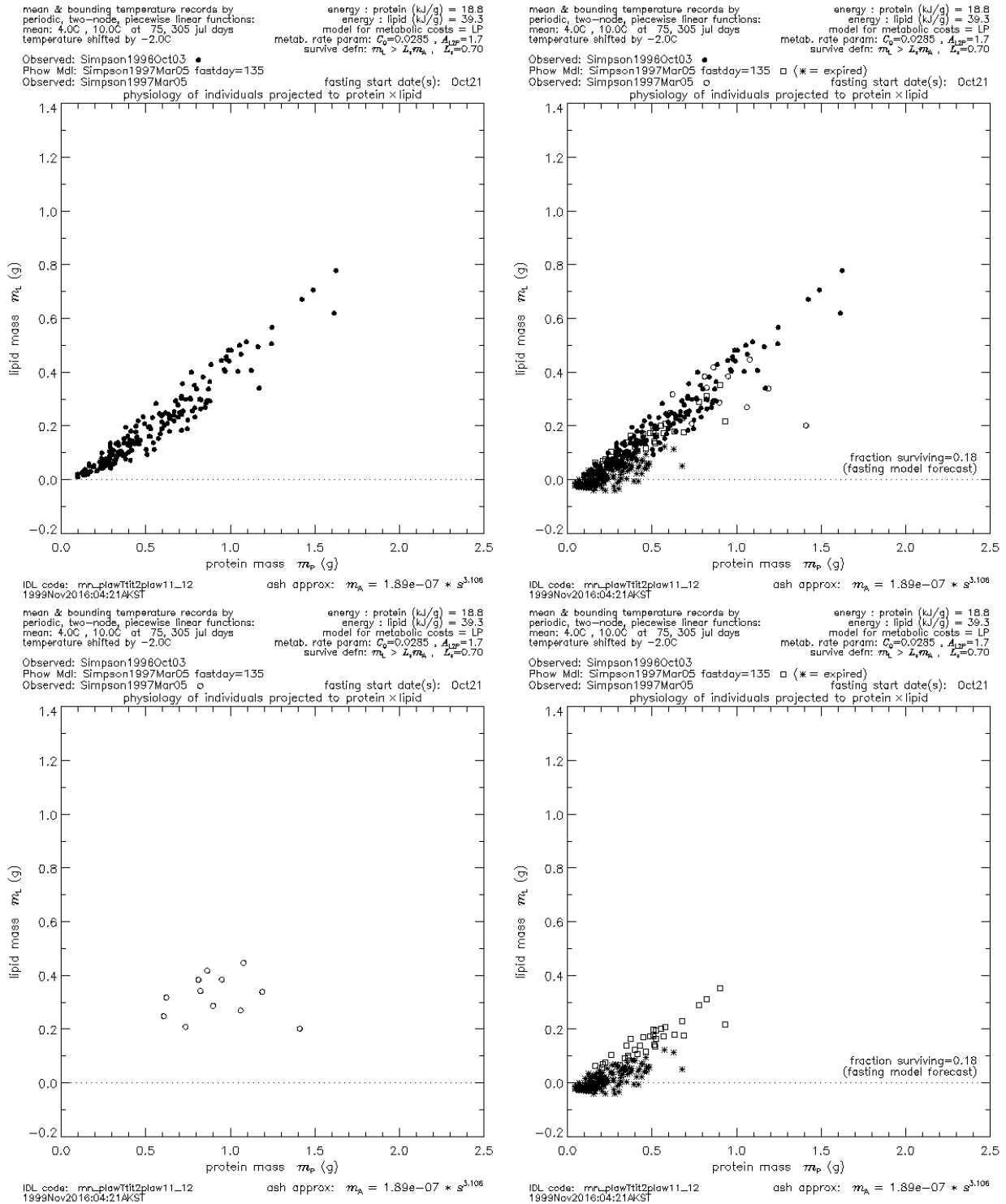


Figure 1.10 Simpson Bay 1996 projected to $m_P \times m_L$.

2.1.8 Test results for Simpson Bay 1997

This site-year has survival that is forecast by the simulation to be 0.052. This is the lowest survival obtained for all simulation tests, including 12 for which there was fall but no spring observation.

FEQ 1. *Is the spring observation set consistent with the partition $\mathcal{P} = \mathcal{P}^\square \cup \mathcal{P}^*$ defined by $\mathcal{P}^\square = \{ (m_P, m_L, m_A, m_W) : m_L > L_* m_A, L_* = 0.70 \}$*

Grade. Pass. In this case we have the first instance of strong field evidence for the merit of the boundary defined by the foregoing definition for \mathcal{P}^\square .

FEQ 2. *Does the simulation forecast for the alive subset (or its support) underestimate the physiology relative to that found in the spring observations?*

Grade. Pass, with allowances for the small size of the spring simulation *alive* set. For both $m_A \times m_L$ and $m_A \times m_P$ there is correspondence between spring observations and the simulations for the *alive* set. This correspondence is noteworthy since it holds equally well for $m_A \times m_P$. For this site-year there is a corroborating survival estimate of 0.08 obtained from the Stokesbury relative density measurements. However, the high losses in the simulation leave the only ten members in the spring *alive* set with which to define the supports. The spring observed sample is, however, quite large.

FEQ 3. *Is the upper bound for m_A in spring observations no greater than that for fall?*

Grade. Pass, with allowances for the few elements in the *alive* set. The upper bounds are within 10% of each other.

FEQ 4. *Does the support of the spring observed distribution reflect the change in support forecast by fasting mortality losses?*

Grade. Pass, with allowances for the small number in the *alive* set. The small *alive* sample size indicates total loss to fasting over an interval of m_A with surviving members in the spring observed sample. This is not inconsistent given the sample size differences.

FEQ 5. *Is the support for the spring observation sample set essentially the same as the support of the *alive* set from the simulation except for a translation in the direction of the m_L coordinate?*

FEQ 6. *Is the support of the spring observation sample set the same as the support of the *alive* set from the simulation?*

Grade. Pass for both 5 and 6 with allowances for the small number in the *alive* set.

FEQ 7. *In $m_P \times m_L$ does the spring observed set reflect the assumed linear relationship between the rates of consumption of protein and lipid, $\frac{dm_P}{dt} = A_{L2P} \frac{dm_L}{dt}$, where $A_{L2P} = 1.7$?*

Grade. Pass, with the allowances. Clearly the support for the observed set in $m_P \times m_L$ is larger than that for the *alive* set, however the *alive* set is easily a subset of the observed set, hence the pass.

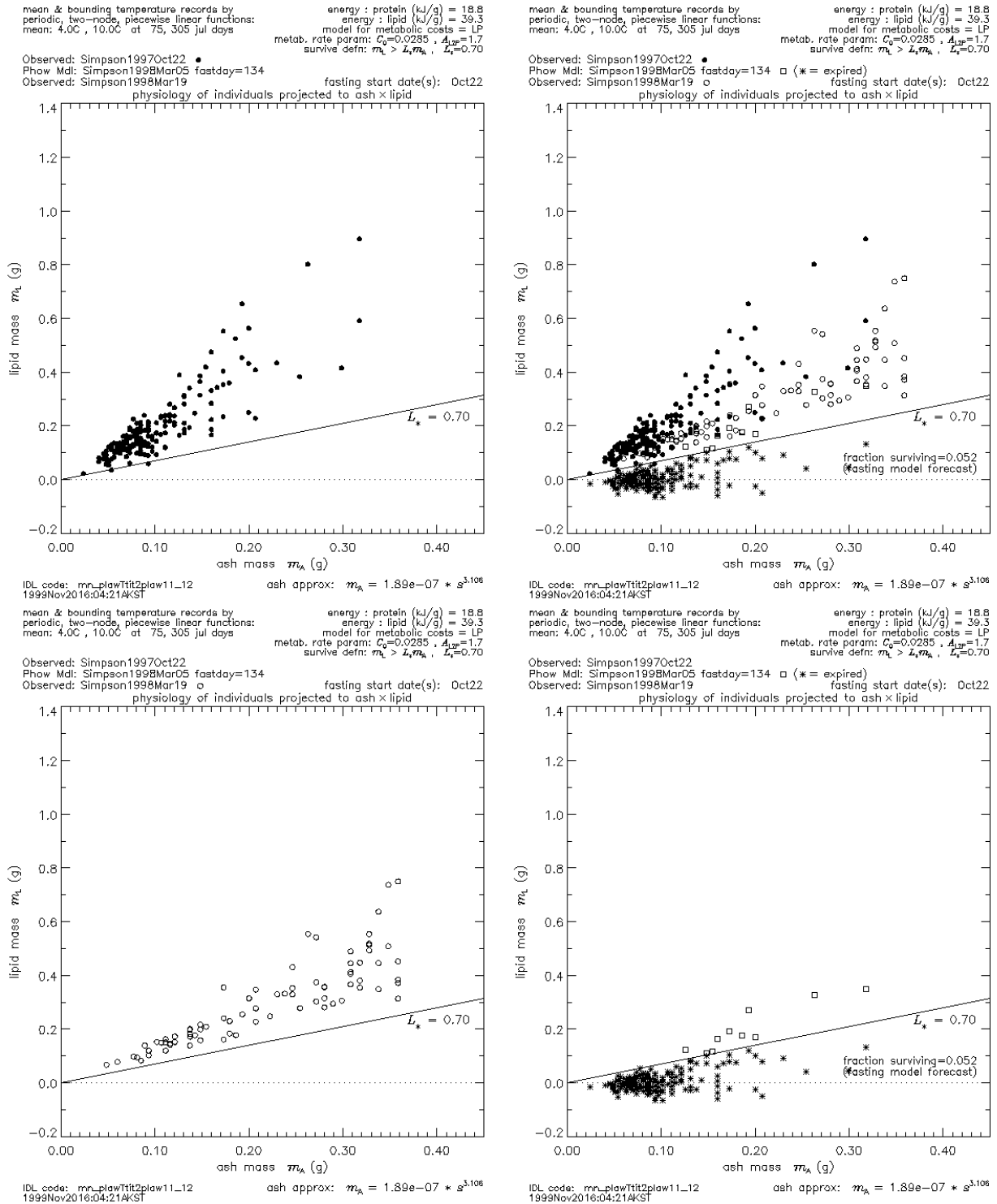


Figure 1.11 Simpson Bay 1997 projected to $m_A \times m_L$.

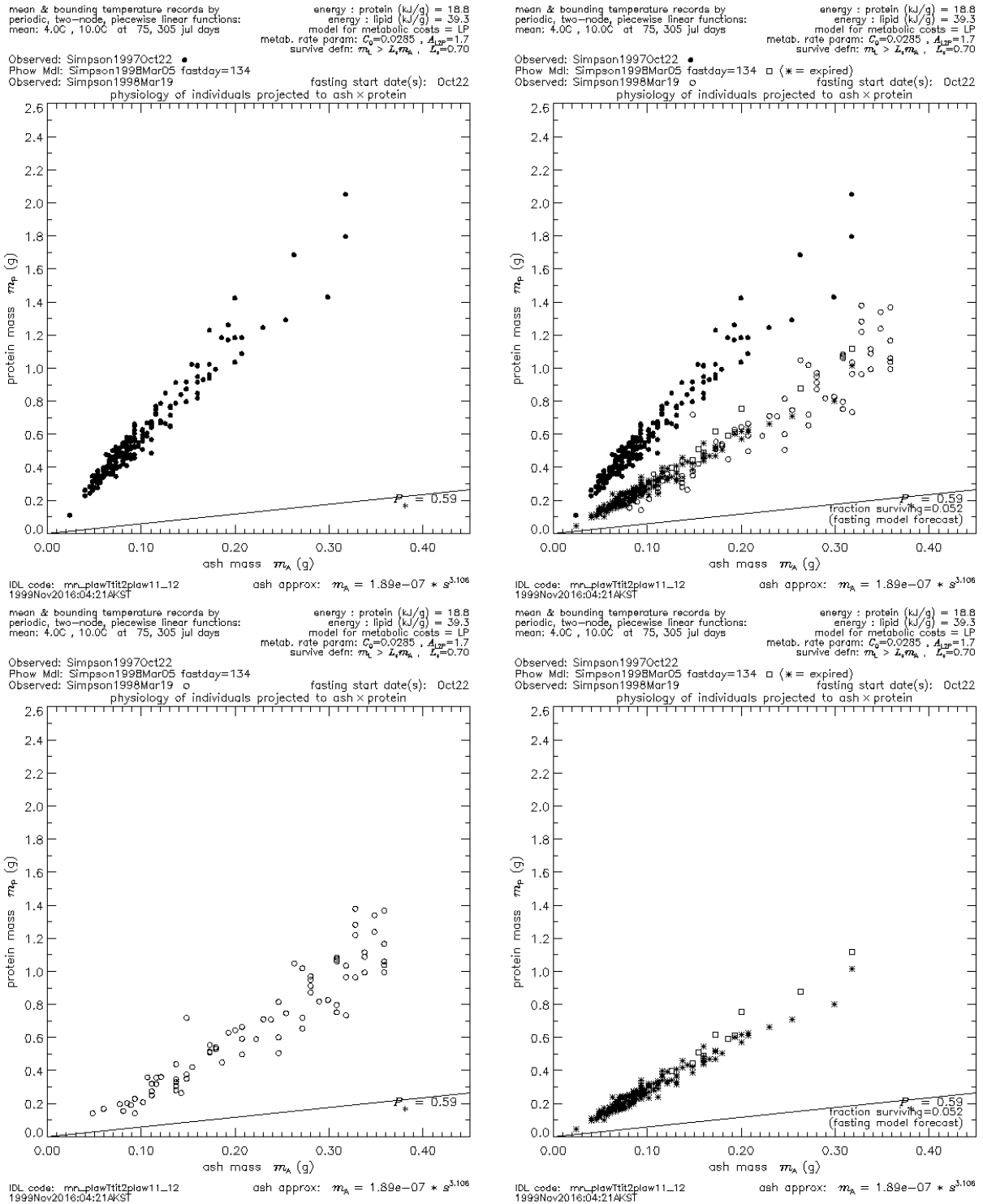


Figure 1.12 Simpson Bay 1997 projected to $m_A \times m_P$.

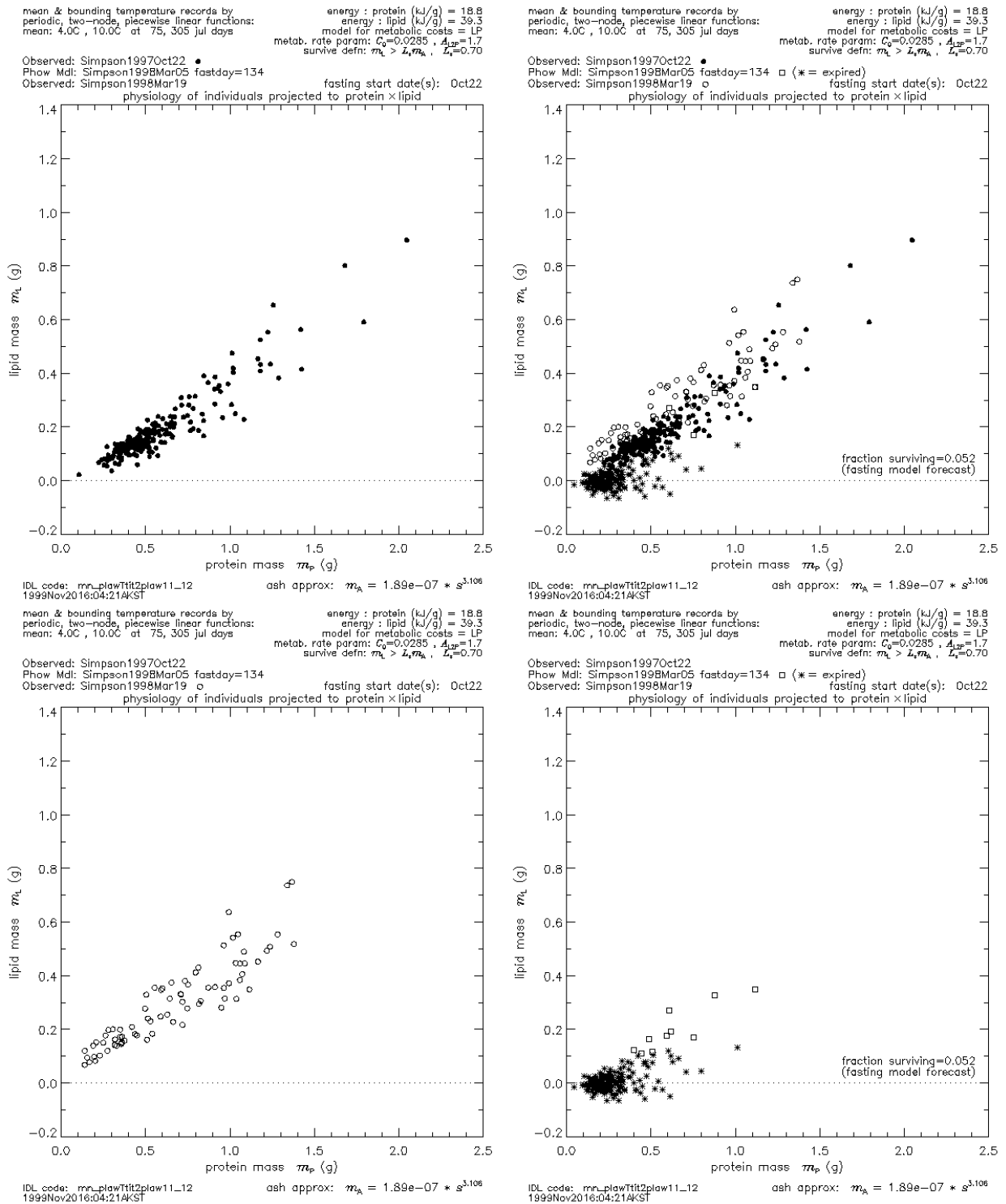


Figure 1.13 Simpson Bay 1997 projected to $m_P \times m_L$.

2.1.9 Test results for Whale Bay 1995

The survival forecast for this site 0.86.

FEQ 1. *Is the spring observation set consistent with the partition $\mathcal{P} = \mathcal{P}^\square \cup \mathcal{P}^*$ defined by $\mathcal{P}^\square = \{ (m_P, m_L, m_A, m_W) : m_L > L_* m_A, L_* = 0.70 \}$*

Grade. Pass. This case is the second case in which there is strong evidence that the partition definition above has merit.

FEQ 2. *Does the simulation forecast for the alive subset (or its support) underestimate the physiology relative to that found in the spring observations?*

Grade. Pass. The simulation estimate is substantially lower than the spring observations for m_P . The estimate is also lower for m_L except possibly at the upper end of the m_A interval of support.

FEQ 3. *Is the upper bound for m_A in spring observations no greater than that for fall?*

Grade. Pass, while noting the upper bound for m_A for spring observations is approximately 20% higher. The spring sample is 19 days after the assumed end of fasting. Although m_P is higher than the simulation forecast and the upper bound is higher, there is no difference for m_L .

FEQ 4. *Does the support of the spring observed distribution reflect the change in support forecast by fasting mortality losses?*

Grade. Pass. Only a small impact is forecast and the spring observations are consistent with the forecast.

FEQ 5. *Is the support for the spring observation sample set essentially the same as the support of the alive set from the simulation except for a translation in the direction of the m_L coordinate?*

FEQ 6. *Is the support of the spring observation sample set the same as the support of the alive set from the simulation?*

Grade. Pass for 5 and 6 for $m_A \times m_L$, fail for $m_A \times m_P$. The support in $m_A \times m_P$ is largely unchanged between fall and spring for the observed sets.

FEQ 7. *In $m_P \times m_L$ does the spring observed set reflect the assumed linear relationship between the rates of consumption of protein and lipid, $\frac{dm_P}{dt} = A_{L2P} \frac{dm_L}{dt}$, where $A_{L2P} = 1.7$?*

Grade. The simulation overestimates the use of protein relative to lipid.

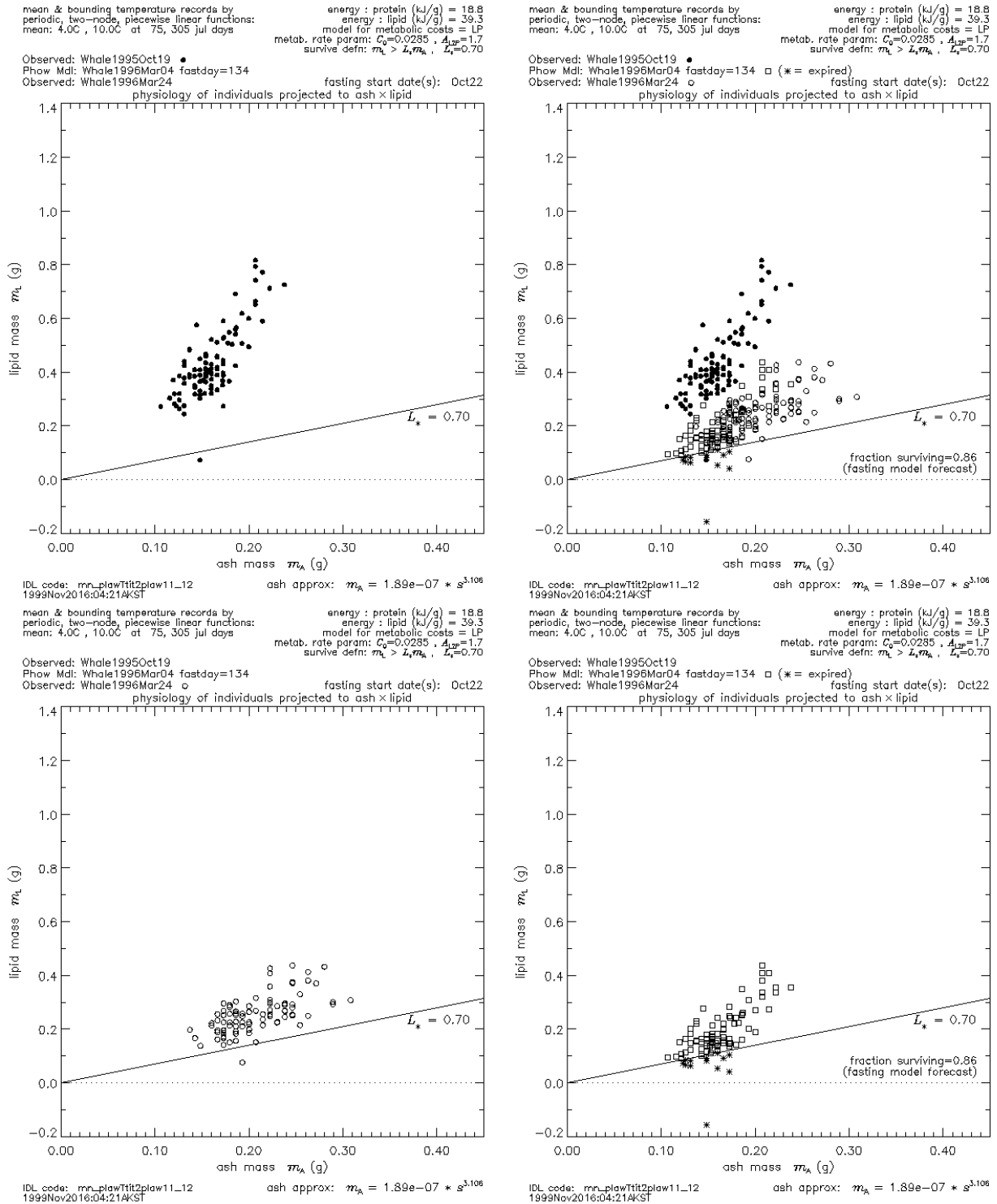


Figure 1.14 Whale Bay 1995 projected to $m_A \times m_L$.

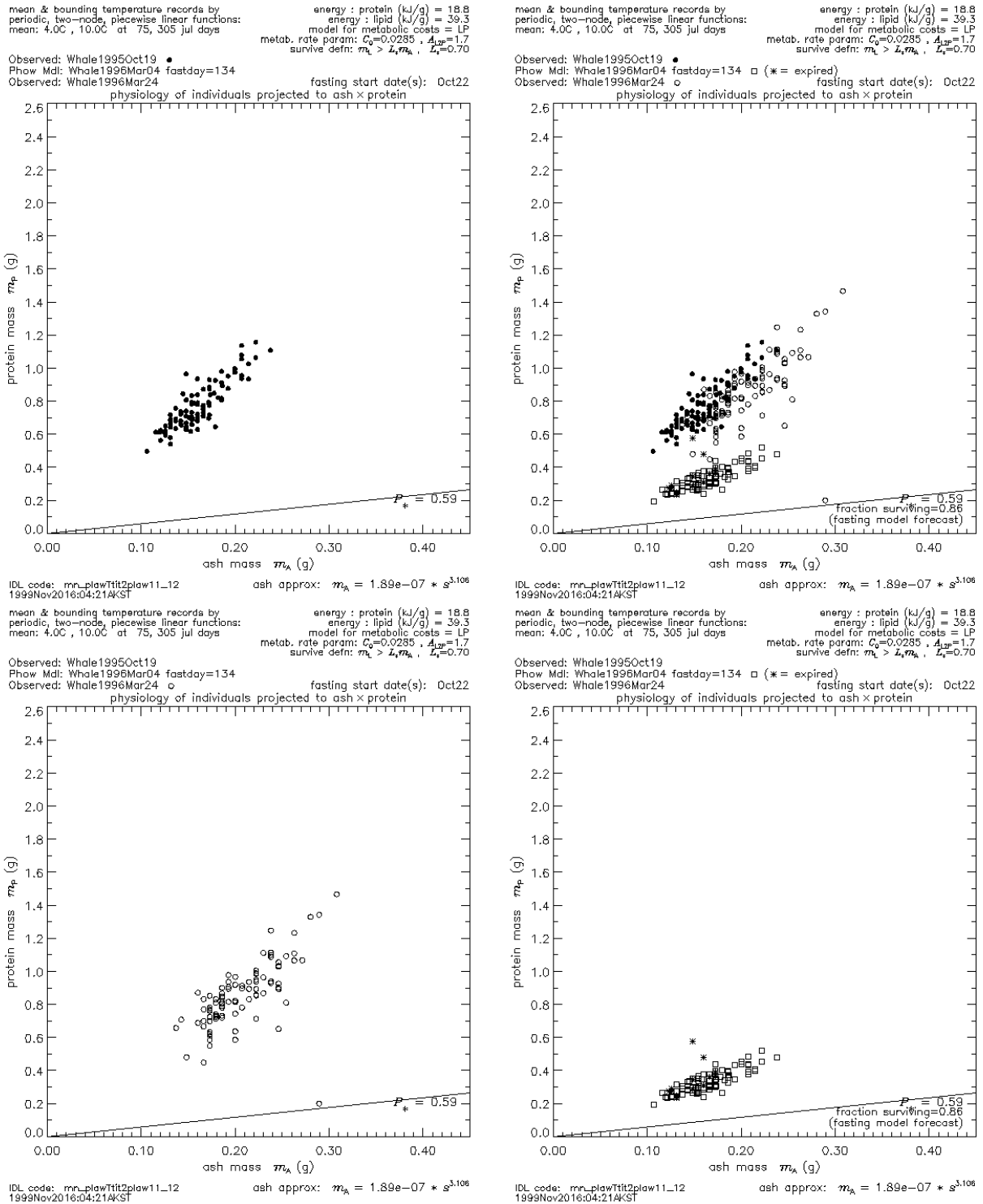


Figure 1.15 Whale Bay 1995 projected to $m_A \times m_P$.

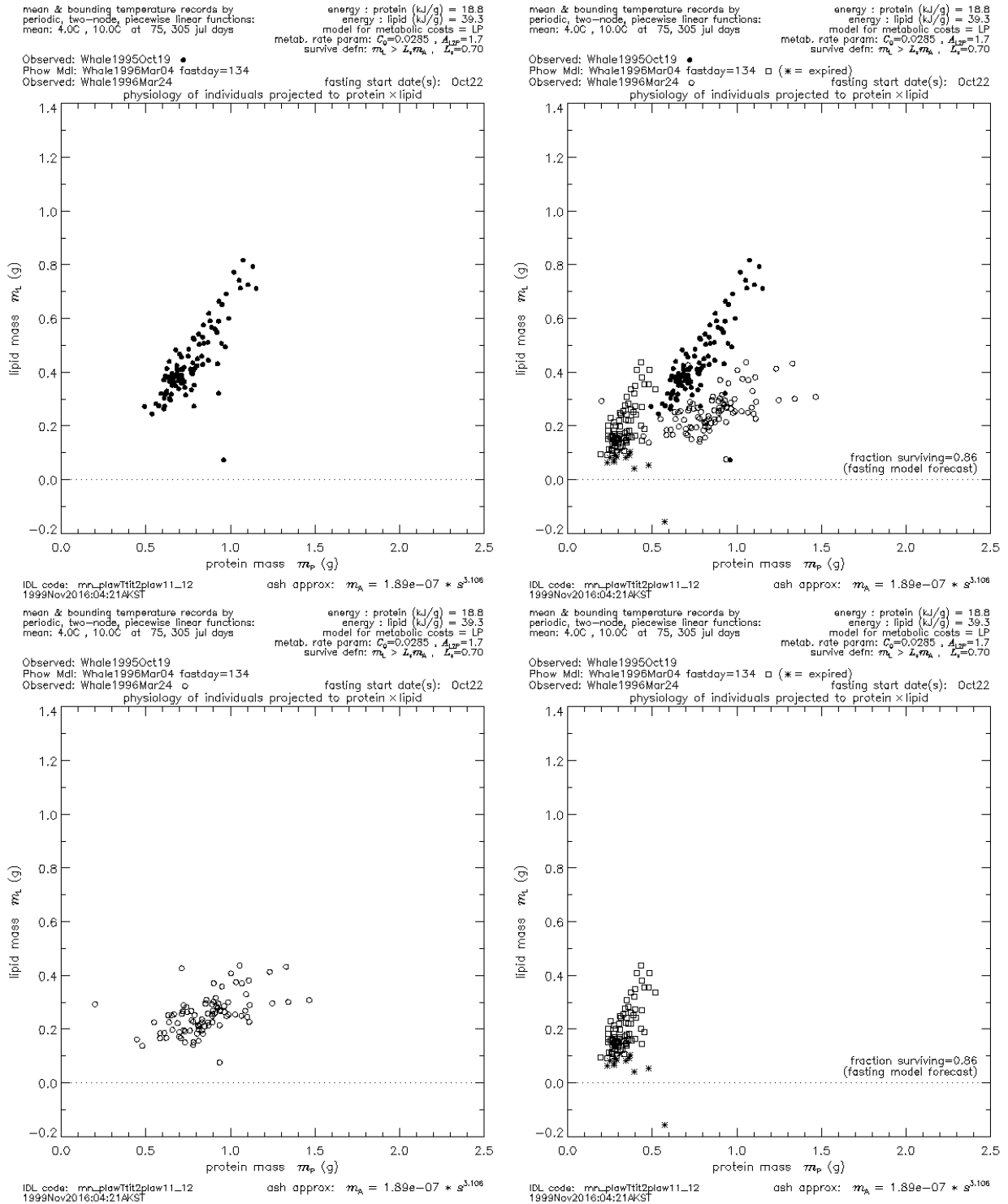


Figure 1.16 Whale Bay 1995 projected to $m_P \times m_L$.

2.2 Validation tests using relative density survival estimates

This section presents the results of comparing the winter survival estimates based upon the Stokesbury relative density measurements to those computed from the winter fasting model. Table 2.1 shows the values for the survival estimates from both sources and Figure 2.1 shows how the fasting survival estimate develops over the course of the winter. From the figure one can immediately assess the impact of errors in start and stop times for fasting and also the effect of errors in estimates of winter water temperature. In this way one has a functional basis for assigning confidence to the survival estimates presented in the table.

Table 2.1 Survival estimates used for validation testing
relative density measurements due to JHGH project [NBF⁺99]

site	fall sample date			fast duration	survival estimates by source		
	year	mon	da		fasting model simulation	relative density measurement spring	relative density measurement fall (age-1)
Simpson	1997	Oct	22	134	0.052	0.080	na
Zaikof	1997	Oct	23	133	0.56	0.17	na
Simpson	1996	Oct	03	135	0.18	1.4	0.20
Whale	1996	Oct	07	135	0.86	na	0.99

The fall sample date in Table 2.1 is the date for the initial physiological conditions for the age-0 herring for the indicated site. If the sample date is prior to Julian day 295 (Oct 22 for non-leap years) the conditions were held fixed until Julian day 292 at which time fasting is assumed to begin; otherwise fasting simulation begins on the date of the sample. For purposes of estimating survival in Table 2.1, fasting is assumed to end on Julian day 64 (Mar 05 for non-leap years). With this one obtains the fast durations shown in Table 2.1. In contrast, the time evolution of the model simulated survival in Figure 2.1 does not end at the foregoing presumed end of fasting but continues with total fasting assumed. The survival in Figure 2.1 has the value in Table 2.1 at the “time since start of fasting” corresponding to the fast duration (essentially 135 da) shown in Table 2.1. One sees immediately that only in the most extreme case (e.g., Simpson 1997) is survival materially changed by a 10 day or even 20 day error in the specification of fasting start and stop times. Further, from the “temperature error lemma” of the “Concise User’s Reference” we have seen that a shift in the mean water temperature of +1C has the effect of contracting the graph relative to the start of fasting by the factor 0.947 (a 5.6% decrease). The effect on survival fast day 135 is to reduce the value to what it would otherwise be at day $135 \times 1.056 = 143$. One can check that a +2C mean shift in water temperature (equivalent to a 15 day shift) is of consequence for survival estimation accuracy only in years in which spring survival is 0.2 and lower.

During the same fall monitoring activities that produced the physiology determinations, Stokesbury conducted bay-specific population density assessments. These assessments provide a bay-specific and age-specific relative density value that can be compared across time to estimate year-class survival. (See the JHGH Final Report, Ch 10 of the *SEA* Final Report [NBF⁺99].) Stokesbury conducted the density assessments in the fall and spring but not always for the same sites.

Table 2.1 shows two site-years, Simpson 1997 and Zaikof 1997, having fall and spring relative density assessments for age-0 herring. The survival estimates computed from those assessments are shown

in the table along with the survival estimates from the winter fasting simulations. Two further site-years are shown in Table 2.1, Simpson 1996 and Whale 1996. These two provide additional but less direct validation information by means of comparing the simulated age-0 winter fasting survival with the survival from the relative density assessments for that cohort over the time period of first fall to second fall.

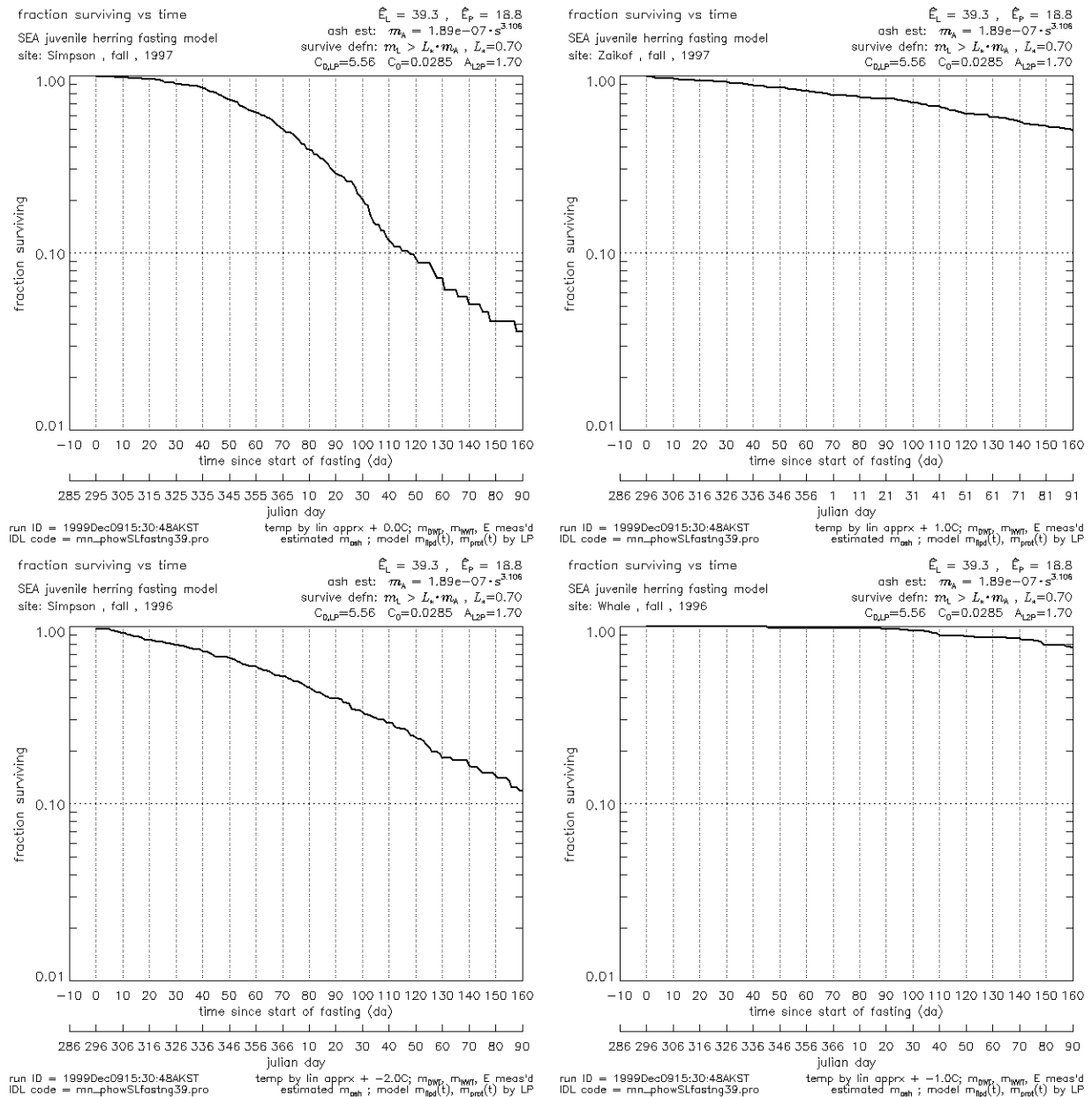


Figure 2.1 Time evolution of age-0 fasting survival for the four site-years of Table 2.1.

Recall that the evaluation of survival comparisons must be considered differently from the physiology comparisons. In the case of the physiology the model design is such that the simulated physiology should be an underestimate of the real-world physiology. For starvation-induced mortality, fasting survival forecasts from simulations are a lower bound for what should occur *due to fasting alone* in the real-world system. However, the *overall* real-world winter survival will have the fasting-only survival as an upper bound: the overall real-world survival can be lower due to predation losses. Therefore one must keep in mind that the simulated winter fasting is a lower bound on the physiology hence a worst case estimate for fasting-only survival, but real-world fasting survival is an upper bound for overall real-world winter survival. Hence, both simulated fasting survival and real-world overall winter survival are bounded above by real-world fasting-only survival. We cannot say more about the relationship between simulated winter fasting survival and real-world winter survival without placing more complete error bounds on the various estimations.

It is, however, a long standing *conjecture* of the juvenile herring model development that the simulated winter fasting survival is indeed a reliable *upper bound* for the overall real-world survival of juvenile herring from their first fall through their first spring as adult herring. In this sense, the survival values in Table 2.1 serve as “best case” survival values for the period from first fall to recruitment. This conjecture is based on the assumption that predation and other losses during the age-1 and age-2 years more than overtake the conservative underestimation of first winter survival from simulations with full fasting during winter.

2.2.1 Simpson Bay 1997

For Simpson 1997 there is the companion validation tests in §2.1 of the fasting model simulation of fall-to-spring change in population physiology. Those companion validation tests were successful albeit qualified by the small number of simulation survivors with which to conduct the comparisons. The validation comparison based on survival is similarly good. The simulation-determined survival estimate of 0.052 is in very good agreement with the relative density survival estimate of 0.080.

2.2.2 Zaikof Bay 1997

The second site-year in Table 2.1 does not have the benefit of a companion validation test for the physiology. No spring 1998 laboratory analysis for age-0 herring was available.

Table 2.1 shows that the survival forecast based solely on fasting is quite high relative to the survival determined by the relative density assessment. Because we have no spring validation datasets for any of the years for Zaikof we cannot say anything regarding any physiological features that are unique to Zaikof that could contribute mortality beyond what is represented in the model. However, we doubt there are any. Figure 2.1 shows that at 0.56 survival the model is very stable with respect to time and temperature parameters. In this sense the survival value of 0.17 from relative density is indeed “significantly” different from 0.56. A change in the survival forecast by that amount requires a major revision of the physiological structure of the initial fall population.

One view is that the relative density, if accurate, is a good illustration of the foregoing “best case” conjecture: in the case of Zaikof 1997 the additional factors for survival already impact the overall real-world survival such that it is lower than the conservative estimate from the total fasting simulation. This scenario is, however, what was expected to occur after the first winter and not to this extent during the first winter. This scenario, however, is consistent with local knowledge

reports that Zaikof Bay is an active feeding area during winter for large marine mammals, so much so that the Bay is an audibly noisy place in January. This report has not been heard for the other bays of this study. Regardless of the origin of the difference, this difference, in conjunction with knowledge of the larval drift population distribution, is a factor to attend to in the design of an implementation plan.

2.2.3 Simpson Bay 1996

Only three site-years have fall-spring relative density assessments for age-0 herring, and the third, Simpson 1996, has the unexpected winter survival estimate of 1.4. However, there is a relative density assessment for Simpson Bay for the following fall which includes a report for the age-1 population. It is that report which is used to obtain the 0.20 survival for the cohort from first fall to second fall.

This case is presented not so much as a validation but as an example. The “best case” conjecture is that the fasting survival forecast will be with high probability be an upper bound for survival from first fall to recruitment. This case illustrates that by one means or another the survival at “second fall” is indeed close to “passing through” the conservative model forecast for fasting related survival.

A corollary is that an implementation plan need not place undue emphasis on a spring monitoring schedule for post-winter age-0. For purposes of tracking the population development the first priority is an annual fall survey in which densities—relative or, preferably, absolute—for age-0 -1 and -2 are separately determined. Anything beyond this is warranted only in the context of very low survival (e.g., Simpson 1997) with prior knowledge that the low survival is acting upon a major fraction of the overall population for that year-class.

2.2.4 Whale Bay 1996

The fourth site-year in Table 2.1 is a much less ambiguous example of the “best case” conjecture. For Whale 1996 there was no spring relative density estimate. There was, however, an estimate for age-1 in the following fall which indicated that there had to have been extremely good first winter survival. Specifically, the estimate for first fall to second fall is 0.99. This estimate, although almost surely an over-estimate, is nevertheless consistent with the survival forecast from the winter fasting model of 0.86. Although the validation is one step removed from the fasting process it nevertheless is an experimental finding that is consistent with the use of the fasting simulation estimate as prescribed by the “best case” conjecture.

2.3 Validation tests using the ADF&G ASA reports

This section presents the full collection of winter survival estimates obtained by applying the current version of the winter fasting model to the 15 fall monitoring datasets provided by the JHGH and FE projects. The totality of all survival estimates, grouped by year, are shown in Table 3.1. The time evolution of the survival from start of fast through fast day 160 is shown in Figures 3.1 through 3.4. This section will not present validation tests but rather is providing the survival forecasts so that others may use these as part of forthcoming analyses whereby the ADF&G ASA reports are established. It is hoped that the ASA analyses will be able to add new and unanticipated insights into the roles of these winter survival estimates in forthcoming adult populations.

Table 3.1 Survival estimates from the winter fasting model

site	fall sample date			fast duration (da)	temperature offset (C)	fasting model survival	Fig
	year	mon	da				
Green	1995	Oct	25	131	+0.0	0.91	3.1
Hogg	1995	Nov	08	117	+0.0	0.071	3.1
Jack	1995	Nov	03	122	+0.0	0.92	3.1
Sawmill	1995	Nov	07	118	+0.0	0.99	3.1
Snug	1995	Nov	03	122	+0.0	0.64	3.2
Simpson	1995	Oct	16	134	+0.0	0.64	3.2
Whale	1995	Oct	19	134	+0.0	0.86	3.2
Zaikof	1995	Oct	20	134	+0.0	0.39	3.2
Eaglek	1996	Oct	00	135	+0.0	0.76	3.3
Simpson	1996	Oct	03	135	-2.0	0.18	3.3
Whale	1996	Oct	07	135	-1.0	0.86	3.3
Zaikof	1996	Oct	09	135	+0.0	0.56	3.3
Eaglek	1997	Oct	26	130	+1.0	0.95	3.4
Simpson	1997	Oct	22	134	+0.0	0.052	3.4
Zaikof	1997	Oct	23	133	+1.0	0.56	3.4

The Fig column in the table identifies in which of the following figures is the display of the time evolution of the survival. The temperature offset is the shift used in the 2-node linear element approximation of the water column temperature.

The figures contain four site-years each except for Figure 3.4; there is no fall information for Whale Bay 1997. For Figure 3.2 Snug 1995 appears in the position that is occupied by Eaglek in Figures 3.3 and 3.4. There is no fall information for Eaglek 1995.

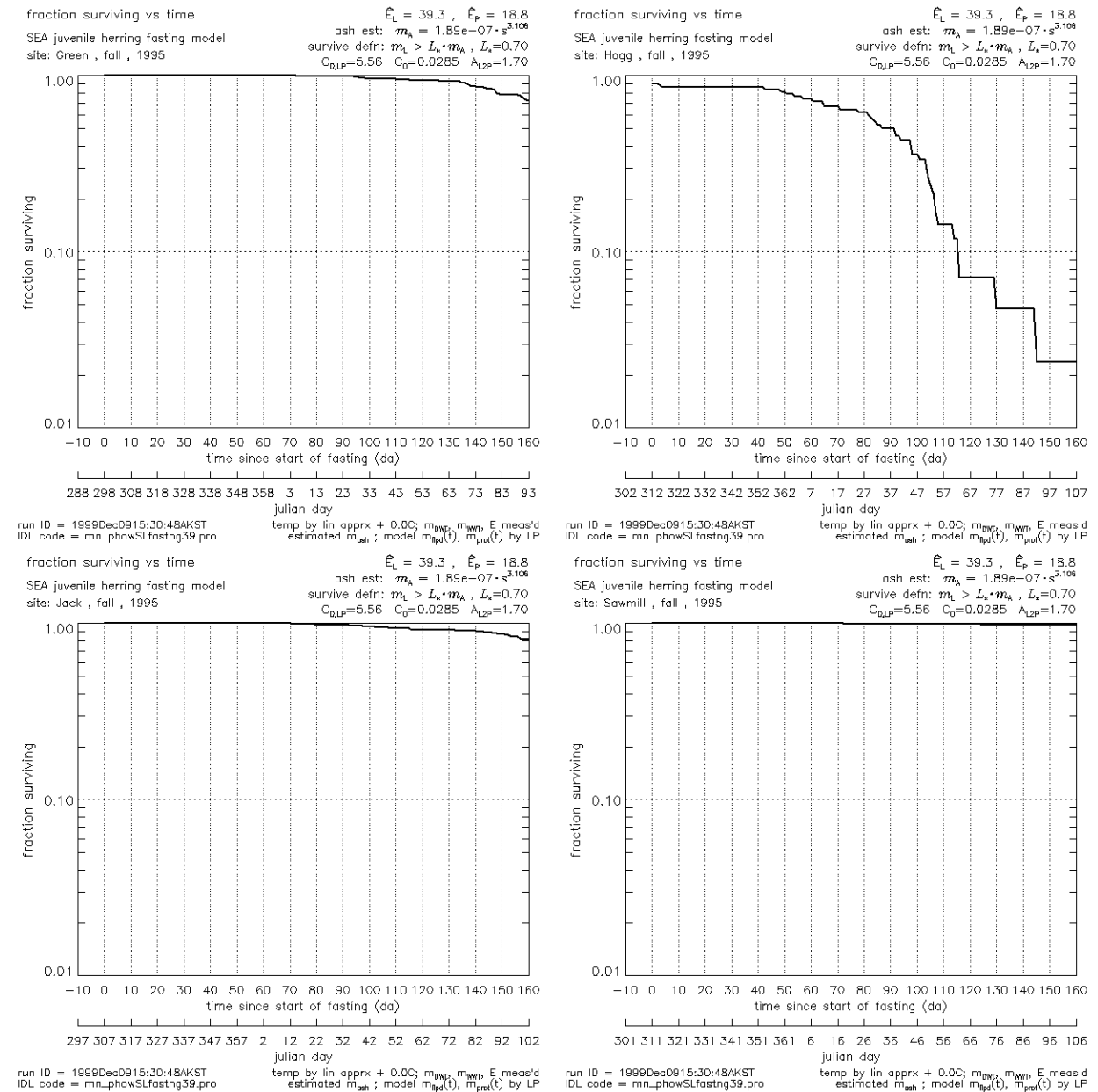


Figure 3.1 Survival versus time during fasting for sites Green, Hogg, Jack, Sawmill, Fall 1995

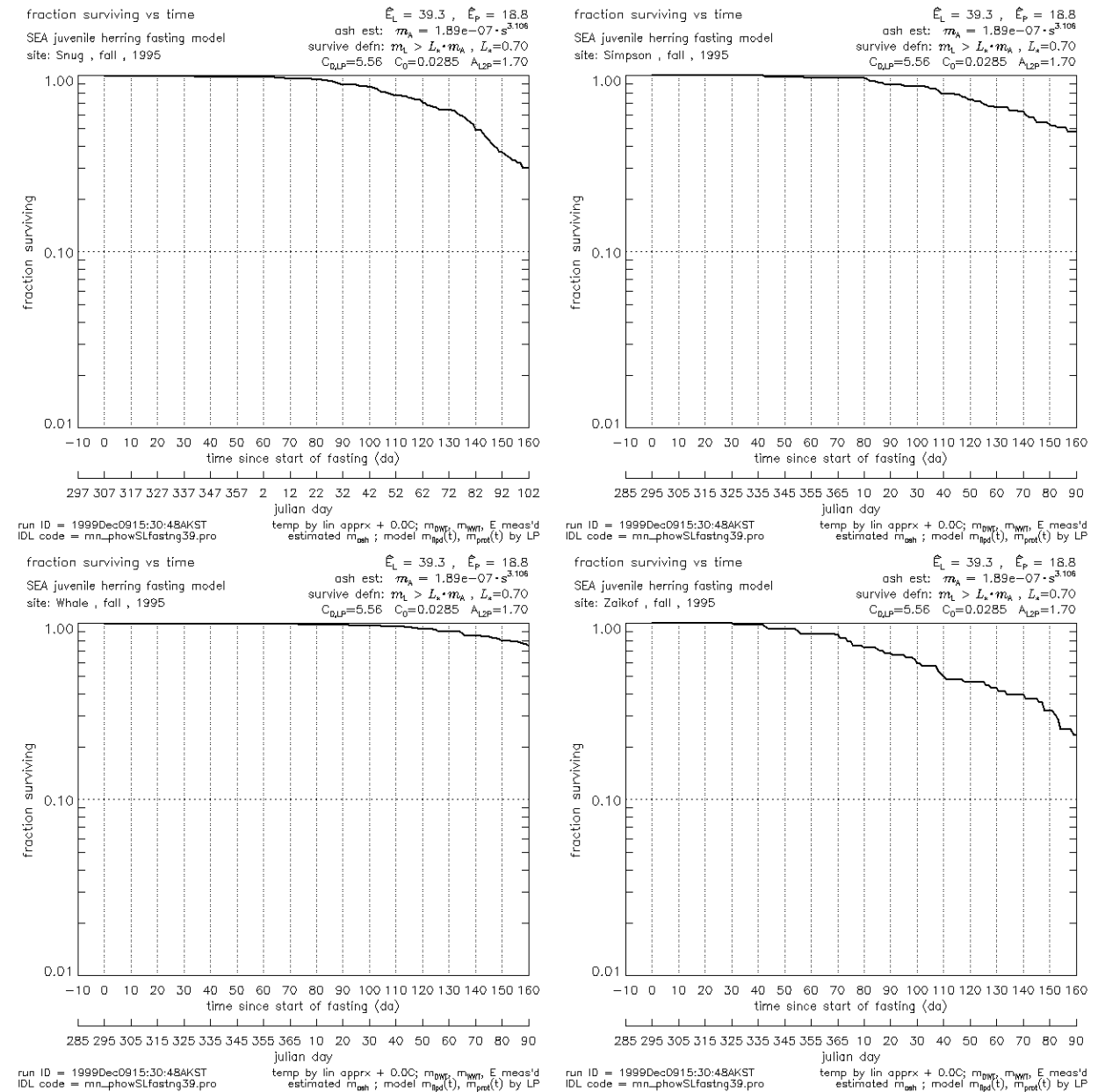


Figure 3.2 Survival versus time during fasting for sites Snug, Simpson, Whale, Zaikof, Fall 1995

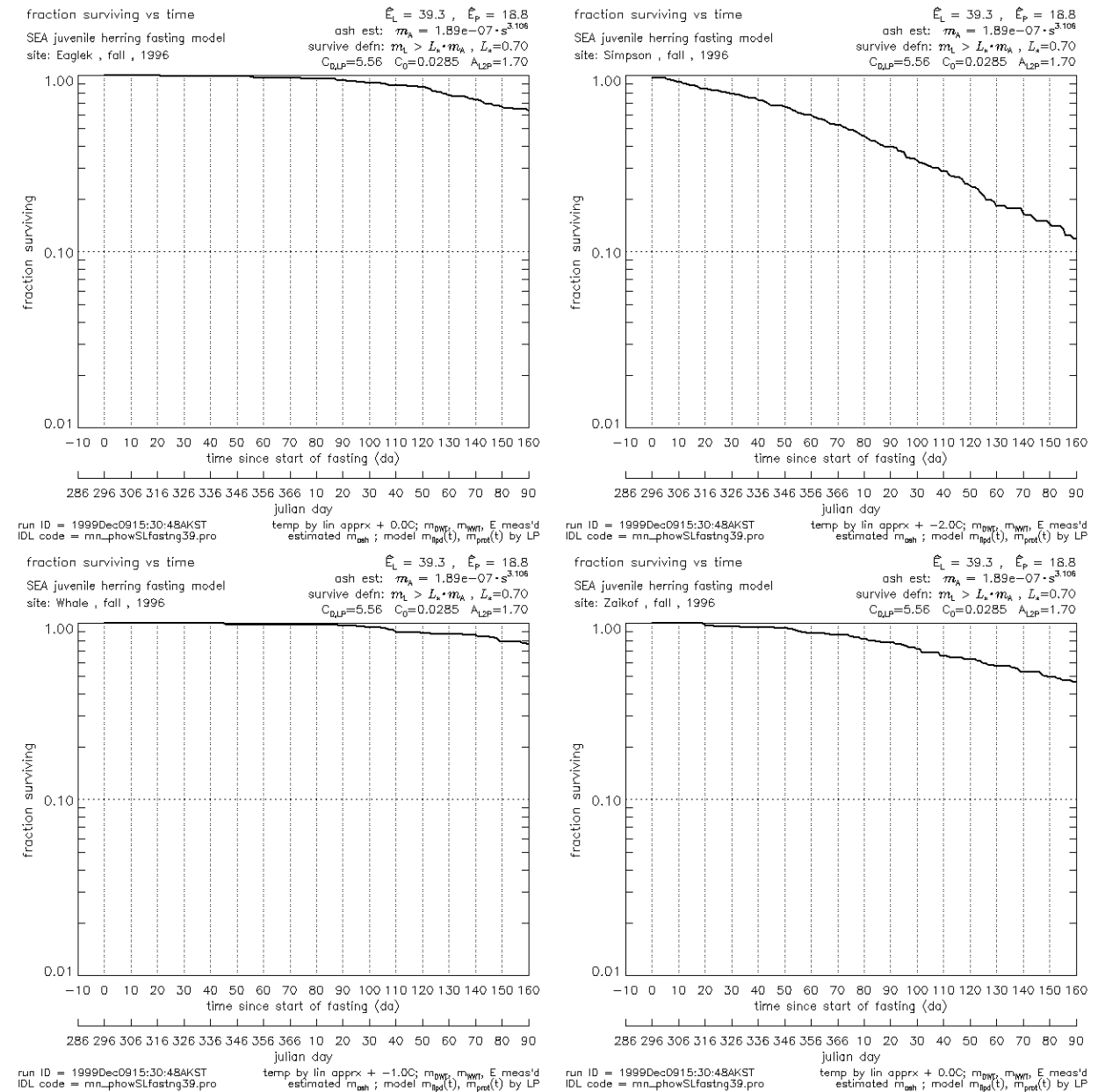


Figure 3.3 Survival versus time during fasting for sites Eaglek, Simpson, Whale, Zaikof, Fall 1996

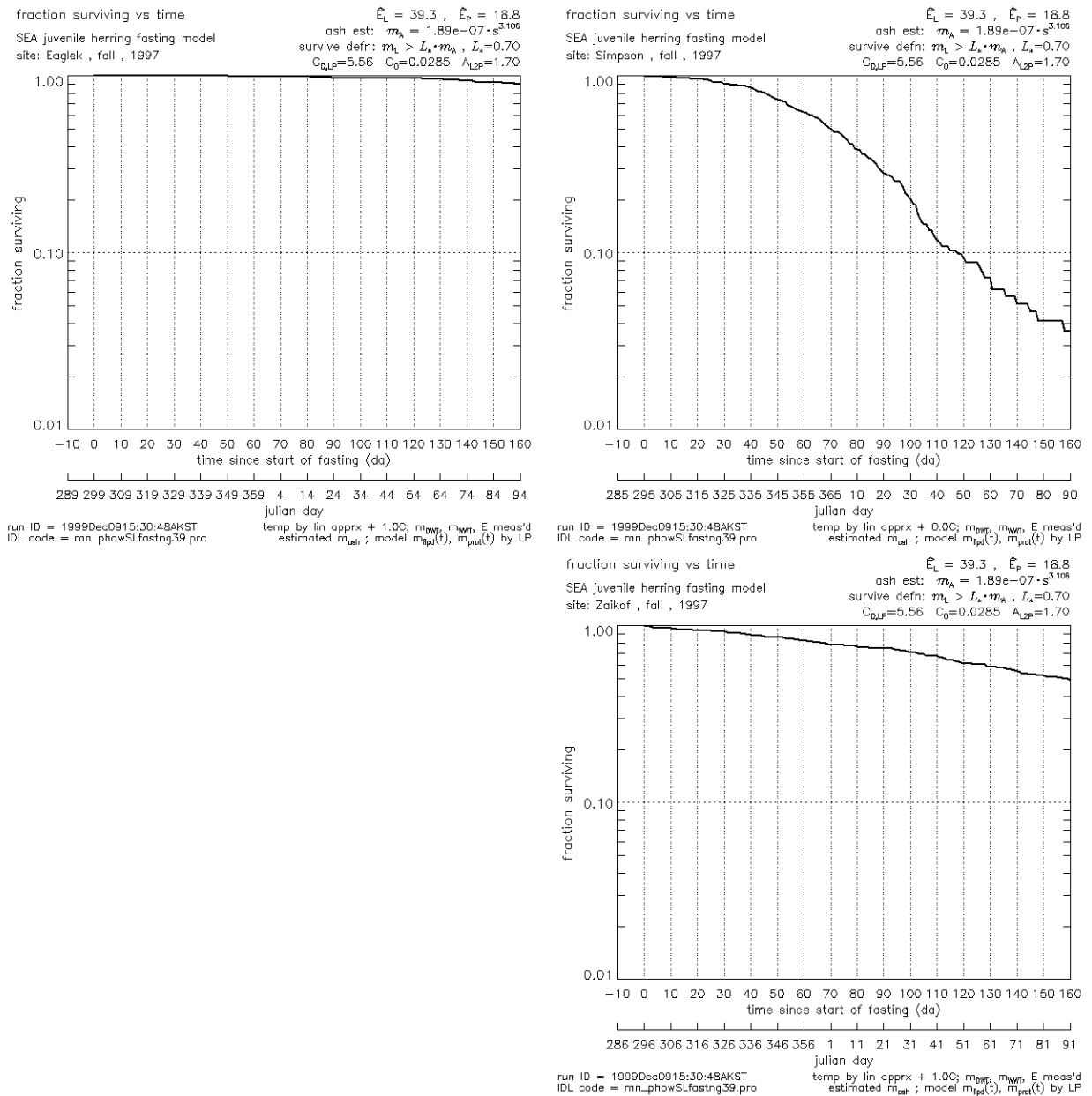


Figure 3.4 Survival versus time during fasting for sites Eaglek, Simpson, Zaikof, Fall 1997

Bibliography

- [Kli99] T. C. Kline. Stable Isotopes as Food-Web Tracers. In R. T. Cooney, editor, *Sound Ecosystem Assessment (SEA) - An Integrated Science Plan for the Restoration of Injured Species in Prince William Sound*, Final Report, Ch 6. Exxon Valdez Oil Spill Trustee Council, June 1999.
- [NBF⁺99] Brenda L. Norcross, Evelyn D. Brown, Robert J. Foy, Michele Frandsen, Jody Seitz, and Keven Stokesbury. Juvenile Herring Growth and Habitats. In R. T. Cooney, editor, *Sound Ecosystem Assessment (SEA) - An Integrated Science Plan for the Restoration of Injured Species in Prince William Sound*, Final Report, Ch 10. Exxon Valdez Oil Spill Trustee Council, June 1999.
- [Pau99] A. J. Paul. Fish Energetics. In R. T. Cooney, editor, *Sound Ecosystem Assessment (SEA) - An Integrated Science Plan for the Restoration of Injured Species in Prince William Sound*, Final Report, Ch 11. Exxon Valdez Oil Spill Trustee Council, June 1999.

Chapter 7 Document 4

Calibration Reference for the models for physiological response and survival of age-0 Pacific herring during winter fasting

J. SEA
and
U. SEA, T. SEA, I. SEA

1. Introduction

This is the reference documentation for the calibration of Version 3.1 of the model for fasting and subsequent survival of age-0 Pacific herring during winter.¹ The model and the calibration procedures described herein are the product of the Information Systems and Model Development (ISMD) project² of the Sound Ecosystem Assessment (SEA) Program in collaboration with the Fish Energetics (FE) project [Pau99]. Also included in this document is a comparison of the physiological determinations obtained from bomb calorimetry and from nitrogen analysis. This comparison was made possible by nitrogen analyses provided by the Stable Isotopes project [Kli99].

This document, like the others in this series, is tailored to the interests and requirements of an informed end-user. The specific requirements addressed by this “Calibration Reference” are the capability and the means to assess the fundamental merit of the models and of the methods and the resources that serve as the basis for the models. In Document 2, the “Concise User’s Reference,” the models have been presented as a sequence of application steps, and in Document 3, the “Validation Reference,” those procedures were tested using an independently acquired collection of field monitoring data sets. These two documents provide the end-user with full view of the model steps but a “black-box” view of the merit of those steps.

In contrast, the “Calibration Reference” shows the end-user a “ground-up” reconstruction of the models. It does not address the underlying technical issues for each of the construction steps.

¹ Version 3, Jul 1999, implemented the model processes associated with parameters L_* , P_* , and A_{L2P} . Version 3.1, Nov 1999, is a full recalibration of the model based on a more complete assessment of the physiological structure of the sample populations used in the Seward Laboratory fasting experiment.

² Primary support during 1994–1999 provided by the Exxon *Valdez* Oil Spill Trustee Council, Restoration Project 320J.

Sustaining support during 1998–1999 for implementation of the circulation model and for the PWSSC computing infrastructure provided by the Oil Spill Recovery Institute, Cordova Alaska.

Version 3 of the model and all of the final documentation for the ISMD project are due to private financing from V. Patrick for ISMD IR&D and continued long term sustaining support from Grafikon Ltd and from the Advanced Visualization Lab of the University of Maryland.

**Structure of the documentation for the solutions to the PWSFERPG problems
contained in the Final Report of the
Information Systems and Model Development Project**

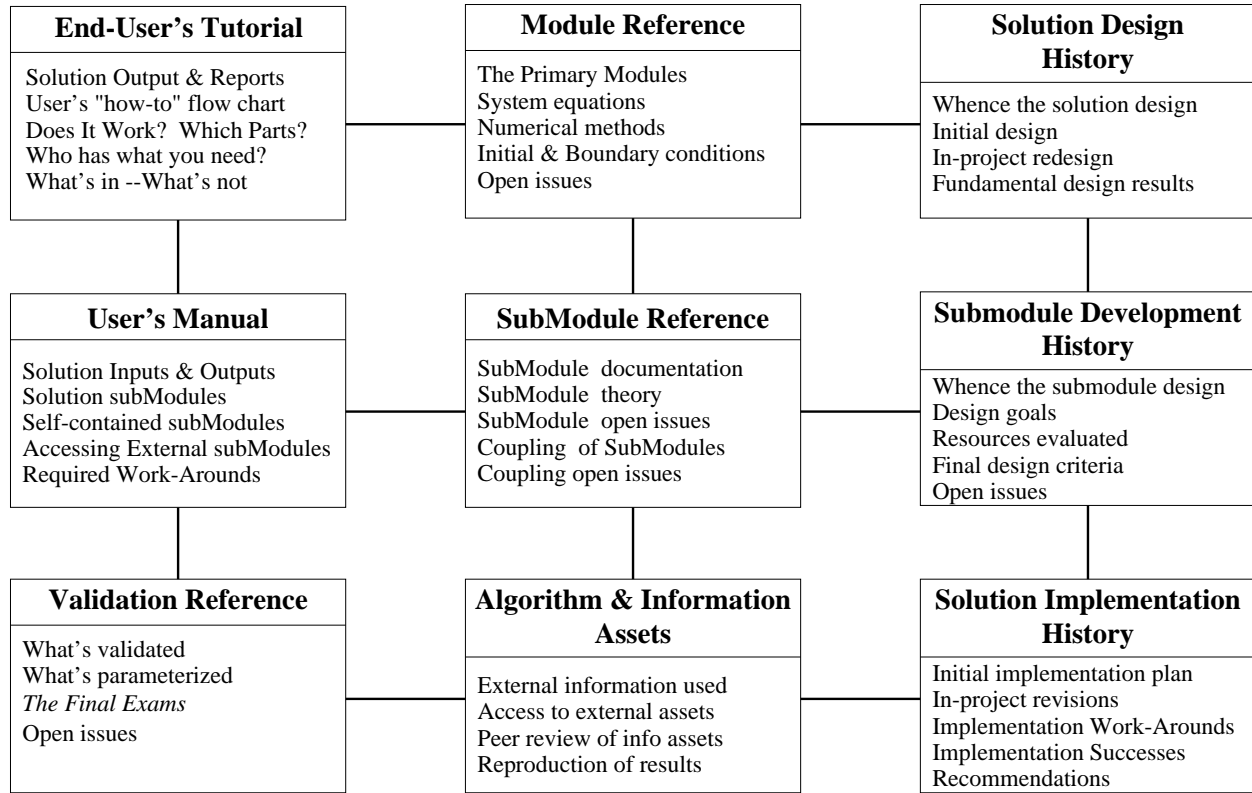


Figure 1. Structure of the document and the relationships between sections. (All sections in the figure do not appear in this first draft of the Final Report.)

However, as a necessity of presenting the calibration, it does proceed step-by-step through the construction process. At each step it identifies the manner in which the model components within that step were quantitatively specified, i.e., “calibrated.” As a consequence, it shows the end-user each submodel component, the information resources that are the basis for the calibration of that component, the “calibrateability” of each component, and any open-issues or qualifications associated with the present specification of that component. In particular, the “Calibration Reference” provides the end-user the means to reproduce the construction of the model from beginning to end and to conduct a “hand-on” structural evaluation of the model.

To facilitate this purpose, this document requires some degree of familiarity with the purposes of the model and with the companion documentation. It uses the formulation of the problem and the presentation of the solutions provided by the “Concise User’s Reference” and by the companion on-line and printed demonstrations and tutorials.

The reader will find herein somewhat more than is conveyed by the strict meaning of “calibration.”

This is because in many cases the calibration procedure provides results which are an overdetermination of the specific parameter in question. That is, procedures will yield information regarding the efficacy and suitability of the model representation, information that supplements the more strictly constrained “Validation Reference.” Because the information arises from controlled laboratory experiments, as opposed to field samples used in the “Validation Reference,” the results are often “sharper” and more clearly delineated than those of the “Validation Reference.”

Figure 1 shows a two-dimensional representation of the structure and interrelationships of the full collection of documents for the Pacific herring models. The reader will note that Figure 1 does not include a “Calibration Reference.” In the context of Figure 1 this “Calibration Reference” is a hybrid of four entries. It is in part a User’s Manual, a Validation Reference, a Submodel Reference, and documentation regarding Information Assets and Algorithms. It is a feature of the history of this development effort that these calibration procedures and the calibration data resources have a large and central role. For information on the development of the models see the “Project History” documentation.

The remainder of the “Calibration Reference” is structured as follows.

Section 2. Calibration requirements

The calibration issues are extracted from §2.4–§2.7 of the “Concise User’s Reference” and organized into a collection of calibration requirements. In this section those aspects of the calibration procedures that are due to the history of the development effort or to constraints imposed by the state of the art are made explicit.

Section 3. Calibration resources

The information resources used in the calibration are made explicit. To fulfill the document objective of full reproducibility, the information resources required to calibrate the model are identified and made accessible through this document.

Section 4. Calibration procedures

The requirements and the resources are brought together through a sequence of calibration procedures identified as “Steps” and numbered 1 through 5. The reader will find that the description above is in some cases too limited: there are sets of parameters that “interact.” That is, some parameters must be established as an n -tuple of values (simultaneously) rather than as n independent scalar values. Consequently some steps will tackle at one time several of the individual calibration requirements identified in Section 2.

2. Calibration requirements

In this section all of the calibration tasks are collected from the companion documentation and assembled into a preliminary sequential order.

The first calibration issues to appear in the ‘‘Concise User’s Reference’’ are those associated with the transformation from laboratory measurement variables to those of the physiology of the organism. In the case of ‘‘bomb calorimetry,’’ the measured variables E , m_{DWT} , m_{WWT} , m_{A} are converted to the physiology variables m_{P} , m_{L} , m_{A} , m_{W} by the linear transformation (6.1-6.4) §2.6 Doc 2

$$\begin{aligned} m_{\text{P}} &= \frac{-E + \widehat{E}_{\text{L}}(m_{\text{DWT}} - m_{\text{A}})}{\widehat{E}_{\text{L}} - \widehat{E}_{\text{P}}} \\ m_{\text{L}} &= \frac{E - \widehat{E}_{\text{P}}(m_{\text{DWT}} - m_{\text{A}})}{\widehat{E}_{\text{L}} - \widehat{E}_{\text{P}}} \\ m_{\text{A}} &= m_{\text{A}} \\ m_{\text{W}} &= m_{\text{WWT}} - m_{\text{DWT}} \end{aligned} \quad (2.1)$$

It will be helpful to have a name for this coordinate transformation. Let L_{bc} denote the linear map from $(m_{\text{P}}, m_{\text{L}}, m_{\text{A}}, m_{\text{W}})$ to $(E, m_{\text{DWT}}, m_{\text{WWT}}, m_{\text{A}})$. The inverse is given by (2.1) and denoted L_{bc}^{-1} . An alternative set of four measurements was m_{N} , m_{DWT} , m_{WWT} , m_{A} obtained by ‘‘nitrogen analysis.’’ These are converted to m_{P} , m_{L} , m_{A} , m_{W} by the linear transformation (6.5-6.8) §2.6 Doc 2

$$\begin{aligned} m_{\text{P}} &= \frac{m_{\text{N}}}{k_{\text{N}}} \\ m_{\text{L}} &= m_{\text{DWT}} - m_{\text{A}} - m_{\text{N}}/k_{\text{N}} \\ m_{\text{A}} &= m_{\text{A}} \\ m_{\text{W}} &= m_{\text{WWT}} - m_{\text{DWT}} \end{aligned} \quad (2.2)$$

In the same manner let this transformation be denoted by L_{N}^{-1} . The parameters required to transform bomb calorimetry data are \widehat{E}_{P} and \widehat{E}_{L} , and the parameter required with nitrogen analysis is k_{N} .

A number of parameters appear through the adaptation of prior methods to the case at hand. Rather than restate much of §2.7 we shall simply restate the solution Φ for the time evolution of the physiology expressed in the coordinates m_{P} , m_{L} , m_{A} , m_{W} since each of the parameters appears explicitly in the solution. From (7.24) §2.7 Doc 2, the solution

$$(m_{\text{P}}(t), m_{\text{L}}(t), m_{\text{A}}(t), m_{\text{W}}(t)) = \Phi(t; (m_{\text{P},0}, m_{\text{L},0}, m_{\text{A},0}, m_{\text{W},0}), \tilde{t}_{0,k}^{\bullet}, \tilde{T}_k)$$

is

$$\begin{aligned} m_{\text{P}}(t) &= A_{\text{L2P}} (m_{\text{L}}(t) - m_{\text{L},0}) + m_{\text{P},0} \\ m_{\text{L}}(t) &= m_{\text{L},0} + \frac{m_{\text{L},0} + m_{\text{P},0}}{1 + A_{\text{L2P}}} \left[-1 + \left[1 - \frac{C_0 C_{0,\text{LP}}^k (1-k)(1 + A_{\text{L2P}}) \int_0^t e^{\gamma T}}{(\widehat{E}_{\text{L}} + A_{\text{L2P}} \widehat{E}_{\text{P}})(m_{\text{L},0} + m_{\text{P},0})^{1-k}} \right]^{1/(1-k)} \right] \\ m_{\text{A}}(t) &= m_{\text{A},0} \\ m_{\text{W}}(t) &= m_{\text{W},0} \end{aligned} \quad (2.3)$$

The solution Φ requires the specification of the parameters A_{L2P} , C_0 , $C_{0,\text{LP}}$, k , and γ .

To use Φ to answer questions about survival we need the specification of the partition

$$\mathcal{P}^\square \cup \mathcal{P}^* = \mathcal{P}, \quad \text{and} \quad \mathcal{P}^\square \cap \mathcal{P}^* = \emptyset$$

where $(m_P, m_L, m_A, m_W) = h_{\mathcal{P}}(\omega)$ is in \mathcal{P}^\square if and only if ω is alive (2.4)

The specification in (2.4) is properly viewed as a conjecture of the model. It is not something known *a priori*. According to (2.4) the calibration will show a region \mathcal{P}^\square in \mathcal{P} such that the physiological state $(m_P, m_L, m_A, m_W) = h_{\mathcal{P}}(\omega)$ for every individual ω known to be alive at the time of collection will be in \mathcal{P}^\square . Conversely, for every individual ω known to be expired at the time of collection will be outside the region \mathcal{P}^\square . In (2.4) the exterior of \mathcal{P}^\square is defined to be \mathcal{P}^* . If in fact the calibration shows that (2.4) holds, then, since the state of an individual should cease to change at death we can expect to find that if the individual ω is expired then the physiological state $(m_P, m_L, m_A, m_W) = h_{\mathcal{P}}(\omega)$ should be on the boundary of \mathcal{P}^\square . That is, although \mathcal{P}^* may be quite large, the subset of \mathcal{P}^* occupied by the state of an actual individual ω will be quite “thin.” The occupied subset will be only the boundary.

If the foregoing holds then we can take advantage of a basic theorem: if the boundary meets certain smoothness conditions then the boundary is the zero-set of a scalar valued function of the coordinate variables. That is, the calibration issue is the identification of $G(m_P, m_L, m_A, m_W)$ such that the boundary between \mathcal{P}^\square and \mathcal{P}^* is (at least locally) the set of all points m_P, m_L, m_A, m_W such that $G(m_P, m_L, m_A, m_W) = 0$. Equivalently, we seek $G(m_P, m_L, m_A, m_W)$ such that

$$\mathcal{P}^\square = \{ (m_P, m_L, m_A, m_W) \text{ in } \mathcal{P} : G(m_P, m_L, m_A, m_W) > 0 \} \quad (2.5)$$

From §2.7 we have the result $\mathcal{P}^\square = \{ (m_P, m_L, m_A, m_W) : m_L - L_* m_A > 0 \}$, where L_* is a constant. We will show in this document the obvious refinement $\mathcal{P}^\square = \{ (m_P, m_L, m_A, m_W) : m_L - L_*(m_A - Q m_P) > 0 \}$, where L_* and Q are constants. That is, the two categories *alive* and *expired* can be represented as a partitioning of \mathcal{P} and, moreover, the boundary between the two partitions is a hyperplane in \mathcal{P} . The calibration is then the specification of the constants of the linear equation for the hyperplane.

The conjecture (2.4) is equivalent to the assumption that a single point (m_P, m_L, m_A, m_W) in \mathcal{P} cannot be the physiological state for both an alive individual and an expired individual. In particular, the assumption is that the dimensionality of \mathcal{P} is sufficient to distinguish between viable and unviable physiological states. One can readily anticipate situations in which the state (m_P, m_L, m_A, m_W) for one individual sustains life but for another does not. The immediate example is if the two individuals are of different age. This example is more realistic for adults for whom there is greater uniformity of state (m_P, m_L, m_A, m_W) among individuals of significantly differing ages. For age-0 juveniles, the rate of physiological change is such that this example involving age is much less applicable. Nevertheless, this illustrates that the space \mathcal{P} is already a projection from a larger space, for example, one in which the coordinates are $(m_P, m_L, m_A, m_W, \beta)$, where the variable β denotes date at which the individual hatched. The conjecture was that this larger space (and consequently otolith readings) would not be necessary for an unambiguous determination of alive versus dead.

One further calibration issue is due to the unique circumstances of the model development. This part of the calibration is not an inherent part of the model and calibration structure and hence is

identified in this document as an “optional” step in the calibration. However, this requirement may well arise with other pre-existing datasets, and that is one reason for providing a careful account of the procedure. In addition, the step may well have a role in an extension of \mathcal{P} to a space of higher dimensionality. The role and the extension are described in this document.

The circumstances are that it was routine practice that the bomb calorimetry analysis at Seward Laboratory not include a determination of mass of ash. From (2.1) and a few example calculations, it is clear that a determination of m_A is required. For example, increasing m_A causes an increase in m_L and a decrease in m_P . In cases in which one would expect m_L to be low, as would be the case in spring, then an under-estimation of m_A can cause the computed value for m_L to be negative.

One way to obtain a low estimate of m_A is to use a fixed value for the ratio m_A/m_{DWT} . In the marine science technical literature proximate analyses frequently are reported using pooled sample set means and variances for such ratios in conjunction with the mean and variance for one measured variable. [AR97, VPPLR97] For our purposes here this takes the a variable out of context as one of four coordinate variables jointly characterizing the state of an individual in \mathcal{P} .

This calibration issue was tackled and a resolution was developed wherein standard length ℓ is used for a fourth variable. Specifically, the resolution is to identify a minimum error transformation F

$$F : (E, m_{DWT}, m_{WWT}, \ell) \mapsto (m_P, m_L, m_A, m_W) \quad (2.6)$$

This is specified as a minimum error solution because it is not at all certain that F is a one-to-one correspondence. Specifically, for F in (2.6) to have the same property as, say, the linear transformation in (2.1), then each set of four variables $E, m_{DWT}, m_{WWT}, \ell$ must uniquely determine one and only one point (m_P, m_L, m_A, m_W) in \mathcal{P} . This *is* the case for the transformations (2.1) and (2.2) to the extent the assumption holds regarding parameters $\widehat{E}_P, \widehat{E}_L$, and k_N being constant. In the case of (2.6) there is nothing fundamental whereby one can assume a one-to-one correspondence. The choice for F is due to D. M. Mason. An approximate relation between ℓ and m_A is chosen to define a function $F_{\ell 2A}$ such that $m_A = F_{\ell 2A}(\ell)$ in some generalized sense. This then defines F in (2.6) by the composition of maps

$$(E, m_{DWT}, m_{WWT}, \ell) \mapsto (E, m_{DWT}, m_{WWT}, F_{\ell 2A}(\ell)) \mapsto (m_P, m_L, F_{\ell 2A}(\ell), m_W) \\ \text{where } F_{\ell 2A}(\ell) = \alpha_1 \ell^{\alpha_0} \quad (2.7)$$

(2.7) is referred to as an “allometric” function. Specifically, $\frac{d \log F_{\ell 2A}}{d \log \ell}$ is a assumed constant and equal to α_0 and $F_{\ell 2A}(1)$ is assigned the value α_1 .

The calibration requirements associated with the relation F of (2.7) are of two types. On the one hand the parameters of F require specification. On the other hand the use of an approximation for m_A requires that an error analysis be carried out for each of the steps in which that approximation is used. Both of these requirements are addressed.

In Table 2.1 the foregoing collection is assembled into six calibration topics. The number associated with each topic is a subsection number for §4, Calibration procedures. The topics with section number “0” are all items wherein preexisting values from the literature have been adopted. These are all addressed in the introduction to §4.

Topics shown with the section number with square brackets “[]” are “optional.” in the sense that each is not fundamentally required by any of the model structure or assumptions.

Table 2.1: calibration requirements

section	calibration issue	procedure & resources
0	$C_{0,LP}=5.56 \text{ gm}^{-1}$	arbitrary but fixed; selected to adjust LP to WWT
0	$\gamma=0.548 \text{ C}^{-1}$	prior bio-energetics [Arr95]
0	$k=0.773$	prior bio-energetics [Arr95]
0	$\widehat{E}_L=39.3 \text{ kJ g}^{-1}$	animal physiology [SN90, Mor78]
[1]	$\alpha_0=3.106$	$F_{\ell 2A}(\ell) = \alpha_1 \ell^{\alpha_0}$
[1]	$\alpha_1=1.89 \times 10^{-7} \text{ mm}$	new measures; calibration from fall 1995 field surveys
2	$\widehat{E}_P=18.8 \text{ kJ g}^{-1}$	upper bnd \widehat{E}_P by $m_L > 0$ globally [Pau99] [NBF+99]
[3]	compare bomb cal. to N_2	Stable Isotope Proj [Kli99] & Fish Ener Proj [Pau99]
4	$L_* = 0.70$	\mathcal{P}^* & \mathcal{P}^\square in \mathcal{P} defined by Ω^ℓ , Seward Lab Exp [Pau99]
5	reconstruct Ω^s rel. to Ω^ℓ	apply \mathcal{P} structure to Seward Lab Exp [Pau99]
5	$C_0=0.0285 \text{ kJ da}^{-1}$	advance Ω^s in time, fit to Ω^ℓ , Seward Lab Exp [Pau99]
5	$A_{L,2P}=1.7$	back projection of $\Omega^s \cup \Omega^\ell$, Seward Lab Exp [Pau99]

3. Calibration resources

There are four calibration resources which have contributed to the present status of the model for age-0 Pacific herring fasting and survival.

the Ph.D. dissertation of F. Arrhenius in the context of contemporary modelling

The dissertation of F. Arrhenius [Arr95] was called to the attention of this project by A. J. Paul shortly after it appeared. Although the topic was Baltic herring, it nevertheless is a comprehensive treatment of juvenile herring from a bioenergetics perspective. The data and the characterizations for age-0 herring presented by Arrhenius are the basis for the calibration used in Version 1 [SS97] of the Pacific herring fasting and survival model.

The model structure in Version 1 is relevant here, although not in itself a calibration issue. The model structure is due to three influences. The first is the work of the ISMD group prior to this project. That work had established already many of the basic approaches. That prior work had involved the use of the existing formulations of the bioenergetics model, work that had led to efforts to have a more complete physiological representation than the single variable wet mass. The second influence was a set of conjectures put forth regarding the expected time evolution for the physiology of fasting herring by A. J. Paul. These conjectures shaped a number of the assumptions used in Version 1 of the model. The third influence was prior modelling and observational work in two areas, compensatory feeding and “dynamic energy budgets.” D. M. Mason had been tracking this work; he provided the ISMD project with its up to date resources regarding contemporary developments in these areas. The work in compensatory feeding and dynamic energy budgets included fasting as one of the scenarios. This work had led to initial extensions of the bioenergetics models to multiple mass types. However, these investigations had retained much of the old baggage associated with the dimension-reducing projection to a “carbon-equivalent” canonical mass type. The demands of fasting had forced a reformulation to something beyond the single variable wet mass and the canonical “carbon equivalent” mass. However, the approach of *two* carbon equivalent mass types—a structure and a reserve—seemed to be over the top.

These specific resources and the circumstances in which they were encountered influenced both the parameter selection and the parameter values found in Version 1 (Nov 1997).

the Seward Laboratory fasting experiment

By far the most important resource for the calibration of the model is the Seward Laboratory fasting experiment. The major part of the remainder of this section is devoted to a review and description of that resource. The experiment has provided far more than values for a handful of constants. It has contributed so much because of specific properties of the experimental design and because of the sheer size and scope of the experiment—the calibration had the benefit of a sample population of over 147 individuals, with values for four variables for each of 114 of these individuals, with measurements distributed over the time interval of winter fasting.

This resource was made available to ISMD in two phases. The first submission was made following the distribution of Version 1 of the fasting model to collaborating projects and to ADF&G both for critical review and for implementation by those having applicable

observational information. The information contained in the first datasets from the Seward Laboratory fasting experiment led to Version 2 [SS98] of the model (June 1998).

Additional information from the fasting study was provided in conjunction with the submissions of the information from the field surveys. This new information was used in the development of the late form of Version 2 of the model, the version presented at the March 1999 public presentation of the *SEA* Program.

the Juvenile Herring Growth & Habitats surveys

The measurements from the field surveys of the JHGH project have been used with but one exception solely for validation and not for calibration. That one exception is the use of the totality of the measurements to define upper and lower bounds, and, specifically, only one of these is used in the calibration. The significance of the field surveys in this regard is simply their number. The sheer size of the sample population and the wide range of conditions is a valuable resource in establishing the bounds of the reachable set of physiological states in \mathcal{P} . Those bounds were not as well delineated by the much smaller population used in the controlled environment Seward Laboratory study.

the ash, standard length, nitrogen analysis dataset

The need to develop a work around for the absence of ash measurements for all of the herring laboratory analyses led to the development of a small sample set for which ash was measured. This dataset provided the calibration of the relation $F_{\ell_{2A}}$.

At the same time there was an interest in applying the measurements of nitrogen that were a by-product of the isotope studies of T. Kline. Therefore, this same dataset has paired replicates for the determination of “whole body mass of nitrogen.”

3.1 The design of the Seward Laboratory fasting experiment

It is a fundamental and near-universal experimental design constraint in fisheries that observations are destructive. This constraint imposes significant overhead as well as limitations upon any experimental procedure—what is conceptually an experiment in to observe the time evolution of one individual at times $t_i, i = 1, \dots, n$, in practice requires, at each time t_i , replicated observations involving a sample set of r_i individuals. The test that conceptually could be carried out by observing one individual in practice requires $\sum_{i=1}^n r_i$ distinct observations. The situation is even more severe than might be apparent. Since each observation is destructive, we can never know the direction in which the individual was going—we can know only his state at the time of the observation and nothing about his future state. A corollary is that we can know nothing of his history either: the determination of a prior state would have been destructive. Even more constraining is that nearly any process that could “filter” for some limited range of a variable is likewise destructive. At each observation time one must be prepared to consider necessarily the full range of occurrence for each and every variable. There is no means to limit that range.

We shall see at several points how these considerations were essential design factors for Paul and Paul in designing the experiment that addressed their purposes. Although this calibration uses that study in a manner different from its original purpose, this use nevertheless must tend to the fundamental constraints due to destructive testing.

Because the destructive testing constraint is so fundamental to the experimental design and to our use here of the experimental results, we need a notation sufficient for expressing this constraint. First, consider the “conceptual experiment” for a fasting individual introduced just above. Let Ω be a population of age-0 herring and let ω be a *single* individual selected for the “conceptual” non-destructive experiment. We wish to observe the individual at time t_0, t_1 , and t_2 to determine (conceptually, that is)

$$\begin{aligned}
 & (m_{P,0}, m_{L,0}, m_{A,0}, m_{W,0}) = \Phi(t_0; (m_{P,0}, m_{L,0}, m_{A,0}, m_{W,0}), t_0, T) \\
 \text{this is not} & \quad (m_{P,1}, m_{L,1}, m_{A,1}, m_{W,1}) = \Phi(t_1; (m_{P,0}, m_{L,0}, m_{A,0}, m_{W,0}), t_0, T) \\
 \text{possible} & \quad (m_{P,2}, m_{L,2}, m_{A,2}, m_{W,2}) = \Phi(t_2; (m_{P,0}, m_{L,0}, m_{A,0}, m_{W,0}), t_0, T) \\
 & \quad \quad \quad = \Phi(t_2; (m_{P,1}, m_{L,1}, m_{A,1}, m_{W,1}), t_1, T)
 \end{aligned} \tag{3.1}$$

where $(m_{P,i}, m_{L,i}, m_{A,i}, m_{W,i})$ is the state of the individual at observation time t_i and T is the temperature time series for the time interval from t_0 to t_2 . In such a scenario we may have noise associated with Φ and we may wish to make several tests. Or we may wish to see the dependence upon the initial condition $(m_P, m_L, m_A, m_W)_0$ or the temperature T and therefore conduct additional tests using a range of initial conditions or a range of temperatures. Note that by (3.1) we have already (conceptually) some information on dependence upon initial state to the extent the states we are interested in appear in this individual during the experiment.

But such is not possible. Instead, we must construct three sample sets $\Omega_0, \Omega_1, \Omega_2$, each contained in and representative of the overall population Ω . The usual notation for “contained in” is \subset and we write $\Omega_i \subset \Omega$, for $i = 0, 1, 2$. Further, the three sets are disjoint—no individual in one can be in another. This is written $\Omega_i \cap \Omega_j = \emptyset$, for $i \neq j$. The experiment we must conduct in place of

(1.1) in order to learn substantially less than is shown in (3.1) is

$$\begin{array}{ll}
\text{for each } i = 0, 1, 2 & S_0 = \{ (m_P, m_L, m_A, m_W) = \Phi(t_0; h_{\mathcal{P}}(\omega), t_0, T) : \omega \text{ in } \Omega_0 \} \\
\text{determine set } S_i & S_1 = \{ (m_P, m_L, m_A, m_W) = \Phi(t_1; h_{\mathcal{P}}(\omega), t_0, T) : \omega \text{ in } \Omega_1 \} \\
\text{where } \Omega_i \subset \Omega & \\
\text{and } \Omega_i \cap \Omega_j = \emptyset, i \neq j & S_2 = \{ (m_P, m_L, m_A, m_W) = \Phi(t_2; h_{\mathcal{P}}(\omega), t_0, T) : \omega \text{ in } \Omega_2 \}
\end{array} \quad (3.2)$$

With the bookkeeping assistance provided by the foregoing notation we can discuss the two major sample sets, the three subsample sets, and the five datasets used in the Seward Laboratory experimental design. Since each calibration procedure uses different sample sets and subsample sets, and uses them in different ways, the notation will help in keeping things straight. The Seward Laboratory fasting experiment is actually two distinct experiments. The fact that the experimental design had these two distinct and independent tests within it turned out to be the most important feature for the model calibration. Therefore, in the following we take some trouble in keeping the distinction clear.

The two experiments are referred to here as the “short” and the “long” experiment. As one can anticipate from (3.2), things began with the construction of two sample sets Ω^s and Ω^ℓ for the short and the long experiment respectively. Both Ω^s and Ω^ℓ were intended to be representative of each other. To that end they were created as subsets of a common set Ω' , where Ω' is a single cast net sample taken from Resurrection Bay on December 1, 1995. That is,

$$\Omega^s \subset \Omega' \quad \text{and} \quad \Omega^\ell \subset \Omega', \quad \text{where} \quad \Omega^s \cap \Omega^\ell = \emptyset$$

3.1.1 Design of the “short” fasting experiment

The goal of the “short” experiment was in effect that of (3.1) and the design is essentially that of (3.2). The sample set Ω^s for the “short” fasting experiment consisted of 99 individuals. These were retained in the Seward Laboratory unfiltered sea water system from December 1 1995 until the end of the experiment. Water temperature for the experimental group was recorded daily. As in (3.1), the experiment was to determine three sets by means of yet another subsample construction. At each of three regularly spaced times, t_0 , t_1 , and t_2 , 22 individuals from Ω^s were selected to construct Ω_0^s , Ω_1^s , and Ω_2^s . Each of the 22 was then subjected to the laboratory analyses whereby its physiological state at the sample time was determined. This established the sets S_0 , S_1 , S_2 in terms of the coordinate variables E , m_{DWT} , m_{WWT} , and m_A . The specific details of the design are collected in the following table

Table 3.1: design plan for the “short” experiment

i	plot	$ \Omega_i^s $	t_i			
set index	symbol	number	fastday	date	Julian day	year
0	●	22	0	Dec 01	335	1995
1	○	22	27	Dec 28	362	1995
2	▽	22	55	Jan 25	25	1996

3.1.2 Design of the “long” fasting experiment

The sample set Ω^ℓ for the “long” experiment consisted of 48 individuals. These were held in a manner designed to be equivalent to that of the “short” experiment. The experimental design for sample times was different. Rather than a predefined discrete set of sample times the event of mortality due to fasting was used to define the set of times $t_3 = t^*(h_{\mathcal{P}}(\omega))$, where t^* is the survival time function of individual ω whose initial conditions (at time t_0 in this context) are $h_{\mathcal{P}}(\omega)$ (see the “Concise User’s Reference” for full definitions of t^*). Fasting was continued in this “long” experiment until April 1 1996. Those individuals expiring during the time period from December 1 1995 through April 1 1996 define sample set Ω_3^ℓ and the corresponding set of physiological conditions S_3 . The end of the experiment also defines the time t_4 , the time at which all ω still alive (i.e., in the subset \mathcal{P}^\square of \mathcal{P}) are collected to define sample set Ω_4^ℓ . The analysis of the states of individuals in Ω_4^ℓ defines S_4 .

$$\begin{aligned}
 S_3 = & \{ (m_{\mathcal{P}}, m_{\mathcal{L}}, m_{\mathcal{A}}, m_{\mathcal{W}}) = \Phi(t; h_{\mathcal{P}}(\omega), t_0, T) : \omega \text{ in } \Omega^\ell \\
 & \text{and } (m_{\mathcal{P}}, m_{\mathcal{L}}, m_{\mathcal{A}}, m_{\mathcal{W}}) \text{ in } \mathcal{P}^* \text{ and } t = t^*(h_{\mathcal{P}}(\omega)) \text{ and } t \leq 122 \text{ fastdays} \} \\
 \text{with } t_3 & \text{ defined to be a set of times} \\
 t_3 = & \{ t^*(h_{\mathcal{P}}(\omega)) : \omega \text{ in } \Omega^\ell \text{ and } t \leq 122 \text{ fastdays} \} \\
 S_4 = & \{ (m_{\mathcal{P}}, m_{\mathcal{L}}, m_{\mathcal{A}}, m_{\mathcal{W}}) = \Phi(t_4; h_{\mathcal{P}}(\omega), t_0, T) : \omega \text{ in } \Omega^\ell \\
 & \text{and } (m_{\mathcal{P}}, m_{\mathcal{L}}, m_{\mathcal{A}}, m_{\mathcal{W}}) \text{ in } \mathcal{P}^\square \}
 \end{aligned} \tag{3.3}$$

Table 3.2: design plan for the “long” experiment

i	plot	$ \Omega_i^\ell $	t_i			
set index	symbol	number	fastday	date	Julian day	year
3	*	30	<i>in</i> 0–122	<i>in</i> Dec 01–Apr 01	<i>in</i> 335–92	1995 & 1996
4	◇	18	122	Apr 01	92	1996

In (3.2) and (3.3) we have expressed the sets S_i , for $i = 0, 1, 2$, in terms of the coordinate variables $m_{\mathcal{P}}, m_{\mathcal{L}}, m_{\mathcal{A}}, m_{\mathcal{W}}$ although we noted that the laboratory analysis was given in terms of the coordinate variables $E, m_{\text{DWT}}, m_{\text{WWT}}, m_{\mathcal{A}}$. The reader will recall from the “Concise User’s Reference” that the two sets of coordinate variables $m_{\mathcal{P}}, m_{\mathcal{L}}, m_{\mathcal{A}}, m_{\mathcal{W}}$ and $E, m_{\text{DWT}}, m_{\text{WWT}}, m_{\mathcal{A}}$ are equivalent—one can convert from one to the other and back. The laboratory analysis variables $E, m_{\text{DWT}}, m_{\text{WWT}}, m_{\mathcal{A}}$ do, however, have a distinct role in the history of this fasting model. We provide a brief summary of the two models, one for rate of energy loss and one for the partition \mathcal{P}^\square and \mathcal{P}^* , reported by Paul and Paul as results from the above Seward Laboratory fasting experiment.[PP98]

3.2 Initial findings from the Seward Laboratory fasting experiment

The structure of the sample sets used in the Seward Laboratory fasting experiment is apparent if the sample sets are viewed in the context of their experimental purpose. Such a view is shown in Figure 3.1.

energy density (wwt) vs time
for fasting age-0 Pacific herring

from laboratory study of U. SEA

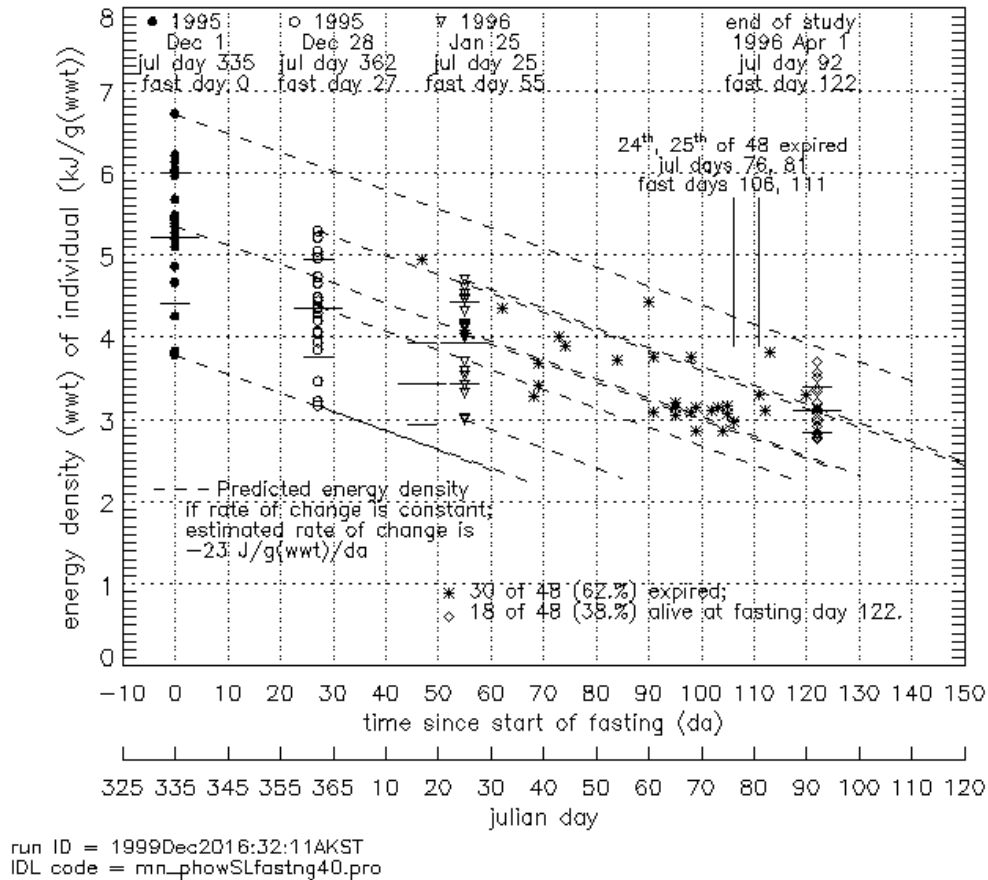


Figure 3.1 The results of the Seward Laboratory fasting experiment presented in the context of the Paul and Paul models for energy utilization and survivability.[PP98]

Figure 3.1 shows the temporal structure of the sample sets Ω^s and Ω^l in the context of the variable that was the primary focus of the experiment, energy per unit wet mass. It shows, in addition, the two time scales that have been mentioned in the tables above: “fast day,” or elapsed time in days since the beginning of the experiment; and Julian day.

The individuals comprising sample set Ω^s were used to establish the values shown in the three “columns” of points over fast days 0, 27, and 55. Above each “column” is a legend displaying the plot symbol followed by the date in calendar format, the Julian day, and then the fast day. The

three columns, in order of increasing fast day, correspond to the three subsets of individuals Ω_0^s , Ω_1^s , and Ω_2^s , and they display values from the three corresponding physiological datasets S_0 , S_1 , and S_2 . Each column records values from the measurement of 22 individuals; the three columns together represent 66 separate measurements of 66 of the 99 individuals involved in the experiment.

The individuals comprising sample set Ω^ℓ appear in Figure 3.1 as indicated by the legend at the bottom of the figure. Data with the symbols $*$ and \diamond denote individuals expired and alive respectively. Collectively they correspond to sets of individuals Ω_3^ℓ and Ω_4^ℓ and to sets of physiological data S_3 and S_4 . Dataset S_3 is unique among the five in that it consists of physiological conditions for a range of times rather than for one specific time. Dataset S_4 has a temporal structure like that of the three from Ω^s . However it is important to keep in mind that S_4 is part of an experimental design distinct from that for S_0 , S_1 , and S_2 . In particular, datasets S_3 and S_4 are a partitioning of the single sample set Ω^ℓ into the two disjoint categories *alive* and *expired*. This distinction is highlighted by the legend in Figure 3.1 identifying fast days 106 and 111 as the days at which the 24th and the 25th individuals out of the total of 48 in Ω^ℓ succumbed to fasting. In particular, at fast day 106 50% of the individuals in the “long” experimental group Ω^ℓ have expired.

The purpose of the two sample sets and the overall experimental objective should be apparent from the foregoing and from the additional information in Figure 3.1. The function of sample set Ω^s is to provide an estimate of the rate at which energy is lost during fasting in terms of the variable energy per unit wet mass. This estimate has been reported by Paul and Paul [PP98] and is widely cited. In Figure 3.1 we have noted by the legend in the lower left the Paul and Paul determination of the rate of decrease of “energy density by wet weight” \hat{E}_{WWT} by linear regression applied to \hat{E}_{WWT} from Ω^s .

In contrast the second sample set Ω^ℓ is to provide the lower bound for viability in terms of \hat{E}_{WWT} . The threshold 3.2 kiloJoule per gram wet mass is a second finding from the Seward Laboratory study.

The Seward Laboratory study during the winter 1995-1996 makes apparent the contribution of A. J. Paul to the development of the original *SEA* Science Plan during the fall of 1993. Although there were many who contributed to the formulation of the problem statement for Pacific herring—John Wilcock, Evelyn Brown, Lew Halderson along with many others—it was the insight that Paul had in 1993 as to what Figure 3.1 would look like that provided much of the “strength” for the case of winter fasting as both a relevant and realizable problem to address in *SEA*. Within one year of the start of *SEA* and prior to the formal start of the herring component of *SEA* Paul had in hand the results to quantify his insights.

The reports by Paul of his findings provided this effort with the datasets that would be used to calibrate the winter fasting model described in the “Concise User’s Reference.” As will be seen, we use the datasets from the Seward Laboratory study in a different manner than that shown in Figure 3.1. We do, however, draw heavily upon the structure that the datasets inherit by virtue of the experimental design. It is for this reason that we have provided the detailed review of that structure.

We do not use the data shown in Figure 3.1 directly in any of the calibrations procedures. However, the findings in Figure 3.1 have provided indirectly related key development objectives. These objective were established on the one hand by the massive redundancy and large experimental effort, evident from Figure 3.1, to estimate but two constant parameters. On the other hand they were

established by the “variability” clearly evident in Figure 3.1 It has required a sample population of 147 individuals of whom 114 were measured to obtain that many records of instantaneous physiological condition. After such a major effort the conclusions from Figure 3.1 remain dominated by what is routinely characterized as inherent biological and ecosystem “variability.” This is most evident in the capability of the viability threshold to distinguish between individuals who are alive or expired. While there is clear evidence of a lower bound for viability, there is no power at all in the threshold from a decision theoretic perspective. Individuals have expired far above the threshold and many individuals remain alive well below the threshold.

Figure 3.1 established for this effort the following set of test question. These test questions are not model validation tests in the usual sense. Rather, they test more basic structural capabilities.

Seward Lab study test question 1. *Would a more comprehensive model be capable of unambiguously distinguishing between the two categories alive and expired? That is, could the so-called “variability” of mortality condition evident in Figure 3.1 be totally eliminated?*

The second question, though of little real practical utility, was nevertheless one which for us was as compelling as the first.

Seward Lab study test question 2. *Could a more comprehensive model of physiological response actually reproduce in simulation the “variability” of the conditions of mortality found in the experimental record. Specifically, if the “short” sample population Ω^s were advanced in time under model simulation would the results exhibit a similar widely ranging, random-like set of physiological conditions at the time of simulated mortality?*

That is, would the model be capable of removing the variability and then putting it back?

3.3 The calibration datasets from the Seward Laboratory fasting experiment

The laboratory analyses from the Seward Laboratory fasting experiment are shown in Figure 3.2. Each of the four variables E , m_{DWT} , m_{WWT} , m_A is displayed using the same format as was used in Figure 3.1 to display the variable $\hat{E}_{WWT} = E/m_{WWT}$.

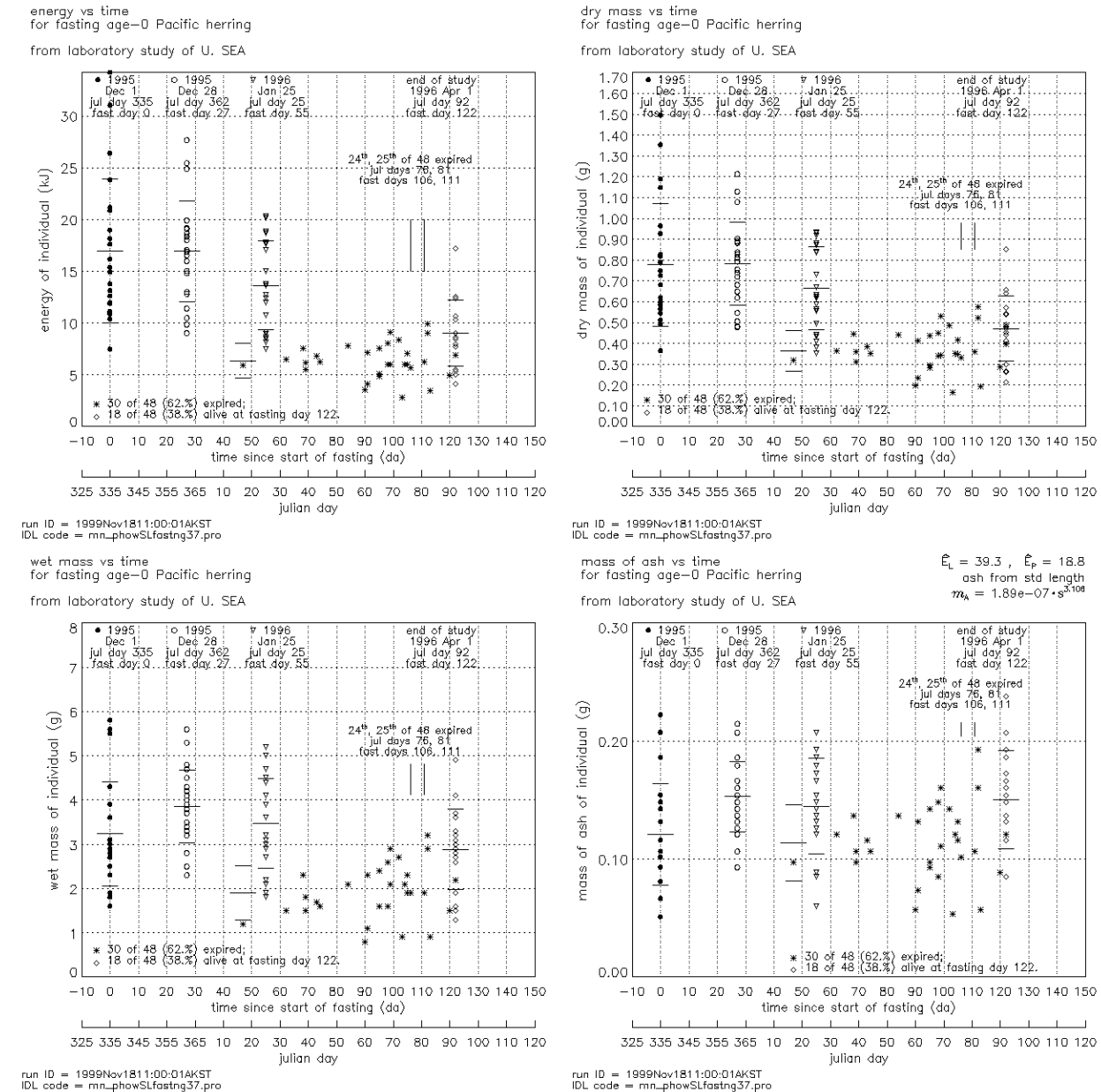


Figure 3.2 The model calibration data provided by the Seward Laboratory fasting experiment. The four variables E , m_{DWT} , m_{WWT} , m_A are shown in the format used in Figure 3.1. See the text regarding the computation of m_A from standard length.

Following the distribution of Version 1 of the model [SS97] at the end of 1997 it was determined that the measurement of ash was not routinely done as Seward Laboratory. (A brief summary of the model versions and a history of the various model calibrations is provided in the introduction to §3.) The data displayed for m_A in the lower right panel are not measured values but rather values computed using the relationship described in §2. D. M. Mason of this project together with A. J. Paul implemented a constant relative rate of change ($\frac{d \log m_A}{d \log \ell}$) relationship between m_A and standard length ℓ by means of a small set of measurements of ash for still available samples from field surveys for fall 1995. Standard length had been measured for all samples in the Program. The inclusion of values for the variable standard length in the fasting experiment dataset provided the means to compute m_A as shown in Figure 3.2.

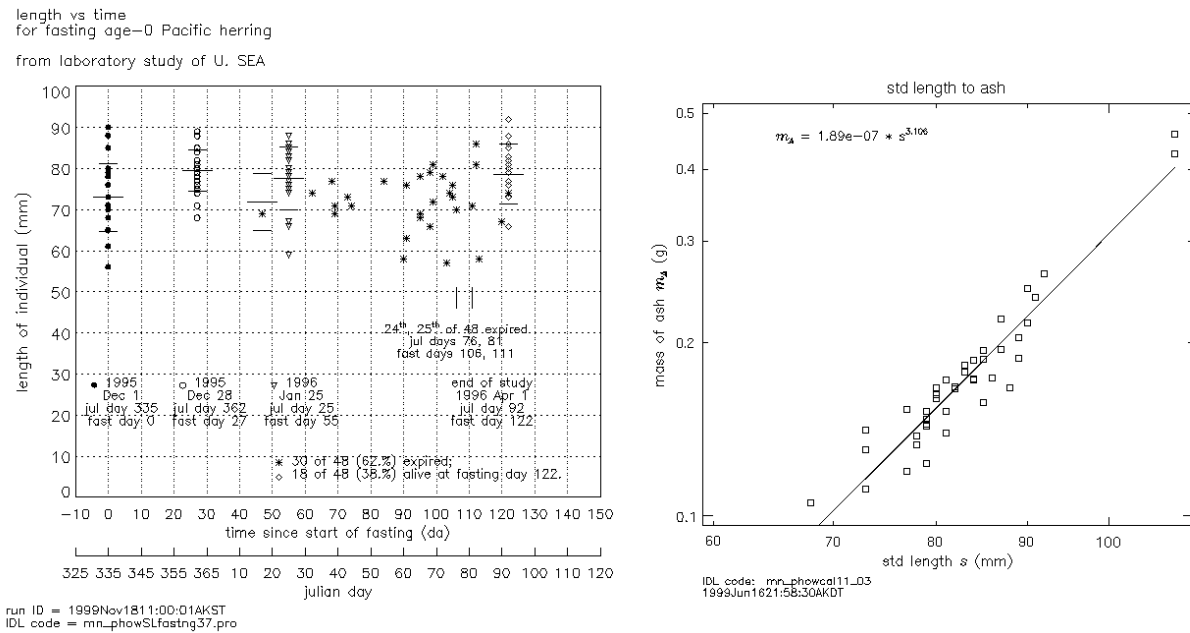


Figure 3.3 The variable standard length for the Seward Laboratory fasting experiment together with the relationship used to convert standard length to mass of ash. This is the source of the values for m_A shown in Figure 3.2.

The values for standard length are shown in the left panel of Figure 3.3. The conversion between standard length and mass of ash is shown in the panel on the right along with the set of pairs (ℓ, m_A) whereby the relationship is established by minimizing the mean square error for $\log m_A$. This conversion is described more fully in §4 along with an assessment of the impact of this approach. This, of course, is an approach appropriate for legacy data and not a preferred or recommended approach.

The complete Seward Laboratory fasting experiment dataset³ used in the calibration of the fasting and survival model consists of the 66 records of sample set Ω^s and 48 records for Ω^ℓ . To illustrate

³ Maintained by the originator. A. J. Paul, UAF Inst. of Marine Science, Seward Marine Center Laboratory, P.O. Box 730, Seward, Alaska 99664; ffajp@uaf.edu

the structure of the dataset 11 records are shown in Table 3.1: individuals 1 and 22 from each of Ω_0^s , Ω_1^s , and Ω_2^s ; individuals 1, 15, and 30 from Ω_3^l ; and individuals 1 and 18 from Ω_4^l .

Table 3.1: example records from the Seward Laboratory fasting experiment

Seward Laboratory fasting exp.					N ₂ analysis									
E	m_{DWT}	m_{WWT}	m_A	slen	m_P	m_P	survey	site	file	fish	file	fish	ash	
kJ	g	g	g	mm	g	g	date	name	ajp	ajp	tk	tk	by	
23.80	1.147	5.60	0.2222	90.0	-9.999	-9.999	1995 12 01	SewardLabExp	0	1	none	none	s12ash	
34.17	1.496	5.50	0.1860	85.0	-9.999	-9.999	1995 12 01	SewardLabExp	0	22	none	none	s12ash	
12.82	0.649	3.70	0.1482	79.0	-9.999	-9.999	1995 12 28	SewardLabExp	1	1	none	none	s12ash	
11.41	0.506	2.30	0.0930	68.0	-9.999	-9.999	1995 12 28	SewardLabExp	1	22	none	none	s12ash	
20.31	0.929	4.70	0.1929	86.0	-9.999	-9.999	1996 01 25	SewardLabExp	2	1	none	none	s12ash	
11.97	0.623	3.60	0.1482	79.0	-9.999	-9.999	1996 01 25	SewardLabExp	2	22	none	none	s12ash	
5.935	0.321	1.20	0.0973	69.0	-9.999	-9.999	1996 01 17	SewardLabExp	3	1	none	none	s12ash	
6.019	0.340	1.60	0.0848	66.0	-9.999	-9.999	1996 03 08	SewardLabExp	3	15	none	none	s12ash	
6.879	0.398	2.20	0.1210	74.0	-9.999	-9.999	1996 04 01	SewardLabExp	3	30	none	none	s12ash	
7.998	0.443	2.90	0.1369	77.0	-9.999	-9.999	1996 04 01	SewardLabExp	4	1	none	none	s12ash	
4.995	0.261	1.60	0.0848	66.0	-9.999	-9.999	1996 04 01	SewardLabExp	4	18	none	none	s12ash	

The format in which the dataset is shown is one that was developed to serve as a temporary schema. It solves problems that are unique to the development but are not important for future model applications. In principle the format requires only the first four columns (or fields)—the laboratory analysis variables E , m_{DWT} , m_{WWT} , m_A —and fields for the date, site, and for provider ID’s. However, the other columns became necessary for the duration of the development effort. The two columns with header “N₂ analysis” were required for the data provided by the Stable Isotope project. These data in turn required two provider ID fields. Lastly, a column was added for a flag string indicating whether the m_A value is due to measurement or a calculation.

Four example records are shown in Table 3.2 from the dataset that is now an integral part of the model calibration, the dataset which establishes the length-to-ash relationship shown in Figure 3.3 This same dataset contains the values used in the comparison of bomb calorimetry with nitrogen analysis, data provided for this purpose by the Stable Isotope project. [Kli99] There are 41 records in the complete dataset.⁴

Table 3.2: dataset for length to ash & bomb calorimetry to nitrogen

Seward Laboratory analysis					N ₂ analysis									
E	m_{DWT}	m_{WWT}	m_A	slen	m_P	m_P	survey	site	file	fish	file	fish	ash	
kJ	g	g	g	mm	g	g	date	name	ajp	ajp	tk	tk	by	
19.57	0.879	4.00	0.1407	73.0	0.616	0.611	1995 11 03	Jack Bay	j21	4	TK1997	HE26	lab_ajp	
38.89	1.700	6.80	0.1863	84.0	0.998	1.001	1995 11 07	Sawmill Bay	j23	24	TK1997	HE81	lab_ajp	
29.88	1.343	5.90	0.1671	80.0	0.822	0.892	1995 10 25	Green Bay	j24	4	TK1997	HE101	lab_ajp	
38.97	1.643	6.40	0.1868	85.0	1.041	1.044	1995 10 19	Whale Bay	j25	24	TK1997	HE132	lab_ajp	

The interest in the use of nitrogen analysis data arose initially as a means to “confirm” the conversion from bomb-calorimetry variables to physiology variables. It is clear, however, that this was an ill-stated problem. The conversion from nitrogen analysis variables to physiological variables is inherently identical to the conversion of bomb calorimetry measurements. A proper formulation

⁴ The dataset is maintained and managed by the provider of the measurement. Bomb calorimetry measurements are due to A. J. Paul. Nitrogen analyses are due to T. C. Kline, PWSSC, P.O. Box 705, Cordova, Alaska 99574; tkline@pwssc.gen.ak.us

is a comparison between the two methods and possibly a check for consistency between the two. Nitrogen analysis and bomb calorimetry are compared and the results are provided later in this document. The data for the comparison was developed as part of the effort to construct the standard length to ash dataset. The data appears in Table 3.2 as replicate pairs of values estimating m_P by means of the routinely used parameter of 16% for the percentage of “mean” protein mass consisting of nitrogen. The actual nitrogen mass is obtained by undoing this conversion.

The temperature at which all of the foregoing happens is of course a required data resource. A graphical representation of the temperature during the fasting experiment is shown in Figure 3.4.

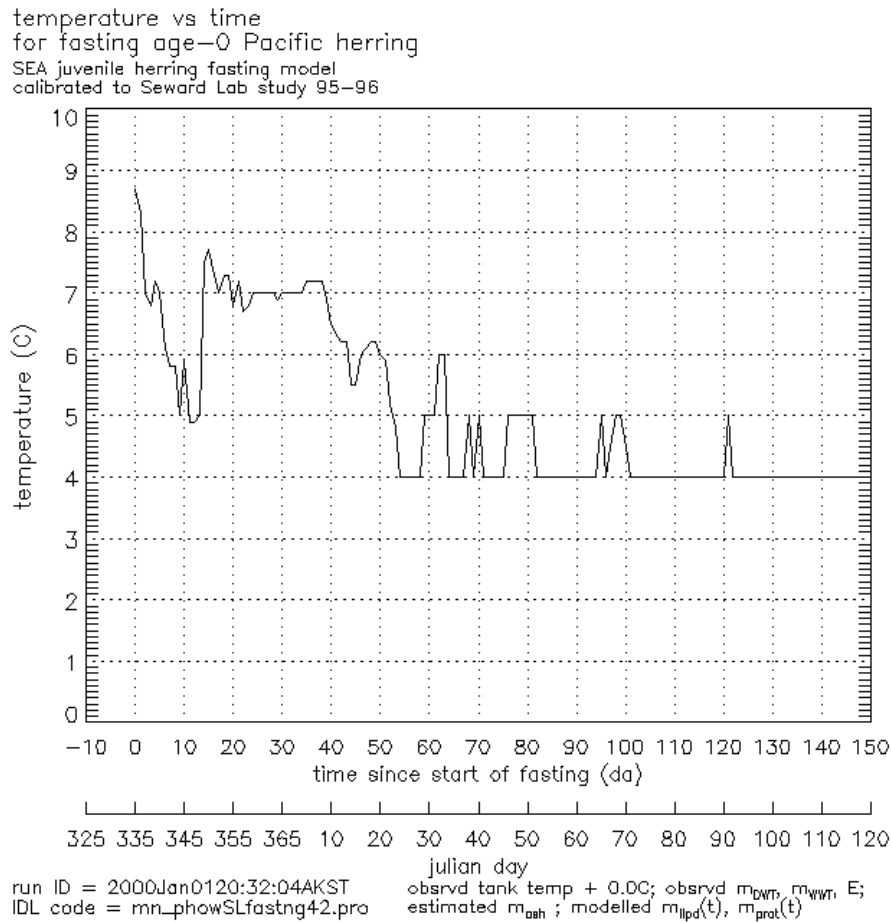


Figure 3.4 Temperature time series for the Seward Laboratory fasting experiment. The record shown is a composite of Fig. 2 (p80) for the “short” experiment and Fig. 3 (p81) for the “long” experiment reported by Paul and Paul [PP98].

4. Calibration Procedures

A reassuring result from this section is that calibration procedures 2, 4, and 5 serve to strongly constrain the model to the behavior exhibited by the individuals in the Seward Lab fasting experiment. That is, the value for any one parameter in Table 2.1 really matter very little as long as *all* of the calibration procedures in Table 2.1 have been carried out. The list of procedures insures that the values in Table 2.1 *as a set* produce a system that reacts as much like the record contained in the Seward Laboratory fasting study as the model structure and the parameter values allow.

If one wished to configure a “sensitivity analysis” then one must construct a variation analysis of a constrained system of equations. The final calibration step, step 5, is the constraint. At the conclusion of all of the prior calibration procedures Step 5 will set C_0 so that the values for all of the other parameters are compensated for in the sense of getting the model to reproduce the survival exhibited by the fasting experiment. One can, and should during any application design review, attempt to break the model by introducing bizarre parameters. This has been done to quite some degree during the development: despite major changes between Versions 1 and 3, the results regarding physiological responses and patterns of survival remain basically the same. For example, the ordering of initial fall conditions with respect to spring survival is stable. The actual survival may change but the order persists. And even if the survival values differ it is difficult to find changes such that the qualitative survival classifications (e.g., “high” versus “low”) change.

This robustness is due to the action of three constraints.

- (1) $m_L > 0$: acts on \widehat{E}_P
- (2) boundary of \mathcal{P}^\square set by Ω_3^ℓ : acts on L_* , with L_* adapting to changes to \widehat{E}_P .
- (3) advance Ω^s in time to the boundary of \mathcal{P}^\square and constrain to Ω^ℓ : acts on C_0 , which adjusts in response to changes in L_* and to A_{L2P}

The effect of these constraints is to force the model to exhibit the survival properties contained within the Seward Laboratory study. As a consequence, the behavior of the model cannot deviate widely regardless how one cooks the parameters. From this it should be clear why in the “Validation Reference” there was a strong emphasis on testing the capability of the model to correctly forecast the location of the set \mathcal{P}^\square . This robustness does not mean that the model does not reveal the details of the time evolution of the physiology. Examples of such detail will be a second result of this section.

We now proceed to substantiate the foregoing claims.

Step 0, part a. $C_{0,LP}$, γ , k , \widehat{E}_L and \widehat{E}_P in the solution Φ

If we examine the solution Φ in (2.3) we can quickly see why the final calibration step in Step 5 will compensate for the values assumed by each of the parameters identified as “Step 0” in Table 2.1. We only need to consider the solution for m_L for, as we will see, it alone is the variable which determines survival. From (2.3) we have that all of the parameters in question act through the single time dependent factor $Q(t)$ where

$$Q(t) = \frac{C_0 C_{0,LP}^k (1-k) \int_0^t e^{\gamma T(s)} ds}{\widehat{E}_L + A_{L2P} \widehat{E}_P} \quad (4.1)$$

Here we are holding A_{L2P} and \widehat{E}_P fixed for these two will be set in a later step. We also hold k fixed for it appears elsewhere in the solution as well.

We can expose the role of γ much more clearly than in (4.1).⁵ Let $\langle T \rangle_t$ denote the mean of the temperature time series T over the time interval $[0, t]$, $\langle T \rangle_t = \frac{\int_0^t T(s) ds}{t}$. Since $e^{\gamma T(s)} = e^{\gamma \langle T \rangle_t} e^{\gamma(T(s) - \langle T \rangle_t)}$ we can take advantage of our knowledge that the upper bound for $|T(s) - \langle T \rangle_t|$ for any t and for all s in $[0, t]$ is approximately 3C. (See the 2-node approximation in §2.7 Doc 2.) From Arrhenius⁶ $\gamma = 0.055\text{C}^{-1}$. Therefore the first order approximation $e^{\gamma(T(s) - \langle T \rangle_t)} \approx 1 + \gamma(T(s) - \langle T \rangle_t)$ is quite accurate. Hence

$$\int_0^t e^{\gamma T(s)} ds = e^{\gamma \langle T \rangle_t} \int_0^t e^{\gamma(T(s) - \langle T \rangle_t)} ds \approx e^{\gamma \langle T \rangle_t} \int_0^t (1 + \gamma(T(s) - \langle T \rangle_t)) ds = e^{\gamma \langle T \rangle_t} t$$

Returning to Q

$$Q(t) = C_0 \frac{C_{0,LP}^k (1-k) e^{\gamma \langle T \rangle_t} t}{\widehat{E}_L + A_{L2P} \widehat{E}_P} \quad (4.2)$$

It is now clear that the value for C_0 obtained in Step 5 will correct for the effects of all of the other factors in Q . For example, the constant $C_{0,LP}$ was defined in Version 1 using values Baltic herring so that C_0 would not have to correct for the difference between the “LP” and the standard “WWT” formulation for the tissue-type metabolic cost function. It makes no difference how it is defined. It can be set to any value other than 0.

The value selected for γ will be “compensated” for by calibration step 5. The Seward Laboratory study has a well-defined temperature time series that fixes $\langle T \rangle_t$ for each t . The calibration step 5 will adjust C_0 to make whatever γ is chosen “work.” That adjustment, however, is in the sense of getting the “mean response” to be consistent with observations. *If γ is increased significantly then the magnitude of the physiological change in response to temperature change above and below the*

⁵ One should not overdue the effort to cope with the specific functional form for the temperature dependence. This functional form is itself an empirical approximation whose origins are difficult to determine. We are about to see that a first order polynomial would have yielded identical results.

⁶ It is a curiosity that empirical constants such as γ are commonly reported to three or more significant figures. The value given by Arrhenius is $\gamma = 0.0546$.

mean will be greater. The mean behavior will be the same. In particular, the midpoint survival (e.g., 0.50) will be effectively the same. The model and the measurements are far from a stage where we can begin to parameterize in the tangent space, i.e., for the magnitude and direction of change in response to temperature change. Therefore we use the conventionally accepted value for γ for the foreseeable future.

The value for the exponent k is well established both empirically and more recently theoretically. The consistency with which the value 0.7 occurs has generated a significant history of inquiry. A recent paper establishes a theoretical basis for the value. There is no reason to use any other value.

There is ambiguity over just what the exponent k is applied to. This ambiguity permeates throughout more than just the topic of respiration. The ambiguity is due to the widely differing methods to characterize “size” combined with the overuse of “size,” once formulated, as the argument for functions of physiological state, now assumed to dependent on only a single scalar variable. Throughout this model we have taken pains to introduce no scalar valued function of physiological state which can mistakenly be interpreted as a definition of the “size.”

This is the reason for constructing the generalized metabolic cost function in §2.7 Doc 2. Early tests at Version 1 indicated some difference would be seen with the various options. However, the work with the Seward Laboratory results showed that the lipid to protein ratio was lower than that presumed in Version 1 and that there was in fact little difference between the options for metabolic cost functions. Therefore, Version 2 focused on the “LP” formulation, that option being the simplest of the group. Version 3 similarly uses the “LP” cost function. However, that assumption is due to be reconsidered. With the addition of significant protein use in Version 3, a primary assumption of Version 2 (low protein usage) is replaced. We have continued with the “LP” formulation and expect to find it fully adequate. At most we expect any increased sensitivity to choice of cost function to tend to favor the “LP” costs over either “wet mass” or “carbon equivalent mass” for the reasons described in §2.7 Doc 2.

The expression for Q in (4.2) also explains why we have not gone to efforts to distinguish between values for \widehat{E}_p for protein energy recovered in bomb calorimetry and for protein energy recovered by an individual to meet basal metabolic requirements during fasting. If we were to use a different value for \widehat{E}_p in the solution Φ that value would appear as shown in (4.2) and simply lead to a different calibration value for C_0 . We have no means to determine that one choice of \widehat{E}_p is better than another.

Step 0., part b. \widehat{E}_L and \widehat{E}_P in the conversion to physiological variables

From (4.2) we know that the choices for \widehat{E}_P and \widehat{E}_L will be compensated for by C_0 within the solution Φ . However, the solution Φ acts on initial conditions in terms of (m_P, m_L, m_A, m_W) and in Step 5 is calibrated relative to final conditions in terms of (m_P, m_L, m_A, m_W) . These initial and final conditions are established by the linear transformation L_{bc}^{-1} from observed variables to physiological variables. L_{bc}^{-1} is given explicitly in (2.1). The significance of (4.2) is that, since we are using the Seward Laboratory fasting experiment to determine the parameter C_0 , the model solution Φ “sees” the transformation L_{bc}^{-1} *only* through the physiological states (m_P, m_L, m_A, m_W) used in the calibration of Φ ; although the parameters \widehat{E}_L and \widehat{E}_P appear explicitly in (4.2), they are absorbed into the unspecified C_0 as part of the calibration. As a consequence, when we deal with these two parameters we can focus solely on the realism of L_{bc}^{-1} without regard for the realism of Φ .

We begin, then, to examine L_{bc}^{-1} . We take the current values of \widehat{E}_L and \widehat{E}_P and carry out the conversions from laboratory variables to physiological variables to see what we have. After that we will look at the consequences and how these are effected by the choices used in that conversion.

Figure 4.1 shows the variables m_P, m_L, m_A, m_W from the Seward Laboratory fasting experiment displayed in the same format as was used to display the four laboratory variables in Figure 3.1. To make this more explicit, we show in Table 4.1 the same records that were shown in Table 3.1 but now converted to the coordinates m_P, m_L, m_A, m_W .

Table 4.1: example records from the Seward Laboratory fasting experiment

m_P g	m_L g	m_A g	m_W g	slen mm	survey date	site name	file	fish ajp	ash ajp by
0.6119	0.3129	0.2222	4.453	90.0	1995 12 01	SewardLabExp	0	1	s12ash
0.8445	0.4655	0.186	4.004	85.0	1995 12 01	SewardLabExp	0	22	s12ash
0.3347	0.1661	0.1482	3.051	79.0	1995 12 28	SewardLabExp	1	1	s12ash
0.2352	0.1778	0.093	1.794	68.0	1995 12 28	SewardLabExp	1	22	s12ash
0.4204	0.3157	0.1929	3.771	86.0	1996 01 25	SewardLabExp	2	1	s12ash
0.3263	0.1485	0.1482	2.977	79.0	1996 01 25	SewardLabExp	2	22	s12ash
0.1393	0.08436	0.0973	0.879	69.0	1996 01 17	SewardLabExp	3	1	s12ash
0.1956	0.05957	0.0848	1.26	66.0	1996 03 08	SewardLabExp	3	15	s12ash
0.1955	0.08153	0.121	1.802	74.0	1996 04 01	SewardLabExp	3	30	s12ash
0.1967	0.1094	0.1369	2.457	77.0	1996 04 01	SewardLabExp	4	1	s12ash
0.09413	0.08207	0.0848	1.339	66.0	1996 04 01	SewardLabExp	4	18	s12ash

The four variables in the format of Figure 4.1 will be useful later in these calibration procedures. But first we will want to see these same variables in their appropriate “context,” that is, as the coordinate variables of the physiological states of the individuals in the fasting experiment. Figure 4.1 shows each coordinate variable for each individual “taken out of context” of the physiological state for that individual. In contrast, our first priority is to see the collection of physiological states (m_P, m_L, m_A, m_W) that comprise the findings of the Seward Laboratory fasting experiment.

There are methods to view the 4-dimensional distribution of states in \mathcal{P} , but such methods are beyond the scope of these documents. As a substitute we will use a collection of projections of \mathcal{P} to 2-dimensional planes. The planes are selected on the basis of structure that has been built into the model, structure which implements the basic assumptions about the nature of the physiological

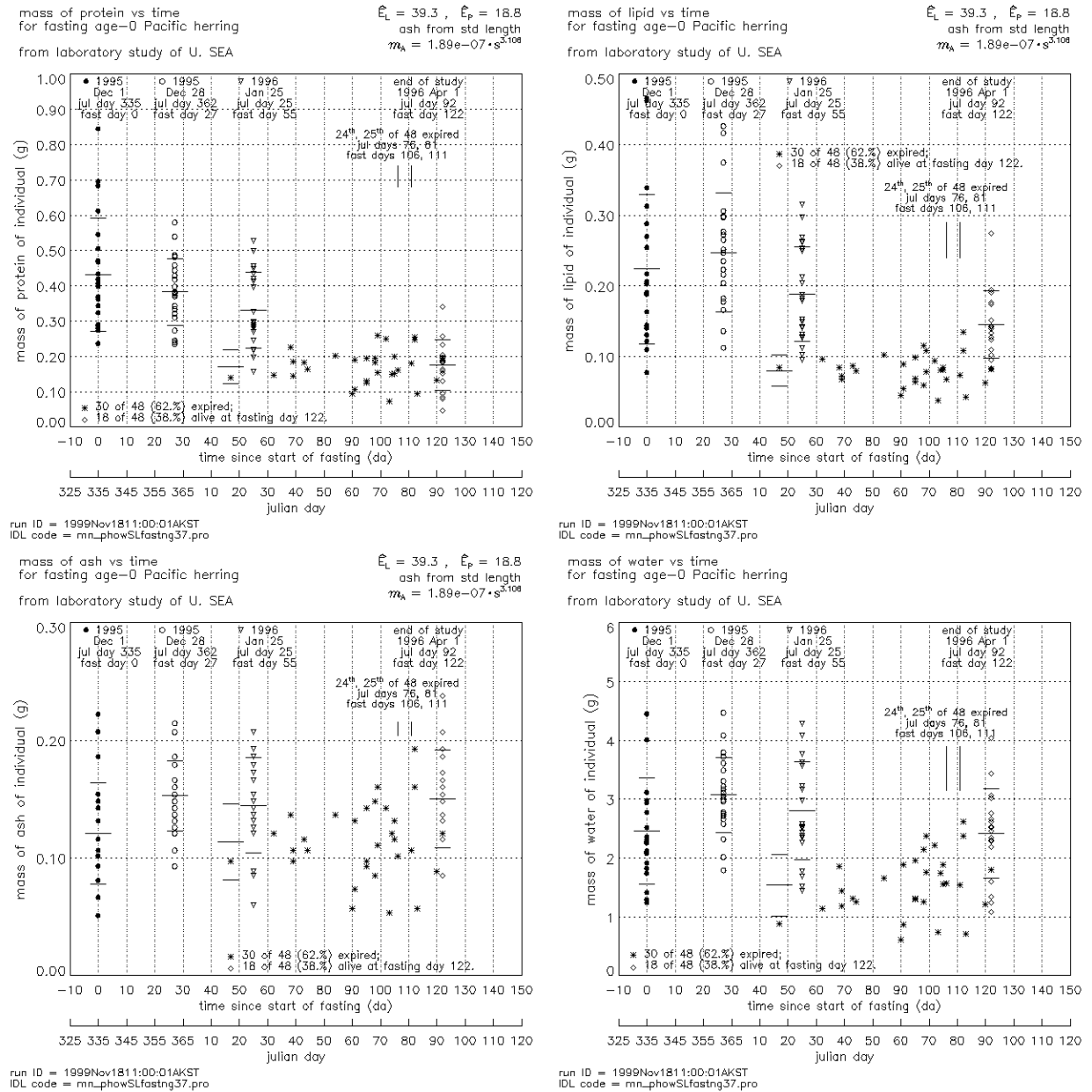


Figure 4.1 The physiological variables m_P , m_L , m_A , m_W from the Seward Laboratory fasting experiment obtained using $\hat{E}_P = 18.8 \text{ kJ g}^{-1}$ and $\hat{E}_L = 39.3 \text{ kJ g}^{-1}$

responses during fasting. Figure 4.2 shows the four projections diagramed in (4.3) applied to the Seward Laboratory study.

The first three projections in (4.3) and their graphical display (the top and lower left panels of Figure 4.2) are the primary workhorses of this document. They take advantage of the model structure in the manner shown by the single arrow in the upper left of each panel. Each arrow

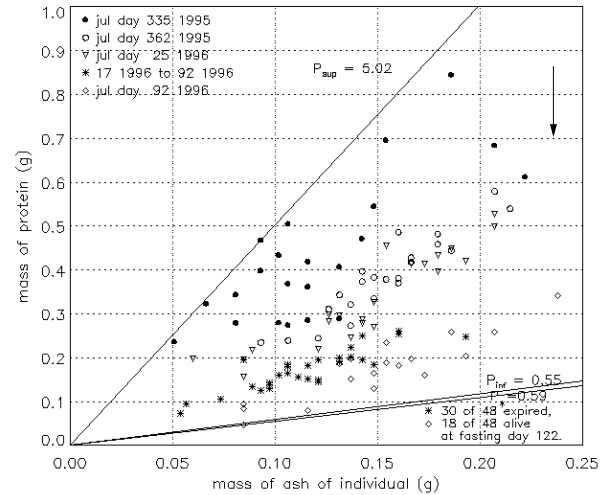
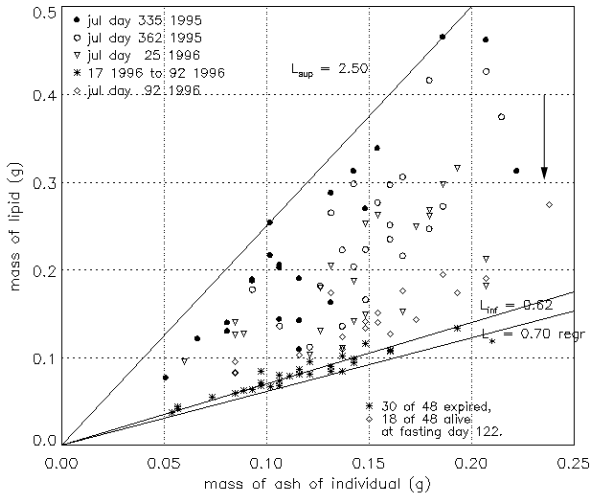
$$\begin{array}{c}
 (m_P, m_L, m_A, m_W) \\
 \swarrow \quad \searrow \quad \swarrow \quad \searrow \\
 (m_A, m_L) \quad (m_A, m_P) \quad (m_P, m_L) \quad (m_A, m_W)
 \end{array}
 \tag{4.3}$$

mass of lipid vs mass of ash
for fasting age-0 Pacific herring
SEA juvenile herring fasting model
calibrated to Seward Lab study 95-96

$\hat{E}_L = 39.3$, $\hat{E}_P = 18.8$
ash from std length
 $m_A = 1.89e-07 * s^{3.108}$

mass of protein vs mass of ash
for fasting age-0 Pacific herring
SEA juvenile herring fasting model
calibrated to Seward Lab study 95-96

$\hat{E}_L = 39.3$, $\hat{E}_P = 18.8$
ash from std length
 $m_A = 1.89e-07 * s^{3.108}$



run ID = 1999Nov1719:34:27AKST
IDL code = mn_phowSLfastng37.pro

obsrvd tank temp + 0.0C; obsrvd $m_{W(t)}$, $m_{W(t)}$, E_i ;
estimated m_{ash} ; modelled $m_{L(t)}$, $m_{P(t)}$

run ID = 1999Nov1719:34:27AKST
IDL code = mn_phowSLfastng37.pro

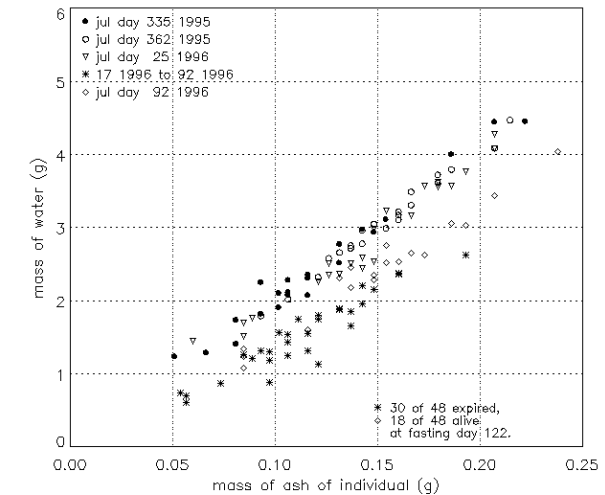
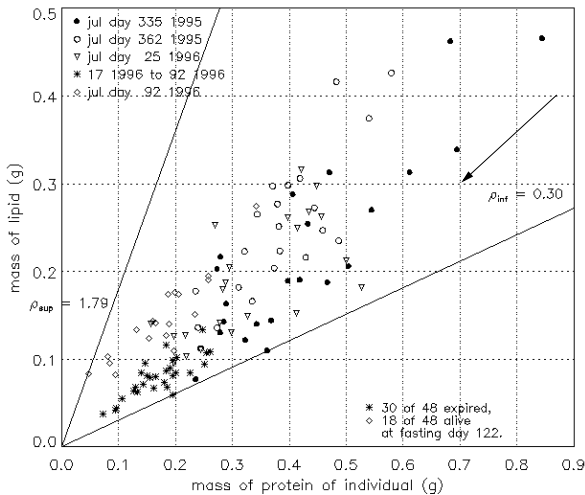
obsrvd tank temp + 0.0C; obsrvd $m_{W(t)}$, $m_{W(t)}$, E_i ;
estimated m_{ash} ; modelled $m_{L(t)}$, $m_{P(t)}$

mass of lipid vs mass of protein
for fasting age-0 Pacific herring
SEA juvenile herring fasting model
calibrated to Seward Lab study 95-96

$\hat{E}_L = 39.3$, $\hat{E}_P = 18.8$
ash from std length
 $m_A = 1.89e-07 * s^{3.108}$

mass of water vs mass of ash
for fasting age-0 Pacific herring
SEA juvenile herring fasting model
calibrated to Seward Lab study 95-96

$\hat{E}_L = 39.3$, $\hat{E}_P = 18.8$
ash from std length
 $m_A = 1.89e-07 * s^{3.108}$



run ID = 1999Nov1719:34:27AKST
IDL code = mn_phowSLfastng37.pro

obsrvd tank temp + 0.0C; obsrvd $m_{W(t)}$, $m_{W(t)}$, E_i ;
estimated m_{ash} ; modelled $m_{L(t)}$, $m_{P(t)}$

run ID = 1999Nov1719:34:27AKST
IDL code = mn_phowSLfastng37.pro

obsrvd tank temp + 0.0C; obsrvd $m_{W(t)}$, $m_{W(t)}$, E_i ;
estimated m_{ash} ; modelled $m_{L(t)}$, $m_{P(t)}$

Figure 4.2 The physiological conditions of the Seward Laboratory fasting experiment projected to the four 2-dimensional planes $m_A \times m_L$, $m_A \times m_P$, $m_P \times m_L$, and $m_A \times m_W$.

shows the direction of the vector field determining the motion of an individual through \mathcal{P} during fasting. In the top panels the vector field is vertically downward because $dm_A/dt = 0$. The relative sizes of the arrows correspond to $A_{L2P} = 1.7$, where $dm_P/dt = A_{L2P}dm_L/dt$. The arrow shown is to be interpreted as applicable at only the specific point (m_P, m_L, m_A, m_W) at which the tail of the arrow is located. The arrows (or vectors) in the top panels represent the rate at which m_P and m_L is being used for basal metabolic requirements. Those requirements depend on (m_P, m_L, m_A, m_W) and are modelled by (7.23) of §7 Doc 2, hence the size of the arrow varies over each of the top planes. Moreover, we *cannot* use one arrow at any point in either of the upper planes because the rate depends on *both* m_P and m_L , but we see only the projection. However, the direction is vertically downward for all vectors; only the length will differ.

The foregoing ambiguity regarding projection does not occur in the case of the lower left panel. This is because the rate is assumed independent of m_A and m_W . Hence, the vector we have shown in the lower left panel at the projected point $(m_P, m_L) = (0.87, 0.4)$ is the same for all (m_P, m_L, m_A, m_W) such that $m_P = 0.87$ and $m_L = 0.4$. (However, we have not attempted to show an exact magnitude for the vector, we show only the correct direction for $A_{L2P} = 1.7$ and a reference length.)

With these utilities and with the example of their use with the current calibration, we can now turn to the procedures whereby that calibration was established. The first calibration procedure is not strictly a calibration of the model and the procedure will leave us with an Open Issue for any new implementation plan.

4.1 Step 1. [optional] Determination of ash with legacy datasets

In the preceding discussion of Figure 4.2 we noted that the projection to the 2-dimensional plane $X \times m_A$ had the property that the time evolution of an individual in \mathcal{P} would appear in the plane $X \times m_A$ as a downward movement. We noted that this was an assumption of the model equations (7.23) §2.7 Doc 2; to the degree the model is a good approximation of the physiology then we should see the same this reflected in observations.

The circumstances whereby m_A was not measured (except for a small test set of 41 individuals) was described in §2 of this document. To address this limitation an empirical approximation was developed by Mason and Paul wherein the unknown m_A is estimated by a function $F_{\ell 2A}$ which depends only on standard length ℓ

$$F_{\ell 2A}(\ell) = \alpha_1 \ell^{\alpha_0}$$

with the present calibration being $\alpha_1 = 1.893 \times 10^{-7}$ and $\alpha_0 = 3.106$ for ℓ in millimeters. These parameter values overstate the appropriate accuracy since ℓ in millimeters is reported only to two significant figures for the case at hand.

In this section we seek to understand the significance of this approximation for the model. A picture of the situation is helpful.

$$\begin{array}{ccc}
 & \mathcal{P} \times \mathbb{R}_+ & \\
 \swarrow & & \searrow \\
 (E, m_{\text{DWT}}, m_{\text{WWT}}, m_A, \ell) & \xrightarrow{L_{\text{bc}}^{-1} \times \text{id}} & (m_P, m_L, m_A, m_W, \ell) \\
 \downarrow F \times \text{id} & & \searrow \text{id} \times F_{\ell 2A} \\
 & & (m_P, m_L, m_A, m_W, F_{\ell 2A}(\ell)) \\
 & & \\
 (E, m_{\text{DWT}}, m_{\text{WWT}}, F_{\ell 2A}(\ell), \ell) & \xrightarrow{L_{\text{bc}}^{-1} \times \text{id}} & (\tilde{m}_P, \tilde{m}_L, F_{\ell 2A}(\ell), m_W, \ell)
 \end{array} \tag{4.4}$$

In (4.4) $\mathcal{P} \times \mathbb{R}_+$ simply means add one new variable, standard length ℓ to the four we already have in physiological space \mathcal{P} . The next row shows two coordinate systems for $\mathcal{P} \times \mathbb{R}_+$: one consisting of the bomb calorimetry variables with standard length, the other the physiological variables with standard length. If we append the identity map to L_{bc}^{-1} , denoted by $L_{\text{bc}}^{-1} \times \text{id}$, then we have a coordinate variable transformation as before.

In the bottom row we make a change. We replace the variable m_A in $(E, m_{\text{DWT}}, m_{\text{WWT}}, m_A, \ell)$ with $F_{\ell 2A}(\ell)$. We denote the map that made this change by $F \times \text{id}$. The map $F \times \text{id}$ goes from a point in $\mathcal{P} \times \mathbb{R}_+$ to another point in $\mathcal{P} \times \mathbb{R}_+$ that to some degree is close to the first. When we apply the transformation $L_{\text{bc}}^{-1} \times \text{id}$ to the approximating point in laboratory coordinates we get the approximating point in the physiological coordinate variables. In particular, from the form of L_{bc}^{-1} in (2.1) we have that m_W is not changed by that m_P and m_L are replaced by approximations \tilde{m}_P and \tilde{m}_L . We shall look at some error estimates for those approximations.

The function $F_{\ell_{2A}}$ can be used in a second way, and this is indicated by the map $\text{id} \times F_{\ell_{2A}}$ on the right of the diagram in (4.3). The effect of $F_{\ell_{2A}}$ is to transform ℓ into a mass with a value that happens to be an approximation of the mass of ash. The map $\text{id} \times F_{\ell_{2A}}$ transforms $\mathcal{P} \times \mathbb{R}_+$ such that all variables are mass. The coordinate variable $F_{\ell_{2A}}(\ell)$ retains the physiological order associated with ℓ but scales as a mass.

The conclusions from this section are collected in a set of “comments.”

Comment 1. *All conclusions regarding site fidelity are not affected by the approximation for m_A ; in fact, the conclusions can be said to be stronger because they are based on the variable $F_{\ell_{2A}}(\ell)$ rather than measured ash.*

Explanation. The variable m_A has been mentioned for the information it provides regarding consistency between experimental results and assumptions regarding populations permanence—that is, that populations are not changing during winter due to factors other than fasting survival. The basis for this role is the assumption that $\frac{dm_A}{dt} = 0$. Since in all cases the variable used for this purpose is $F_{\ell_{2A}}(\ell)$ and since there is general consensus that $\frac{d\ell}{dt} = 0$, there is, in fact, a higher confidence with the use of $F_{\ell_{2A}}(\ell)$ than would be the case with measured m_A . \square

The next comments address the error in \tilde{m}_P and \tilde{m}_L .

Comment 2. *The relative change in \tilde{m}_P and \tilde{m}_L due to relative change in the estimated \tilde{m}_A , with E , m_{DWT} , and m_{WWT} fixed, increases as m_P and m_L decrease. In particular, the magnitude of the relative change increases as fasting progresses during winter. Explicitly,*

$$\frac{m_A}{m_L} \frac{\partial m_L}{\partial m_A} = + \frac{\widehat{E}_P}{\widehat{E}_L - \widehat{E}_P} \frac{m_A}{m_L} \quad (4.5)$$

$$\frac{m_A}{m_P} \frac{\partial m_P}{\partial m_A} = - \frac{\widehat{E}_P}{\widehat{E}_L - \widehat{E}_P} \frac{\widehat{E}_L}{\widehat{E}_P} \frac{m_A}{m_P} \quad (4.6)$$

In terms of approximate upper bounds, given a 10% error in m_A , for fall physiological conditions the change for m_P will be at most 3% and for m_L from 3% up to 10%; for near fatal spring conditions the change for m_P and m_L will be at most 10%.

Explanation. (4.5) and (4.6) are obtained by taking the partial derivatives of L_{bc}^{-1} with respect to m_A . A useful approximation is that \widehat{E}_L is twice \widehat{E}_P , hence $\widehat{E}_P/(\widehat{E}_L - \widehat{E}_P) \approx 1$. (A second useful but less reliable approximation is that m_P is about twice m_L . Hence, $\frac{\widehat{E}_L}{\widehat{E}_P} \frac{1}{m_P} \approx \frac{1}{m_L}$, and the righthand side of both equations is approximately m_A/m_L . but we shall be slightly more precise and identify two fall scenarios.) Approximation for the ratios $m_A:m_L:m_P$ are as follows. In fall, with m_L near its upper bound in the set of reachable physiological states, the ratios are 1:3:6. The m_L component is not necessarily near the upper bound and ratios similar to 1:1:6 are possible. In spring the ratios for post-fasting, near fatal conditions are 1:1:2. Thus $\frac{m_A}{m_L}$ is in the range 0.3 to 1 in fall and

approximately 1 in spring. For $\frac{\widehat{E}_L}{\widehat{E}_P} \frac{m_A}{m_P}$ the value is 0.3 in fall and approximately 1 in spring. \square

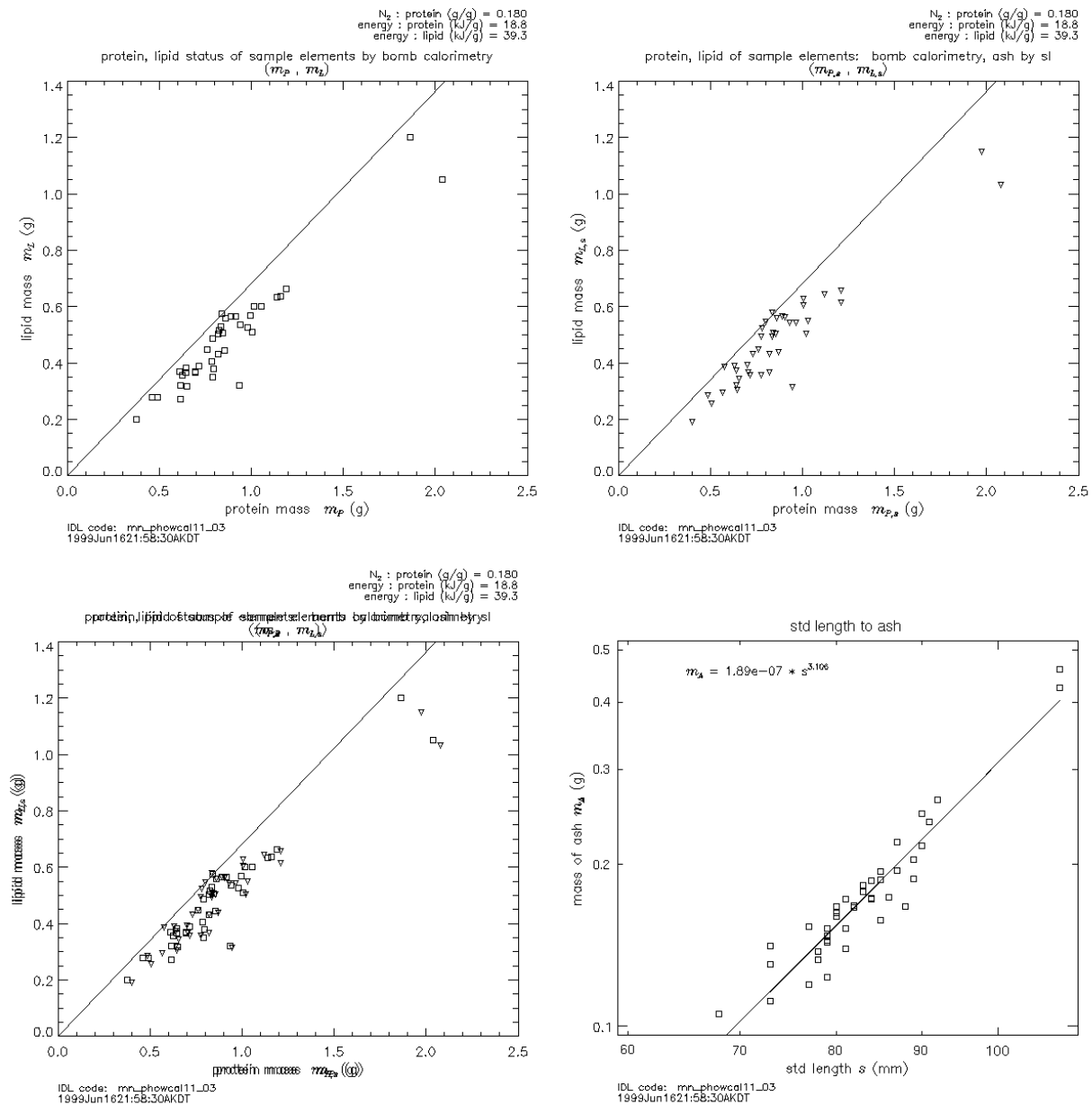


Figure 4.3 The manner in which estimation errors for m_A appear in m_P and m_L .

Comment 2 can be made more graphic. Figure 4.3 displays the comparison of (m_P, m_L) from L_{bc}^{-1} using measured m_A (upper left panel) with $(\tilde{m}_P, \tilde{m}_L)$ from L_{bc}^{-1} using estimated $\tilde{m}_A = F_{\ell 2A}(\ell)$ (upper right panel) for the case of the 41 individuals used to establish $F_{\ell 2A}$. The lower left panel is the overlay of the upper two. The lower right is a redisplay of a previous figure, the logarithmic plot of the pairs (ℓ, m_A) . The information in Figure 4.3 is consistent with Comment 2: for all 41 individuals used to establish $F_{\ell 2A}$ were from fall 1995 monitoring surveys. The the errors and

the aforementioned ratios for the samples in Figure 4.3 are consistent with the fall scenario of Comment 2.

Comment 3. *If in fact $\frac{dm_A}{dt} < 0$ but m_A is assumed constant then the estimated magnitude for the rate of decrease of m_P is too large and the estimated magnitude for the rate of decrease of m_L is too small.*

Explanation. Apply Comment 2; note the sign difference and use a change in time for m_A in place of an estimation error.

Comment 4. *The assumption $\frac{dm_A}{dt} = 0$ must remain an Open Issue. With existing information it cannot be confirmed. On the other hand, nothing is found that is inconsistent with the assumption. The present conclusion is that this Open Issue can be resolved with ash measurements for post-fasting juveniles in spring and for low lipid pre-fasting juveniles in fall from any convenient field location, that a controlled experiment is not a necessary requirement.*

Explanation. There is evidence that the approximation $F_{\ell_{2A}}$ is good for fall conditions. There is an analytic estimate for the sensitivity to error as m_P and m_L decline. The missing information is whether m_A is indeed an invariant of fasting and whether the error in the approximation of ash from standard length degrades as conditions degrade. If m_A is an invariant, then the properties of the approximation in Figure 4.3 should be constant. If, however, m_A declines, that process will need to be identified. \square

To the extent that m_A is dominated by skeletal structures that are in fact the mechanism by which standard length remains fixed during fasting, then indeed m_A is a constant of fasting. This has been a conjecture throughout, and there has been no reason seen to discard the conjecture. But the foregoing is required to make the end-user aware that the confirmation of the conjecture is not yet complete. It is, however, a straightforward task to complete the confirmation. Since it is well accepted that length is an invariant, then a comparison of spring m_A relative to standard length will determine if the relationship changes between fall and spring as fasting progresses.

A second scenario for which Figure 4.3 may be inadequate is one which is highlighted in the next calibration procedure. In this scenario the fall physiological state has integrated prior conditions such that protein is near normal but m_L is significantly below its reachable upper bound for given the values for the other three physiological coordinate variables. For this scenario the question is whether ash is lower for a given standard length than is specified by the function $F_{\ell_{2A}}$. This scenario has less effect upon the conclusions of these documents so we have not presented this as a separate comment. However, we have included in Comment 4 the recommendation of ash measurements for both fall and spring because of this second scenario.

Those using the graphics from this work should note that in all cases wherein computed ash has been used to compute L_{bc}^{-1} this fact is indicated in the legends in the graphic. The parameters for the function $F_{\ell_{2A}}$ are provided as part of the legend.

4.2 Step 2. Upper bound for \widehat{E}_P

This section continues with the calibration of L_{bc}^{-1} . There are two parameters, \widehat{E}_P and \widehat{E}_L , both of which have been measured for a wide diversity of organisms. These are, however, constants only in the sense of whole body averages for a specific class of organisms. Neither constant is traceable to a specific biochemical structure whose thermodynamic state can be established from physical chemistry principles. Rather, each “constant” may well vary within a specific class. For example, the “constant” is to our knowledge not tested at the initial and final times of an extended interval of severe physiological stress such as fasting. It seems reasonable to not exclude the possibility of non-uniform use of tissues with differing energy content per unit mass during fasting. It seems prudent to view reported values as approximations of a value that may well vary within some small but not insignificant range.

Because of this conditional perspective on the values for \widehat{E}_P and \widehat{E}_L , we have looked to the system under investigation for all possible clues regarding the most appropriate values for the two “constants”

In this calibration procedure we look at the information regarding \widehat{E}_P obtained by considering the most basic of all constraints for m_L

$$m_L > 0 \quad (4.7)$$

This constraint applied to the m_L component of the transformation L_{bc}^{-1} (see (2.1)) provides an upper bound for \widehat{E}_P

$$\widehat{E}_P < \frac{E}{m_{DWT} - m_A} \quad (4.8)$$

Let Ω denote the entire collection of all individual age-0 herring measured for physiological state, let ω be a member of Ω , and use ω as an index on the laboratory variables, as in $m_{DWT,\omega}$ and $m_{A,\omega}$. Then

$$\widehat{E}_P < \widehat{E}_{P,\text{lub}} = \inf \left\{ \frac{E_\omega}{m_{DWT,\omega} - m_{A,\omega}} : \omega \text{ in } \Omega \right\} \quad (4.9)$$

Each quotient $\frac{E_\omega}{m_{DWT,\omega} - m_{A,\omega}}$ for each individual juvenile ω provides an upper bound for \widehat{E}_P ; the infimum (or minimum) of such upper bounds for the entire collection Ω of all individuals is the “least upper bound” (lub) $\widehat{E}_{P,\text{lub}}$ for \widehat{E}_P as defined by that collection.

Table 4.2 shows the output of the shell script filter⁷ written to find $\widehat{E}_{P,\text{lub}}$ from datasets in the format shown in Tables 3.1 and 3.2. The output of the script computes the quotient in (4.8), sorts the archive by that quotient in ascending order, then writes the quotient to the first column followed by those columns relevant to the calculation.

The records in Table 4.2 are the 29 smallest values for the quotient out of the 2544 records for age-0 herring from the field monitoring program. The result in Table 4.2 indicates that almost surely \widehat{E}_P is less than 20. Note that if $\widehat{E}_P = 20$, then an individual whose physiological state is such that

⁷ See the documentation “Algorithms and Information Assets” for information on locations for code and scripts developed to implement these models.

Table 4.2: initial 29 of all field records, in ascending order for $\widehat{E}_{P,\text{lub}}$

$\frac{E}{m_{\text{DWT}} - m_{\text{A}}}$ kJ/g	E kJ	m_{DWT} g	m_{A} g	slen mm	survey date	site name	file ajp	fish ajp	ash by
19.17	4.665	0.3132	0.06983	62.0	1997 10 23	Zaikof Bay	j133	4140	s12ash
19.96	15.71	0.973	0.186	85.0	1996 03 19	Drier Bay	j40	5	s12ash
20.23	20.93	1.183	0.1482	79.0	1995 10 19	Whale Bay	j25	4	s12ash
20.33	20.58	1.205	0.1929	86.0	1996 03 24	Whale Bay	j42	46	s12ash
20.45	10.07	0.5988	0.1064	71.0	1995 11 08	Hogg Bay	j29	25	s12ash
20.57	2.275	0.133	0.02241	43.0	1996 10 03	Simpson Bay	j50	376	s12ash
20.67	2.226	0.127	0.01933	41.0	1996 10 03	Simpson Bay	j50	350	s12ash
20.77	15.74	0.9439	0.186	85.0	1996 03 23	Paddy Bay	j41	52	s12ash
20.86	12.83	0.7312	0.116	73.0	1995 11 08	Hogg Bay	j29	30	s12ash
20.9	3.163	0.179	0.02763	46.0	1996 10 03	Simpson Bay	j50	392	s12ash
20.93	3.356	0.188	0.02763	46.0	1996 10 03	Simpson Bay	j50	356	s12ash
20.94	7.048	0.3904	0.05378	57.0	1997 10 22	Simpson Bay	j130	3677	s12ash
20.96	10.36	0.6006	0.1064	71.0	1997 10 23	Zaikof Bay	j133	4094	s12ash
20.96	3.74	0.208	0.02954	47.0	1996 10 03	Simpson Bay	j50	393	s12ash
21.14	10.82	0.6049	0.09303	68.0	1997 10 22	Simpson Bay	j130	3586	s12ash
21.17	13.88	0.8221	0.1664	82.0	1996 03 23	Paddy Bay	j41	53	s12ash
21.21	23.38	1.34	0.2379	92.0	1996 03 13	Eaglek By.	j36	62	s12ash
21.22	13.58	0.7611	0.121	74.0	1995 11 08	Hogg Bay	j29	40	s12ash
21.25	3.518	0.188	0.02241	43.0	1996 10 03	Simpson Bay	j50	360	s12ash
21.27	3.216	0.172	0.02083	42.0	1996 10 03	Simpson Bay	j50	382	s12ash
21.35	3.895	0.2101	0.02763	46.0	1996 10 03	Simpson Bay	j50	357	s12ash
21.36	34.46	1.931	0.3179	101.0	1997 03 05	Simpson Bay	j90	1872	s12ash
21.37	3.594	0.194	0.02581	45.0	1996 10 03	Simpson Bay	j50	353	s12ash
21.38	7.172	0.381	0.04547	54.0	1996 10 03	Simpson Bay	j50	397	s12ash
21.39	12.34	0.6742	0.09735	69.0	1997 10 23	Zaikof Bay	j133	4095	s12ash
21.4	5.226	0.28	0.0358	50.0	1996 10 03	Simpson Bay	j50	377	s12ash
21.43	10.05	0.5801	0.1111	72.0	1996 03 23	Paddy Bay	j41	3	s12ash
21.43	12.91	0.7043	0.1018	70.0	1997 10 23	Zaikof Bay	j133	3991	s12ash
21.43	16.95	0.9839	0.1929	86.0	1996 03 19	Drier Bay	j40	10	s12ash

$\frac{E}{m_{\text{DWT}} - m_{\text{A}}} = 20$. must necessarily have completely used all lipid. These practicalities lead us to use the quotients as strictly larger than \widehat{E}_{P} . Based on Table 4.2, along with other development considerations, we have used $\widehat{E}_{\text{P}} = 18.8 \text{ kJ g}^{-1}$ in Version 3.1. This choice makes \widehat{E}_{P} in fact a lower bound for all records in Table 4.2, including the first. The quotient for the first record is admittedly 4% lower than the second record. On the other hand, we viewed the value 18.8 as being no more than 5% lower than 19.7 which seems the largest value one could use in light of the results in Table 4.2. All experience with the model is that such a difference will not materially alter the conclusions the model provides regarding the issues that are its primary purpose. We collect this into a “calibration statement” for Step 2.

Step 2 calibration result for \widehat{E}_{P} . By virtue of the constraint $m_{\text{L}} > 0$ applied to the m_{L} -component of the transformation L_{bc}^{-1} , with m_{A} estimated from standard length by the approximation $F_{\ell_{2\text{A}}}$, the current estimate for \widehat{E}_{P} is 18.8 kJ g^{-1} . The estimate is the result of the constraint applied to 2544 physiology records for age-0 herring from the field survey program. In terms of that information archive, the estimate $\widehat{E}_{\text{P}} = 18.8 \text{ kJ g}^{-1}$ satisfies the necessary condition that it be a lower bound for all quotients $\frac{E}{m_{\text{DWT}} - m_{\text{A}}}$; the estimate increased by 5% is almost surely not such a lower bound.

It is of interest both technically and as it relates to the project history that the physiology records

for the Seward Laboratory fasting experiment define a least upper bound that is significantly larger than that for the field studies. This same is true for the small set of states used to define the map $F_{\ell 2A}$. Of course, these two archives are very much smaller: 114 records in the fasting study and 41 records in the special ash-measurements archive. The least upper bound for \hat{E}_P determined by each of these is shown by means for the first 19 records in the output of the shell script. Table 4.3 shows the output from the Seward Laboratory study; Table 4.4 shows the output from the special ash-measurements archive.

Table 4.3: initial 19 of the records of Seward Lab study, ascending order for $\hat{E}_{P,\text{lub}}$

$\frac{E}{m_{\text{DWT}}-m_A}$ kJ/g	E kJ	m_{DWT} g	m_A g	slen mm	survey date	site name	file ajp	fish ajp	ash by
23.57	11.1	0.587	0.116	73.0	1995 12 01	SewardLabExp	0	6	sl2ash
23.59	6.019	0.34	0.0848	66.0	1996 03 08	SewardLabExp	3	15	sl2ash
23.85	7.466	0.364	0.0509	56.0	1995 12 01	SewardLabExp	0	13	sl2ash
24.06	17.08	0.917	0.2072	88.0	1996 01 25	SewardLabExp	2	11	sl2ash
24.32	6.142	0.359	0.1064	71.0	1996 02 08	SewardLabExp	3	4	sl2ash
24.33	13.76	0.732	0.1664	82.0	1996 01 25	SewardLabExp	2	9	sl2ash
24.39	7.539	0.446	0.1369	77.0	1996 02 07	SewardLabExp	3	3	sl2ash
24.4	10.85	0.511	0.0664	61.0	1995 12 01	SewardLabExp	0	18	sl2ash
24.42	8.413	0.487	0.1425	78.0	1996 03 12	SewardLabExp	3	19	sl2ash
24.56	12.59	0.619	0.1064	71.0	1995 12 01	SewardLabExp	0	15	sl2ash
24.67	16.16	0.748	0.093	68.0	1995 12 01	SewardLabExp	0	16	sl2ash
24.72	6.268	0.36	0.1064	71.0	1996 03 21	SewardLabExp	3	25	sl2ash
24.74	11.95	0.564	0.0809	65.0	1995 12 01	SewardLabExp	0	14	sl2ash
24.74	17.58	0.817	0.1064	71.0	1995 12 01	SewardLabExp	0	19	sl2ash
24.82	9.155	0.529	0.1602	81.0	1996 03 09	SewardLabExp	3	17	sl2ash
24.83	5.666	0.33	0.1018	70.0	1996 03 16	SewardLabExp	3	24	sl2ash
24.83	6.879	0.398	0.121	74.0	1996 04 01	SewardLabExp	3	30	sl2ash
24.86	7.075	0.416	0.1314	76.0	1996 03 15	SewardLabExp	3	23	sl2ash
24.91	17.73	0.919	0.2072	88.0	1996 01 25	SewardLabExp	2	19	sl2ash

Table 4.4: initial 19 of the ash measurement archive, ascending order for $\hat{E}_{P,\text{lub}}$

$\frac{E}{m_{\text{DWT}}-m_A}$ kJ/g	E kJ	m_{DWT} g	m_A g	slen mm	survey date	site name	file ajp	fish ajp	ash by
24.04	30.14	1.414	0.1601	80.0	1995 10 19	Whale Bay	j25	28	lab_ajp
25.11	22.27	1.01	0.1231	79.0	1995 10 19	Whale Bay	j25	96	lab_ajp
25.11	28.62	1.312	0.1721	84.0	1995 10 19	Whale Bay	j25	92	lab_ajp
25.41	29.88	1.343	0.1671	80.0	1995 10 25	Green Bay	j24	4	lab_ajp
25.5	24.76	1.114	0.1429	79.0	1995 10 19	Whale Bay	j25	32	lab_ajp
25.69	38.89	1.7	0.1863	84.0	1995 11 07	Sawmill Bay	j23	24	lab_ajp
25.78	79.6	3.513	0.4254	109.0	199x mo da	-999 Bay	j20	12	lab_ajp
25.79	30.7	1.348	0.1576	85.0	1995 10 19	Whale Bay	j25	52	lab_ajp
25.81	24.13	1.088	0.153	77.0	1995 10 19	Whale Bay	j25	48	lab_ajp
25.84	33.61	1.495	0.1941	85.0	1995 11 07	Sawmill Bay	j23	36	lab_ajp
25.86	32.37	1.418	0.1663	82.0	1995 11 07	Sawmill Bay	j23	60	lab_ajp
25.89	27.52	1.235	0.1722	81.0	1995 10 19	Whale Bay	j25	44	lab_ajp
25.89	27.64	1.219	0.1516	79.0	1995 10 19	Whale Bay	j25	80	lab_ajp
25.92	15	0.684	0.1053	68.0	1995 11 03	Jack Bay	j21	52	lab_ajp
25.96	39.13	1.674	0.1669	88.0	199x mo da	-999 Bay	j20	52	lab_ajp
26.01	28.67	1.275	0.1729	84.0	1995 10 19	Whale Bay	j25	56	lab_ajp
26.07	46.83	2.06	0.2639	92.0	1995 11 03	Jack Bay	j21	64	lab_ajp
26.14	46.38	1.978	0.2037	89.0	199x mo da	-999 Bay	j20	76	lab_ajp
26.15	48.46	2.093	0.2399	91.0	1995 11 03	Jack Bay	j21	44	lab_ajp

During the first half of 1998 model development was carried out with only the Seward Laboratory records. Throughout that period there was no inconsistency with the use of published values for \hat{E}_P , values from 22 kJ g^{-1} to 23 kJ g^{-1} . The reason for this is immediately clear from Table 4.3—the

least upper bound is 23.57kJ g^{-1} . However, in the second half of 1998 development effort turned to the field survey archives. Immediately there was a problem with the constraint $m_L > 0$. It is clear from the quotients in Table 4.2 that using a value for \hat{E}_P greater than 22 will result in many cases in which m_L is negative.

A final note regarding the choice of \hat{E}_P is to assess the degree to which error in m_A affects the the estimation of $\hat{E}_{P,\text{lub}}$. From Table 4.2 the individuals responsible for the least upper bound $\hat{E}_{P,\text{lub}}$ are all ones for whom m_A is computed. It is straightforward to compute the change in the quotient (4.8) resulting from a 10% change in m_A : for the first six records in Table 4.2 the consequent change is 2.9%, 2.4%, 1.4%, 1.9%, 2.2%, and 2.0%.

It is of separate interest to note that the majority of individuals in Table 4.2 are by a wide margin from fall surveys rather than spring surveys. A moments thought makes clear that our search has been for individuals in whom the mass of lipid *relative* to the mass of protein is small. Although the spring brings with it depletion of lipid, it is not necessarily the time of a minimum value for the ratio of lipid mass to protein mass.

4.3 Step 3. [optional] \widehat{E}_L and bomb calorimetry vs nitrogen analysis

In this section the results appear as “Comments” in an opening “Summary” (rather than throughout the section). The explanation and construction of the results is in the second part of this section, “Review of Results.”

4.3.1 Summary

The first issue is a constraint which will better define \widehat{E}_L . We find none. In particular, we find no bound for \widehat{E}_L that is as informative as the one for \widehat{E}_P in the previous section. Specifically we find

Comment 1. *The inequality $\widehat{E}_L > \frac{E}{m_{DWT} - m_A}$ does not provide a “tight” bound; the values for the righthand side reflect the boundary of the domain of realizable physiological states in \mathcal{P} and provide no information about \widehat{E}_L .*

Not to stop there, we then expand the search possibilities by adding a second system of measurement, the determination of the physiological state by nitrogen analysis. However, the new system of observations brings its own parameter k_N in need of some constraint to overcome the ambiguity in its definition. The best we are able to do with \widehat{E}_L and k_N is to establish that the value $k_N = 0.18$ is consistent with $\widehat{E}_P = 18.8$ and $\widehat{E}_L = 39.3$. This is obtained with a dataset providing results from both nitrogen analysis and bomb calorimetry for a common set of 41 age-0 herring. This set was provided by T. C. Kline [Kli99] in collaboration with A. J. Paul. [Pau99]

Comment 2. *The relation*

$$m_P = \frac{-E + \widehat{E}_L(m_{DWT} - m_A)}{\widehat{E}_L - \widehat{E}_P}$$

$$m_P = \frac{m_N}{k_N}$$

holds (in the sense described in the text) for the sample set from Kline and Paul for $\widehat{E}_P = 18.8 \text{ kJ g}^{-1}$, $\widehat{E}_L = 39.3 \text{ kJ g}^{-1}$, and $k_N = 0.18$. The value for k_N differs from the commonly used value of 0.16 but is well within the range of values reported for k_N .

The foregoing provided a first comparison between bomb calorimetry and nitrogen analysis as alternative or complementary methods for establishing the physiological variables E , m_{DWT} , m_{WWT} , m_A or m_N , m_{DWT} , m_{WWT} , m_A specifically for use in age-0 fasting survival forecasts. From the results of the comparison we have a number of preliminary conclusions.

Comments 3 **The first comparison of bomb calorimetry and nitrogen analysis.** *In a special comparison test involving a test set consisting of 41 individuals, the two methods produced remarkably similar determinations of the physiological states for the 41 individuals in the test set. The extent of the consistency is shown in Figure 4.4: there is near coincidence for the determinations of (m_P, m_L) for all but 8 of the 41 individuals; 4 of those 8 are in good agreement although not coincident. The following results from the comparison are noted:*

(i) the individual states in \mathcal{P} are more broadly distributed in the nitrogen analysis estimate than in the bomb calorimetry estimate;

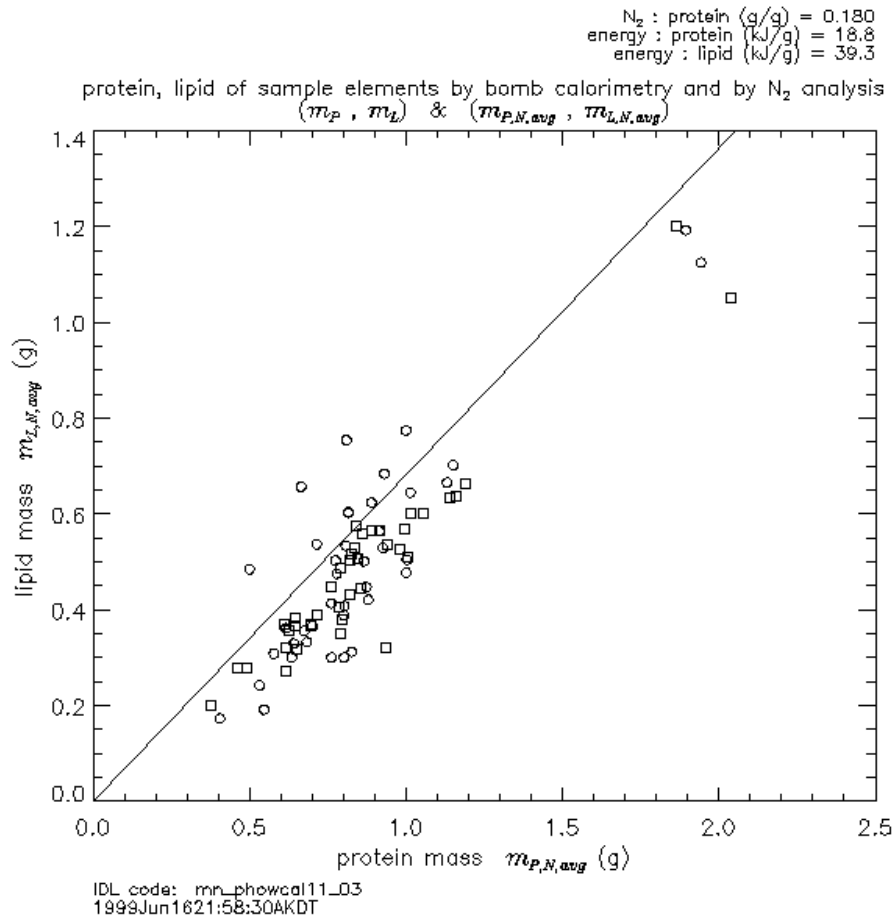


Figure 4.4 Overlay of the determinations of (m_P, m_L) for a test set of 41 age-0 herring by \circ nitrogen analysis and by \square bomb calorimetry. There is near coincidence for all but 8 of the 41.

- (ii) the increased spread (i.e., support) of the distribution obtained by nitrogen analysis is tentatively judged due to greater inherent measurement error;
- (iii) the estimates wherein nitrogen analysis differs from bomb calorimetry are underestimations of protein mass;
- (iv) in the case of underestimation the direction of the error is lower protein, higher lipid, and longer survival time;
- (v) the replicates used in the nitrogen analysis protocol exhibit differences (at a frequency of roughly 10–20%) sufficiently high to make a noteworthy difference in subsequent estimates of survival time.

(Note that these conclusions are made for nitrogen analysis in part because replicates are a standard and routine part of the protocol. Replicates are not routine for bomb calorimetry and for that reason alone there is no similar evaluation.)

The foregoing findings are conjectured to be in large measure due to the following.

Comment 4 The fundamental difference. Nitrogen analysis measures (only) protein and deduces lipid by subtraction. One consequence of this and the fact that protein mass is twice that

of lipid is that a relative measurement error ϵ for protein necessarily becomes the relative error 2ϵ for lipid. In contrast, bomb calorimetry measures a weighted sum of both lipid and protein (i.e., the factors \hat{E}_L and \hat{E}_P) with the weighting for lipid twice that for protein.

Comment 5 Scoring errors. The representation of the error in \mathcal{P} using the projection $m_A \times m_L$ or the related $m_{P,res} \times m_{L,res}$ provides the means to relate errors in estimation of physiological state to errors in estimates of survival time: for example, 10% lipid error is approximately equivalent to 2 weeks fasting time.

Comment 6 Conclusions. The results suggest continuing the present practice of using bomb calorimetry as the primary method of laboratory analysis for the determination of physiology variables. The findings provide an explicit migration path whereby nitrogen analysis can undergo a second-stage assessment followed by a cost-benefit analysis for its use either as a alternative primary laboratory analysis or as a part of a combined protocol utilizing both methods of laboratory analysis.

4.3.2 Review of results

In the remainder of this section the basis for each of the Comments is described.

The constraint $m_P > 0$ applied to the m_P -component of L_{bc}^{-1} (2.1) provides a lower bound for \hat{E}_L

$$\hat{E}_L > \frac{E}{m_{DWT} - m_A} \tag{4.10}$$

The quotient on the right is the same as (4.8), the quotient which provided the upper bound for \hat{E}_P . In this case each record provides a lower bound for \hat{E}_L . The totality of all records defines a “greatest lower bound” (glb) $\hat{E}_{L,glb}$. However, one can guess that this bound is not so “great.” One may already know to expect only very rare occurrences of m_L approximately equal to m_P and even less frequently m_L greater than m_P . That is, one may know that the largest value for the righthand side of (4.10) will split the difference between \hat{E}_P and \hat{E}_L . Tables 4.5 and 4.6 show the upper ends of the same records as were shown in Tables 4.2 and 4.3 in the last section.

Table 4.5: upper 15 of all field records, in ascending order for $\hat{E}_{L,glb}$

$\frac{E}{m_{DWT}-m_A}$ kJ/g	E kJ	m_{DWT} g	m_A g	slen mm	survey date	site name	file ajp	fish ajp	ash by
28.16	24.08	1.055	0.2	87.0	1995 10 25	Green Island	j24	18	s12ash
28.2	38.8	1.562	0.186	85.0	1995 11 07	Sawmill Bay	j23	13	s12ash
28.23	48.96	1.901	0.1664	82.0	1997 10 23	Zaikof Bay	j133	3964	s12ash
28.24	67.79	2.63	0.2299	91.0	1995 11 07	Sawmill Bay	j23	83	s12ash
28.26	7.36	0.3535	0.09303	68.0	1998 03 19	Simpson Bay	j999	4151	s12ash
28.36	47.92	1.869	0.1793	84.0	1995 11 07	Sawmill Bay	j23	92	s12ash
28.39	39.11	1.632	0.2543	94.0	1996 03 13	Eaglek By.	j36	12	s12ash
28.44	39.22	1.565	0.186	85.0	1995 11 07	Sawmill Bay	j23	11	s12ash
28.7	188.2	7.494	0.936	143.0	1996 03 11	Boulder By	j34	38	s12ash
28.72	13.27	0.578	0.116	73.0	1996 03 12	Jack Bay	j35	38	s12ash
29.08	65.12	2.469	0.2299	91.0	1995 11 03	Jack Bay	j21	62	s12ash
29.37	90.13	3.315	0.246	93.0	1997 10 23	Zaikof Bay	j133	4103	s12ash
29.58	64.71	2.536	0.3481	104.0	1996 03 12	Jack Bay	j35	132	s12ash
29.77	54.79	2.055	0.2146	89.0	1995 11 07	Sawmill Bay	j23	17	s12ash
31	15.26	0.7816	0.2894	98.0	1996 03 24	Whale Bay	j42	123	s12ash

Table 4.6: upper 15 of the records of Seward Lab study, ascending order for \widehat{E}_L ,glb

$\frac{E}{m_{\text{DWT}}-m_A}$ kJ/g	E kJ	m_{DWT} g	m_A g	slen mm	survey date	site name	file ajp	fish ajp	ash by
27.93	18.65	0.828	0.1602	81.0	1995 12 28	SewardLabExp	1	14	sl2ash
27.98	7.725	0.413	0.1369	77.0	1996 04 01	SewardLabExp	4	3	sl2ash
28.22	10.7	0.572	0.1929	86.0	1996 04 01	SewardLabExp	4	6	sl2ash
28.27	8.644	0.454	0.1482	79.0	1996 04 01	SewardLabExp	4	17	sl2ash
28.3	25.43	1.078	0.1793	84.0	1995 12 28	SewardLabExp	1	12	sl2ash
28.35	4.995	0.261	0.0848	66.0	1996 04 01	SewardLabExp	4	18	sl2ash
28.46	10.66	0.541	0.1664	82.0	1996 04 01	SewardLabExp	4	16	sl2ash
28.48	8.463	0.382	0.0848	66.0	1996 01 25	SewardLabExp	2	10	sl2ash
28.48	8.634	0.476	0.1728	83.0	1996 04 01	SewardLabExp	4	2	sl2ash
28.7	10.35	0.492	0.1314	76.0	1996 04 01	SewardLabExp	4	13	sl2ash
28.73	15.02	0.671	0.1482	79.0	1996 01 25	SewardLabExp	2	7	sl2ash
29.15	7.69	0.412	0.1482	79.0	1996 04 01	SewardLabExp	4	14	sl2ash
29.65	5.343	0.265	0.0848	66.0	1996 04 01	SewardLabExp	4	9	sl2ash
30.31	5.546	0.299	0.116	73.0	1996 04 01	SewardLabExp	4	8	sl2ash
31.96	4.161	0.215	0.0848	66.0	1996 04 01	SewardLabExp	4	12	sl2ash

A second source of a information regarding \widehat{E}_L is through a second method of laboratory analysis applied to a common set of samples. T. C. Kline of the Stable Isotope Project provided such a sample. Nitrogen analysis is a routine component of his procedures for determining carbon isotopes. Kline collaborated with A. J. Paul in the preparation of the sample set that was to provide ash measurements: each of the 41 samples had both a bomb calorimetry analysis with ash measurements as well as a determination of protein mass by nitrogen analysis. Therefore, for this sample set both transformations (2.1) and (2.2) apply,

$$m_P = \frac{-E + \widehat{E}_L(m_{\text{DWT}} - m_A)}{\widehat{E}_L - \widehat{E}_P} \quad (4.11)$$

$$m_P = \frac{m_N}{k_N}$$

However, we gain only the one relation in (4.11): the equations for m_L in (2.1) and (2.2) are identical—in both cases $m_L = m_{\text{DWT}} - m_A - m_P$.

The value $k_N = 0.18$ was obtained in the following non-standard manner. From (4.11) \widehat{E}_L is expressed in terms of k_N and the laboratory variables; then by a simple search a value is found for k_N which yields 39.3 for the average of \widehat{E}_L over all 41 records.

This is about as much as one can do regarding \widehat{E}_L and a value for k_N without explicit laboratory calibration tests. The second part of this section presents the results of using the nitrogen analysis to obtain a proximate analysis then comparing that analysis with the one from bomb calorimetry. A question carried over from the foregoing: What was the origin of the magnitude of the variation in the computed values for \widehat{E}_L ? This question is illustrated by Table 4.7 which shows records extracted from that calculation. The range of the computed values for \widehat{E}_L is higher than expected. This question in part motivated what follows.

The structure of the measurement records for the nitrogen analysis was described in §3.3 and illustrated by the four records shown in Table 3.2. In particular note that for each sample the mass of nitrogen is determined twice, i.e., there are replicate pairs for each estimate of whole body mass of nitrogen. In Table 3.2 the values are as received, as “protein mass estimates,” that is, $m_N/0.16$.

Table 4.7: extractions from calculations of \hat{E}_L using (4.11)

\hat{E}_L kJ	m_N g	E kJ	m_{DWT} g	m_A g	slen mm	survey date	site name	file ajp	fish ajp	ash by
38.53	0.07304	15	0.7018	0.1053	68.0	1995 11 03	Jack Bay	j21	52	lab_ajp
33.86	0.09	25.84	1.115	0.1301	73.0	1995 10 25	Green Island	j24	44	lab_ajp
44.93	0.0956	20.29	0.871	0.1114	73.0	1995 11 03	Jack Bay	j21	100	lab_ajp
45.39	0.09816	19.57	0.8904	0.1407	73.0	1995 11 03	Jack Bay	j21	4	lab_ajp
39.3	0.126	27.64	1.219	0.1516	79.0	1995 10 19	Whale Bay	j25	80	lab_ajp
35.16	0.1284	32.37	1.418	0.1663	82.0	1995 11 07	Sawmill Bay	j23	60	lab_ajp
37.47	0.1371	29.88	1.343	0.1671	80.0	1995 10 25	Green Island	j24	4	lab_ajp
43.67	0.1371	27.52	1.235	0.1722	81.0	1995 10 19	Whale Bay	j25	44	lab_ajp
38.21	0.1463	38.43	1.562	0.1445	79.0	1995 10 19	Whale Bay	j25	36	lab_ajp
37.7	0.1467	38.12	1.586	0.1673	82.0	1995 11 07	Sawmill Bay	j23	80	lab_ajp
41.59	0.1488	28.62	1.312	0.1721	84.0	1995 10 19	Whale Bay	j25	92	lab_ajp
39.21	0.1524	35.86	1.532	0.1779	83.0	1995 10 19	Whale Bay	j25	40	lab_ajp
44.55	0.1802	39.4	1.71	0.2487	90.0	1995 11 03	Jack Bay	j21	92	lab_ajp
37.83	0.1824	43.54	1.847	0.1877	89.0	1995 11 07	Sawmill Bay	j23	100	lab_ajp
39.12	0.2033	46.83	2.046	0.2639	92.0	1995 11 03	Jack Bay	j21	64	lab_ajp
41.39	0.2071	48.46	2.037	0.2399	91.0	1995 11 03	Jack Bay	j21	44	lab_ajp

In Figure 4.5 the nitrogen masses have been converted to protein mass using $k_N = 0.18$. The upper left panel of Figure 4.5 displays the replicate measurements by means of a scatter plot wherein one replicate is the first coordinate and the second replicate is the second coordinate.

Each panel in Figure 4.5 uses the logarithm of mass as the coordinate axes in order to make the inference of relative error immediate. Note that 1g falls in the middle of each axis and that the tick just below on each scale is 0.9g or a 10% change. That same distance is a 10% change at all positions in each of the panels. For the plot of the replicated measurements we see that very few replicates differ by more than 10% however a noticeable fraction does differ by nearly 10%.

An error of 10% for protein mass is significant because (i) lipid mass is computed from $m_L = m_{DWT} - m_A - m_P$ and (ii) m_P is typically twice as large as m_L . These two facts together mean that the relative error ϵ in m_P translates directly into a relative error 2ϵ for m_L . For example, a 10% error in the estimate of m_P means an error of 20% for m_L .

In §2.7 of the “Concise User’s Guide” the technique is shown wherein lines of constant survival are plotted on a plane whose x-coordinate and y-coordinate are the variables $m_P + L_*m_A$ and $m_L - L_*m_A$ respectively. An example plot is shown in which the lines are at 30da intervals. The lines for 120da and for 150da are upper and lower bounds for the typical winter fast. These two lines provide an indicator of the consequences to an individual for changes in m_L and m_P . One will see that in the y-axis direction—the m_L direction—these lines are approximately 20% apart. That is, a 10% increase in lipid adds 2 weeks of survival time, 20% adds four weeks. It is based on this that the 10% error in the protein mass estimates is of concern.

When the estimates of protein mass by nitrogen analysis are compared with the estimates from bomb calorimetry, the deviation increases significantly over that exhibited by the replicates. This is shown in the right two panels of 4.5. In the upper right panel the estimate of protein mass by bomb calorimetry is the x-coordinate and the estimate by nitrogen analysis is the y-coordinate. The upper panel shows the replicates and the lower panel shows the average of the two replicates. In the bottom right panel the difference between the bomb calorimetry estimate and that from nitrogen analysis is quite often greater than 10%. Roughly speaking, the range of difference is +10% to

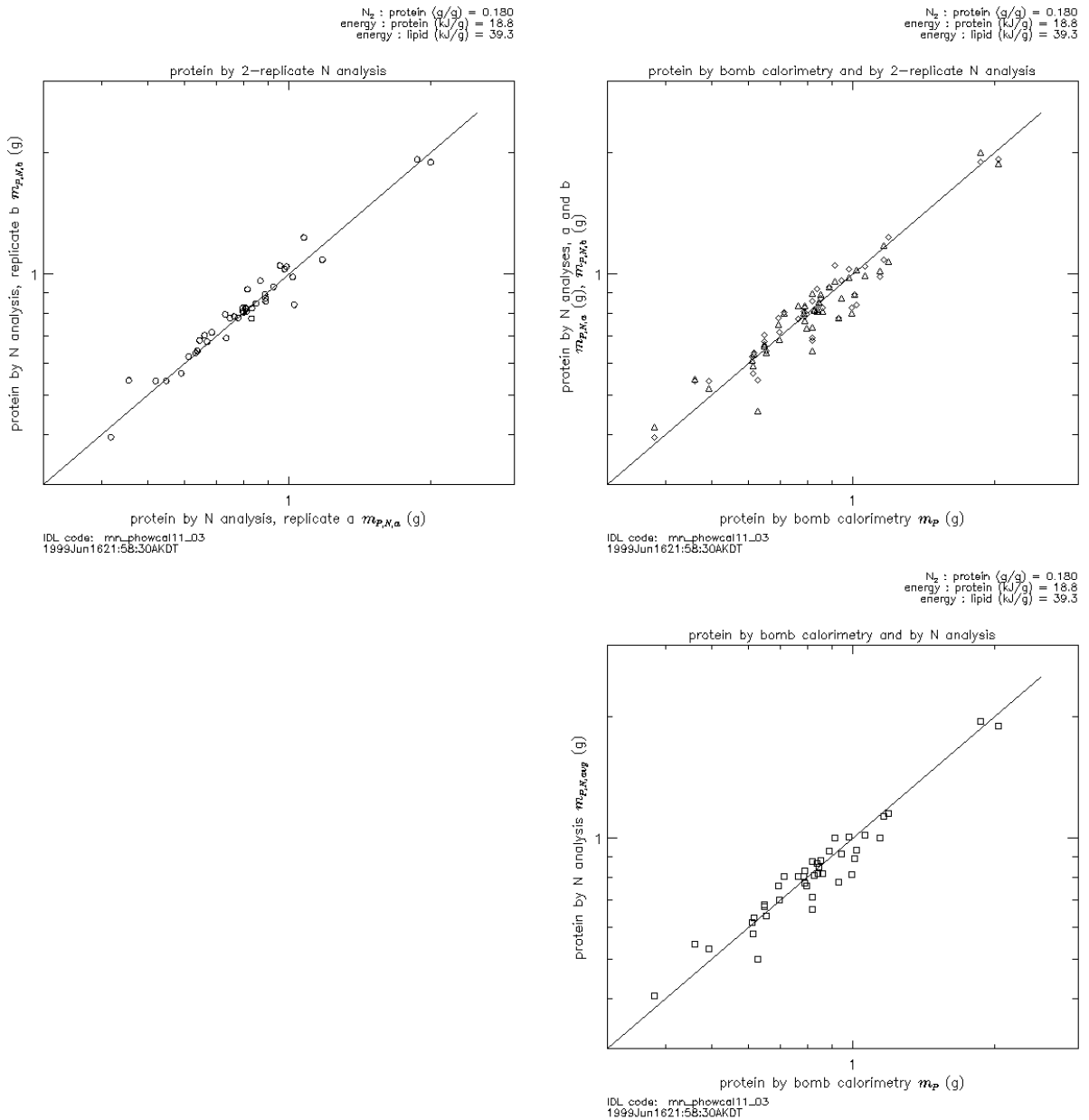


Figure 4.5 Review of the mass of nitrogen measurements provided by T. C. Kline for use in the development of the winter fasting model.

-20%. However, this does not give any indication as to which measurement is correct—only that the two differ.

In Figure 4.6 the results from the two measurement methods are shown in a manner that better displays the location of a measurement as a point in \mathcal{P} . The measurements are shown as points in the $m_p \times m_L$ plane. In the upper left panel a plot symbol is shown for each of the two replicate

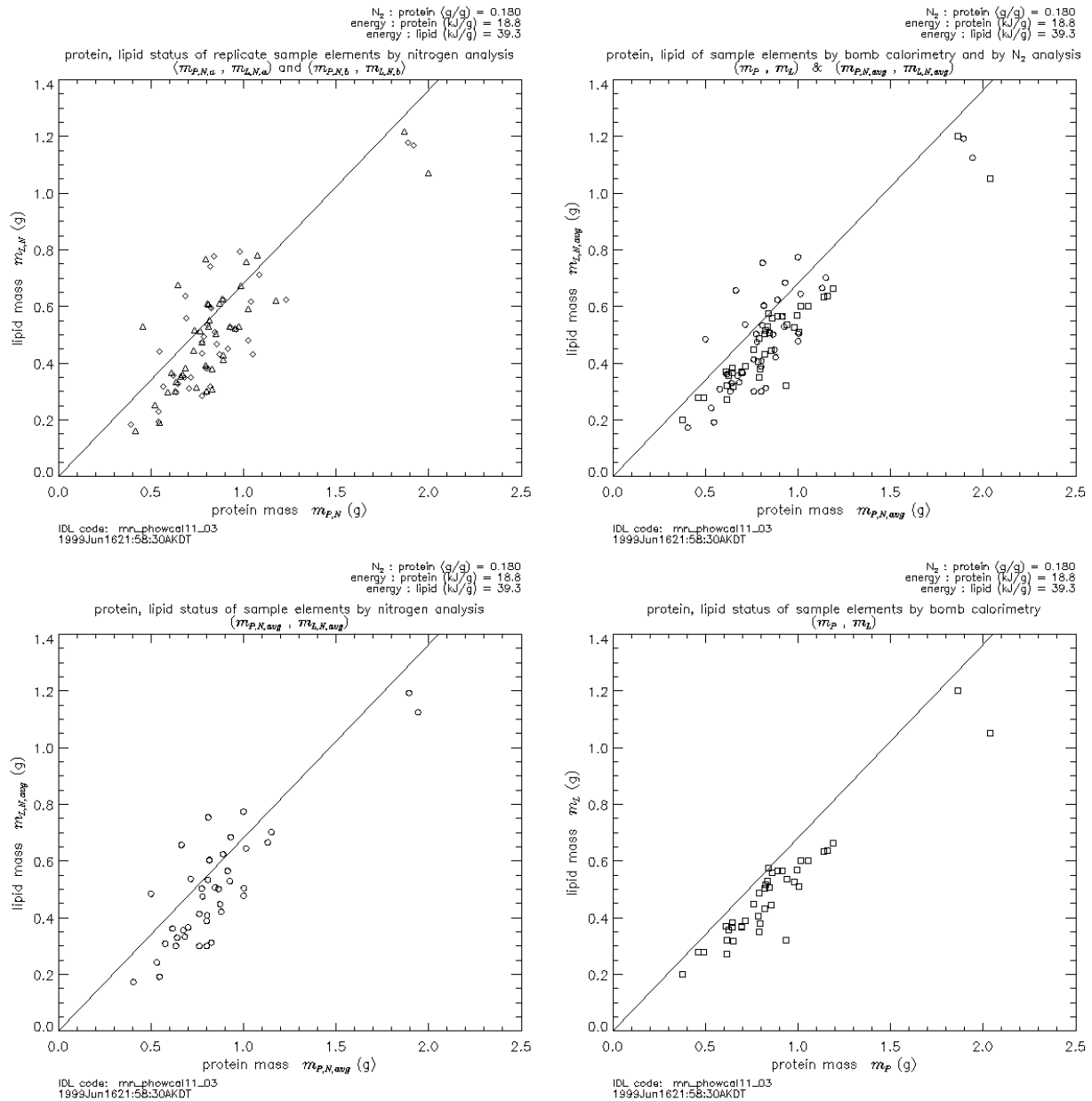


Figure 4.6 The physiology for 41 individuals as measured by two methods, listed counterclockwise: (top lt) nitrogen analysis, two replicate measurements displayed; (bot lt) \circ nitrogen analysis, average of two replicate measurements; (bot rt) \square bomb calorimetry; (top rt) overplot \circ nitrogen analysis (avg) / \square bomb calorimetry

measurements for each of the 41 individuals: replicate “a” is shown with a triangle plot symbol; replicate “b” is shown with a diamond plot symbol. By means of the two symbols on can see explicitly the displacement between the replicates in a context that is readily interpreted in terms of fasting survival. It is possible to pair the replicates because the nitrogen analysis determines only protein. Replicate pairs necessarily lie along a diagonal line with slope of -1. (The replicate

with higher protein is located to the right and down an equal amount in absolute units.) It is not difficult to identify pairs in the neighborhood of $0.8 < m_p < 1.0 \times 0.4 < m_L < 0.5$ wherein the difference in m_p and in m_L is about 0.1g. That is, and error of 10% for protein and 20% for lipid.

The bottom left panel displays the averages for the replicate pairs shown in the top left panel. The support for the distribution has contracted somewhat.

The bottom right panel displays the position in $m_p \times m_L$ as determined by the bomb calorimetry measurements. The support of the distribution in $m_p \times m_L$ for bomb calorimetry is markedly more compact than that to the left for nitrogen analysis. Since one expects measurement error to “blur” the distribution and expand the support, and not to contract it, one is inclined to suspect that it is nitrogen analysis that has the greater measurement error—one of the two must be in error to account for the differences shown in the right panels of 4.6.

One must, however, also note the extent to which the distributions are extremely similar. To be explicit, there are only 8 of the 41 individuals of the sample set who were positioned by nitrogen analysis above the diagonal line in Figure 4.6. If these 8 were removed, the two distributions would be very difficult—nearly impossible—to distinguish. It is a subset of 20% which is significantly displaced relative to the bomb calorimetry results. In addition, the displacement is large in only the direction of underestimation of protein—which increases lipid and hence survival time. Consequently, the difference is for 20% of the sample for whom survival time improves. Further, not all of the 20% are strongly displaced. Only four of the eight are in that category. Four are only mildly outside the support defined by bomb calorimetry. From this counting 90% of the sample set is distributed in $m_p \times m_L$ by nitrogen analysis such that the results for fasting survival will be essentially identical to the results from bomb calorimetry.

4.4 Step 4. Identification of \mathcal{P}^* and \mathcal{P}^\square in \mathcal{P}

This section brings together Calibration Steps 1 and 2 to establish the procedure whereby a state (m_P, m_L, m_A, m_W) in \mathcal{P} is judged suitable or unsuitable for life. The result from this Step is shown in Figure 4.7 and described in a “short form” statement below the figure.

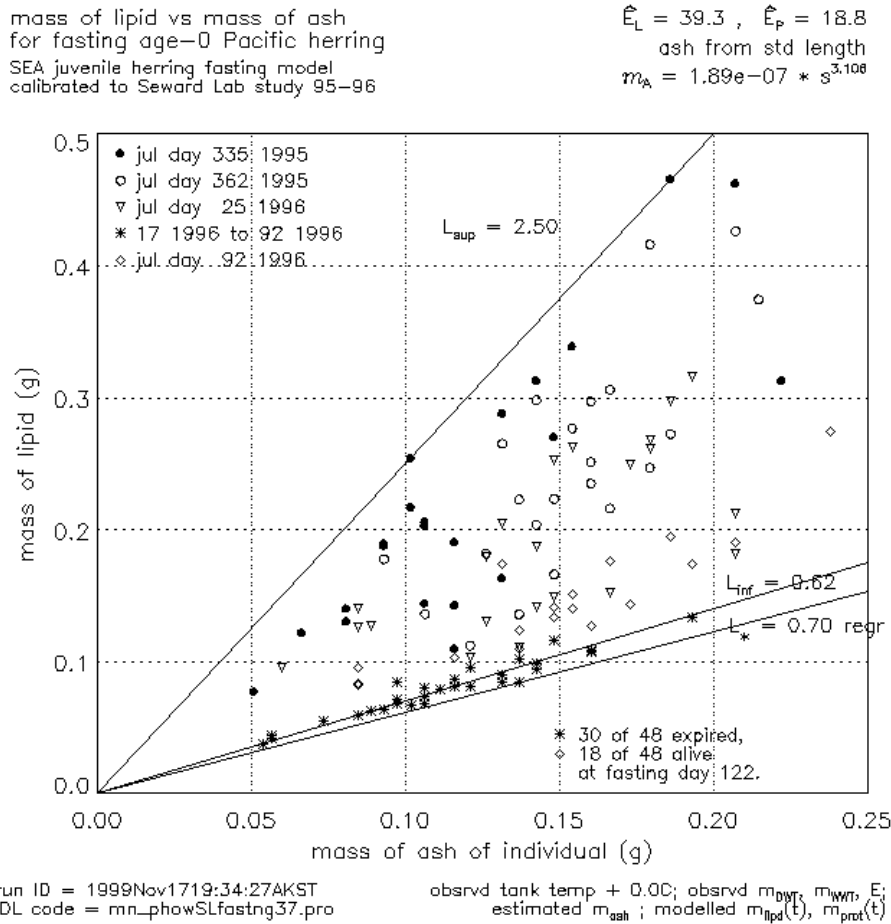


Figure 4.7 The discrimination between *alive* and *expired* of the Seward Laboratory fasting experiment obtained with Version 3.1 of the fasting model. All subsets S_i , $i = 0, \dots, 4$, are shown projected to $m_A \times m_L$. Each subset is distinguished by a unique plot symbol identified in the legend in the upper left of the figure. There is a special interest in the separation of *alive* and *expired* for the two subsets from the “long” experimental group Ω^ℓ ; this special status is noted by the legend in the lower right of the figure. The two lines L_{sup} and L_{inf} provide estimates of the (projected) upper and lower boundaries of the reachable set within \mathcal{P} . Note that the label “ $L_* = 0.70$ regr” is below and to the right of the line it labels; the label “ $L_{inf} = 0.62$ ” is above and to the left of the line it labels.

Calibration of the decision boundary in \mathcal{P} for viability (short form).

$$\text{alive: } \mathcal{P}^\square = \{m_L > L_* m_A\}, \quad \text{expired: } \mathcal{P}^* = \{m_L \leq L_* m_A\}, \quad \text{where } L_* = 0.70$$

The remainder of this section presents the calibration procedures whereby Figure 4.7 and the result in the “short form” statement can be reproduced.

4.4.1 Descriptions of the procedures

In order to present the procedures whereby the results are obtained we will first need a more complete and more precise statement of those results—a “long form” of the calibration results.

Calibration of the decision boundary in \mathcal{P} for the classification of states as either viable or unviable (long form). *The representation of the Seward Laboratory fasting experiment in \mathcal{P} by Version 3.1 of the fasting model has the following properties:*

(1) *The distributions of the two categories expired and alive in \mathcal{P} are compatible with a representation wherein \mathcal{P} is partitioned into two disjoint subsets \mathcal{P}^\square and \mathcal{P}^* such that the distribution of alive is contained in \mathcal{P}^\square , expired contained in \mathcal{P}^* , and the support of the distribution of expired approximates the boundary of \mathcal{P}^\square .*

(2) *The distribution of the expired category in \mathcal{P} exhibits support which, as an approximate boundary for \mathcal{P}^\square , can be specified as the zero-set of a smooth function G ;*

(3) *A suitable choice for G is the linear function $m_L - L_* m_A$,*

$$\mathcal{P}^\square = \{ (m_P, m_L, m_A, m_W) \text{ in } \mathcal{P} : m_L - L_* m_A > 0, \quad L_* = 0.70 \} \quad (4.12)$$

(4) *An alternative choice for G is the linear function $m_L - L_*(m_A + Qm_P)$,*

$$\mathcal{P}^\square = \{ (m_P, m_L, m_A, m_W) \text{ in } \mathcal{P} : m_L - L_*(m_A + Qm_P) > 0, \quad L_* = 0.85 \text{ and } Q = -0.11 \} \quad (4.13)$$

Explanation. Version 3.1 refers to the parameters whose values were established by Steps 1, 2, and 3 of these procedures and the use of those parameters in the two transformations L_{bc}^{-1} (2.1) and $F_{\ell_{2A}}$ (2.7). For quick reference every figure in these documents contains within the figure the parameters whereby the figure can be reproduced.

The case for the first result is essentially a graphical one: Figure 4.7. The distributions for *alive* and *expired* exhibit all of the anticipated properties: they are disjoint in \mathcal{P} , they are adjacent, and the *expired* distribution is “thin” in a direction “outward” from \mathcal{P}^\square . The projection to $m_A \times m_L$ is expected, of course, to necessarily spread the support of *expired* and to cause the two distributions to overlap. The fact that the simple projection to one of the planes defined by two coordinate variables exhibits the degree of conformance to the model prescriptions is a good indicator that the representation in (1) is realistic.

Although the second result was anticipated in the form stated, it was not anticipated that the boundary would have the trivial shape exhibited in Figure 4.7. There was no reason to expect that the boundary would be so well approximated by a hyperplane. Indeed, one could apply a variety of methods to approximate the boundary of \mathcal{P}^\square regardless of the shape, but this result makes a first approximation trivial.

The trivial approximation is the third result. A linear regression is used to determine a “center” for the support—the small width that does appear for the support is collapsed to zero and the regression equation is used to define the boundary of \mathcal{P}^\square .

A less trivial approximation one due to a multilinear regression, similarly forced through the origin. The projection $(m_P, m_L, m_A, m_W) \mapsto (m_A + Qm_P, m_L)$ is used to provide a 2-dimensional visualization, the result of which is shown in Figure 4.8. Result (4) is *not* part of the Version 3.1 calibration.

mass of lipid vs $m_A + Q m_P$
 for fasting age-0 Pacific herring
 SEA juvenile herring fasting model
 calibrated to Seward Lab study 95-96

$\hat{E}_L = 39.3$, $\hat{E}_P = 18.8$
 ash from std length
 $m_A = 1.89e-07 * s^{3.108}$

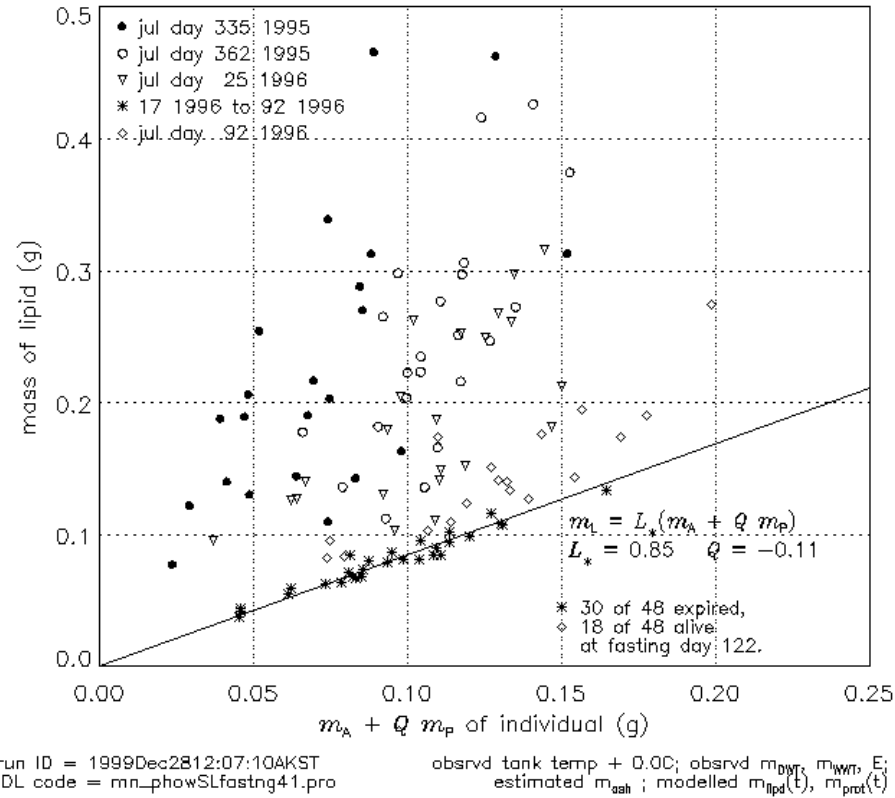


Figure 4.8 The projection of \mathcal{P} to the plane $(m_A + Qm_P, m_L)$ where $Q = -0.11$.

It is introduced because it is the obvious refinement of the trivial approximation in result (3) and it better illustrates the use of result (2). Result (4) will be used in selected comparisons in this section. The full calibration in §4.5 is based upon the approximation in result (3); the current documentation is based on result (3). □

The foregoing calibrations provide explicit representations for the set \mathcal{P}^\square . In particular, if the calibrations are in fact realistic then we should find the entire collection of individuals from field surveys “inside” \mathcal{P}^\square . Figure 4.9 shows the test of the calibrations. The left panel is the projection of \mathcal{P} to $m_A \times m_L$ with the boundary of \mathcal{P}^\square approximated by the simple approximation in result (3). The right panel does the same thing for the totality of field samples as was done in Figure 4.8: the approximation in result (4) is used with the projection of \mathcal{P} to $(m_A - Qm_P, m_L)$. There are over 2500 individuals in the combined archive for the physiology of age-0 herring, each of which is in the *alive* category. Figure 4.9 provides a quick visual assessment of the number of individuals misclassified by the two approximations for the boundary of \mathcal{P} .

Figure 4.9 is provided as a validation of the foregoing calibrations rather than as part of the calibration. As is evident from the presentation, the information from the field surveys was not

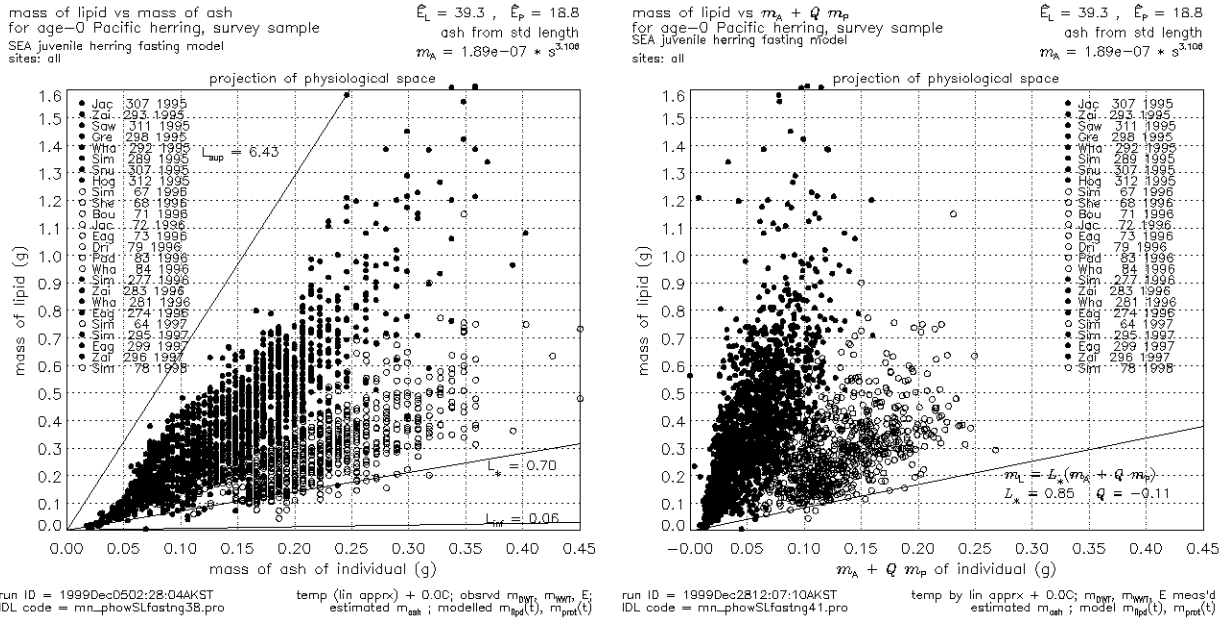


Figure 4.9 The projection from of all field survey records from \mathcal{P} to two planes: (left) to $m_A \times m_L$, with the boundary of \mathcal{P}^\square approximated by $m_L - L_* m_A = 0$, $L_* = 0.70$; (right) to $(m_A - Q m_P, m_L)$, with the boundary of \mathcal{P}^\square approximated by $m_L - L_*(m_A + Q m_P) = 0$, $L_* = 0.85$, $Q = -0.11$.

used in the construction of the approximations in (4.12) and (4.13). One *could* use the field survey archive to construct an upper bound for \mathcal{P}^* using, say, one of the projections in Figure 4.9. But that leaves a lot of items inadequately specified.

This test provided by Figure 4.9 does not appear in that “Validation Reference.” The test is closely related to the details of the construction of the model calibration and seemed more appropriate to this context than to the tests appearing in the “Validation Reference.”

The remaining procedure for the calibration of \mathcal{P}^\square is an error analysis for the use of F_{l2A} as an approximation of m_A . Clearly, everything in this calibration step involves m_A and hence relies on the approximation F_{l2A} . We see three areas of dependence upon F_{l2A} . This error analysis consists of an estimation of the scope and magnitude of the revisions that will be required as a result of transitioning from the use of F_{l2A} as an approximation of m_A to a direct measurement of m_A . In summary, the results are that the transition should necessitate only minor revisions for everything in this section. The following is the basis for this conclusion.

1. m_A as the x-coordinate in Figure 4.7. If it turns out that a significant difference is found between measured m_A and F_{l2A} for near-fatal states in \mathcal{P} , then the presentation in Figure 4.7 can remain essentially unchanged by the following revisions. Adopt the expanded space $\mathcal{P} \times \mathbb{R}_+$ described in §4.1. Adopt for Figure 4.7 the projection $(m_P, m_L, m_A, m_W, F_{l2A}(\ell)) \mapsto (F_{l2A}(\ell), m_L)$. Since this is in fact what we have actually shown in Figure 4.7 there will be no change with respect to the x-coordinate in the display.

2. *The impact on the separation of alive and expired.* The separation of the two categories *alive*

and *expired* involves discrimination between individuals who are relatively close to one another in \mathcal{P} . That is, we will be dealing with a change induced by a transition from $F_{\ell 2A}$ to measured m_A only over a small region in \mathcal{P} . Based on continuity considerations we fully expect that even if the location of the boundary is moved using m_A instead of $F_{\ell 2A}$ that the separation of the points near that boundary will be insignificantly changed.

3. *The change of the location of the boundary.* The location of the boundary may change. With adoption of measured ash the values for m_L may differ even if we do follow recommendation 1 above and retain the x-coordinate as it presently is and not switch to actual m_A . We have evaluated in §4.1 Comment 1 the magnitude of the change expected in m_L due to a change in m_A . Applying the result in (4.5) one has that since the set *expired* is characterized by constant m_A/m_L that the revised boundary—to first order—will have a similar characterization. Consequently, at most there will be a revision to L_* but not to the approximate shape of the boundary between \mathcal{P}^\square and \mathcal{P}^* .

4.5 Step 5. Rate coefficient C_0 and protein:lipid utilization A_{LP}

In this final section the values for the two remaining parameters are established.

4.5.1 Summaries

The calibration of C_0 is shown graphically by Figure 4.10. A concise statement of the results follows the figure. The left panel of the figure recalls the test groups of the Seward Laboratory experiment: three groups at fast days 0, 27, and 55 (plot symbols \bullet , \circ , and ∇) are subgroups $\Omega_0^s, \Omega_1^s, \Omega_2^s$ (or simply 0, 1, and 2) of the “short (duration)” test group Ω^s ; the two remaining groups, one not fixed in time the other at fast day 122, (plot symbols $*$ and \diamond) are subgroups Ω_3^ℓ and Ω_4^ℓ (or 3 and 4) of the “long (duration)” test group Ω^ℓ . The variable of the figure is not significant to this calibration. The calibration of C_0 is to minimize the “distance” between two functions of time:

- (1) the surviving fraction of the test group Ω^ℓ (right panel, dashed line);
- (2) the surviving fraction of the test group Ω^s when that group is advanced in time in simulation by the model Φ (right panel, solid line).

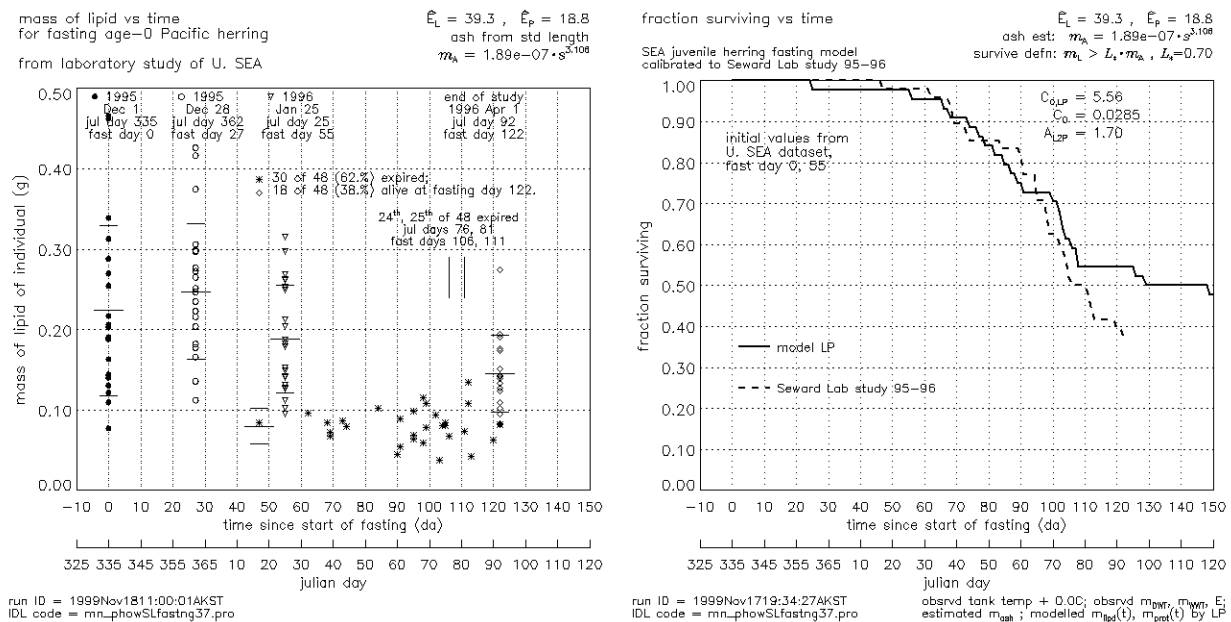


Figure 4.10 C_0 “minimizes” the difference between the simulated fate of Ω^s and the actual fate of Ω^ℓ .

The calibration of C_0 . This calibration of C_0 had the following results.

- (i) The procedure applied to subgroups Ω_0^s and Ω_2^s of Ω^s resulted in a very close correspondence between simulated and observed survival time functions (Figure 4.10, right panel);
- (ii) The calibration was successful when applied to the subgroups of Ω^s having a frequency distribution for the coordinate variable m_A (equivalently standard length) similar to that of Ω^ℓ . The calibration was unsuccessful if the distributions were dissimilar.

The calibration of A_{L2P} is described by Figure 4.11 and by the brief statement that follows.

A_{L2P} is calibrated by minimizing the dissimilarity between the distributions of the five experimental groups, $\Omega_0^s, \Omega_1^s, \Omega_2^s, \Omega_3^\ell,$ and Ω_4^ℓ , advanced or “back-projected” so that all five are compared at a common time. The minimization of dissimilarity can be approached by seeking the smallest support for the distribution of all five subgroups combined after back-projection to a common time. The left panel shows the projection to $m_A \times m_P$ of all five experimental subgroups with each individual having the state (m_P, m_L, m_A, m_W) corresponding to the time of either collection or expiration. The right panel shows those same five subgroups after each individual has been back-projected by the model Φ to the common time fast day 0 (1995 December 01). For the calibration of A_{L2P} the projection $m_A \times m_P$ is of primary significance: the similarity of the back-projections viewed from $m_A \times m_L$ is due to C_0 .

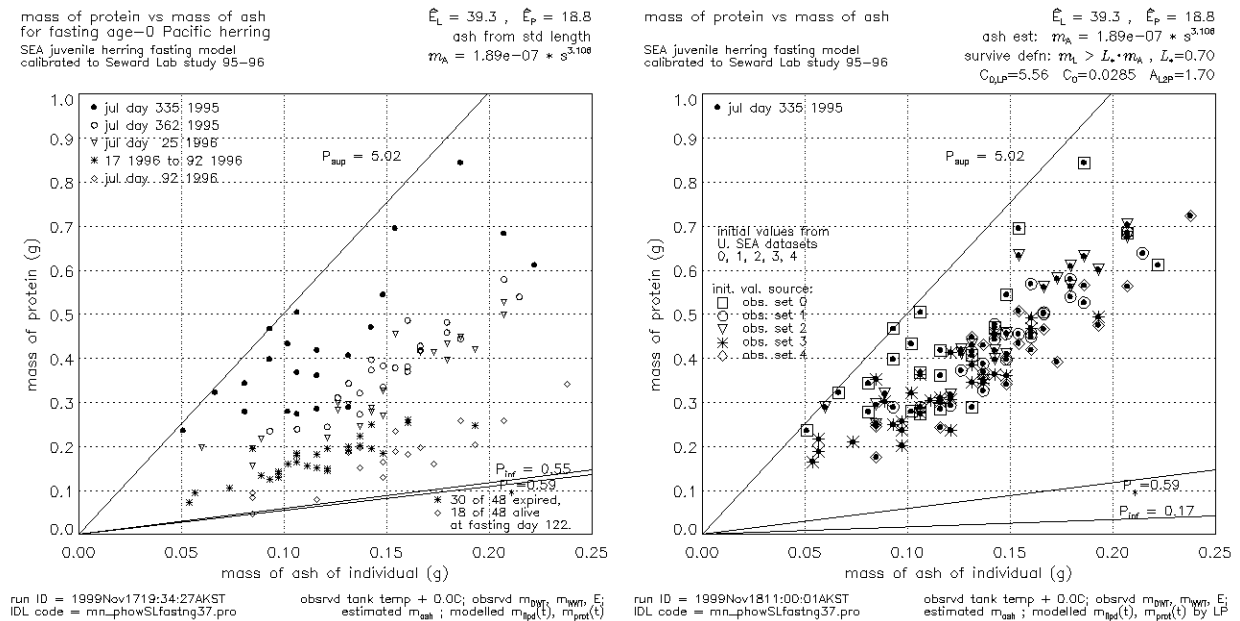


Figure 4.11 A_{L2P} minimizes the difference between the distributions of each of the five experimental groups advanced or back-projected to a common time.

The calibration of A_{L2P} . The calibration was successful in recovering a “virtual” combined test group $\Omega^s \cup \Omega^\ell$ whose distribution in $m_A \times m_P$ corresponds very closely to that of any one of the test subgroups known a priori to have been measured at a common time. Four of the five subgroups are essentially coincident, including the subgroup of expired individuals wherein each is back-projected from a wide diversity of times. The poorly conforming subgroup Ω_0^s has a uniquely high protein content relative to the other two groups of Ω^s . The shift to higher m_P for Ω_0^s is consistent with inter-group analyses described herein.

4.5.2 The description of the procedures for the calibration of C_0

The procedure adopted here is arguably the most important one. This procedure links the model structure established in the foregoing steps to actual phenomena. Much of the prior work has had the effect of adjusting by small amounts values for empirical constants that were already reasonable. In this step we are largely without guidance. There are values for C_0 for bioenergetics models based on growth studies and on the use of wet mass as the basis for metabolic energy requirements. Arrhenius uses a rate coefficient that after recasting into the form used here is 0.045. There is mention of rate reductions during fasting, some dropping to as low as 20% of non-fasting values. This suggests a rate coefficient as low as 0.01 is possible.

But we are not seeking to confirm an independently determined value for C_0 . Our purpose is to *determine* the value for C_0 for this model. In so doing we will actually be setting the combined value of all of the factors multiplying C_0 , a fact described at the beginning of §4. Given this significance, it is appropriate to look for all of the available structure within the Seward Laboratory fasting experiment whereby we can overdetermine C_0 . That is, we ought not take the first convenient relation. Rather we should find as many relations as possible to be satisfied simultaneously.

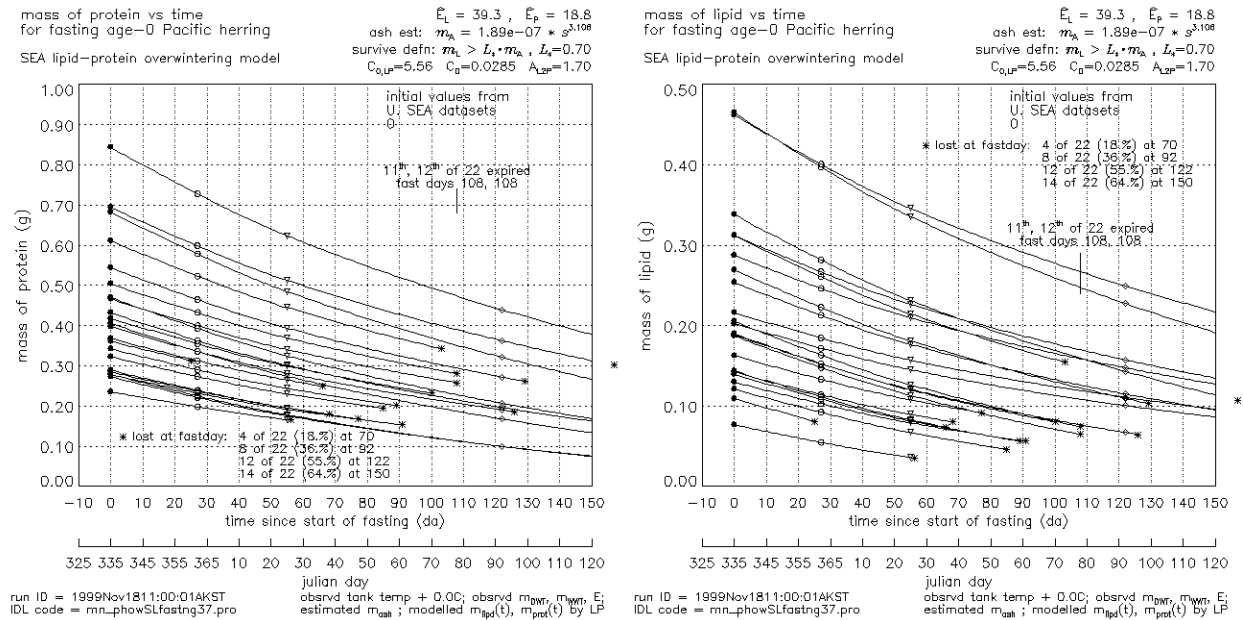


Figure 4.12 The time evolution of m_P and m_L for each of the individuals of the test group Ω_0^s . The plot symbols at fast days 27 and 55 show the values group Ω_0^s would have if measured at the special times subgroups Ω_1^s and Ω_2^s had been measured.

The basic issue in the calibration of C_0 is making the time evolution determined by the model Φ , and illustrated in Figure 4.12, “fit” the record contained in the Seward Laboratory study. In the figure the graphs of m_P and m_L versus time are shown for the case of advancing in time only subgroup Ω_0^s . The plot symbol—and only the plot symbol—has been borrowed from the other two

subgroups temporarily to indicate a special measurement time. In this case the symbol denotes a special measurement time.

Figure 4.12 shows many aspects of the model. All of these aspects will somehow have to be “captured” and compared to the Seward Laboratory study. Adjusting the parameter C_0 will superimpose an overall rate adjustment for everything that is happening in the figure. The detailed structure will be the same, just declining faster or slower. The question is how to choose how much faster or slower.

We can take this question and Figure 4.12 and return to Figure 4.1 in §4.0. The top two panels of that figure are the Seward Laboratory study records for the same two variables, for m_P (top left) and m_L (top right), and displayed in the same variable versus time format. Maybe we are done! Comparing Figure 4.12 with Figure 4.1 one could say we have both quantitative fits and a qualitative fit.

- A The time record for m_P in the simulation is much the same as for the experiment at fast days 0, 27 and 55. That is, we could set C_0 for a best fit at the three observation times.
- B Second, the time for 50% survival in the simulation agrees very well with the time for 50% survival in the experiment.
- C And there is a qualitative agreement: the simulation has recreated quite well the “variability” of the values assumed by m_P and m_L at the time of death.

However, in the case of m_L the time evolution of the simulation at fast days 0, 27, and 55 is not in good agreement with the experiment. How can this be?

The answer is in Figures 3.3, 3.2, and 4.1. Since $m_A = F_{\ell_{2A}}$ the record for standard length and for m_A convey the same information. (The advantage for m_A here is that it is a mass.) From Figure 3.3 and from Figure 3.2 we have the following.

Length, wet mass, and ash are quite low for Ω_0^s but quite high for Ω_1^s , yet energy and dry mass are close to the same for these two subgroups.

If energy and dry mass are both fixed, then if ash is increased, protein decreases and lipid increases. Hence we have lipid high in Ω_1^s with large lengths and high ash; lipid is low in Ω_0^s with small lengths and low ash. And it makes sense to see protein mass is flipped relative to lipid. This means, however, that there is substantial difference between the subgroups Ω_0^s , Ω_1^s , and Ω_2^s . This explains why the simulation and the observation sequence for m_L differed. It also suggests that the sample groups differ too greatly to use in a simple direct comparison of one group advanced to the sample time of a second group.

We set aside A and consider B.

In plan B we can do more than merely the time at which 50% survival is reached. We can examine the full survival function or, alternatively, the cumulative mortality function. In either case, the big difference between plan A and plan B is that plan A works within the 66 measurements of group Ω^s , whereas plan B compares the 66 measurements of group Ω^s with the 48 measurements of Ω^ℓ . This change immediately brings to bear on the calibration much more than simply more samples; it brings into the procedure two independent experiments. A further favorable feature is that it uses a transition that is well defined both experimentally and numerically—as we have seen in §4.4. A third favorable feature is that the comparison will be by means of what in effect is an integration.

The cumulative mortality or the survival is an integral over all of the differences in the sample populations, the details of the model, and the specifics of the environmental conditions. Although this integration should filter out issues that are thought not relevant, it will remain fully sensitive to changes in C_0 . Indeed, the rate at which mortality accumulates, the purpose for which these models were developed, should be very sensitive to changes in C_0 . And most important in practical terms, by allowing pooling of Ω_0^s , Ω_1^s , and Ω_2^s to simply Ω^s , plan B provides the means to neglect the differences identified above regarding the subgroups. Since Ω^s and Ω^ℓ are two subsamples from the same net cast, there should be no difference in the structure of the two groups.

Figure 4.13 shows the extent to which the foregoing forecast proved to be correct. Each panels shows the survival function (dashed line) for the Ω^ℓ group. This function is in effect the “target” function we seek to fit with this calibration.

The Seward Laboratory experiment ended on fast day 122, hence the plotted survival function ends at that time, with survival of 0.38 for the test group Ω^ℓ . This is a good point to recall the significance of these fast day units to actual field scenarios. The experiment started well after fasting is generally assumed to have begun, specifically 30–40 days after the start of fasting. Hence fast day 122 is more appropriately day 150 or 160 of the fast. The last day is similarly late. Spring feeding is assumed to begin no later than mid-March or Julian day 75. (The model uses March 05 for end of fasting, Julian day 64.) The last day for the Seward Experiment, fast day 122, Julian day 92, is 15–20 days beyond the expected end of fasting. Therefore, the end of the plot as shown in the figure is not a limitation for the calibration. Already the end of the plot is beyond a time that is relevant. In particular, Julian day 75 and fast day 105 (with observed survival 0.50) are the appropriate spring limits for any calibration procedure.

The overlay plot displayed in the top left panel of Figure 4.13 shows the results of the Version 3.1 calibration applied to the test group Ω^s .

From the restricted viewpoint that the model is to forecast survival and that a very good fit through Julian day 64 is the requirement, then the fit shown in the top left of Figure 4.13 is passable. From the viewpoint with which we opened this section, the results are not acceptable: The experimental results are from a well controlled study; the physiological system in question should be within the capabilities of this albeit simple model; and the merit of the model remains ambiguous if such results must stand. These results require an explanation. An explanation was found. And the answer was not within the domain of the model representation; rather, too much had been expected from the Law of Large Numbers.

The other three panels in Fig 4.13 show the overplots for the model applied to each subgroup of Ω^s individually. These overplots make evident the source of the problem in the top left panel, and for some time that source had been overlooked. The overplots make evident that the same differences between the subgroups of Ω^s that were identified above with respect to the distributions of m_P and m_L are also a factor in the survival function. Recall that Ω_0^s has low ash and low lipid; and Ω_1 has high ash and high lipid. We see that the survival trend is according to this ash and lipid trend. This provides sufficient motivation to visit again the physiological structure of subgroups.

However, there is now an additional aspect. The subgroups in question are no longer only those of Ω^s . The issue now is the structure of the subgroups of Ω^s relative to one another *and* relative to the test group Ω^ℓ . It is the survival function due to Ω^ℓ in Figure 4.13 that establishes the reference function (dashed line) appearing in each panel. It is this reference that we now use to classify Ω_0^s

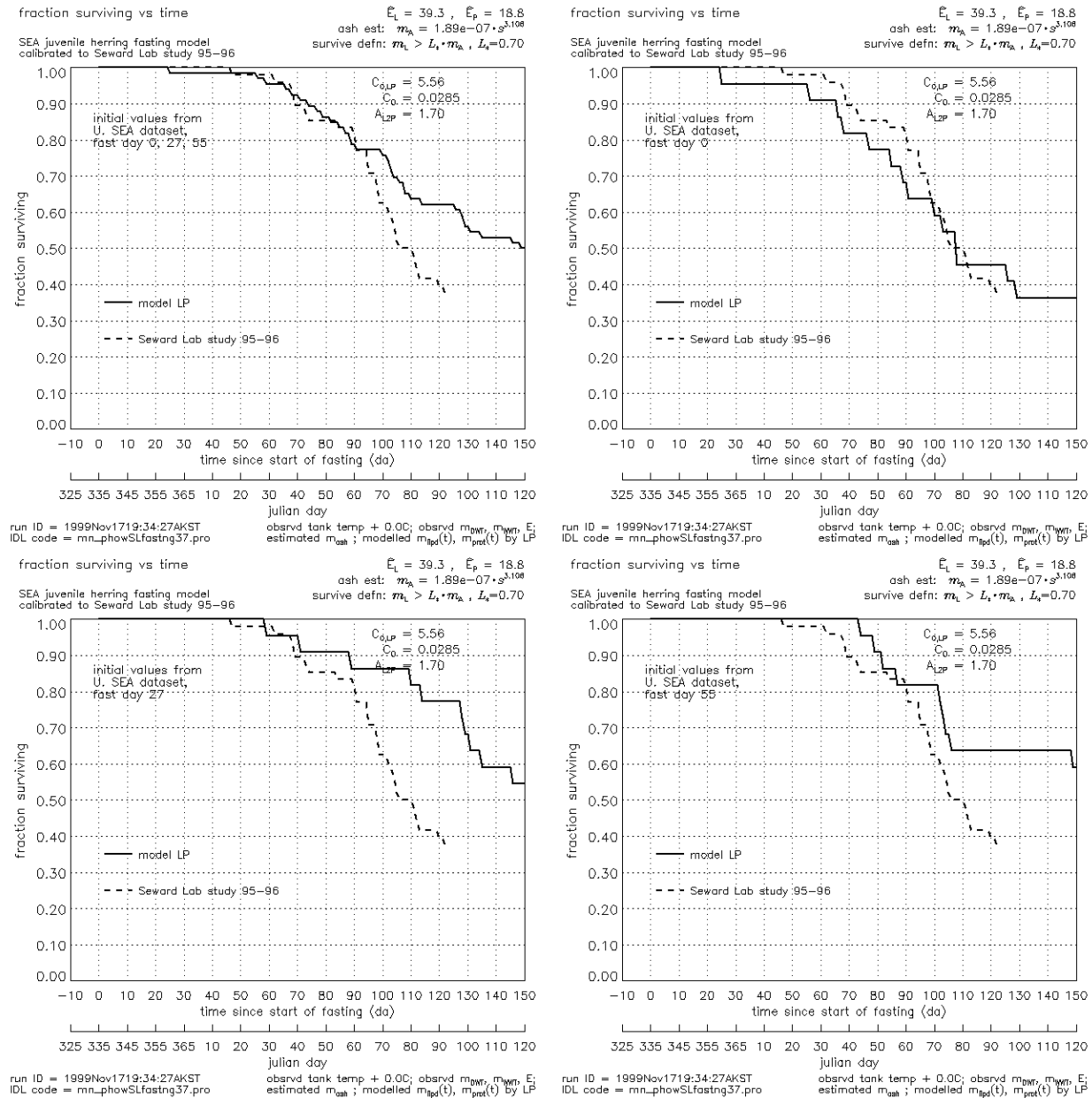


Figure 4.13 The survival function as for Ω^ℓ is the calibration “objective” (dashed line); the survival functions for Ω^s (top left), Ω_0^s (top right), Ω_1^s (bot left), and Ω_2^s (bot right) are shown in overlay (solid line).

as somewhat low, Ω_1^s as extremely high, and Ω_2^s as somewhat high. We have made progress in that instead of the four variables m_P, m_L, m_A, m_W for each of five subgroups we have for each of three subgroups the distance between a function of time and one common “calibration” function. But what is it with Ω^s and Ω^ℓ that prevents the simulated survival from being “aligned” with the “real” survival? The problem now centers on Ω^ℓ . All information about Ω^ℓ was acquired only at the end

of long periods of continuous and unmonitored physiological change. The change was substantial; in particular, most individuals died.

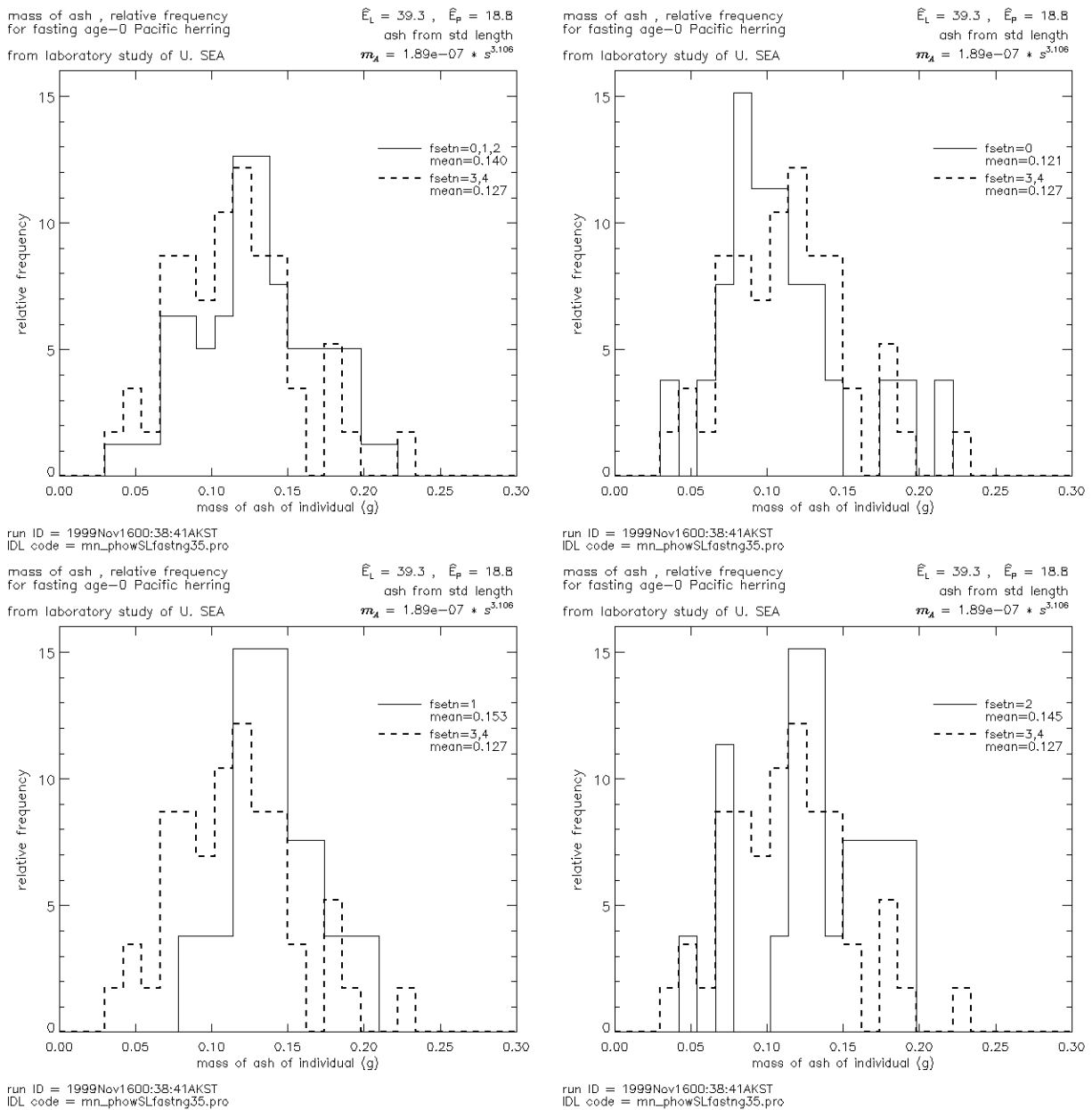


Figure 4.14 Histograms for the variable m_A for each of the test subgroups of Ω^s : Ω^s itself (top left), Ω_0^s (top right), Ω_1^s (bot left), Ω_2^s (bot right).

We have, however, the variable $m_A = F_{\ell 2A}(\ell)$ for each individual. This variable is an invariant of fasting. Independent of its utility as an approximation for m_A , $F_{\ell 2A}$ is extremely useful as a

mass-like quantity which is an invariant of the fasting process. Figure 4.14 shows the manner in which the function $F_{\ell 2A}$ (due to Mason and Paul) is used to conclude the calibration of C_0 .

Each panel in Figure 4.14 shows two histogram plots of relative frequency. The dashed-line histogram is the same in each panel and shows the relative frequency of m_A for the test group Ω^ℓ ; the solid-line histogram displays the relative frequency of m_A for the four test subgroups Ω^s (top left), Ω_0^s (top right), Ω_1^s (bot left), and Ω_2^s (bot right). By relative frequency we mean that each histogram integrates to 1. Each panel has a legend for the mean for each of the two histograms. The variable “fsetn” is the test group index as it has been used in this document. For example, fsetn = 3, 4 means $\Omega_3^\ell \cup \Omega_4^\ell = \Omega^\ell$. From left to right, top to bottom, the means for the subgroups of Ω^s less the mean for Ω^ℓ are, respectively, +0.13, -0.06, +0.26, +0.18.

This may or not have anything to do with the fact that the survival functions are greater than or less than the calibration function at a given time in the simulation. The fact that the histogram with mean closest to that for Ω^ℓ may not mean anything. It is for the model to sort out how the four system variables appear in the system time evolution. What we *can* say is that to the extent the histograms in a given panel are different then we are not in a comparable situation and any calibration is in doubt. Clearly, the physiological structure for the test group Ω_1 (bot left) is very different from that for Ω^ℓ for the variable m_A —and we know how survival depends upon m_A from §4.4. We can also now rank test groups according to the similarity between its frequency distribution and that for the test group Ω^ℓ . The best of the four shown is Ω_0^s (top right), and, by the way, that is the best fit between any subgroup survival function and the calibration survival function (see Figure 4.13).

If we look at pairwise unions of the subgroups of Ω^s we find a pair with a relative frequency that is extremely close to that for Ω^ℓ . This is shown in in the left panel of Figure 4.15. The absolute value of the difference in the means in Figure 4.15 is the same as the best we had. It seems clear, however, if we were to use a norm like L^1 or L^2 this new example would be “nearer” to the calibration case. In addition, this union $\Omega_0^s \cup \Omega_2^s$ has twice as many elements in the group. With this union the comparison is between 44 individuals and the 48 individuals of Ω^ℓ .

The right panel of Figure 4.15 shows the survival function obtained with $\Omega_0^s \cup \Omega_2^s$. The difference has increased for the time outside the time interval of interest—110 fast days. But for fast days less than 110 the difference is smaller.

We now have a calibration of the type appropriate for this model and its purposes. In the next section we describe how to extend this procedure to one in which the time evolution of protein is calibrated.

4.5.3 Using back-projections

In Figure 4.12 the individuals from the test subgroup Ω_0^s were used for the initial conditions of Φ and advanced in time. By this means the individuals in one test subgroup can be compared with the individuals in another test subgroup. More precisely, this is the *only* way the individuals in from subgroup Ω_0^s can be compared with the individuals in Ω_1^s or Ω_2^s since there is a time difference between the groups and a time difference means a change in the physiological state.

Figure 4.12 displayed the time evolution of the two variables m_p and m_L for each individual in Ω_0^s

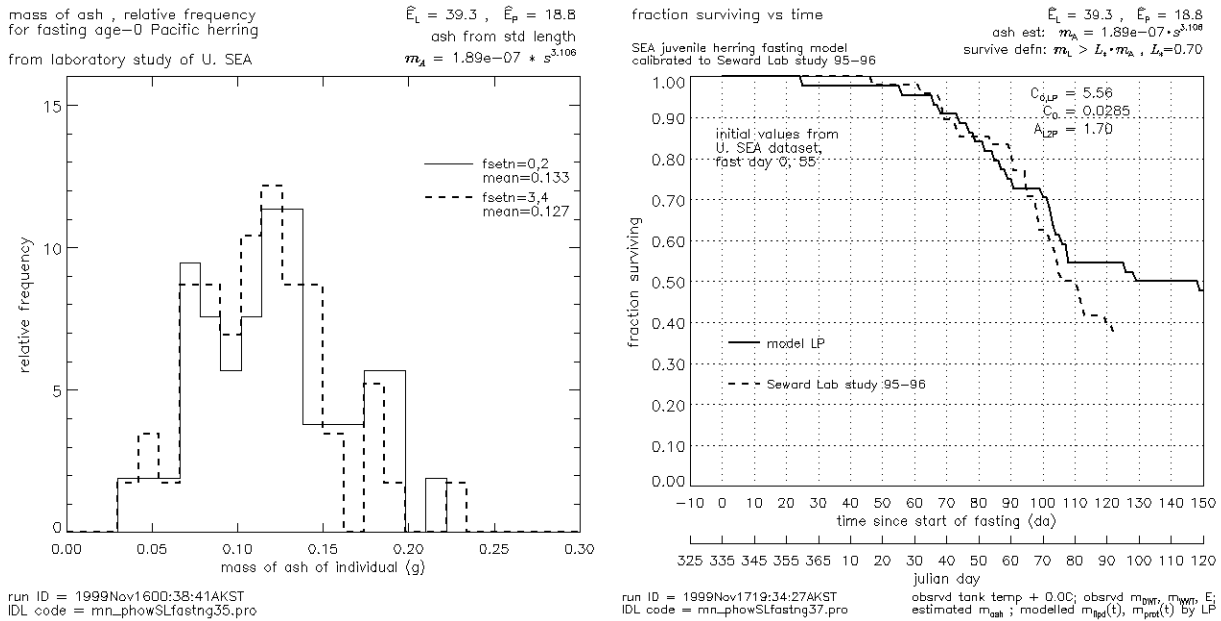


Figure 4.15 The calibration results for C_0 with Version 3.1 of the fasting model. (left) Relative frequency of m_A in $\Omega_0^s \cup \Omega_2^s$ (solid line); overplot of relative frequency of m_A in Ω^ℓ (dashed line). (right) Survival fraction of $\Omega_0^s \cup \Omega_2^s$, advancing in time by fasting model with Vers 3.1 calibration (solid line); overplot of survival fraction time series for Ω^ℓ (dashed line).

by means of two separate graphs,

$$\{(t, m_P(t)) : 0 < t < 150\} \quad \text{and} \quad \{(t, m_L(t)) : 0 < t < 150\} \quad (4.14)$$

displayed in side-by-side panels. In each panel there is a graph (or “curve”) for each individual. Consequently each panel has 22 graphs or curves, one curve for each individual. The figure provides a good illustration that

One or more graphs of the time dependence of a single coordinate variable for a system of more than a few dimensions typically provides little information about the system.

What we really want to know is all of the variables at each time t

$$\{(m_P(t), m_L(t), m_A(t), m_W(t)) : 0 < t < 150\}$$

that is, the “path” followed through, in this case, \mathcal{P} . In §4.4 we were interested in the boundary of \mathcal{P}^\square because we want to know when the path through \mathcal{P} leaves \mathcal{P}^\square and enters \mathcal{P}^* . Now that we know where the boundary is we could plot the projection to the orthogonal complement of the boundary against time—but that will be in another document.

It is often possible to view paths in \mathcal{P} in fewer than four dimensions and have the information be useful. For example, we can take Figure 4.12 and use just the $m_P(t)$ and $m_L(t)$ parts—discarding the time axis—to draw a path in the $m_P \times m_L$ plane. This is useful since within the model m_A and

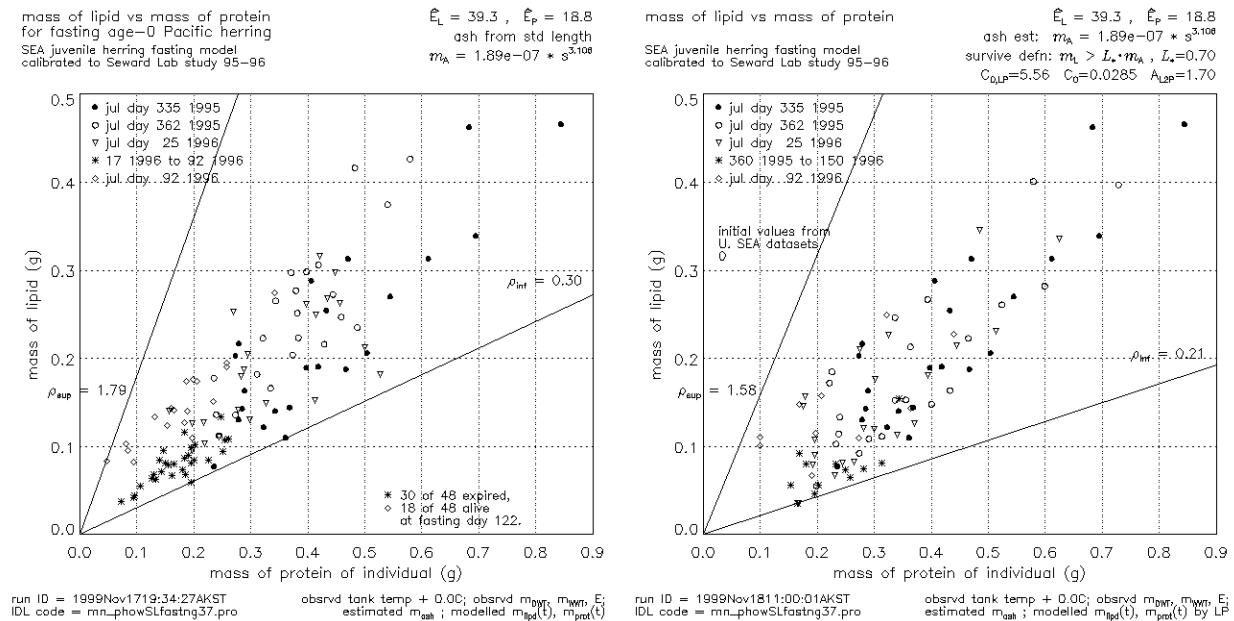


Figure 4.16 Left: data from each Ω_i , $i = 0, 1, 2, 3, 4$.
Right: snapshots of path of Ω_0 at fast days 0, 27, 55, 122.

m_W are assumed to not vary. These two *do* affect the course of events for a path, such as how close the path is to the boundary of \mathcal{P}^{\square} , but they do not change while things are underway.

An example is shown in Figure 4.16. The left and the right are *different* and the interpretation requires tending to the fact that:

left This is the Seward Lab data. Every plot symbol is a different individual. The plot symbols change to denote sample time, and sample groups are organized by the sample time. This is the “as measured state,” with measurements at sample times 0, 27, 55, and 122 fast day.

right Only subgroup Ω_0^s appear in the right plot. The same 22 individuals are reused. Each is measured at each sample time, 0, 27, 55, 122, then continues on until the next time. The path is that which was shown in a previous figure, in the direction (-1.7, -1). The position changes between sample times. Each individual is shown as if a snapshot were taken at times 0, 27, 55, and 122 fast day.

After a bit of thought one can see how subgroup Ω_0^s advanced to fast day 27 compares with Ω_1^s at fast day 27: this comparison is made by comparing the open circles in the left figure with the open circles in the right figure.

This is one view. Another is to take the same snapshots at fast days 0, 27, 55, and 122, but use the $m_A \times m_L$ plane. Since m_A does not change, the path is a bit easier to see, especially since we have to track a group. But we would like to see all the groups brought to the same time. So we take all five subgroups and “back-project” each to the 4 sample times. This lets us see how well the original group is reconstructed from the samples. If the reconstructed group is as well defined

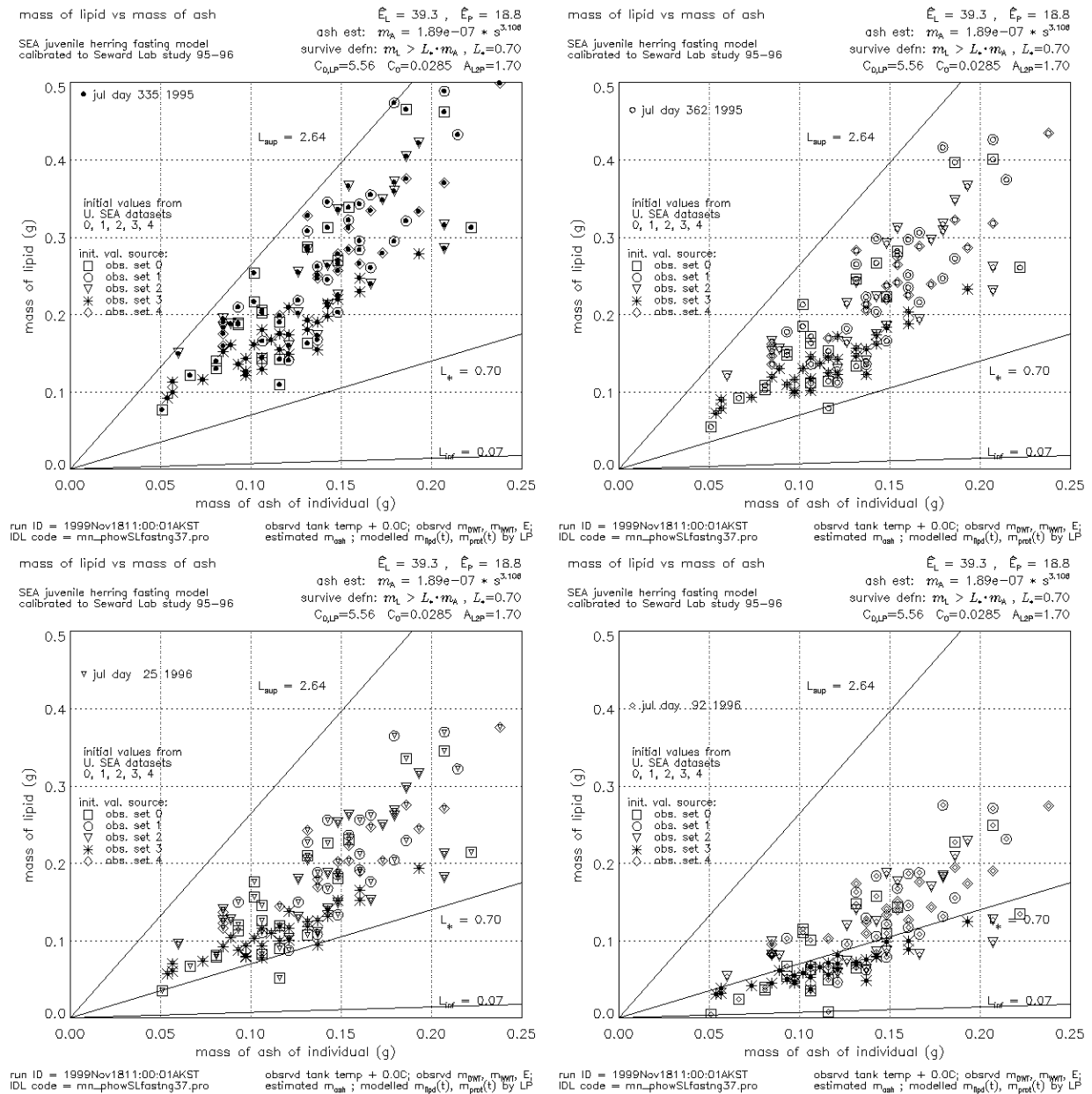


Figure 4.17 Back-projection of all test groups in $m_A \times m_L$, using snapshot times 0, 27, 55, 122 fast day.

as any one of the sample groups, then we have an indication that the model is reasonable. If, however, the group reconstruction is not localized, then probably (but not necessarily) the model is not accurately representing the path.

The result of doing this for the Seward Laboratory study is shown in Figure 4.17. One can evaluate how well the full test group has been “recreated” by back-projecting all measurements to the original collection day (fast day 0) then advancing the full group ahead in time and measuring each

one at 27, 55, and 122 fast days. Each individual is identified as to his origins by the large outer symbol. The small inner symbol identifies the snapshot time. So when inner and outer are the same, the measurement shows the initial conditions.

This back-projection is essentially a check on the calibration above. In the next section we show the back-projection in the plane $m_A \times m_P$. This back-projection was used to calibrate A_{L2P} .

4.5.4 Calibration of A_{L2P}

The model does not have to be calibrated for protein usage. The model forecasts survival based upon the boundary \mathcal{P}^\square , and that boundary lies essentially tangent to the direction of the m_P coordinate—a path cannot cross the boundary by changing the value of m_P alone. We have found no evidence of a boundary transversal to the m_P direction. There may be one but nothing has been in a state whereby it is revealed.

The effect is that A_{L2P} can be any value from 0 to, say, 1.9. The effect of using an inaccurate estimate for A_{L2P} is that protein use is incorrect and C_0 was calibrated to increase or reduce respiration rates so that at the time of death the correct amount of lipid is used. The model calibrates to lipid use from start of fast to death and adjusts C_0 so that the respiration matches that. If there is no protein usage, respiration is reduced to make that “work.”

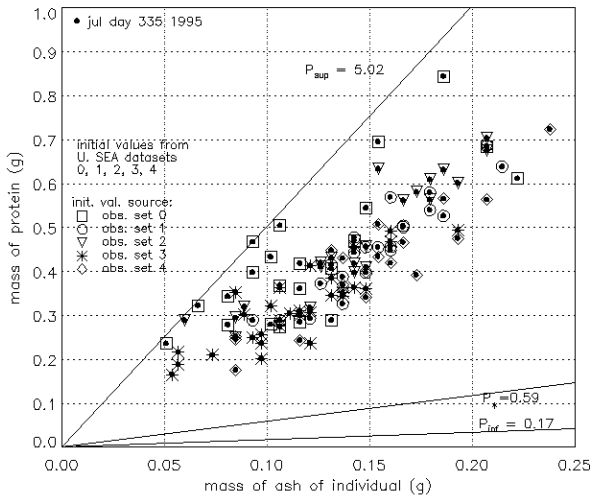
A practical effect is that the simulations get survival correct but not things that measure protein: energy, energy densities (any flavor), and wet or dry mass. Therefore, challenging the model with energy densities or dry mass misses the point of the model. The model forecasts life versus death and lipid usage. All else is lost in the calibration constant.

However, the model *can* be configured to attempt a realistic forecast of protein utilization. This process is only weakly coupled to the lipid usage (through the mass dependence of respiration). Hence, the survival works no matter what. Conversely, the protein approximation does not depend on the lipid being correct. This situation is ideal, for validation is indicating that protein is not consistent but lipid is. We have a conjecture for why which will appear in another document. For now, we show the calibration of Version 3.1 for protein usage using the back-projection method of the previous section.

Figure 4.18 shows the same set of four graphics for the plane $m_A \times m_P$ as was shown in the last section. The calibration for A_{L2P} was done by first setting C_0 for whatever was the existing choice for A_{L2P} . Then A_{L2P} is adjusted to have the tightest collection of overlapping distributions in the plane A_{L2P} by examining the effect of variations in terms of the display shown in Figure 4.18. After choosing a new A_{L2P} the calibration for C_0 is rerun. This continues until one is convinced that things can get no better.

mass of protein vs mass of ash
SEA juvenile herring fasting model
calibrated to Seward Lab study 95-96

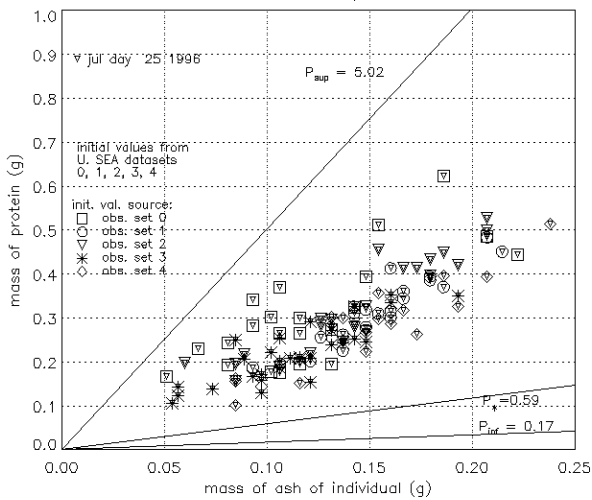
$\hat{E}_L = 39.3$, $\hat{E}_P = 18.8$
ash est: $m_A = 1.89e-07 * s^{3.108}$
survive defn: $m_L > L_s * m_A$, $L_s=0.70$
 $C_{0,LP}=5.56$ $C_0=0.0285$ $A_{LP}=1.70$



run ID = 1999Nov1811:00:01AKST
IDL code = mn_phovSLfastng37.pro
obsrvd tank temp + 0.0C; obsrvd m_{bWT} , m_{wWT} , E_i
estimated m_{ash} ; modelled $m_{pp}(t)$, $m_{pr}(t)$ by LP

mass of protein vs mass of ash
SEA juvenile herring fasting model
calibrated to Seward Lab study 95-96

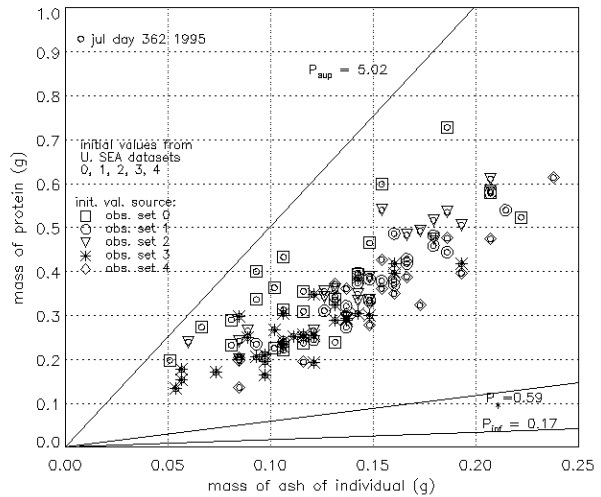
$\hat{E}_L = 39.3$, $\hat{E}_P = 18.8$
ash est: $m_A = 1.89e-07 * s^{3.108}$
survive defn: $m_L > L_s * m_A$, $L_s=0.70$
 $C_{0,LP}=5.56$ $C_0=0.0285$ $A_{LP}=1.70$



run ID = 1999Nov1811:00:01AKST
IDL code = mn_phovSLfastng37.pro
obsrvd tank temp + 0.0C; obsrvd m_{bWT} , m_{wWT} , E_i
estimated m_{ash} ; modelled $m_{pp}(t)$, $m_{pr}(t)$ by LP

mass of protein vs mass of ash
SEA juvenile herring fasting model
calibrated to Seward Lab study 95-96

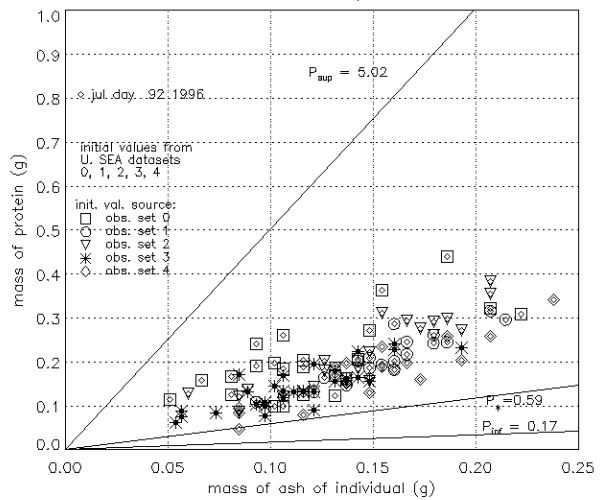
$\hat{E}_L = 39.3$, $\hat{E}_P = 18.8$
ash est: $m_A = 1.89e-07 * s^{3.108}$
survive defn: $m_L > L_s * m_A$, $L_s=0.70$
 $C_{0,LP}=5.56$ $C_0=0.0285$ $A_{LP}=1.70$



run ID = 1999Nov1811:00:01AKST
IDL code = mn_phovSLfastng37.pro
obsrvd tank temp + 0.0C; obsrvd m_{bWT} , m_{wWT} , E_i
estimated m_{ash} ; modelled $m_{pp}(t)$, $m_{pr}(t)$ by LP

mass of protein vs mass of ash
SEA juvenile herring fasting model
calibrated to Seward Lab study 95-96

$\hat{E}_L = 39.3$, $\hat{E}_P = 18.8$
ash est: $m_A = 1.89e-07 * s^{3.108}$
survive defn: $m_L > L_s * m_A$, $L_s=0.70$
 $C_{0,LP}=5.56$ $C_0=0.0285$ $A_{LP}=1.70$



run ID = 1999Nov1811:00:01AKST
IDL code = mn_phovSLfastng37.pro
obsrvd tank temp + 0.0C; obsrvd m_{bWT} , m_{wWT} , E_i
estimated m_{ash} ; modelled $m_{pp}(t)$, $m_{pr}(t)$ by LP

Figure 4.18 Back-projection of all test groups in $m_A \times m_P$, using snapshot times 0, 27, 55, 122 fast day.

Bibliography

- [AR97] J. A. Anthony and D. D. Roby. Variation in lipid content of forage fishes and its effects on energy provisioning rates to seabird nestlings. In *Forage Fishes in Marine Ecosystems*, volume AK-SG-97-01, pages 725–729. Alaska Sea Grant College Program, 1997.
- [Arr95] Fredrik Arrhenius. *Feeding Ecology of Baltic Sea Herring (Clupea harengus L.)—field and model studies of a dominant zooplanktivor*. PhD dissertation, Stockholm University, Department of Systems Ecology, 1995.
- [Kli99] T. C. Kline. Stable Isotopes as Food-Web Tracers. In R. T. Cooney, editor, *Sound Ecosystem Assessment (SEA) - An Integrated Science Plan for the Restoration of Injured Species in Prince William Sound*, Final Report, Ch 6. Exxon Valdez Oil Spill Trustee Council, June 1999.
- [Mor78] H. J. Morowitz. *Foundations of Bioenergetics*, chapter 14, pages 197–212. Academic Press, New York, 1978.
- [NBF⁺99] Brenda L. Norcross, Evelyn D. Brown, Robert J. Foy, Michele Frandsen, Jody Seitz, and Keven Stokesbury. Juvenile Herring Growth and Habitats. In R. T. Cooney, editor, *Sound Ecosystem Assessment (SEA) - An Integrated Science Plan for the Restoration of Injured Species in Prince William Sound*, Final Report, Ch 10. Exxon Valdez Oil Spill Trustee Council, June 1999.
- [Pau99] A. J. Paul. Fish Energetics. In R. T. Cooney, editor, *Sound Ecosystem Assessment (SEA) - An Integrated Science Plan for the Restoration of Injured Species in Prince William Sound*, Final Report, Ch 11. Exxon Valdez Oil Spill Trustee Council, June 1999.
- [PP98] A. J. Paul and J. M. Paul. Comparisons of whole body energy content of captive fasting age zero Alaskan Pacific herring (*Clupea pallasii Valenciennes*) and cohorts overwintering in nature. *J. Exp. Mar. Biol. Ecol.*, 226:75–86, 1998.
- [SN90] Knut Schmidt-Nielsen. *Animal Physiology: Adaptation and Environment*. Cambridge University Press, Cambridge, 4 edition, 1990.
- [SS97] J. T. U. SEA and M. N. R. SEA. Cookbook for age-0 Pacific herring during inactive fasting. 27 November 1997.
- [SS98] J. T. U. SEA and M. N. R. SEA. A Cookbook for Fasting Pacific herring: Algorithms for forecasting the maximum period of inactive fasting for age-0 Pacific herring during winter in Prince William Sound, AK. Technical note to SEA, Sound Ecosystem Assessment Program, 23 June 1998.
- [VPPLR97] T. I. Van Pelt, J. F. Piatt, B. K. Lance, and D. D. Roby. Proximate composition and energy density of some north Pacific forage fish. *Comp. Biochem Physiol.*, 118A(4):1393–1398, 1997.